THESE DE DOCTORAT DE
SORBONNE UNIVERSITE

Spécialité

Biomathématiques

ECOLE DOCTORALE PIERRE LOUIS DE SANTE PUBLIQUE A PARIS : EPIDEMIOLOGIE ET SCIENCES DE L'INFORMATION BIOMEDICALE

Présentée par

M. Francesco Pinotti

Pour obtenir le grade de

DOCTEUR de SORBONNE UNIVERSITE

Sujet de la thèse :

Dynamique multi-souche sur réseaux

soutenue le 27/11/2019

devant le jury composé de : (préciser la qualité de chacun des membres).

M. Christian L. ALTHAUS (University of Bern)	Examinateur
M. Pierre-Yves BOËLLE (Inserm, Sorbonne Université)	Directeur de thèse
Mme Clémence MAGNIEN (Sorbonne Université)	Examinateur
Mme Lulla OPATOWSKI (Université de Versailles Saint Quentin)	Rapporteur
Mme Chiara POLETTO (Inserm, Sorbonne Université)	Co-encadrante
M. Michele TIZZONI (Institute for Scientific Interchange Foundation)	Rapporteur

Sorbonne Université
Bureau d'accueil, inscription des doctorants et base de données
Esc G, 2ème étage
15 rue de l'école de médecine
75270-PARIS CEDEX 06

Tél. Secrétariat : 01 42 34 68 35
Fax : 01 42 34 68 40
Tél. pour les étudiants de A à EL : 01 42 34 69 54
Tél. pour les étudiants de EM à MON : 01 42 34 68 41
Tél. pour les étudiants de MOO à Z : 01 42 34 68 51
E-mail : scolarite.doctorat@upmc.fr

Résumé de la thèse

Introduction

La propagation des pathogènes résulte de l'interaction complexe entre plusieurs facteurs, y compris les interactions entre un pathogène et ses hôtes, l'environnement ou d'autres pathogènes. Les interactions entre pathogènes sont de plus en plus étudiées. En effet, la propagation de certaines maladies ne peut être analysée sans la prise en compte de ces interactions.

La modélisation mathématique représente un outil d'intérêt dans la lutte contre les maladies infectieuses. En particulier, les modèles mathématiques permettent de comprendre les données épidémiologiques en formulant des hypothèses mécaniques sur la propagation des maladies. Dans le cas particulier de plusieurs pathogènes et de leurs interactions mutuelles, les modèles mathématiques peuvent être utilisés pour répondre à une série de questions écologiques et épidémiologiques. Par exemple, ils peuvent clarifier les effets des interactions spécifiques sur la co-existence ou la dominance de plusieurs souches. Cependant, bien qu'il soit important de tenir compte des interactions entre pathogènes, plusieurs études mettent en évidence le rôle des facteurs environnementaux et ceux liés à l'hôte.

Les contacts entre les hôtes ont une importance reconnue dans la propagation d'épidémie. De récentes avancées technologiques ont permis d'aquérir des quantités massives de données, à une résolution spatiale et temporelle sans précédent, sur différents types de contacts humains [1, 2, 3, 4, 5, 6, 7, 8, 9, 10, 11, 12, 13, 14, 15, 16, 17, 18, 19, 20, 21, 22, 23, 24, 25]. Ces informations détaillées sur les individus et leurs relations mutuelles peuvent être pris en compte dans des modèles épidémiques en utilisant des réseaux [26, 27]. Ici, les hôtes sont représentés sous forme de noeuds dans un réseau, tandis que leurs connexions mutuelles sont représentées par des arêtes. La transmission s'effectue sur les arêtes émanant de noeuds infectés. Au cours des dernières années, notre compréhension théorique des processus de diffusion sur les réseaux de contacts s'est considérablement améliorée [28]. Néanmoins, l'étude des propriétés des contacts humains en cas de co-existence de plusieurs souches est encore préliminaire. En effet, la majorité des études ne concerne que l'interaction de deux agents pathogènes [29, 30, 31, 32, 33, 34, 35, 36, 37, 38, 39, 40, 41, 42]. Les connaissances de l'effet des interactions simultanées et hétérogènes liées aux pathogènes sont donc limitées.

Interactions entre pathogènes

Plusieurs mécanismes d'interaction ont été observés. Tout d'abord, les interactions peuvent être concurrentielles ou coopératives. La concurrence peut survenir en raison de ressources limitées. Il a été démontré, par exemple, que la colonisation par *Staphylococcus aureus* prévient l'invasion par d'autres souches de *S. aureus* [43]. Certains pathogènes comme *Streptococcus pneumoniae* peuvent également nuire aux concurrents en produisant des composés chimiques [44]. Enfin, certaines infections confèrent un certain degré d'immunité croisée contre d'autres pathogènes, protégeant efficacement l'hôte des infections secondaires [45].

Les pathogènes peuvent également interagir de manière synergique, facilitant ainsi leur propagation mutuelle. Par exemple, les infections grippales d'origine virale peuvent augmenter temporairement la susceptibilité aux infections bactériennes par *S. pneumoniae* et *Neisseria meningitidis* [46, 47, 48]. Le VIH est connu pour partager une synergie avec de nombreux pathogènes, comme *Mycobacterium tuberculosis*, *Plasmodium falciparum* ou le HPV [49, 50, 51, 52, 53, 54, 55, 56]. En effet, l'immunosuppression induite par le VIH favorise l'acquisition de plusieurs infections. En retour, le HPV endommage la barrière épithéliale du tractus génital, ce qui augmente le risque de contracter le VIH. *P. falciparum*, au contraire, semble augmenter la virulence de l'infection au VIH, en augmentant sa transmissibilité.

Les interactions entre les pathogènes et/ou les différentes souches d'un même agent pathogène ont des implications épidémiologiques et de santé publique importantes. Par exemple, pour comprendre les mécanismes à l'origine de l'émergence et du maintien de la résistance aux antibiotiques des bactéries *S. aureus*, *S. pneumoniae* et *Neisseria gonorrhoeae*, il faut prendre en compte des facteurs écologiques qui façonnent leurs écosystèmes, notamment la concurrence entre les différentes souches [57, 58, 59, 60]. Une interprétation correcte des modèles éco-épidémiologiques est également fondamentale pour évaluer l'efficacité des vaccins. Étant donné que les vaccins peuvent ne cibler que quelques souches, la compréhension de l'impact des interactions concurrentielles peut aider à quantifier le risque de remplacement des souches cibles par les souches non-cibles. Dans le passé, le remplacement post-vaccinal a été observé dans le cas du pneumocoque [61, 62]. Des augmentations sporadiques de la prévalence des types de HPV non ciblés ont également été signalées [63, 64, 65, 66], bien que le remplacement fasse encore l'objet de débats [67, 68].

Modèles mathématiques en épidémiologie

Les modèles épidémiologiques sont souvent formulés en termes de compartiments, c'est-à-dire de groupes d'hôtes partageant des propriétés similaires telles que l'état de santé. Les individus peuvent passer d'un compartiment à l'autre lors de la survenue de certains événements tels que l'infection et le rétablissement [69]. Dans le modèle *Susceptible-Infected-Susceptible* (SIS), par exemple, les individus peuvent être sensibles (S) ou infectés (I). Les infectés peuvent

transmettre l'infection aux individus sensibles à un taux de transmission β et se rétablir à un taux μ. Une fois rétablies, les personnes redeviennent sensibles aux nouvelles infections. Par conséquent, le modèle SIS décrit la propagation d'infections qui n'accordent pas l'immunité en cas de rétablissement. C'est le cas par exemple des bactéries commensales de l'homme comme *S. aureus*, qui entraînent généralement une colonisation asymptomatique.

Dans le contexte des systèmes multi-souches, les modèles compartimentaux sont essentiels pour répondre à un grand nombre de questions écologiques et épidémiologiques, e.g. les conditions menant à la co-existence des souches [70, 71, 72, 73, 74, 75, 76]. Les modèles mathématiques peuvent également être utilisés pour comprendre l'émergence de pathogènes envahissants qui peuvent apparaître à la suite d'importations externes ou de mutations. Par exemple, des modèles multi-souches ont été utilisés pour comprendre l'émergence des bactéries résistantes aux antibiotiques [77] et des souches pandémiques de grippe [78, 79, 80, 81]. L'analyse de modèles multi-souches peut également aider à évaluer l'efficacité des interventions de santé publique, par exemple en évaluant l'impact à long terme d'un vaccin sur une population de pathogènes et le risque de remplacement [82, 83, 84].

Les modèles compartimentaux supposent souvent que les hôtes sont bien mélangés, c'est-à-dire que chaque individu a la même probabilité de rencontrer tous les autres. Toutefois, cette approximation peut représenter une limite dans certains cas. La discipline de *network epidemiology* fournit le cadre approprié pour tenir compte de la complexité inhérente à la structure des contacts et à la dynamique épidémique. Les effets de la structure des contacts sur la propagation de l'épidémie ont été largement étudiés au cours des deux dernières décennies [28]. Les résultats les plus importants concernent le seuil épidémique [85, 86, 87, 88], la prévalence [89, 90, 91, 92, 93, 94, 95] et les stratégies de vaccination [96, 97, 98, 99, 100, 101]. Les développements théoriques ont permis de traiter également des hétérogénéités découlant de la nature temporelle des contacts entre hôtes [102, 103, 104, 105, 106, 107, 108, 109].

Plusieurs travaux ont porté sur la dynamique des pathogènes en interaction sur des réseaux de contacts. La plupart des études se sont concentrées sur deux souches qui interagissent par exclusion mutuelle ou par immunité croisée [110, 111, 32, 34, 33, 112, 113, 40, 29, 31, 39, 30, 41, 42]. Il a été démontré que les hétérogénéités de la structure des contacts influent sur la probabilité de l'émergence de nouvelles souches ainsi que sur la taille des nouvelles épidémies. En ce qui concerne la coopération sur des réseaux de contacts, de nombreuses études ont considéré une susceptibilité accrue comme mécanisme d'interaction [35, 38, 36, 37, 114]. Dans ce contexte, il a été démontré qu'à mesure que la transmissibilité augmente, les pathogènes coopératifs peuvent donner lieu à des flambées épidémiques discontinues en termes de prévalence. Néanmoins, la nature (continue ou discontinue) de cet événement dépend de la topologie du réseau.

Dynamique des contacts et écologie des souches multiples

Les travaux présentés dans la section précédente ne considèrent que deux souches en interaction. Les modèles à deux souches peuvent souvent être étudiés analytiquement, ce qui permet une caractérisation approfondie de la co-existence et de ses conditions. Cependant, l'impact de ces résultats avec un plus grand nombre de souches a été peu étudié. En effet, cela doit être abordé d'un point de vue écologique, avec la prise en compte simultanée de la stochasticité et de la sélection exercée par l'environnement, ou de la transmission entre hôtes. Les auteurs de [115] ont étudié par exemple plusieurs communautés de *S. aureus*, *S. pneumoniae* et *N. meningitidis*. Ils ont mis en place un modèle minimal de transmission avec des mutations neutres, capable d'expliquer la diversité génétique entre les souches. Les auteurs de [116] ont plutôt constaté que l'immunité croisée favorise l'organisation d'une population multi-souches en groupes antigéniques distincts, ce qui explique les tendances observées chez *N. meningitidis*. Les effets de l'immunité croisée sur la diversité des souches ont également été étudiés dans le contexte de réseaux de contacts [117, 118]. Les contacts en réseau favorisent la diversité par rapport à un mélange homogène où chaque individu a la même probabilité de rencontrer tout le monde. Cela s'explique par la nature localisée des contacts, qui permet aux groupes de souches d'occuper différentes parties du réseau.

Dans [119] nous avons étudié l'impact des hétérogénéités structurales et temporelles des contacts sur une population de souches. Nous avons simulé la propagation des souches multiples suivant une dynamique SIS sur des réseaux synthétiques variant dans le temps, en caractérisant les écosystèmes simulés par des indicateurs écologiques, e.g. la richesse (le nombre de souches en co-circulation) et l'indice de Berger-Parker, défini comme la fraction de prévalence associée à la souche la plus fréquente. Afin de mieux évaluer l'impact de la structure de contacts, nous avons considéré un modèle épidémiologique neutre où toutes les souches partagent les mêmes paramètres épidémiologiques. De plus, on a supposé que le statut de "porteur" confère une protection complète contre les nouvelles infections.

Nous avons montré que l'hétérogénéité des contacts réduit le nombre de souches en co-circulation, tout en favorisant la dominance de quelques souches (Fig. R1). Nous attribuons ce résultat au double rôle des individus les plus actifs, aussi connus sous le nom de *hubs* : ces derniers agissent comme *super-spreaders*, favorisant la propagation de certaines souches, et comme *super-blockers*, entravant l'émergence de nouvelles souches. La répartition des hôtes en différentes groups (communautés) a eu l'effet contraire, même si son impact était faible. Nous avons également constaté que le nombre de souches en co-circulation dépendait de manière non-linéaire de la durée moyenne du séjour des hôtes en raison d'un compromis entre le taux d'immigration de nouvelles espèces et le taux d'extinction de souches qui circulaient auparavant.

Nos résultats sont robustes lorsqu'il y a peu d'hétérogénéités des paramètres

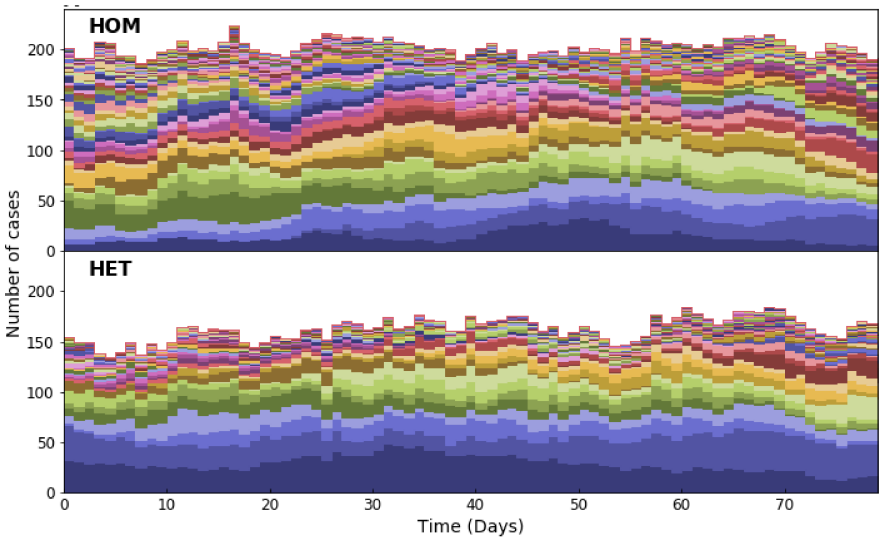

Fig. R1. Évolution temporelle d'un écosystème multi-souche. Chaque couleur indique une souche différente ; toutes les séries temporelles ont été empilées, de sorte que la hauteur des barres indique le nombre total de porteurs. Les deux vignettes correspondent respectivement à une structure de contacts homogène et hétérogène partageant les mêmes propriétés moyennes, notamment le nombre d'individus, l'activité et le nombre individuel de contacts. Les paramètres épidémiologiques sont également les mêmes pour tous les souches. On observe que la prévalence et la richesse sont plus faibles dans le cas d'un réseau hétérogène ; de plus, dans le réseau hétérogène la dominance de la souche la plus fréquente est amplifiée par rapport au cas homogène.

épidémiologiques entre les souches, comme par exemple la taux de transmission. Cependant, si l'ampleur de ces hétérogénéités est supérieure à un certain seuil, une souche super-adaptée devient dominante, assurant une fraction finie de la prévalence.

Comme étude de cas, nous avons examiné l'écologie de *S. aureus* en milieu hospitalier. *S. aureus* est une bactérie commensale de l'homme, présente chez 30 % des individus environ. Néanmoins, *S. aureus* est responsable de la majorité des infections nosocomiales dans les hôpitaux. Plusieurs études ont décrit l'écologie des souches de *S. aureus*, révélant une diversité remarquable à plusieurs échelles [120, 121, 11, 122]. Ici, nous avons utilisé un ensemble de données combinées d'interactions face-à-face et de portage nasal de *S. aureus* chez les patients et le personnel hospitalier, collectées dans le cadre de l'étude I-Bird (individual-based investigation of resistance dissemination) [123, 11, 124, 125, 12]. Le caractère hebdomadaire des données de portage, les informations sur le spa-type et le profil de résistance aux antibiotiques, ont permis de reconstituer l'écologie de *S. aureus* au cours de l'étude (Fig. R2 (A)). Nous avons montré que

les caractéristiques temporelles et topologiques du réseau conduisent à une prévalence et une richesse plus faibles par rapport à un mélange homogène. Par ailleurs, des valeurs de prévalence et de richesse similaires sont associées à différents niveaux de dominance (indice de Berger-Parker) dans différents réseaux ; les valeurs obtenues en utilisant les données de contact étaient plus proches des valeurs empiriques (Fig. R2 (B)). Ce comportement s'explique par les résultats théoriques et peut être attribué essentiellement à l'effet des hétérogénéités de contacts.

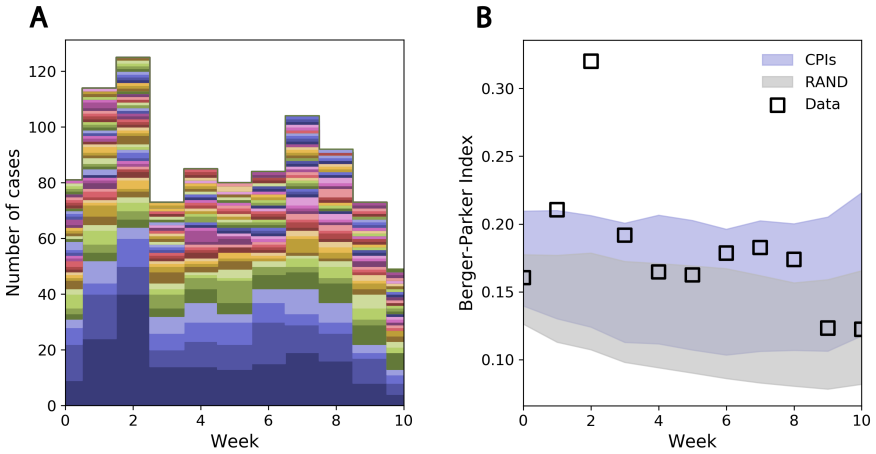

Fig. R2. Écologie de *S. aureus* et réseau hospitalier. (A) montre la composition hebdomadaire de l'écosystème de *S. aureus* au cours de l'étude i-Bird. La visualisation est la même qu'en Fig. R1. (B) montre l'indice de Berger-Parker obtenue respectivement par les données de portage (carrées noirs) et par les simulations sur le réseau des contacts hospitaliers (bleu) et un réseau randomisé (gris). Les bandes correspondent à des valeurs qui s'écartent d'un écart-type de la moyenne. Pour chaque réseau, les paramètres ont été établis afin de faire correspondre les valeurs empiriques de richesse et de prévalence.

Nos résultats fournissent de nouveaux aperçus sur les effets de la structure de contacts sur la concurrence des souches et pourraient améliorer notre compréhension de la diversité écologique des souches.

Interactions hétérogènes

Dans la section précédente nous avons étudié une population de souches interagissant seulement par exclusion mutuelle. Toutefois, la co-existence de souches peut être affectée par des interactions supplémentaires, exercées par exemple par d'autres pathogènes en co-circulation. Néanmoins, peu d'études ont été réalisées sur ce sujet. Les auteurs de [76] ont étudié l'interaction entre *Haemophilus influenzae* et les sérotypes de *S. pneumoniae* en co-circulation.

Leur étude suggère que *H. influenzae* pourrait favoriser la diversité des sérotypes de *S. pneumoniae* en modifiant la réponse immunitaire des hôtes.

Dans [126], nous avons approfondi les connaissances actuelles sur les effets des interactions hétérogènes dans les systèmes multi-pathogènes. En particulier, nous avons considéré le cas où deux pathogènes, A et B, suivent une dynamique SIS (un schéma du modèle est montré dans Fig. R3) ; pour simplifier, A et B ont le même taux de récupération μ. A et B coopèrent de manière symétrique par une susceptibilité accrue, c'est-à-dire qu'une infection primaire par l'un augmente la susceptibilité à une infection secondaire par l'autre. Nous avons supposé que l'interaction coopérative n'affecte pas la transmissibilité, de sorte que les individus doublement infectés, c'est-à-dire infectés simultanément par A et B, transmettent les deux maladies selon leur taux d'infection respectif. B est structuré en deux souches, B_1 et B_2, qui sont en concurrence en raison de l'exclusion mutuelle et de leurs différentes valeurs de transmissibilité. Plus précisément, nous avons indiqué les taux d'infection pour les pathogènes A et B_i avec α et β_i $(i = 1, 2)$, respectivement. Nous avons introduit les paramètres $c_i > 1$ pour représenter la susceptibilité accrue après une infection primaire.

Sans perte de généralité, nous avons examiné le cas où la souche B_2 est plus transmissible que B_1, c'est-à-dire $\delta_\beta = \beta_2 - \beta_1 > 0$. En outre, nous nous sommes concentrés sur le cas d'un compromis entre transmissibilité et coopération, pour limiter l'exploration des paramètres : la souche la moins transmissible, B_1, est plus coopérative ($\delta_c = c_1 - c_2 > 0$).

Dans les cas d'une population bien mélangée (Fig. R3 B), nous avons effectué une analyse de stabilité pour classer le résultat de la compétition entre B_1 et B_2 en fonction de δ_c et δ_β. Nous avons calculé des expressions analytiques explicites pour les conditions de faisabilité et de stabilité de chaque point d'équilibre dans plusieurs cas. Nous avons montré qu'il est possible pour une souche plus coopérative de dominer une souche plus transmissible. Nous avons constaté que le jeu entre interactions différentes (compétitives et coopératives) conduit à un diagramme de phase complexe dont les propriétés ne peuvent être facilement anticipées à partir de travaux antérieurs qui considéraient séparément chaque interaction. Pour certaines valeurs des paramètres, par exemple, les zones de stabilité associées à des équilibres différents sont superposées, donnant lieu à un comportement bistable ou multistable (Fig. R4 A,B). Dans certains cas, notre modèle conduit à un comportement apparemment paradoxal : nous constatons que l'augmentation de la capacité de coopération de la souche la plus transmissible peut entraîner son extinction. Fig. R4 C montre ce phénomène : dans le cadre inférieur, correspondant au marqueur noir en Fig. R4 A, B_2 est dominant. Par contre, en augmentant son facteur coopératif (marqueur gris en Fig. R4 A), B_1 gagne la compétition (Fig. R4 C, cadre supérieur). En fait, dans ce dernier cas B_2 favorise la propagation de A, ce qui profite en fin de compte à la souche la plus coopérative.

Nous avons étudié les effets de la répartition des hôtes en communautés différentes en considérant une population divisé en deux communautés bien mélangées (Fig. R3 B). Le couplage entre les deux sous-populations est réglé par un paramètre ϵ (une faible valeur de ϵ indique peu de mélange entre des commu-

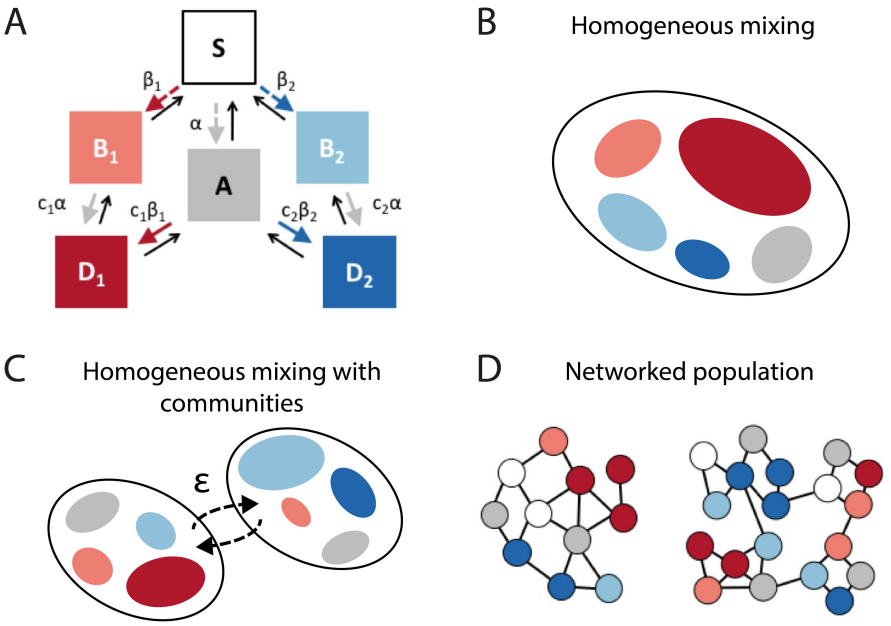

Fig. R3. Schéma du modèle. (A) Modèle épidémique. Les flèches de couleur représentent les transitions dues à la transmission de l'infection. Les flèches pointillées renvoient aux infections primaires, tandis que les flèches pleines renvoient aux infections secondaires ; les paramètres de transmission sont également indiqués à proximité de chaque flèche. Les flèches noires représentent les transitions de récupération. (B) Population homogène. (C) Deux populations homogènes avec couplage réglé par le paramètre ϵ. (D) Population structurée en réseau.

nautés distinctes). Dans ce cas, les calculs analytiques n'étaient pas possibles et nous avons donc eu recours à l'intégration numérique d'équations dynamiques. Nous avons montré que la répartition en communautés joue un rôle important sur la dynamique. En fait, cela permet la co-existence des deux souches dans de la population. Dans ce cas, les souches sont séparées en différentes communautés afin de minimiser la compétition pour les hôtes. La co-existence est finalement maintenue grâce au pathogène coopératif, dont la présence permet d'équilibrer localement la plus faible transmissibilité de la souche B_1.

Le cadre déterministe continu analysé jusqu'à présent ne tient pas compte du caractère aléatoire et de la nature discrète des individus et de leurs interactions. Afin de tenir compte de ces aspects, nous avons fondé notre modèle sur un cadre discret dans lequel les individus sont représentés par des noeuds dans un réseau statique. Nous avons considéré des réseaux à la Erdős-Rényi et des réseaux structurés en communautés (Fig R3 D). Les diagrammes de phase étaient semblables à ceux obtenus dans le cadre déterministe. Néanmoins, le cadre discret/stochastique a permis d'observer la nature des transitions de phase : dans

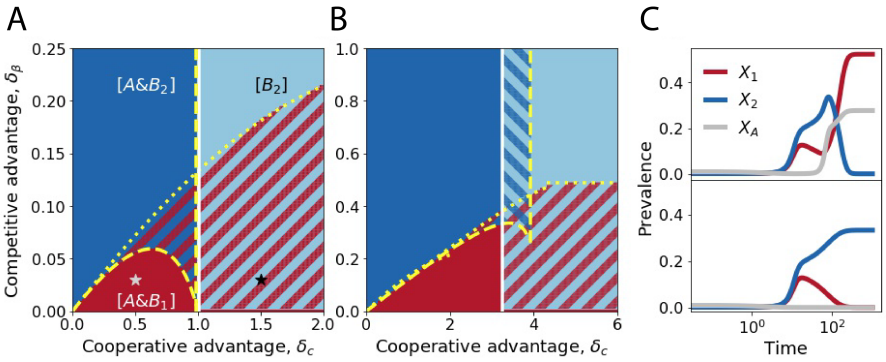

Fig. R4. Diagramme de phase pour une population homogène. (A, B) Diagrammes de phase obtenue pour différentes valeurs de α, c_1 et β_2 ($\alpha = 0.6$, $c_1 = 4$, $\beta_2 = 1.5$ en A et $\alpha = 0.8$, $c_1 = 7$, $\beta_2 = 1.1$ en B). Sur les axes x et y nous avons respectivement l'avantage coopératif de la souche B_1, $\delta_c = c_1 - c_2$ et l'avantage en transmission de la souche B_2, $\delta_\beta = \beta_1 - \beta_2$. Dans A et B, chaque couleur indique la région de stabilité associée à chaque point d'équilibre. Les motifs hachurés représentent les régions de bi-stabilité ou de multi-stabilité, i.e. des valeurs des paramètres où plusieurs équilibres sont simultanément stables. Les limites de chaque phase sont également indiquées. Les deux panneaux en C montrent les trajectoires dynamiques de la prévalence de B_1 (rouge), B_2 (bleu) et A (gris). Ces trajectoires ont été obtenues pour des valeurs de paramètres correspondant aux marqueurs gris et noir figurant dans le panneau A.

certains cas la transition d'une phase a l'autre était hybride, c'est-à-dire continue dans la probabilité d'atteindre l'un ou l'autre régime et discontinue dans la prévalence, selon la valeur de la différence entre les taux de cooperativité de chaque souche. Ces résultats concordent avec les constatations antérieures selon lesquelles la topologie du réseau peut influer sur la nature de la transition de phase. Cependant, une analyse numérique plus complexe est nécessaire afin de mieux comprendre les propriétés des transitions de phase, en faisant varier la valeur de δ_c.

Cette analyse fournit de nouvelles perspectives sur les facteurs écologiques qui déterminent la dynamique des souches concurrentes. De plus, ce travail souligne comment le jeu entre de multiples facteurs, par exemple la concurrence, la coopération et la répartition des hôtes en communautés, peut conduire à la co-existence ou à la domination de la souche la plus faible.

Conclusions

Dans cette thèse, nous avons étudié les effets de la structure des contacts sur la diversité des souches en utilisant une approche écologique. Grâce a cette approche nous avons été en mesure d'affronter des problématiques épidémiolo-

giques et écologiques qui, jusqu'à présent, étaient généralement abordées dans le cadre de modèles à deux souches. Nos résultats confirment l'importance de tenir compte simultanément de l'hétérogénéité des pathogènes et des hôtes dans les modèles à souches multiples. De plus, nos résultats fournissent de nouvelles perspectives écologiques et suggèrent des mécanismes susceptibles d'influer sur la dynamique des épidémies en interaction qui représentent une préoccupation pour la santé publique.

Références

[1] Ciro Cattuto, Wouter Van den Broeck, Alain Barrat, Vittoria Colizza, Jean-François Pinton, and Alessandro Vespignani. Dynamics of Person-to-Person Interactions from Distributed RFID Sensor Networks. *PLOS ONE*, 5(7) :e11596, 15-lug-2010.

[2] Marcel Salathé, Maria Kazandjieva, Jung Woo Lee, Philip Levis, Marcus W. Feldman, and James H. Jones. A high-resolution human contact network for infectious disease transmission. *Proceedings of the National Academy of Sciences*, 107(51) :22020–22025, December 2010.

[3] Juliette Stehlé, Nicolas Voirin, Alain Barrat, Ciro Cattuto, Lorenzo Isella, Jean-François Pinton, Marco Quaggiotto, Wouter Van den Broeck, Corinne Régis, Bruno Lina, and Philippe Vanhems. High-Resolution Measurements of Face-to-Face Contact Patterns in a Primary School. *PLOS ONE*, 6(8) :e23176, 16-ago-2011.

[4] Juliette Stehlé, Nicolas Voirin, Alain Barrat, Ciro Cattuto, Vittoria Colizza, Lorenzo Isella, Corinne Régis, Jean-François Pinton, Nagham Khanafer, Wouter Van den Broeck, and Philippe Vanhems. Simulation of an SEIR infectious disease model on the dynamic contact network of conference attendees. *BMC Medicine*, 9 :87, July 2011.

[5] Lorenzo Isella, Juliette Stehlé, Alain Barrat, Ciro Cattuto, Jean-François Pinton, and Wouter Van den Broeck. What's in a crowd ? Analysis of face-to-face behavioral networks. *Journal of Theoretical Biology*, 271(1) :166–180, February 2011.

[6] Mathieu Génois, Christian L. Vestergaard, Julie Fournet, André Panisson, Isabelle Bonmarin, and Alain Barrat. Data on face-to-face contacts in an office building suggest a low-cost vaccination strategy based on community linkers. *Network Science*, 3(3) :326–347, September 2015.

[7] Moses C. Kiti, Michele Tizzoni, Timothy M. Kinyanjui, Dorothy C. Koech, Patrick K. Munywoki, Milosch Meriac, Luca Cappa, André Panisson, Alain Barrat, Ciro Cattuto, and D. James Nokes. Quantifying social contacts in a household setting of rural Kenya using wearable proximity sensors. *EPJ Data Science*, 5(1) :21, December 2016.

[8] Laura Ozella, Francesco Gesualdo, Michele Tizzoni, Caterina Rizzo, Elisabetta Pandolfi, Ilaria Campagna, Alberto Eugenio Tozzi, and Ciro Cattuto. Close encounters between infants and household members measured through wearable proximity sensors. *PLOS ONE*, 13(6) :e0198733, 7-giu-2018.

[9] Lorenzo Isella, Mariateresa Romano, Alain Barrat, Ciro Cattuto, Vittoria Colizza, Wouter Van den Broeck, Francesco Gesualdo, Elisabetta Pandolfi,

Lucilla Ravà, Caterina Rizzo, and Alberto Eugenio Tozzi. Close Encounters in a Pediatric Ward : Measuring Face-to-Face Proximity and Mixing Patterns with Wearable Sensors. *PLOS ONE*, 6(2) :e17144, 28-feb-2011.

[10] Philippe Vanhems, Alain Barrat, Ciro Cattuto, Jean-François Pinton, Nagham Khanafer, Corinne Régis, Byeul-a Kim, Brigitte Comte, and Nicolas Voirin. Estimating Potential Infection Transmission Routes in Hospital Wards Using Wearable Proximity Sensors. *PLOS ONE*, 8(9) :e73970, September 2013.

[11] Thomas Obadia, Romain Silhol, Lulla Opatowski, Laura Temime, Judith Legrand, Anne C. M. Thiébaut, Jean-Louis Herrmann, Éric Fleury, Didier Guillemot, Pierre-Yves Boëlle, and on behalf of the I.-Bird Study Group. Detailed Contact Data and the Dissemination of Staphylococcus aureus in Hospitals. *PLOS Computational Biology*, 11(3) :e1004170, 19-mar-2015.

[12] Audrey Duval, Thomas Obadia, Pierre-Yves Boëlle, Eric Fleury, Jean-Louis Herrmann, Didier Guillemot, Laura Temime, Lulla Opatowski, and the i-Bird Study Group. Close proximity interactions support transmission of ESBL-K. pneumoniae but not ESBL-E. coli in healthcare settings. *PLOS Computational Biology*, 15(5) :e1006496, 30-mag-2019.

[13] Ken T. D. Eames and Matt J. Keeling. Monogamous networks and the spread of sexually transmitted diseases. *Mathematical Biosciences*, 189(2) :115–130, June 2004.

[14] Peter S. Bearman, James Moody, and Katherine Stovel. Chains of Affection : The Structure of Adolescent Romantic and Sexual Networks. *American Journal of Sociology*, 110(1) :44–91, July 2004.

[15] Luis E. C. Rocha, Fredrik Liljeros, and Petter Holme. Information dynamics shape the sexual networks of Internet-mediated prostitution. *Proceedings of the National Academy of Sciences*, 107(13) :5706–5711, March 2010.

[16] Chaoming Song, Zehui Qu, Nicholas Blumm, and Albert-László Barabási. Limits of Predictability in Human Mobility. *Science*, 327(5968) :1018–1021, February 2010.

[17] Mikko Kivelä, Raj Kumar Pan, Kimmo Kaski, János Kertész, Jari Saramäki, and Márton Karsai. Multiscale analysis of spreading in a large communication network. *Journal of Statistical Mechanics : Theory and Experiment*, 2012(03) :P03005, March 2012.

[18] Lauri Kovanen, Kimmo Kaski, János Kertész, and Jari Saramäki. Temporal motifs reveal homophily, gender-specific patterns, and group talk in call sequences. *Proceedings of the National Academy of Sciences*, 110(45) :18070–18075, November 2013.

[19] Zhi-Qiang Jiang, Wen-Jie Xie, Ming-Xia Li, Boris Podobnik, Wei-Xing Zhou, and H. Eugene Stanley. Calling patterns in human communication dynamics. *Proceedings of the National Academy of Sciences*, 110(5) :1600–1605, January 2013.

[20] Ming-Xia Li, Vasyl Palchykov, Zhi-Qiang Jiang, Kimmo Kaski, János Kertész, Salvatore Miccichè, Michele Tumminello, Wei-Xing Zhou, and Rosario N. Mantegna. Statistically validated mobile communication networks : The evolution of motifs in European and Chinese data. *New Journal of Physics*, 16(8) :083038, August 2014.

[21] Lijun Sun, Kay W. Axhausen, Der-Horng Lee, and Xianfeng Huang. Understanding metropolitan patterns of daily encounters. *Proceedings of the National Academy of Sciences*, 110(34) :13774–13779, August 2013.

[22] Marta C. González, César A. Hidalgo, and Albert-László Barabási. Understanding individual human mobility patterns. *Nature*, 453(7196) :779–782, June 2008.

[23] Filippo Simini, Marta C. González, Amos Maritan, and Albert-László Barabási. A universal model for mobility and migration patterns. *Nature*, 484(7392) :96–100, April 2012.

[24] Cecilia Panigutti, Michele Tizzoni, Paolo Bajardi, Zbigniew Smoreda, and Vittoria Colizza. Assessing the use of mobile phone data to describe recurrent mobility patterns in spatial epidemic models. *Royal Society Open Science*, 4(5) :160950, May 2017.

[25] Michele Tizzoni, Paolo Bajardi, Adeline Decuyper, Guillaume Kon Kam King, Christian M. Schneider, Vincent Blondel, Zbigniew Smoreda, Marta C. González, and Vittoria Colizza. On the Use of Human Mobility Proxies for Modeling Epidemics. *PLOS Computational Biology*, 10(7) :e1003716, July 2014.

[26] Alain Barrat, Marc Barthélemy, and Alessandro Vespignani. Dynamical Processes on Complex Networks by Alain Barrat. /core/books/dynamical-processes-on-complex-networks/D0173F07E0F05CEE9CF7A6BDAF48E9FC, October 2008.

[27] Mark Newman. *Networks : An Introduction*. Oxford University Press, March 2010.

[28] Romualdo Pastor-Satorras, Claudio Castellano, Piet Van Mieghem, and Alessandro Vespignani. Epidemic processes in complex networks. *Reviews of Modern Physics*, 87(3) :925–979, August 2015.

[29] M. E. J. Newman. Threshold Effects for Two Pathogens Spreading on a Network. *Physical Review Letters*, 95(10) :108701, September 2005.

[30] Brian Karrer and M. E. J. Newman. Competing epidemics on complex networks. *Physical Review E*, 84(3) :036106, September 2011.

[31] Shweta Bansal and Lauren Ancel Meyers. The impact of past epidemics on future disease dynamics. *Journal of Theoretical Biology*, 309 :176–184, September 2012.

[32] Qing-Chu Wu, Xin-Chu Fu, and Meng Yang. Epidemic thresholds in a heterogenous population with competing strains. *Chinese Physics B*, 20(4) :046401, April 2011.

[33] Gabriel E. Leventhal, Alison L. Hill, Martin A. Nowak, and Sebastian Bonhoeffer. Evolution and emergence of infectious diseases in theoretical and real-world networks. *Nature Communications*, 6 :6101, January 2015.

[34] Ruud van de Bovenkamp, Fernando Kuipers, and Piet Van Mieghem. Domination-time dynamics in susceptible-infected-susceptible virus competition on networks. *Physical Review E*, 89(4) :042818, April 2014.

[35] Laurent Hébert-Dufresne and Benjamin M. Althouse. Complex dynamics of synergistic coinfections on realistically clustered networks. *Proceedings of the National Academy of Sciences*, 112(33) :10551–10556, August 2015.

[36] Weiran Cai, Li Chen, Fakhteh Ghanbarnejad, and Peter Grassberger. Avalanche outbreaks emerging in cooperative contagions. *Nature Physics*, 11(11) :936–940, November 2015.

[37] Peter Grassberger, Li Chen, Fakhteh Ghanbarnejad, and Weiran Cai. Phase transitions in cooperative coinfections : Simulation results for networks and lattices. *Physical Review E*, 93(4) :042316, April 2016.

[38] Li Chen, Fakhteh Ghanbarnejad, and Dirk Brockmann. Fundamental properties of cooperative contagion processes. *New Journal of Physics*, 19(10) :103041, 2017.

[39] Sebastian Funk and Vincent A. A. Jansen. Interacting epidemics on overlay networks. *Physical Review E*, 81(3) :036118, March 2010.

[40] Joaquín Sanz, Cheng-Yi Xia, Sandro Meloni, and Yamir Moreno. Dynamics of Interacting Diseases. *Physical Review X*, 4(4) :041005, October 2014.

[41] Chiara Poletto, Sandro Meloni, Vittoria Colizza, Yamir Moreno, and Alessandro Vespignani. Host Mobility Drives Pathogen Competition in Spatially Structured Populations. *PLOS Computational Biology*, 9(8) :e1003169, 15-ago-2013.

[42] Chiara Poletto, Sandro Meloni, Ashleigh Van Metre, Vittoria Colizza, Yamir Moreno, and Alessandro Vespignani. Characterising two-pathogen competition in spatially structured environments. *Scientific Reports*, 5 :7895, January 2015.

[43] Elisa Margolis, Andrew Yates, and Bruce R. Levin. The ecology of nasal colonization of Streptococcus pneumoniae, Haemophilus influenzae and Staphylococcus aureus : The role of competition and interactions with host's immune response. *BMC microbiology*, 10 :59, February 2010.

[44] O. T. Avery and H. J. Morgan. THE OCCURRENCE OF PEROXIDE IN CULTURES OF PNEUMOCOCCUS. *The Journal of Experimental Medicine*, 39(2) :275–287, January 1924.

[45] Andrew F. Read and Louise H. Taylor. The Ecology of Genetically Diverse Infections. *Science*, 292(5519) :1099–1102, May 2001.

[46] Sourya Shrestha, Betsy Foxman, Daniel M. Weinberger, Claudia Steiner, Cécile Viboud, and Pejman Rohani. Identifying the interaction between influenza and pneumococcal pneumonia using incidence data. *Science translational medicine*, 5(191) :191ra84, June 2013.

[47] S. Shrestha, B. Foxman, S. Dawid, A. E. Aiello, B. M. Davis, J. Berus, and P. Rohani. Time and dose-dependent risk of pneumococcal pneumonia following influenza : A model for within-host interaction between influenza and Streptococcus pneumoniae. *Journal of The Royal Society Interface*, 10(86) :20130233–20130233, July 2013.

[48] Lulla Opatowski, Marc Baguelin, and Rosalind M. Eggo. Influenza interaction with cocirculating pathogens and its impact on surveillance, pathogenesis, and epidemic profile : A key role for mathematical modelling. *PLOS Pathogens*, 14(2) :e1006770, 15-feb-2018.

[49] Haileyesus Getahun, Christian Gunneberg, Reuben Granich, and Paul Nunn. HIV infection-associated tuberculosis : The epidemiology and the response. *Clinical Infectious Diseases : An Official Publication of the Infectious Diseases Society of America*, 50 Suppl 3 :S201–207, May 2010.

[50] Clara Flateau, Guillaume Le Loup, and Gilles Pialoux. Consequences of HIV infection on malaria and therapeutic implications : A systematic review. *The Lancet Infectious Diseases*, 11(7) :541–556, July 2011.

[51] Christina C. Chang, Megan Crane, JingLing Zhou, Michael Mina, Jeffrey J. Post, Barbara A. Cameron, Andrew R. Lloyd, Anthony Jaworowski, Martyn A. French, and Sharon R. Lewin. HIV and co-infections. *Immunological Reviews*, 254(1) :114–142, July 2013.

[52] James G Kublin, Padmaja Patnaik, Charles S Jere, William C Miller, Irving F Hoffman, Nelson Chimbiya, Richard Pendame, Terrie E Taylor, and Malcolm E Molyneux. Effect of Plasmodium falciparum malaria on concentration of HIV-1-RNA in the blood of adults in rural Malawi : A prospective cohort study. *The Lancet*, 365(9455) :233–240, January 2005.

[53] Cheryl Cohen, Alan Karstaedt, John Frean, Juno Thomas, Nelesh Govender, Elizabeth Prentice, Leigh Dini, Jacky Galpin, and Heather Crewe-Brown. Increased Prevalence of Severe Malaria in HIV-Infected Adults in South Africa. *Clinical Infectious Diseases*, 41(11) :1631–1637, December 2005.

[54] Laith J. Abu-Raddad, Padmaja Patnaik, and James G. Kublin. Dual infection with HIV and malaria fuels the spread of both diseases in sub-Saharan Africa. *Science (New York, N.Y.)*, 314(5805) :1603–1606, December 2006.

[55] Catherine F HOULIHAN, Natasha L LARKE, Deborah WATSON-JONES, Karen K SMITH-MCCUNE, Stephen SHIBOSKI, Patti E GRAVITT, Jennifer S SMITH, Louise KUHN, Chunhui WANG, and Richard HAYES. HPV infection and increased risk of HIV acquisition. A systematic review and meta-analysis. *AIDS (London, England)*, 26(17), November 2012.

[56] Pascale Lissouba, Philippe Van de Perre, and Bertran Auvert. Association of genital human papillomavirus infection with HIV acquisition : A systematic review and meta-analysis. *Sexually Transmitted Infections*, 89(5) :350–356, August 2013.

[57] Caroline Colijn, Ted Cohen, Christophe Fraser, William Hanage, Edward Goldstein, Noga Givon-Lavi, Ron Dagan, and Marc Lipsitch. What is the mechanism for persistent coexistence of drug-susceptible and drug-resistant strains of Streptococcus pneumoniae ? *Journal of The Royal Society Interface*, 7(47) :905–919, June 2010.

[58] Sonja Lehtinen, François Blanquart, Marc Lipsitch, Christophe Fraser, and with the Maela Pneumococcal Collaboration. On the evolutionary ecology of multidrug resistance in bacteria. *PLOS Pathogens*, 15(5) :e1007763, 13-mag-2019.

[59] Stephanie M. Fingerhuth, Sebastian Bonhoeffer, Nicola Low, and Christian L. Althaus. Antibiotic-Resistant Neisseria gonorrhoeae Spread Faster with More Treatment, Not More Sexual Partners. *PLOS Pathogens*, 12(5) :e1005611, 19-mag-2016.

[60] Magnus Unemo and Christian L. Althaus. Fitness cost and benefit of antimicrobial resistance in Neisseria gonorrhoeae : Multidisciplinary approaches are needed. *PLOS Medicine*, 14(10) :e1002423, 31-ott-2017.

[61] M. Lipsitch. Vaccination against colonizing bacteria with multiple serotypes. *Proceedings of the National Academy of Sciences of the United States of America*, 94(12) :6571–6576, June 1997.

[62] Brian G. Spratt and Brian M. Greenwood. Prevention of pneumococcal disease by vaccination : Does serotype replacement matter ? *The Lancet*, 356(9237) :1210–1211, October 2000.

[63] Jessica A. Kahn, Darron R. Brown, Lili Ding, Lea E. Widdice, Marcia L. Shew, Susan Glynn, and David I. Bernstein. Vaccine-Type Human Papillomavirus and Evidence of Herd Protection After Vaccine Introduction. *Pediatrics*, 130(2) :e249–e256, August 2012.

[64] David Mesher, Kate Soldan, Matti Lehtinen, Simon Beddows, Marc Brisson, Julia M.L. Brotherton, Eric P.F. Chow, Teresa Cummings, Mélanie Drolet, Christopher K. Fairley, Suzanne M. Garland, Jessica A. Kahn, Kimberley Kavanagh, Lauri Markowitz, Kevin G. Pollock, Anna Söderlund-Strand, Pam Sonnenberg, Sepehr N. Tabrizi, Clare Tanton, Elizabeth Unger, and Sara L. Thomas. Population-Level Effects of Human Papillomavirus Vaccination Programs on Infections with Nonvaccine Genotypes. *Emerging Infectious Diseases*, 22(10) :1732–1740, October 2016.

[65] Penelope Gray, Tapio Luostarinen, Simopekka Vänskä, Tiina Eriksson, Camilla Lagheden, Irene Man, Johanna Palmroth, Ville N. Pimenoff, Anna Söderlund-Strand, Joakim Dillner, and Matti Lehtinen. Occurrence of human papillomavirus (HPV) type replacement by sexual risk-taking behaviour group : Post-hoc analysis of a community randomized clinical trial up to 9 years after vaccination (IV). *International Journal of Cancer*, February 2019.

[66] Andreas Ährlund-Richter, Liqin Cheng, Yue O. O. Hu, Mikaela Svensson, Alexandra A. L. Pennhag, Ramona G. Ursu, Linnea Haeggblom, Nathalie Grün, Torbjörn Ramqvist, Lars Engstrand, Tina Dalianis, and Juan Du. Changes in Cervical Human Papillomavirus (HPV) Prevalence at a Youth Clinic in Stockholm, Sweden, a Decade After the Introduction of the HPV Vaccine. *Frontiers in Cellular and Infection Microbiology*, 9, 2019.

[67] Courtney Covert, Lili Ding, Darron Brown, Eduardo L. Franco, David I. Bernstein, and Jessica A. Kahn. Evidence for cross-protection but not type-replacement over the 11 years after human papillomavirus vaccine introduction. *Human Vaccines & Immunotherapeutics*, 15(7-8) :1962–1969, August 2019.

[68] Penelope Gray, Johanna Palmroth, Tapio Luostarinen, Dan Apter, Gary Dubin, Geoff Garnett, Tiina Eriksson, Kari Natunen, Marko Merikukka, Ville Pimenoff, Anna Söderlund-Strand, Simopekka Vänskä, Jorma Paavonen, Eero Pukkala, Joakim Dillner, and Matti Lehtinen. Evaluation of HPV type-replacement in unvaccinated and vaccinated adolescent females—Post-hoc analysis of a community-randomized clinical trial (II). *International Journal of Cancer*, 142(12) :2491–2500, 2018.

[69] Roy M. Anderson and Robert M. May. *Infectious Diseases of Humans : Dynamics and Control*. Oxford University Press, Oxford, New York, August 1992.

[70] Roger Kouyos, Eili Klein, and Bryan Grenfell. Hospital-Community Interactions Foster Coexistence between Methicillin-Resistant Strains of Staphylococcus aureus. *PLOS Pathogens*, 9(2) :e1003134, 28-feb-2013.

[71] François Blanquart, Sonja Lehtinen, Marc Lipsitch, and Christophe Fraser. The evolution of antibiotic resistance in a structured host population. *Journal of the Royal Society, Interface*, 15(143), June 2018.

[72] Maia Martcheva, Sergei S. Pilyugin, and Robert D. Holt. Subthreshold and superthreshold coexistence of pathogen variants : The impact of host age-structure. *Mathematical Biosciences*, 207(1) :58–77, May 2007.

[73] Sarah Cobey, Edward B. Baskerville, Caroline Colijn, William Hanage, Christophe Fraser, and Marc Lipsitch. Host population structure and treatment frequency maintain balancing selection on drug resistance. *Journal of The Royal Society Interface*, 14(133) :20170295, August 2017.

[74] Sonja Lehtinen, François Blanquart, Nicholas J. Croucher, Paul Turner, Marc Lipsitch, and Christophe Fraser. Evolution of antibiotic resistance is linked to any genetic mechanism affecting bacterial duration of carriage. *Proceedings of the National Academy of Sciences*, 114(5) :1075–1080, January 2017.

[75] Sarah Cobey and Marc Lipsitch. Niche and neutral effects of acquired immunity permit coexistence of pneumococcal serotypes. *Science (New York, N.y.)*, 335(6074) :1376–1380, March 2012.

[76] Sarah Cobey and Marc Lipsitch. Pathogen diversity and hidden regimes of apparent competition. *The American naturalist*, 181(1) :12–24, January 2013.

[77] François Blanquart. Evolutionary epidemiology models to predict the dynamics of antibiotic resistance. *Evolutionary Applications*, 12(3) :365–383, 2019.

[78] Yuki Furuse and Hitoshi Oshitani. Mechanisms of replacement of circulating viruses by seasonal and pandemic influenza A viruses. *International Journal of Infectious Diseases*, 51 :6–14, October 2016.

[79] Sébastien Ballesteros, Elisabeta Vergu, and Bernard Cazelles. Influenza A Gradual and Epochal Evolution : Insights from Simple Models. *PLOS ONE*, 4(10) :e7426, 20-ott-2009.

[80] Xu-Sheng Zhang, Daniela De Angelis, Peter J. White, Andre Charlett, Richard G. Pebody, and John McCauley. Co-circulation of influenza A virus strains and emergence of pandemic via reassortment : The role of cross-immunity. *Epidemics*, 5(1) :20–33, March 2013.

[81] Spencer J. Fox, Joel C. Miller, and Lauren Ancel Meyers. Seasonality in risk of pandemic influenza emergence. *PLoS Computational Biology*, 13(10), October 2017.

[82] Irene Man, Kari Auranen, Jacco A. Wallinga, and Johannes A. Bogaards. Capturing multiple-type interactions into practical predictors of type replacement following HPV vaccination. *bioRxiv*, page 523472, January 2019.

[83] Erida Gjini, Carina Valente, Raquel Sá-Leão, and M. Gabriela M. Gomes. How direct competition shapes coexistence and vaccine effects in multistrain pathogen systems. *Journal of Theoretical Biology*, 388 :50–60, January 2016.

[84] Margarita Pons-Salort, Véronique Letort, Michel Favre, Isabelle Heard, Benoit Dervaux, Lulla Opatowski, and Didier Guillemot. Exploring individual HPV coinfections is essential to predict HPV-vaccination impact on genotype distribution : A model-based approach. *Vaccine*, 31(8) :1238–1245, February 2013.

[85] Deepayan Chakrabarti, Yang Wang, Chenxi Wang, Jurij Leskovec, and Christos Faloutsos. Epidemic Thresholds in Real Networks. *ACM Trans. Inf. Syst. Secur.*, 10(4) :1 :1–1 :26, January 2008.

[86] Claudio Castellano and Romualdo Pastor-Satorras. Thresholds for epidemic spreading in networks. *Physical Review Letters*, 105(21) :218701, November 2010.

[87] Romualdo Pastor-Satorras and Alessandro Vespignani. Epidemic Spreading in Scale-Free Networks. *Physical Review Letters*, 86(14) :3200–3203, April 2001.

[88] Eugenio Valdano, Luca Ferreri, Chiara Poletto, and Vittoria Colizza. Analytical Computation of the Epidemic Threshold on Temporal Networks. *Physical Review X*, 5(2) :021005, April 2015.

[89] M. E. J. Newman. Spread of epidemic disease on networks. *Physical Review E*, 66(1) :016128, July 2002.

[90] Y. Moreno, R. Pastor-Satorras, and A. Vespignani. Epidemic outbreaks in complex heterogeneous networks. *The European Physical Journal B - Condensed Matter and Complex Systems*, 26(4) :521–529, April 2002.

[91] Yamir Moreno, Javier B. Gómez, and Amalio F. Pacheco. Epidemic incidence in correlated complex networks. *Physical Review E*, 68(3) :035103, September 2003.

[92] Joel C. Miller. Percolation and epidemics in random clustered networks. *Physical Review E*, 80(2) :020901, August 2009.

[93] Zimo Yang and Tao Zhou. Epidemic spreading in weighted networks : An edge-based mean-field solution. *Physical Review E*, 85(5) :056106, May 2012.

[94] Erik Volz. SIR dynamics in random networks with heterogeneous connectivity. *Journal of Mathematical Biology*, 56(3) :293–310, March 2008.

[95] James P. Gleeson. Binary-State Dynamics on Complex Networks : Pair Approximation and Beyond. *Physical Review X*, 3(2) :021004, April 2013.

[96] Romualdo Pastor-Satorras and Alessandro Vespignani. Immunization of complex networks. *Physical Review E*, 65(3) :036104, February 2002.

[97] Petter Holme, Beom Jun Kim, Chang No Yoon, and Seung Kee Han. Attack vulnerability of complex networks. *Physical Review E*, 65(5) :056109, May 2002.

[98] P. Holme. Efficient local strategies for vaccination and network attack. *EPL (Europhysics Letters)*, 68(6) :908, November 2004.

[99] Eben Kenah and Joel C. Miller. Epidemic Percolation Networks, Epidemic Outcomes, and Interventions. https ://www.hindawi.com/journals/ipid/2011/543520/, 2011.

[100] Maria Deijfen. Epidemics and vaccination on weighted graphs. *Mathematical Biosciences*, 232(1) :57–65, July 2011.

[101] Zhen Wang, Chris T. Bauch, Samit Bhattacharyya, Alberto d'Onofrio, Piero Manfredi, Matjaž Perc, Nicola Perra, Marcel Salathé, and Dawei Zhao. Statistical physics of vaccination. *Physics Reports*, 664 :1–113, December 2016.

[102] Naoki Masuda and Petter Holme, editors. *Temporal Network Epidemiology*. Theoretical Biology. Springer Singapore, 2017.

[103] Petter Holme and Jari Saramäki. Temporal networks. *Physics Reports*, 519(3) :97–125, October 2012.

[104] N. Perra, B. Gonçalves, R. Pastor-Satorras, and A. Vespignani. Activity driven modeling of time varying networks. *Scientific Reports*, 2 :469, June 2012.

[105] Giovanna Miritello, Esteban Moro, and Rubén Lara. Dynamical strength of social ties in information spreading. *Physical Review E*, 83(4) :045102, April 2011.

[106] M. Karsai, M. Kivelä, R. K. Pan, K. Kaski, J. Kertész, A.-L. Barabási, and J. Saramäki. Small but slow world : How network topology and burstiness slow down spreading. *Physical Review. E, Statistical, Nonlinear, and Soft Matter Physics*, 83(2 Pt 2) :025102, February 2011.

[107] Luis E. C. Rocha and Vincent D. Blondel. Bursts of Vertex Activation and Epidemics in Evolving Networks. *PLOS Computational Biology*, 9(3) :e1002974, 21-mar-2013.

[108] Dávid X. Horváth and János Kertész. Spreading dynamics on networks : The role of burstiness, topology and non-stationarity. *New Journal of Physics*, 16(7) :073037, July 2014.

[109] Matthieu Latapy, Tiphaine Viard, and Clémence Magnien. Stream graphs and link streams for the modeling of interactions over time. *Social Network Analysis and Mining*, 8(1) :61, October 2018.

[110] Ken T. D. Eames and Matt J. Keeling. Coexistence and Specialization of Pathogen Strains on Contact Networks. *The American Naturalist*, 168(2) :230–241, August 2006.

[111] B. Aditya Prakash, Alex Beutel, Roni Rosenfeld, and Christos Faloutsos. Winner Takes All : Competing Viruses or Ideas on Fair-play Networks. In *Proceedings of the 21st International Conference on World Wide Web*, WWW '12, pages 1037–1046, New York, NY, USA, 2012. ACM.

[112] Jonas I. Liechti, Gabriel E. Leventhal, and Sebastian Bonhoeffer. Host population structure impedes reversion to drug sensitivity after discontinuation of treatment. *PLOS Computational Biology*, 13(8) :e1005704, 21-ago-2017.

[113] Faryad Darabi Sahneh and Caterina Scoglio. Competitive epidemic spreading over arbitrary multilayer networks. *Physical Review E*, 89(6) :062817, June 2014.

[114] Peng-Bi Cui, Francesca Colaiori, and Claudio Castellano. Mutually cooperative epidemics on power-law networks. *Physical Review E*, 96(2) :022301, August 2017.

[115] Christophe Fraser, William P. Hanage, and Brian G. Spratt. Neutral microepidemic evolution of bacterial pathogens. *Proceedings of the National Academy of Sciences of the United States of America*, 102(6) :1968–1973, February 2005.

[116] S. Gupta, M. C. Maiden, I. M. Feavers, S. Nee, R. M. May, and R. M. Anderson. The maintenance of strain structure in populations of recombining infectious agents. *Nature Medicine*, 2(4) :437–442, April 1996.

[117] Caroline O'F Buckee, Katia Koelle, Matthew J. Mustard, and Sunetra Gupta. The effects of host contact network structure on pathogen diversity and strain structure. *Proceedings of the National Academy of Sciences*, 101(29) :10839–10844, July 2004.

[118] Caroline Buckee, Leon Danon, and Sunetra Gupta. Host community structure and the maintenance of pathogen diversity. *Proceedings of the Royal Society of London B : Biological Sciences*, 274(1619) :1715–1721, July 2007.

[119] Francesco Pinotti, Éric Fleury, Didier Guillemot, Pierre-Yves Böelle, and Chiara Poletto. Host contact dynamics shapes richness and dominance of pathogen strains. *PLOS Computational Biology*, 15(5) :e1006530, 21-mag-2019.

[120] Olga Sakwinska, Dominique S. Blanc, Catherine Lazor-Blanchet, Martine Moreillon, Marlyse Giddey, and Philippe Moreillon. Ecological Temporal Stability of Staphylococcus aureus Nasal Carriage. *Journal of Clinical Microbiology*, 48(8) :2724–2728, August 2010.

[121] Lyndsey O. Hudson, Courtney R. Murphy, Brian G. Spratt, Mark C. Enright, Kristen Elkins, Christopher Nguyen, Leah Terpstra, Adrijana Gombosev, Diane Kim, Paul Hannah, Lydia Mikhail, Richard Alexander, Douglas F. Moore, and Susan S. Huang. Diversity of Methicillin-Resistant Staphylococcus aureus (MRSA) Strains Isolated from Inpatients of 30 Hospitals in Orange County, California. *PLOS ONE*, 8(4) :e62117, 24-apr-2013.

[122] F. Di Ruscio, J. V. Bjørnholt, K. W. Larssen, T. M. Leegaard, A. E. Moen, and B. F. de Blasio. Epidemiology and spa-type diversity of meticillin-resistant Staphylococcus aureus in community and healthcare settings in Norway. *Journal of Hospital Infection*, 100(3) :316–321, November 2018.

[123] Thomas Obadia, Lulla Opatowski, Laura Temime, Jean-Louis Herrmann, Éric Fleury, Pierre-Yves Boëlle, and Didier Guillemot. Interindividual Contacts and Carriage of Methicillin-Resistant Staphylococcus aureus : A Nested Case-Control Study. *Infection Control and Hospital Epidemiology*, 36(8) :922–929, August 2015.

[124] Lucie Martinet, Christophe Crespelle, Eric Fleury, Pierre-Yves Boëlle, and Didier Guillemot. The Link Stream of Contacts in a Whole Hospital. *arXiv :1805.05752 [cs]*, May 2018.

[125] Audrey Duval, Thomas Obadia, Lucie Martinet, Pierre-Yves Boëlle, Eric Fleury, Didier Guillemot, Lulla Opatowski, and Laura Temime. Measuring dynamic social contacts in a rehabilitation hospital : Effect of wards, patient and staff characteristics. *Scientific Reports*, 8(1) :1686, January 2018.

[126] Francesco Pinotti, Fakhteh Ghanbarnejad, Philipp Hövel, and Chiara Poletto. Interplay between competitive and cooperative interactions in a three-player pathogen system. *Royal Society Open Science*, Under review.

Abstract

For many human pathogens, distinct strains have been reported to circulate in the host population. However, despite our ability to observe strain diversity, biological, environmental and host-related mechanisms shaping co-existence patterns remain largely unexplored. In this context, the importance of modeling contact structure is becoming increasingly recognized, yet, the study of this aspect is still at the beginning. To date, the majority of works focus on two pathogens that either compete or cooperate. Here, we extend current knowledge about strain co-existence on contact networks in two directions, characterizing the ecology of an open strain population, and analyzing the effect of heterogeneous concurrent interactions. In a first study, we assess the role of important contact properties on ecological diversity in a parsimonious model of strain competition. We found that our theoretical results improve our interpretation of observed patterns in a joint dataset consisting of face-to-face interactions and *Staphylococcus aureus* carriage in a hospital. In a second work, we study a theoretical model accounting for both competition and cooperation. We consider two competing strains that both cooperate with a second pathogen. The interplay between transmissibility and cooperative factor led to a rich phase diagram, showing complex boundaries and bistability. Here, repartition of hosts into communities enables strain co-existence by dynamically creating different ecological niches. Our findings confirm the importance of host contact structure as a driver of strain diversity.

Acknowledgements

First, I would like to thank Chiara, who has been not only a great mentor but also a great friend throughout these four years. I will be always indebted to her for teaching me how to do science and for instilling in me the passion for research. Thanks also to Pierre-Yves, for his guidance throughout my PhD.

I would like to express my gratitude to all my colleagues of any academic ranking, from master's students up to PIs. Thanks to them, my days at the lab have always been full of joy. A special mention to my fellows, Giulia and Alexandre. Together, we shared not just a mere room and a cluster but also the hardships of being PhD students. Thanks also to the other colleagues of the 8th floor, particularly Caroline and Raphaelle, who helped me express my thoughts in a correct French.

There is a chance that if you are an Italian living abroad, you'll be surrounded by plenty of other Italian people. This has definitely been the case for me here in Paris. Although I would like to thank all of them for making me feel at home even in this place, my warmest appreciation goes to the small clique also known as the "Italian Corner". Thanks for sharing this adventure and a flat with me. We have been so close that for some time there were not even walls between us, literally.

Leaving Italy for France meant leaving behind a small part of myself. Yet, my old friends have never left me and I will always be grateful to them for their friendship. I guess certain bonds cannot just fade simply due to distance or time. Also, they make me miss the fog sometimes.

A heartfelt thanks to my family, who has always been supporting me throughout my life and my studies. Without their help, it would not have been possible for me to make it this far. I am what I am because of them.

Last, but by no means the least, my deepest thanks to Giovanna. It is very difficult for me to describe how much I am indebted to her. Despite three long years of living in different countries, she has always been supporting me. This last year together under the same roof has been amazing. With her by my side, the sun finally started shining in Paris.

Research articles published as first author contained in this thesis

- Francesco Pinotti, Eric Fleury, Didier Guillemot, Pierre-Yves Boëlle, Chiara Poletto
  Host contact dynamics shapes richness and dominance of pathogen strains
  PLoS Computational Biology 15(5): e1006530 (2019)
  Cited as [1]

Research articles submitted as first author contained in this thesis

- Francesco Pinotti, Fakhteh Ghanbarnejad, Philipp Hövel, Chiara Poletto
  Interplay between competitive and cooperative interactions in a three-player pathogen system
  Royal Society Open Science, under review
  Cited as [2]

Oral communications

- *Host contact dynamics shapes richness and dominance of pathogen strains* at SPHINx19, Spread of Pathongens in Healthcare Institutions and Networks: a modeling conference, Paris, France.
- *Host contact dynamics shapes population diversity of pathogen strains* at Erice MathCompEpi 2018, Erice, Italy
- *Interplay between cooperative and competitive effects in multi-pathogen interaction systems* at International School and Conference on Network Science 2018, Paris, France.
- *Co-Existence of multiple SIS processes on temporal networks : implications for control of bacterial infections in hospitals* at International School and Conference on Network Science 2017, Indianapolis, Indiana (US)

Poster communications

- *Interplay between cooperative and competitive effects in multi-pathogen interaction systems* at Conference of Complex Systems 2017, Cancun, Mexico.
- *Co-Existence of multiple SIS processes on temporal networks : implications for control of bacterial infections in hospitals* at Epidemics6 Conference 2017, Sitges, Spain.
- *Interplay between cooperative and competitive effects in multi-pathogen interaction systems* at Epidemics6 Conference 2017, Sitges, Spain.

Contents

List of Figures

List of Abbreviations

HIV	Human Immonodeficiency Virus
SARS	Severe Acute Respiratory Syndrome
MERS CoV	Middle East Respiratory Syndrome Coronavirus
TB	Tuberculosis
HPV	Human Papillomavirus
SIS	Susceptible-Infected-Susceptible
SIR	Susceptible-Infected-Recovered
RFID	Radio Frequency Identification Device
CPI	Close-Proximity Interaction
ICT	Inter-Contact Time
RRM	Random Reference Model
ER	Erdős-Rényj
AD	Activity-Driven
HMF	Heterogeneous Mean Field
DFS	Disease-Free State
MRSA	Methicillin-Resistant *Staphylococcus Aureus*
HOM	Homogeneous model
HET	Heterogeneous model
COM	Community model
IPR	Inverse Participation Ratio
MDR-TB	Multi-Drug Resistant Tuberculosis

Introduction

Infectious diseases represent a major burden for public health. While efforts in prevention and control have led to a decline in prevalence for several infections, many diseases are still a source of concern in both developed and under-developed countries. More importantly, during the last 80 years we have witnessed the emergence of new threats such as antibiotic resistance [3], human immunodeficiency virus (HIV) [4], severe acute respiratory syndrome (SARS) [5], Middle East respiratory syndrome coronavirus (MERS-CoV) [6], pandemic influenza [7], Zika [8] and Chikungunya [9], and the re-emergence of Dengue [10] and Tuberculosis [11] (TB) in different parts of the world.

Pathogen spread results from the complex interplay between multiple factors, including interactions between a pathogen and the hosts, the environment and other pathogens as well. Pathogen-pathogen interactions have been drawing increasing attention recently. In fact, the spread of certain diseases cannot be analyzed independently from each other. For example, recurrent patterns of seasonal influenza reflect the co-circulation of antigenically distinct strains that compete for hosts through immune cross-reactions [12]. Competition between resistant and sensitive strains is key to understand the emergence and maintenance of antibiotic resistance [13, 14, 15, 16]. Knowledge of pathogen-pathogen interactions is also fundamental to assess vaccine efficacy and risk of replacement by non-vaccine types. Post-vaccine replacement has been observed in *Streptococcus pneumoniae* [17, 18] and concerns that human papillomavirus (HPV) might meet a similar fate have been raised too [19].

Mathematical modeling represents an invaluable tool in the fight against infectious diseases. In particular, mathematical models provide a way to uncover the mechanisms behind observed epidemiological patterns by formulating mechanistic hypotheses about disease spread [20, 21]. The consequences of hypotheses can be explored by means of mathematical analyses or numerical simulations, while their validity can be assessed by comparing model predictions against epidemiological data. Specifically for the case of multiple pathogens/strains and their mutual interactions, mathematical models can be used to address a range of ecological and epidemiological questions. For example, they may shed light on the consequences of specific interactions – e.g. cross-immunity, altered susceptibility and co-infections – on multi-strain co-existence and dominance. Models also help understanding determinants behind new strain emergence [22, 23, 24, 25, 26, 27, 28]. However, while it is important to account for interactions between pathogens/strains, several studies emphasize the role of environmental and host-related factors. Multi-strain models need to encompass the complexity arising from the simultaneous accounting of ecological interactions and the host dimension.

Host-to-host contacts have been increasingly recognized for their importance to epidemic spread [29, 30]. Up until 20 years ago, however, data about human behavior was limited, thus preventing the accounting of host-to-host contacts into epidemic models. For this reason, early mathematical models were heavily relying on a coarse-grained representation of mixing patterns among individuals [21]. Recent technological breakthroughs have changed this picture, yielding massive amounts of data at unprecedented spatial and temporal resolution about different kinds of human contacts, e.g. face-to-face interactions [31, 32, 33, 34, 35, 36, 37, 38, 39, 40, 41, 42] and sexual encounters [43, 44, 45], as well as about individual mobility at multiple scales [46, 47, 48, 49, 50, 51, 52, 53, 54, 55].

Network epidemiology provides a natural framework to encode detailed information about hosts and their mutual relationships within an epidemic model. According to this description, hosts are represented as nodes embedded in a network, while infection spreads through edges emanating from infected nodes. Our theoretical understanding of dynamical processes unfolding on networks, including epidemic processes, has significantly improved over the last two decades [29]. The study of properties of host contacts on multi-strain co-existence is, however, still in its infancy. In fact, the majority of multi-strain works has been concerned with just two interacting agents [56, 57, 58, 59, 60, 61, 62, 63, 64, 65, 66, 67, 68, 69, 70]. This makes it difficult to draw conclusions about diversity in larger multi-strain assemblies and about the effect of concurrent, heterogeneous interactions. In this thesis we aim to go beyond such limitations in two directions. First, we adopt an ecological perspective to multi-strain dynamics, using tools and concepts from community ecology to characterize strain diversity and to interpret its determinants. Second, we assess the impact of heterogeneous interactions types, i.e. co-operative and competitive, on strain co-existence and dominance on adding a new layer of complexity to the description of strain competition.

This thesis is organized as follows. In Chapter 1 we give an overview of pathogen-pathogen interactions and discuss their implications for epidemiology and public health. At the same time, we also introduce some of the fundamental mathematical tools that will be used throughout this thesis. Chapter 2 is dedicated to networks in epidemiology and epidemic spread on networks; we focus in particular on the spread of interacting pathogens/strains. The work associated to my first research article, entitled *"Host contact dynamics shapes richness and dominance of pathogen strains"* [1], is the subject of Chapter 3. There we investigate the impact of contact structure on diversity of multiple strains that compete for susceptible hosts. More in detail, we assess the impact of contact heterogeneities, community structure and host turnover by simulating synthetic contacts. As a case study, we analyze the spread of *Staphylococcus aureus* in a hospital by leveraging on a combined dataset of host-to-host interactions and carriage data. In my second article, *"Interplay between competitive and cooperative interactions in a 3-player pathogen system"* [2], which is included in Chapter 4, we study how additional, cooperative interactions with a co-circulating pathogen affect the outcome of competition between two strains. We consider both deterministic and stochastic dynamics and investigate the role of networked contacts and community structure.

Chapter 1

Multi-pathogen Systems

1.1 Introduction

The spread of pathogens is a complex and multifaceted phenomenon, thus epidemiology has established as an interdisciplinary research field, drawing attention from many scientific areas, including mathematics and computer science. The use of mathematical models has proven valuable in the fight against infectious diseases. The reasons behind this success are multiple. First, epidemic models provide a way to formulate and investigate mechanistic hypotheses about how diseases spread at the population scale. Second, mathematical models can make quantitative predictions about the temporal evolution of a disease. Models can thus be used both for epidemic assessment and for guiding public health interventions.

Most mathematical models focus on a single pathogen, ignoring interactions between pathogens. Although this is appropriate in some cases, certain problems require a multi-pathogen/strain perspective. For example, the occurrence of pathogen-pathogen interactions can hamper the efficacy of treatment [71, 72, 73] and public health measures such as vaccination [17, 74, 19]. Therefore, it is important to understand pathogen-pathogen interactions and their impact on epidemiological and macro-ecological patterns. This justifies accounting for multiple strains/pathogens and their mutual interactions into mathematical models.

In this chapter we review some of the most common and well-studied interactions between pathogens. We then discuss the importance of accounting for pathogen interactions in epidemiology and public health, highlighting possible biases arising from their neglect. Finally, we introduce compartmental models as well as the fundamental mathematical tools required to describe disease spread. We devote particular attention to the description of additional challenges that arise when accounting for multiple pathogen/strains and their mutual interactions.

1.2 Interaction mechanisms

As a first approximation we may distinguish between competitive and synergistic interactions. Competitive interactions play a fundamental role in shaping pathogen communities [75, 76]. Competition can arise due to limited shared resources or space. Nasal

colonization by *S. aureus* has been shown for example to prevent invasion from other *S. aureus* strains because of the limited amount of attachment sites [77]. Some pathogens can also harm competitors by producing chemical compounds. *S. pneumoniae* for example produces oxygen peroxide [78], which is harmful to other commensal bacteria. Finally, some infections confer some degree of cross-immunity against other pathogens/strains, effectively protecting the host from secondary infections [79]. Owing to their antigenic similarity, *S. pneumoniae* serotypes can elicit serotype-specific cross-immunity [80, 81]. Influenza strains also compete for hosts through cross-immunity; indeed, this mechanism is a fundamental driver of recurrent patterns of seasonal influenza [82].

Pathogens may also interact in a synergistic way, facilitating their mutual spread. For example, primary influenza infections can temporarily increase susceptibility to bacterial infections by, e.g., *S. pneumoniae* and *Neisseria meningitidis* [83, 84, 85]. Within-host mechanisms responsible for such facilitation are multiple, ranging from increased bacterial adherence to host cells [86] to impairment of host immune defenses [87, 88]. Another paradigmatic synergistic interaction between pathogens is the one between HIV and *Mycobacterium tuberculosis*, which appear to fuel each other's spread in Sub-Saharan Africa [89, 72]. On one hand, HIV exacerbates every aspect of tuberculosis infection, increasing also susceptibility [90]; on the other hand tuberculosis impairs highly active antiretroviral therapy, making it difficult to treat patients co-infected with HIV and Tuberculosis [91].

In other cases, however, the nature of a given interaction cannot be identified as purely competitive or purely cooperative. Let us consider for example the case of immune-mediated cross-reactions between Dengue serotypes. Primary Dengue infections grant full immunity against the same serotype and short-term protection against other serotypes [92]. However, secondary Dengue infections are much more severe than primary ones, suggesting a complex immunological scenario. Late disease enhancement may be explained by a non-linear association between cross-protection and antibody concentration, according to a mechanism known as antibody-dependent enhancement [93]. As a consequence, the nature of cross-reactive interactions between Dengue serotypes shifts from protective to enhancing as antibody count decreases over time.

Besides interactions taking place within hosts, pathogens may also interfere at the population level [94]. Sickness arising from some primary infection is likely to be followed by convalescence. Owing to the reduced number of contacts, convalescent individuals are less exposed to secondary infections and they can thus be considered as being effectively removed from the pool of susceptibles. This can hamper the spread of other pathogens, as potential hosts are temporarily unavailable. This kind of interference has been suggested to affect apparently unrelated diseases such as measles and pertussis, which happen to affect the same pool of hosts (children in this case) [95]. Fatal diseases may interfere in a similar manner, owing to the increased mortality and quarantine measures, which ultimately result in the depletion of the susceptible pool [96].

1.3 Implications for epidemiology and public health

In the previous section we discussed several mechanisms through which two or more pathogens can interact. We show here that interactions between pathogens can affect their mutual spread as well as epidemic assessment and public health projections.

Interactions can affect spatial and temporal spreading patterns. Cross-protection due to previous immunity can prevent multiple diseases to co-circulate within the same population; for example, past immunity to chikungunya [97] and Dengue [98] was found to displace or reduce the size of Zika epidemics. Also, cross-protection due to seasonal influenza has been suggested to tighten constraints on the timing of pandemics [99]. In some cases, the depletion of the shared susceptible pool can also induce out-of-phase relationships between diseases and alter disease periodicity [95, 100].

S. pneumoniae, *S. aureus* and *Neisseria gonorrhoeae* bacterial populations are characterized by a multiplicity of strains with varying profiles of antibiotic resistance. Understanding the mechanisms behind the emergence and maintenance of resistance in bacterial populations is fundamental to quantify the impact of resistance on public health. This necessarily requires a proper accounting of the ecological factors that shape bacterial ecosystems, including interactions among different strains [13, 14, 15, 16].

A correct interpretation of eco-epidemiological patterns is also fundamental to assess vaccine effectiveness. Vaccines usually target only a subset of circulating strains. The heptavalent pneumococcal vaccine (PCV7), for example, targets only 7 out of the over 90 known pneumococcus serotypes. In such cases, ignoring eventual competitive interactions between target and non-target types may lead to an overestimation of vaccine effectiveness. PCV7 resulted for example in replacement of target types by non-target types [17, 18]. Sporadic increases in the prevalence of non-target HPV types have been reported as well [101, 102, 103, 104], although replacement is still matter of debate [105, 106].

The burden of emergent diseases such as Zika may also depend on past exposure to other pathogens. Zika recently emerged in the Pacific area and in South America [8], sharing considerable geographical overlap with Dengue. Cross-reactions between Zika and Dengue suggest that exposure to the latter may modulate Zika outbreaks by either protecting against it or by triggering antibody-dependent enhancement [107, 108, 109, 98].

1.4 Modeling multi-pathogen interactions

1.4.1 Compartmental models

Mathematical models describing infectious disease spread date back to 1766 [110]. In his seminal paper, Bernoulli analyzed mortality due to smallpox, discussing the beneficial impact of prevention strategies against the disease. The foundations of modern epidemiology were laid by Ross in 1911 [111], who developed the first mathematical model of malaria transmission.

Epidemiological models are often formulated in terms of compartments, i.e. groups of hosts sharing similar properties such as the health status [20]. Upon certain events like, e.g., infection and recovery, individuals transit from one compartment to the other. Within this framework, it is possible to study the temporal evolution of a disease by tracking the number of individuals within each compartment.

The Susceptible-Infected-Susceptible (SIS) model includes just two categories of individuals, namely susceptibles (S) and infected (I) (Fig. 1.1 A). The SIS model is characterized by two elementary reactions:

$$\begin{aligned} S + I &\xrightarrow{\beta} I + I\,, \\ I &\xrightarrow{\mu} S\,, \end{aligned} \tag{1.1}$$

the first reaction refers to the infection of a susceptible upon contact with an infected, whereas the second refers to the recovery of an infected into a susceptible. Infection and recovery occur at rates β and μ respectively. If we assume that every individual contacts, on average, $\bar{k}$ other individuals chosen fully at random, the evolution equation for the density of infected individuals $\rho_I(t)$ is given by:

$$\dot{\rho}_I = -\mu\rho_I + \beta\bar{k}(1-\rho_I)\rho_I\,, \tag{1.2}$$

the two terms on the right side represent recovery and infection respectively. Notice that, in the case of a closed population, a single variable, namely the density of infected ρ_I, completely characterizes the state of the system. Dynamical trajectories arising from Eq. (1.2) settle around different values as the control parameter $R_0 = \beta/\mu$ (the basic reproductive number) is varied. By setting $\dot{\rho}_I = 0$ in Eq. (1.2), we obtain two possible fixed points, namely $\rho_I = 0$ and $\rho_I = 1 - R_0^{-1}$. The first solution corresponds to a disease-free state, whereas the second one corresponds to an endemic state with stationary prevalence. If $R_0 < 1$ the disease dies out immediately, whereas if $R_0 > 1$ it becomes endemic. At $R_0 = 1$ the model thus undergoes a dynamical transition which changes its qualitative behavior. R_0 has an important epidemiological interpretation: it is the average number of secondary cases originating from a single infected seed in a fully susceptible population.

There is a connection between the SIS model and the theory of critical phenomena in statistical physics. More precisely, the disease-free and endemic states can be regarded as two distinct phases of a physical system such as a ferromagnet. According to this analogy, the critical point at $R_0 = 1$ can be regarded as a phase transition. Furthermore, because total prevalence varies continuously at the transition, a physicist would denote this phase transition as continuous or “second order".

For some diseases, recovery grants lifelong immunity, preventing re-infection by the same pathogen. This situation is described by the Susceptible-Infected-Recovered (SIR) model (Fig. 1.1 B), where infected individuals transit to the recovered (R) compartment. The SIRS model describes yet another scenario, where immunity wanes over time (Fig. 1.1 C).

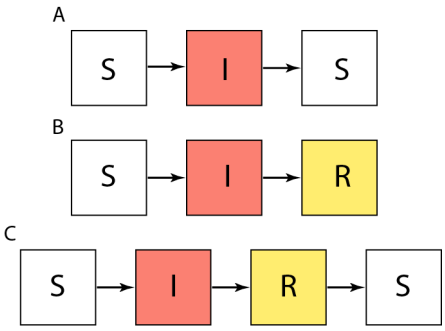

FIGURE 1.1: **Elementary compartmental models.** Transition schemes for (A) the Susceptible-Infected-Susceptible (SIS) model, (B) the Susceptible-Infected-Recovered (SIR) model and (C) the Susceptible-Infected-Recovered-Susceptible (SIRS) model.

Compartmental models that are formulated in terms of deterministic ordinary differential equations (ODE) such as Eq. (1.2) rely on a few critical assumptions. First, they completely ignore stochasticity arising from transmission, recovery and demographic processes. Nonetheless, stochastic fluctuations are usually negligible in the limit of large population size (their typical magnitude is inversely proportional to population size). Thus, the deterministic ODE approach is expected to perform well for large populations. Second, they assume a homogeneously-mixed population where every individual has the same probability to meet everyone else. Within the homogeneous mixing framework, the rate of new infected cases is given by the mass-action law, as if individuals were interacting chemical molecules in a well-stirred vessel. As we will see in the next chapter, the homogeneous mixing hypothesis is a crude approximation of real contact patterns.

We can use compartmental models to describe multi-pathogen/strain systems as well. This usually requires additional compartments. Let us consider the case of N_S mutually-excluding strains, each following SIS dynamics. Here, the number of compartments scales linearly with N_S since we have just one infected compartment per strain (plus a compartment for susceptible individuals). In principle, this model may be characterized by $2N_S$ parameters, namely the N_S infection rates β_i and the N_S recovery rates μ_i. Such model may be used as a basis for more complex models. In Fig. 1.2 we show a variant of the previous model, based on SIR dynamics instead of SIS, where infected compartments are coupled to each other. Transitions of the kind $I_i \to I_j$ can model a whole range of processes, including mutations and superinfection (new infections can clear previous ones). In the original formulation of this model [112], transitions form a nested pattern where I_i can mutate into I_j only if $j > i$. Here, increasing strain number i may be associated, for example, to increasing levels of drug resistance.

If recovery grants some degree of cross-immunity, one should in principle track each host's immune status as well as the set of past exposures [113]. Although exact, this approach is not amenable to analytical techniques as it requires monitoring the state of each individual. An alternative is to adopt either a status-based or a history-based approach [114, 115, 116]. In the former case, one defines compartments which track the set of strains a host is immune to, whereas in the second case one subdivides individuals

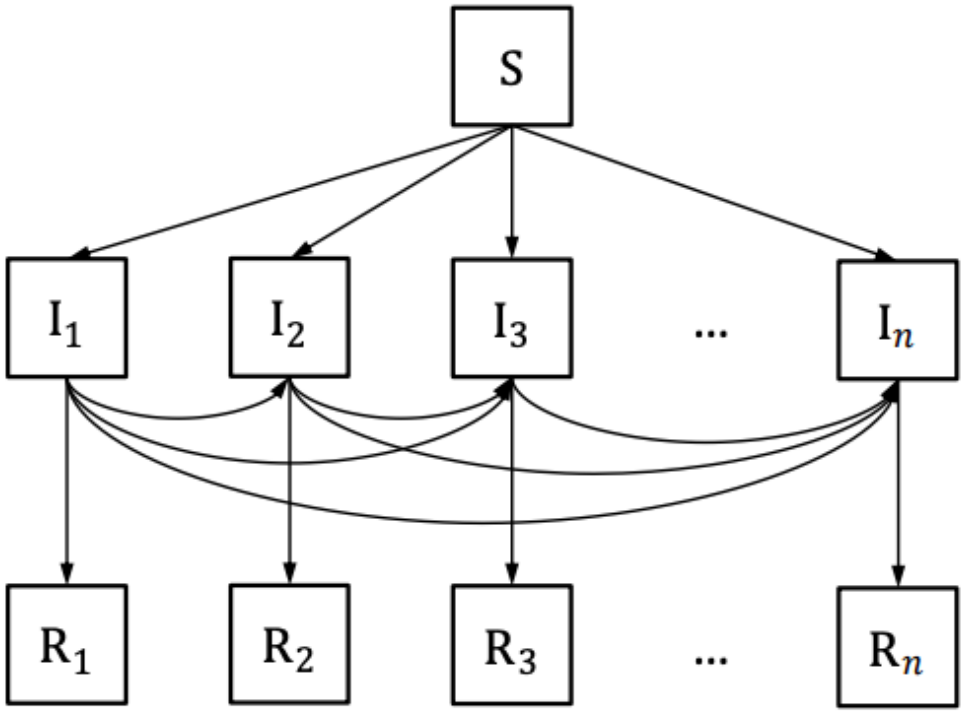

FIGURE 1.2: **Multi-strain compartmental model with couplings between infected.** This model features n strains following each SIR dynamics. The model also allows for mutations between infected compartments. The figure is taken from [112].

according to their set of past infections. While history-based models usually require a large number of variables when N_S is large – typically 2^{N_S} –, certain status-based need much less variables in order to be fully specified. For example, authors in [117] were able to derive a status-based model that requires just $2N_S$ state variables. This model is based on the assumptions that only a fraction of individuals successfully mount an immune response upon infection and that immunity results in reduced transmissibility.

1.4.2 Ecological insights from multi-strain models

Models of multiple, interacting strains or pathogens are key to address a wealth of ecological and epidemiological questions. Under which conditions do two or more interacting species co-exist within a population? How common is a species relative to others? The problem of co-existence is a central one in disease ecology and a highly non-trivial one. Indeed, simple models of competing strains usually fail to predict co-existence [118, 13]. Rather, they predict competitive exclusion, i.e. total domination by the fittest pathogen species or by the one with the largest R_0. However, observed co-circulation patterns of, e.g., drug-sensible and drug-resistant strains in *S. pneumoniae* [119, 120, 121, 122] and *S. aureus* [123, 124] populations, suggest the existence of mechanisms promoting population-level co-existence. Mathematical models have shed light on a few possible such mechanisms. Some mechanisms favor the partitioning of strains into non-overlapping niches, thus minimizing competition. These include, for example, reduced mixing between host sub-groups [22, 23, 24, 25] and heterogeneity in duration of carriage [26]. In some cases, cross-immunity can also promote co-existence by neutralizing fitness differences, curtailing the competitive advantage of certain strains. For example, non-specific cross-immunity, built through multiple, consecutive carriage events, and interference by *Haemophilus influenzae* have been suggested to promote diversity in *S. pneumoniae* serotypes by reducing differences in carriage duration [27, 28].

Multi-strain models shed light on the emergence of invading pathogens. Indeed, new pathogens may appear in a population as a result of external importations, spillover from an animal reservoir or mutations. In all these cases, emergence may be affected not only by environmental and host-related factors, but also by interference with resident pathogens. Multi-strain mathematical models have been used to understand for instance the emergence of antibiotic resistance, providing insights about factors leading to co-existence of sensitive and resistant strains as well as their frequencies under different treatment regimes [23]. Models also allowed studying the probability of reassortant influenza strains developing into a global pandemic, the frequency of replacement of circulating seasonal strains and the timing of pandemic emergence [125, 115, 126, 99].

Insights from multi-strain models can also help the design of public health interventions. Multi-strain models can be employed for example to investigate the long-term impact of vaccination on a pathogen population. In particular, mathematical models can be used to predict post-vaccination size and composition of a pathogen population in order to assess the risk of strain replacement [127, 128, 19].

1.5 Open challenges in modelling multi-strain dynamics

The diversity of multi-strain interactions opens up for several theoretical challenges. One problem of paramount importance concerns the link between within-host dynamics and population-level models. In fact, while within-host processes drive the outcome of strains' interactions, accounting for the full complexity entailing such processes typically requires high-dimensional models that hardly scale to more than a few pathogenic variants. Thus, in order to allow for tractable models, researchers make simplifying assumptions about disease interactions. The challenge is then to define models that represent a compromise between tractability and realism [129].

For example, models dealing with strains that confer only partial cross-immunity should specify how past infections affect the outcome of future exposure and/or transmission events and how immunity is built over time [114, 117, 115, 116]. As already discussed, a full description of such a system would amount to monitoring both the immune status and history of each host [113]. Here, model reduction is possible only under specific assumptions about strain interactions.

Not all interaction mechanisms have drawn equal attention in the literature. In fact, because interactions among strains are typically based on assumptions, most works have focused so far on just a few outcomes of multiple infections, notably co-infection and super-infection. Authors in [130, 131] have shown however that, even in the case of just two co-circulating pathogens, within-host dynamics can give rise to a large number of outcomes after simultaneous or sequential inoculations with different pathogens. The population-level impact of such infection patterns remains largely unexplored and thus calls for further research work.

Authors in [129] have also pointed out the importance of incorporating heterogeneities in host population structure within multi-strain models. In this thesis we elaborate on this aspect and make extensive use of individual-based and spatially-structured models in order to assess the impact of the heterogeneous host behaviour on the ecology of interacting strains.

Chapter 2

Epidemics on Networks

2.1 Introduction

Compartmental models are pervasive in mathematical epidemiology [21, 20]. As seen in Chapter 1, this mathematical framework allows fundamental understandings about factors driving epidemic spread and enables the investigation of outbreaks and the modeling of incidence data for a wide range of diseases [132, 133, 134, 135, 136, 137, 138, 139, 140, 141, 142, 143, 144, 145]. However, compartmental models make several simplifying assumptions, e.g. homogeneous mixing (Fig. 2.1 A), which may represent a limitation in some cases.

Network epidemiology provides the right framework to account for the complexity entailed by contact structure and epidemic dynamics. Within this framework, hosts are represented as nodes in a network while their mutual connections are represented by edges (Fig. 2.1 B). During recent years we have witnessed significant advances in network epidemiology, supported by an increasing amount of data and theoretical advances [29]. Advanced technology has improved our ability to track individual activity, yielding a high throughput of data about different kinds of social interactions, e.g. face-to-face proximity [32, 33, 34, 35, 36, 37, 38, 39, 40, 41, 42] and sexual encounters [43, 44, 45], and human movements [46, 47, 48, 49, 50, 51, 52, 53, 54, 55]. Theoretical development has allowed dealing with several types of heterogeneities emerging from these data, as well as novel frameworks to model complex network architectures, e.g. multi-layer networks [146, 147, 148, 149, 150, 151]. More recently, the availability of time-stamped contact data sparked substantial interest in temporal networks, where nodes and edges vary in time (Fig. 2.1 C) [152, 153, 32, 33, 34, 35, 36, 37, 38, 39, 40, 41, 42, 154, 155, 156, 157, 158].

At the same time, the theory of epidemic processes on networks has progressed as well [29]. Several mathematical frameworks have been proposed [159, 160, 161, 162, 163, 164], allowing for a comprehensive understanding of the role of network structure and dynamics on epidemic spread. Some of the most important analytical results concern the epidemic threshold [165, 166, 160, 167], prevalence [161, 168, 169, 170, 171, 172, 173] and immunization protocols [174, 175, 176, 177, 178, 179]. Several works have addressed the dynamics of interacting pathogens on networked populations. Particular attention has been devoted to a small set of interactions, namely cross-immunity [57, 58, 59], mutual exclusion [60, 63, 64] and increased susceptibility [65, 66, 67, 68], and different network

substrates have been considered, including multi-layer [69, 70] and metapopulation networks [61, 62]. Research work in this direction is however at the beginning. Indeed, the majority of works deal with just two pathogens that either compete or cooperate.

This chapter is organized as follows: in Section 2.2 we give an overview of main sources of networked data that are relevant for epidemic spread. In Section 2.3 we introduce basic network concepts and tools. In Section 2.4 we turn our attention to the mathematical description of epidemic dynamics on networks. Finally, in Section 2.5 we review the literature about multi-strain/pathogen dynamics on networks, describing the outcome of competitive and cooperative interactions.

2.2 Network data in epidemiology

Early studies of human contacts originated in the context of social science in order to better understand human behavior and social relationships [180]. Contact data from different studies may display different levels of detail. For example, a few studies yield only summary statistics about respondents, e.g. their number of individual contacts [181]. In other studies, respondents are asked to report also about characteristics of their acquaintances. Age information, for instance, is often reported [182, 183, 184], and may be used to inform mixing rates in age-structured models [185]. Finally, studies carried at the individual level sometimes report on the identity of respondents' acquaintances, potentially enabling the reconstruction of the underlying contact network [44, 186, 30].

Early attempts to measure individual contacts were based on contact-tracing [187, 188, 189, 190, 191, 192, 182, 44, 193]. The latter aims to identify potential transmission routes by asking subject individuals to report on their past relationships. Contact-tracing is also a standard control tool used, for example, to identify asymptomatic infected individuals in the case of sexually transmitted diseases [194, 195, 196, 192]. Another traditional approach relies on contact diaries [186, 183, 184, 197]: respondents receive a personal diary in order to progressively record their contacts.

Recently, advances in communication technologies allowed measuring contacts with unprecedented temporal and spatial resolution. For example, a recent experimental setup makes use of dedicated sociometric sensors based on Radio Frequency Identification (RFID) technology [31]. RFID devices act as beacons which periodically broadcast a signal that is eventually "listened" by neighboring RFIDs. Whenever two RFID sensors successfully reach each other, a Close Proximity Interaction (CPI) is automatically registered. Experimenters can manually tune the strength of the signal, thus selecting only social interactions occurring within a given radius from the sensor. RFID devices have been used in different settings, such as schools [32, 33], conferences [34], museums [35], workplaces [36], households [37, 38] and hospitals [39, 40, 41, 42]. Other technologies include Bluetooth and/or WiFi signals in mobile phones [154, 155, 156, 157, 158].

The importance of contacts is becoming increasingly recognized in hospital settings, as evidenced by the increasing amount of studies accounting for contact networks [198]. These works have focused on the properties of network structure, the epidemiological

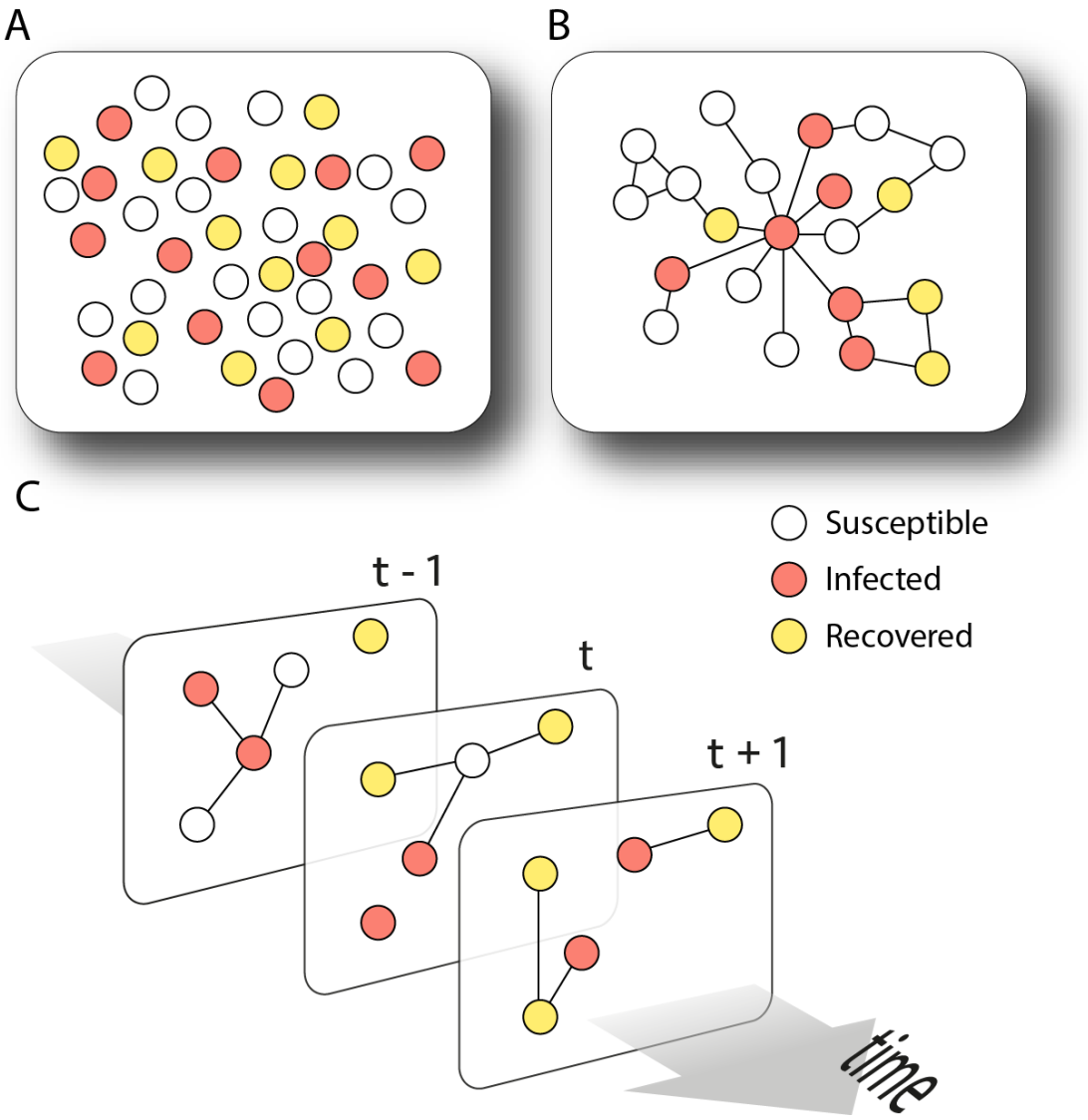

FIGURE 2.1: **Homogeneously mixed vs networked populations.** (A) Homogeneously mixed population. Here every individual has the same probability to meet everyone else. White, red and yellow circles represent different kinds of individuals, e.g. susceptible, infected and recovered individuals in a SIR model. (B) Static contact network. Here every individual is in direct contact with a sub-set of individuals of the whole network. (C) Temporal contact network. Contacts can change from one snapshot to the next one.

relevance of measured contacts and on the impact of contact structure on epidemic spread and prevention and control strategies [199, 200, 201, 202, 203, 204, 205, 206, 207, 208, 41, 42, 209, 210]. On a different scale, increasing attention is devoted to networks of hospitals linked by patient transfer [211, 212, 213, 214, 215].

Further network data is becoming available about human mobility at multiple scales. Air traffic data, for instance, encodes information about long-range movements and is of direct importance for understanding the rapid spread of pandemic diseases [216, 217]. At a shorter scale, census data provides information about commuting trips between neighboring locations. Regional patterns of seasonal influenza [218] and measles [219] have been studied in relation to commuting patterns. More recently, massive data about mobile phone calls provided unique opportunities in the study of human mobility [54, 55]. Indeed, call data records enabled remarkable insights not only about properties of human behavior [53, 52], but also about the impact of human mobility on the spread of several diseases, including malaria [220, 221], cholera [222, 223] and HIV [224].

2.3 Network analysis

2.3.1 Basic definitions

We can represent a network as a set of nodes joined by edges. We will denote an edge between nodes i and j with (i, j). If edges have a direction associated to them, the graph is said to be directed and we must distinguish between the edges (i, j) and (j, i). In principle, a graph can contain multiple edges between two nodes (multi-edges) and self-loops, i.e. edges connecting a node to itself. Because this work is mostly concerned with contact networks, we will not consider self-loops and multi-edges.

We say that an undirected network is connected if there exists a path (i.e. a set of subsequent edges) joining any pair of nodes. Else, the network is made up by multiple components. Empirical networks are usually characterized by a large component, also known as the giant connected component, that includes most of the nodes, plus a number of smaller components.

Edges in a graph may be additionally characterized by a weight $w_{i,j}$. In this case, the graph is said to be weighted. The weight $w_{i,j}$ may represent, e.g., the cumulative duration of a contact, or the number of passengers traveling from one location to the other.

There are multiple ways to represent a static graph. A possible choice is the adjacency matrix A, whose elements take values $A_{i,j} = 1$ if nodes i, j are connected and $A_{i,j} = 0$ otherwise. Notice that the adjacency matrix of an undirected graph is always symmetric. The adjacency matrix is of considerable theoretical interest since many network quantities can be directly written in terms of A. For example, the diagonal elements of the l-th power of the adjacency matrix, namely $(A^l)_{i,i}$, count the number of closed trajectories of length l starting and ending in the same node. Also, the spectral properties of A determine key features of dynamical processes over networks, including epidemic spread.

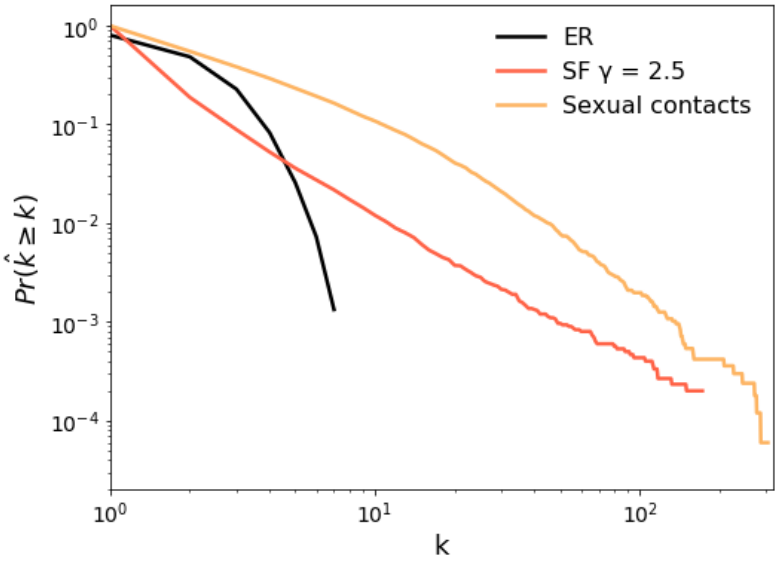

FIGURE 2.2: **Degree distributions in synthetic and empirical contact networks.** Here we show the complementary cumulative degree distribution for a scale-free network with $\gamma = 2.5$ (red), for a homogeneous network with a Poisson degree distribution and with the same average degree (black) and for an empirical network of sexual contacts among sex workers and their clients (orange) [45]. The maximum degree in the scale-free network has been clipped to $\sqrt{N}$.

2.3.2 Topological properties

The number of neighbors of a node is termed degree. An important quantity in a graph is the degree distribution $P(k)$, i.e. the frequency of nodes with degree k. In many empirical networks $P(k)$ is broad (spanning several orders of magnitude, as shown in Fig. 2.2 for a network of sexual contacts (orange)) and has a large variance. These networks are often modeled with a power-law degree distribution $P(k) \propto k^{-\gamma}$. In Fig. 2.2 we compare two different networks with a Poisson (black) and a power-law (red) degree distribution respectively. The former is characterized by a small range of values, indicating that most nodes have a degree concentrated around the average, whereas the second distribution extends to way larger values. Networks whose degree distribution follows a power-law with exponent γ in the range $2 < \gamma < 3$ have been dubbed "scale-free" networks [225]. In this case, the second moment $\bar{k^2}$ becomes divergent. Strictly speaking, this is true only in the limit of infinite network size; in real networks $\bar{k^2}$ is necessarily finite because the maximum degree is bounded by network size. An important feature of scale-free networks is the presence of large hubs, i.e. highly connected nodes.

An important quantity for epidemic spread is the conditional probability to reach a node with degree k by following an edge emanating from a node with degree k'. In absence of degree correlations, the conditional probability is equal to $\tilde{P}(k) = kP(k)/\bar{k}$. Notice that $\tilde{P}(k)$ is shifted towards nodes with a larger degree since it is more likely for a randomly selected edge to lead to a hub than to a peripheral node. As a consequence, its first moment $\sum_k k\tilde{P}(k) = \bar{k^2}/\bar{k}$ is larger than $\bar{k}$. This observation lies at the heart of the

friendship paradox, which states that your acquaintances are on average more connected than you are.

Networks may display additional mesoscopic properties that may affect dynamical processes unfolding on them. It is common in empirical networks to observe communities, i.e. groups of nodes that are highly connected internally while sharing only a few links between each other [29]. Such a modular organization can arise for multiple reasons. In hospitals, for example, community structure may be induced by the organization into wards [41]: two patients assigned to the same ward may be more likely to engage in contact compared to patients belonging to different wards. In this case, inter-community links are likely to be mediated by health-care workers [210], specially peripathetic ones [226]. Community structure has been shown to hinder spread in simple epidemic models. It has been shown for example to reduce the epidemic threshold [227], to slow down spread [228] and to reduce final outbreak size in SIR dynamics [229, 230]

2.3.3 Temporal networks

Some networks are not static but rather evolve in time. Contact networks represent a typical example since the very nature of human contacts is transitory. It is important to distinguish between contacts and edges. The former indicate an interaction between two individuals occurring at some point in time, whereas an edge indicates whether two individuals have ever interacted. There exist several ways to represent both continuous- and discrete-time temporal networks [153, 231]. For example, a discrete-time temporal network can be represented by a sequence of static graphs $\{G_1, \ldots, G_T\}$. Each graph G_t can be seen as a snapshot of a time-varying network at time step t, as depicted in Fig. 2.1 C.

The temporal dimension brings in substantial theoretical challenges. For example, most metrics that are standard in the analysis of static networks cannot be generalized to temporal networks in a straightforward manner [232]. In addition, some properties of temporal networks do not have a counterpart in static networks. For example, the very nature of temporal networks reflects a causal structure that is nowhere present in static networks. Let us elucidate the implications of causality on disease spread by considering a small temporal network with just three nodes, labeled by v_1, v_2, v_3 and depicted in Fig. 2.3 A. Here, node v_1 can infect v_3 in two steps: first v_1 infects v_2 at time t, and in turn v_2 infects v_3 at time $t+1$. Infection can travel from v_1 to v_3 because there exists a time-respecting path joining them. Notice that v_3 cannot infect v_1 because there is no time-respecting path starting in v_3 and ending up in v_1. If we were to collapse the two snapshots in Fig. 2.3 A onto a static aggregated graph (see Fig. 2.3 B), causality would be lost and the disease would instead be able to propagate from v_3 to v_1.

Temporal networks can also exhibit additional sources of heterogeneity compared to static graphs. For example, empirical studies revealed that both nodal and edge contact activities are bursty [233], i.e. they display bursts of contacts followed by long periods of inactivity. This is evident from the distribution of inter-contact times (ICT), i.e. the

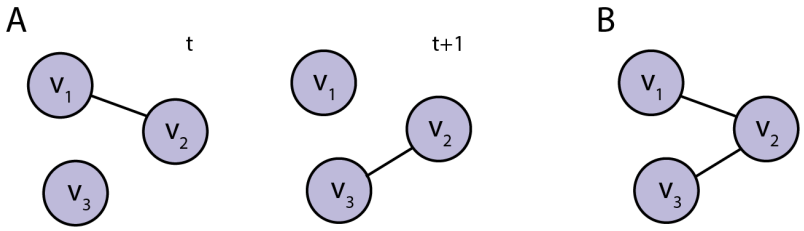

FIGURE 2.3: **Time respecting paths and causality in temporal networks.** (A) shows two consecutive snapshots of a temporal network with just three nodes. (B) shows the corresponding aggregated graph.

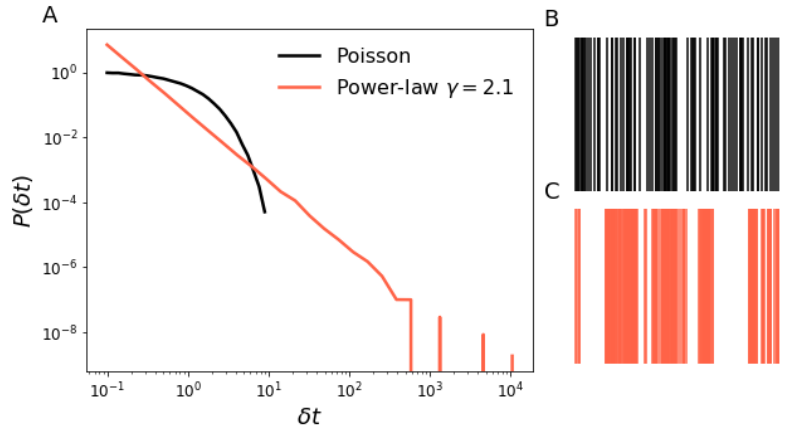

FIGURE 2.4: **Homogeneous vs heterogeneous ICT distributions.** In (A) we compare two inter-contact time distributions, an exponential one (black) and a power-law one with exponent 2.1 (red). The two distributions share the same average value. Two contact sequences sampled from each inter-contact time distribution are shown in panels (B) and (C) respectively.

time elapsed between two successive contacts, which is usually heavy-tailed rather than exponential, as exemplified in Fig. 2.4.

The mathematical treatment of epidemics on networks often relies on some time scale separation argument, i.e. it is often assumed that the network and disease dynamics evolve on different time scales. For some temporal networks, however, time scale separation may not hold as contacts might evolve on a time scale comparable to that of the pathogen [152, 234, 235, 236]. Recently, authors in [167, 237] have developed a general mathematical framework for the computation of the epidemic threshold in arbitrary time-varying networks.

2.3.4 Null models

Often, we are interested in assessing the impact of a single network property, e.g. degree heterogeneities or community structure, on a given dynamical process. A popular approach to isolate the role of specific network properties is based on random reference models (RRM) [153, 238]. In their essence, RRMs consist in randomization schemes that aim at destroying one or more properties of a given network. If a given dynamical process is driven by any of these properties, it is likely that it will differ substantially in the

original network and in the corresponding RRM. This can be checked directly by comparing the realizations of the dynamical process of interest on both the original network and its randomized version.

In weighted static networks, for example, the role of network topology can be highlighted by setting all weights to the average weight value while retaining existing edges. This approach has allowed the assessment of the impact of topology of air travels on the predictability of large-scale outbreaks [239].

RRMs have proven to be particularly useful also in the context of temporal networks. A convenient temporal RRM consists in completely randomizing all contacts by redistributing them over the existing edges. This procedure preserves the topology of the network but destroys any kind of temporal structure. Another scheme consists in permuting the order of network snapshots. This procedure not only preserves the topological and aggregated properties of the network but also the strength of each edge's and each node's activity, while destroying temporal correlations. RRMs that preserve the ICT history of single edges or the global ICT distribution have also been considered in the literature [240]. As pointed out in [241] however, most of these RRMs inevitably alter the turnover of edges and nodes, which in turn is a key property for spreading processes [242]. Thus, if a temporal network is characterized by a strong turnover of nodes, RRMs that preserve this property should be preferred [241, 243].

2.3.5 Generative models

The null-model approach can be identified as "top-down" since it consists in the progressive removal of selected structures from an original network. However, detailed network data may not be fully available in some cases, except perhaps for a few aggregated quantities (e.g. a list of individual degrees). There are also cases where we might want to investigate a specific network property in isolation and in a controlled manner. In both cases we may follow a "bottom-up" approach by specifying a generative model, i.e. a set of algorithmic rules able to produce synthetic graphs displaying a few desired properties.

The Erdős-Rényj (ER) model, or Poisson random graph, is a well-studied generative model for static networks. It is defined as follows: given a set of N nodes, each of the $\binom{N}{2}$ possible distinct edges is present with probability p, independently from each other. It follows that the degree distribution of an ER graph is binomial, i.e. $P(k) = \binom{N-1}{k} p^k (1-p)^{N-1-k}$ and the average degree is given by $\bar{k} = p(N-1)$. If network size is large, we can approximate the degree distribution with a Poisson distribution $P(k) = \bar{k}^k e^{-\bar{k}}/k!$. Despite its simple definition, ER graphs display several non-trivial properties often found in empirical networks: they can exhibit for instance a giant connected component and the so-called small-world property, which amounts to a logarithmic scaling of the average path length with N. The ER model is however not suited to describe most real-world networks because of the Poissonian degree distribution, which fails at capturing degree heterogeneities across nodes.

Degree heterogeneities can be introduced by means of another generative model: the configuration model. The recipe consists in first assigning to each node i a number of

half-edges (stubs) k_i sampled from the desired degree distribution $P(k)$. Given the degree list $\{k_i\}_{i=1,\dots,N}$, we form edges by joining the stubs at random. The configuration model yields by definition networks with custom degree distribution and with no degree-degree correlations. By choosing $P(k) \propto k^{-\gamma}$ it is thus possible to generate heterogeneous networks with power-law degree distribution.

Additional mesoscopic structures, such as communities, can be included by modifying the configuration model algorithm. First we assign a group membership b_i to each node, where $b_i = 1, \dots, B$ and B is the total number of groups. Then, once the stubs have been assigned, we design a random fraction p_{in} of stubs as within-group stubs. During the matching procedure within-group stubs will be matched with other within-group stubs from the same community. The remaining stubs will be directed to nodes in different communities.

For time-varying networks a paradigmatic generative model is the activity-driven (AD) model [234]. It describes a population of N agents, each characterized by a different activity rate a_i which measures its propensity to create contacts. Usually, the activity rate is sampled from some distribution $f(a)$. During each time step (of duration Δt), each agent activates with probability $a_i \Delta t$ and establishes m contacts directed at randomly chosen individuals. Contacts last for a single time step. Individual activity rates define additional time scales over which network connectivity varies. The AD model thus provides a way to investigate the role of network time scales on epidemic spread in a controlled manner.

The AD model accounts for contact heterogeneities across individuals while resulting in geometrically distributed inter-contact times for each single node. However, it has been observed in networks of contacts and phone-calls that individual activities are bursty [233]. A model that yields networks with such properties has been proposed in [244]. The recipe consists in directly sampling nodal activation times from a heavy-tailed distribution [244] instead of using a constant activation probability.

2.4 Epidemics on networks

2.4.1 Static networks

The impact of degree heterogeneities on epidemic spread can be better understood in the context of Heterogeneous Mean Field (HMF) theory [160]. HMF assumes that individuals with the same degree are equivalent. It is thus customary to subdivide individuals into different connectivity classes C_k indexed by their degree k. Let us define the fraction ρ_k of infected individuals within degree class C_k. For the SIS model, and in absence of any degree-degree correlation, the quantities ρ_k satisfy the following differential equations:

$$\dot{\rho}_k = -\mu \rho_k + \beta k (1 - \rho_k) \sum_l \frac{l \rho_l P(l)}{\bar{k}} , \tag{2.1}$$

where the first and the second term on the right represent infection and recovery respectively. Notice that the infection term is given by a sum of contributions from each degree

class, weighted by their degree and the frequency of nodes with that degree. Eq (2.1) admits a disease-free state (DFS) as well as an endemic state. The epidemic threshold can be determined by evaluating Eq. (2.1)'s Jacobian matrix in the DFS:

$$\mathcal{J}^{DFS}_{k,l} = \frac{\partial \dot{\rho}_k}{\partial \rho_l}|_{\{\rho_k=0\}} = -\mu\delta_{k,l} + \frac{\beta k l P(l)}{\bar{k}}\,, \tag{2.2}$$

and computing its largest eigenvalue, which reads $\beta\bar{k^2}/\bar{k} - \mu$. Successful spread occurs whenever this last quantity is positive, i.e. if:

$$\beta > \mu\bar{k}/\bar{k^2}\,. \tag{2.3}$$

As discussed earlier, $\bar{k^2}$ diverges in scale-free networks with degree-exponent γ in the range $2 < \gamma < 3$; in this situation, HMF predicts a vanishing epidemic threshold.

While large attention has been devoted to the epidemic threshold, a few works have focused on the endemic state [30]. Further insights about the role of degree heterogeneities can be obtained by investigating the endemic state. In this case, the stationary, non-zero value of ρ_k satisfies:

$$\rho_k = \frac{\beta k \Theta}{\mu + \beta k \Theta}\,, \tag{2.4}$$

where $\Theta = \sum_k k\rho_k P(k)/\bar{k}$. Θ can be found self-consistently by plugging Eq. (2.4) inside its own definition. Eq. (2.4) implies that large-degree nodes (hubs) are highly vulnerable to epidemic spread since ρ_k approaches 1 as k increases. This result suggests that hubs are responsible for the vanishing epidemic threshold owing to their vulnerability to epidemics. Furthermore, their large connectivity makes them acting as super-spreaders [245, 246, 247, 248]. The HMF framework is not limited to the SIS model and can be generalized to more complex models [249].

2.4.2 Temporal networks

HMF can be adapted to the AD model of time-varying networks in order to understand the impact of heterogeneities in activations on epidemic spread [234]. Paralleling the discussion about degree heterogeneities, we first subdivide hosts into activity classes. Once this division is made, we may write down a closed set of equations for $\rho(a)$:

$$\dot{\rho}_a = -\mu\rho_a + \beta m(1-\rho_a)[a\int da'\rho_{a'}P(a') + \int da'\rho_{a'}P(a')a']\,, \tag{2.5}$$

where we can again recognize the recovery and infection terms. The latter is given by two contributions: the first corresponds to susceptible nodes with activity a becoming active and contacting nodes that are already infected, whereas the second contribution comes from already infected nodes becoming active (at their corresponding rate a') and contacting susceptible nodes in class a. The epidemic threshold is obtained analogously as in the HMF framework, yielding the following condition for spreading:

$$\beta > \frac{\mu}{m} \frac{2\bar{a}}{\bar{a} + \sqrt{\bar{a^2}}}, \tag{2.6}$$

where $\bar{a}$, $\bar{a^2}$ are respectively the first and second moments of the activity distribution. As in the case of degree heterogeneities, variability in host activation patterns facilitates epidemic spread by lowering the epidemic threshold. If the activity distribution is heavy-tailed, i.e. it decays as $a^{-\gamma}$ with $2 < \gamma < 3$, the epidemic threshold vanishes. In the AD model, nodes with a large activity rate play the role of hubs.

Bursty contact behavior, induced by, e.g., a power-law ICT distribution, has been shown to impact the speed of spreading processes [250, 251, 244, 252]. Whether the effect is a speed-up or a slow-down is a complex question whose answer depends on the short-time behavior of the ICT distribution as well as on network topology [252].

2.5 Multi-strain dynamics on networks

2.5.1 Competitive interactions in SIS dynamics

Compared to the large effort on single-pathogen models, less attention has been devoted to the joint spread of multiple interacting pathogens/strains on networks [29]. Moreover, most works have focused on just two pathogenic agents that either compete or cooperate.

In the case of SIS dynamics, the focus is on understanding the impact of network structure on co-existence and dominance. Under the assumption of mutual exclusion, two pathogens that both follow SIS dynamics cannot stably co-exist on static networks if they differ in terms of R_0 [253]. Indeed, the theory predicts that the pathogen with the largest R_0 drives its competitor to extinction, in agreement with the principle of competitive exclusion. The case of competitors with the same R_0 is quite special, since HMF predicts a whole family of co-existence equilibria [60]. This mean-field prediction, however, is fundamentally altered by stochasticity, as highlighted by numerical simulations [64]. An analysis of the average co-existence time, i.e. the time until extinction of either competitor, reveals a linear scaling with population size [254]. Thus the average co-existence time is much shorter than the average extinction time for a single pathogen, which scales exponentially with population size. Also, whenever the extinction of either strain is forbidden, by e.g. preventing the last infected node of either type from recovering, a strong dominance behavior is observed, with the two strains taking turns as the leading competitor. The domination time distribution takes the same functional form, namely a power-law with an exponential cutoff, for different networks. The cutoff position and the average domination time depend on network topology; in particular, the star graph (a network consisting in $N-1$ peripheral nodes with a single connection to a central hub) features longer domination times compared to ER and scale-free graphs [64].

Other studies focus on the case of a newly injected strain in a population where a wild-type is already endemic [63, 255]. These works have shown that contact structure affects the emergence probability of the invader. For example, authors in [63] found that the invader may not invade even if it has the largest R_0. Moreover, they found

that contact heterogeneities reduce the emergence probability compared to homogeneous mixing. This result stems from a hub-holding effect: when the invader appears, most hubs are likely to be already infected by the wild-type, reducing the spreading potential of the mutant. This hub-holding effect is closely related to the friendship paradox since the “patient zero" carrying the initial mutant seed is likely to be be connected to one or more hubs. The same authors also reported the limited role of triangles, i.e. groups of three connected nodes, on the emergence probability. This may be explained by the fact that edges that are involved in triangles direct to nodes that are already infected by the wild-type and can thus be considered as “wasted" edges.

Co-existence of mutually-excluding pathogens is instead possible if the two diseases spread on different layers of a multi-layer network [256]. A multi-layer network can be seen as a sequence of distinct network topologies (the layers), sharing the same set of nodes. Each layer may represent for example a different transmission route, e.g. direct contact or transmission through a vector. A necessary condition for co-existence of mutually-excluding diseases spreading on two distinct layers is that the two layers must have different contact structures, i.e. different sets of edges (if this were not the case, the graph would behave as a single-layer network, and co-existence would not thus be possible). Provided that the two layers are different, co-existence is possible only within a range of transmissibility values. In practice, if the two pathogens have transmissibilities β_1, β_2 respectively, pathogen 2 spreads only if $\beta_{surv}(\beta_1) < \beta_2 < \beta_{dom}(\beta_1)$, where β_{surv}, β_{dom} are the survival and the domination thresholds. Below β_{surv}, pathogen 2 dies out, while above β_{dom} it outcompetes pathogen 1. Importantly, both the survival and domination thresholds are not simple constants but depend on pathogen 1’s transmissibility. Interestingly, the co-existence region becomes wider if the two layers are negatively correlated, as confirmed also by [70], in which the more general scenario of reduced susceptibility and reduced infectious period is discussed.

Heterogeneous contact behavior coupled with sequential monogamy has been shown to enable long-term co-existence of two mutually excluding pathogens with different basic reproductive numbers in a dynamical network of sexual contacts [56]. Moreover, the repartition of hosts into low-risk and high-risk groups favors dominance of pathogens with different traits in each group: a fast, highly transmissible pathogen dominates in the high-risk group where hosts have many potential partners and change partner often, whereas the slower pathogen dominates in the low-risk group, where sexual ties persist for a longer time.

2.5.2 Competitive interactions in SIR dynamics

In the case of SIR dynamics, the focus is on whether two diseases can cause similar-sized outbreaks or not. In particular, two main scenarios have been considered, corresponding to the two pathogens spreading either sequentially or concurrently. In the former case, authors in [57] showed that there exists an intermediate range of transmissibility values for the first pathogen such that both competitors can infect a significant fraction of the network. On one hand, if the first pathogen is not transmissible enough, it will not spread

in the first place. On the other hand, if the first pathogen has a too large transmissibility, it will reach and immunize most nodes, leaving behind a fragmented residual network of susceptibles. Thus, the second pathogen will not be able to propagate even if it has a large transmissibility. Network structure affects vulnerability to sequential invasions; it has been shown for example that networks with larger degree variance are more vulnerable to subsequent invasions [59].

Authors in [69] generalized these results to the case of partial cross-immunity, with the two pathogens spreading on different network layers. They found that increasing degree heterogeneities makes the whole network more resilient to further outbreaks if degrees are positively correlated across the two layers. Degree heterogeneities, however, can also make the system more vulnerable if correlations are negative or absent.

In the case of strains spreading concurrently, the situation is more subtle [58]. Nevertheless, whenever the two strains have different spreading rates, their respective dynamics will unfold on distinct time scales, as if they were invading sequentially. This means that arguments from the sequential case can still be used to recover the phase diagram. Interestingly, the two pathogens can both reach a finite fraction of the nodes if and only if the faster pathogen generates more cases per unit time than the slower one, while not being too transmissible (otherwise it would disrupt the residual network of susceptibles).

By modeling two pathogens competing on a metapopulation network it was found that different pathogens traits may be selected by host mobility: high mobility favors the faster pathogen, whereas low mobility favors the slower one [61, 62].

2.5.3 Cooperative interactions in SIS dynamics

The case of two mutually cooperative SIS processes has been studied thoroughly in the literature [65, 68, 257]. The phenomenology of cooperative contagion can be illustrated through the following paradigmatic model, as shown in Fig. 2.5: let us consider two pathogens, which we denote with A and B, that both follow SIS dynamics. A, B share for simplicity the same recovery rate μ and the same transmission rate β. In this model, co-infection with A, B is possible. Individuals that are already infected by either A or B are subject to increased risk of contagion by the other pathogen. More precisely, singly infected individuals are $C > 1$ times more susceptible to further infections compared to fully susceptible individuals. Cooperative interactions can affect the nature of the epidemic transition compared to the single disease case: if C is sufficiently large, the transition from the disease-free to the endemic state becomes discontinuous in terms of prevalence, as depicted in Fig. 2.6. Abrupt transitions underpin a possible threat to public health since a small increase in transmissibility can lead to large outbreaks. Moreover, stability analysis reveals a bistable region in parameter space where the disease-free and the active states are simultaneously stable. Within this region, the final outcome will be either extinction or co-circulation depending on the actual initial conditions. Bistability is also reflected in the hysteretic behavior of the system: if one introduces a small infectious seed, e.g. a single doubly-infected individual, and progressively increases transmissibility β, a large-scale outbreak will occur at some value β_c, i.e. at the epidemic threshold.

Instead, if the system is initially prepared in the endemic state (the upper line in Fig. 2.6) above the epidemic threshold, progressively reducing β will not result in an epidemic die-out at β_c. Rather, extinction will occur past another threshold $\beta_e < \beta_c$. β_e can be interpreted as the eradication threshold, which represents a distinct concept from that of the usual epidemic threshold β_c. Lowering β below β_c surely reduces prevalence, but it does not allow to get rid completely of the infection. The fact that β_e is smaller than β_c implies that once cooperative pathogens give rise to an outbreak, the effect of intervention strategies will be limited and more resources will be required to achieve full eradication.

2.5.4 Cooperative interactions in SIR dynamics

Cooperative contagion through increased susceptibility has been widely studied also in the context of SIR dynamics [66, 67, 258]. Even in this case, the transition from the disease-free state to the endemic state becomes discontinuous if C is sufficiently large. Simulations on various network topologies revealed however that the nature of the transition highly depends on the underlying contact structure [66, 67, 258]. Discontinuous transitions have been found for instance in 4d lattices, ER [67] and scale-free networks with degree exponent larger than 3 [258], but not on trees and scale-free networks with degree exponent smaller than 3. It has been conjectured that a key element to explain the discontinuous jump in prevalence is the relative abundance of long cycles compared to short ones [67]. This argument explains why the transition is continuous on trees, which do not possess any cycle, but it is discontinuous on ER networks, which indeed contain long cycles while being locally tree-like.

We conclude by mentioning a few works dealing with both competitive and cooperative interactions. Authors in [70] considered a model where two pathogens interact though multiple mechanisms, e.g. altered transmissibility, susceptibility and infectious period during co-infection. Different interaction mechanisms can be either competitive or cooperative according to parameter values. Many results that we reviewed in this section represent limiting cases of this general model.

Temporal properties of contact structure can affect the nature of the transition as well. Authors in [259] found a discontinuous transition in a temporal network of contacts in a hospital, but this was not the case for a related network null model. This result suggests that temporal correlations can drive abrupt transitions in cooperative contagion on temporal networks.

2.5.5 Multiple pathogens on networks

A few works have investigated the impact of network structure on the maintenance of diversity in large multi-strain assemblies [260, 261]. Authors in [261] considered for example a “bit-string" epidemic model [262] where each strain is associated to a different genotype out of 2^n possible configurations, where n is the number of different loci. Competition is mediated by cross-immunity, which is assumed to be strongest between similar strains. They found that networked contacts promote diversity with respect to random

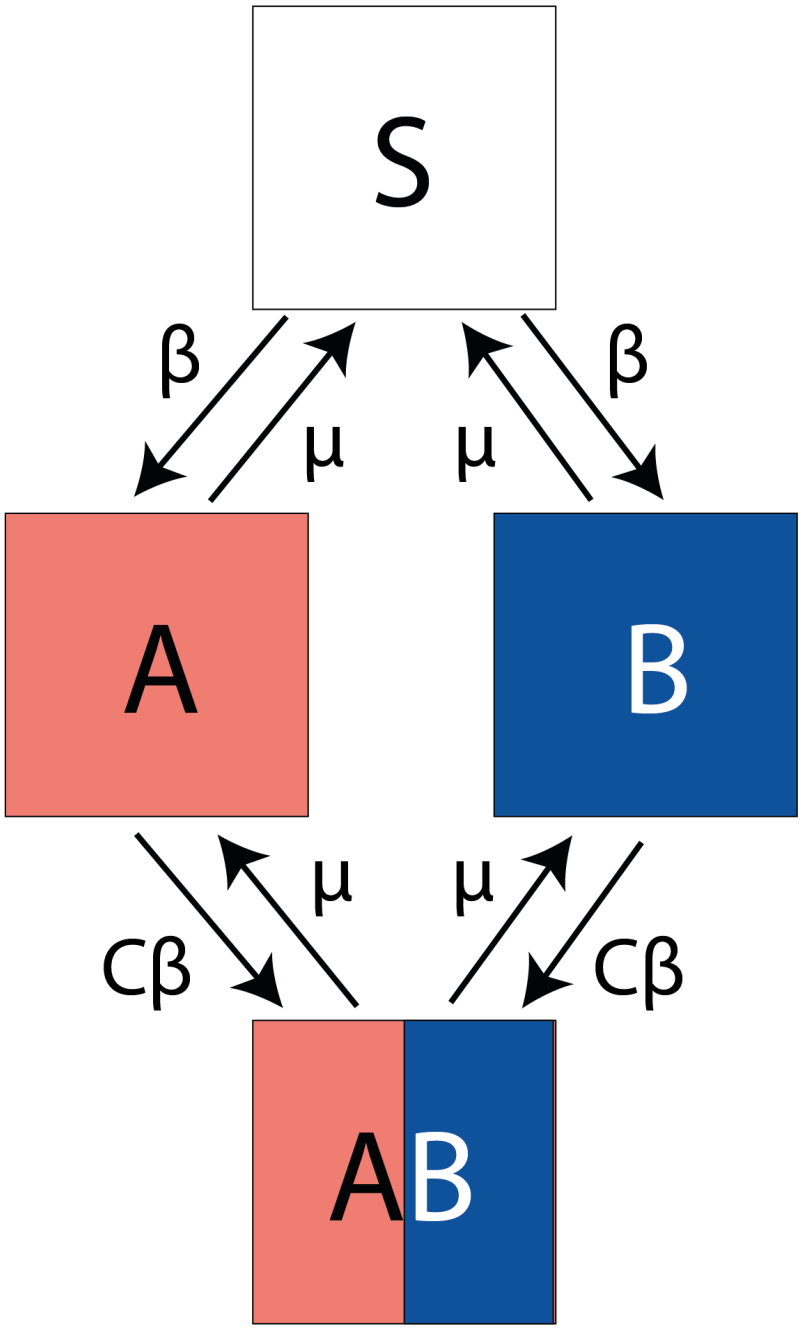

FIGURE 2.5: **Cooperative contagion compartmental model.** In this model, infected individuals can be in either one of 4 states, i.e. susceptible, infected by either strain A or B, or co-infected with A and B. Singly infected individuals are $C > 1$ times more susceptible to further infections compared to susceptible individuals. Both singly and doubly infected individuals transmit the disease(s) at rate β. Recovery from each disease occurs at rate μ.

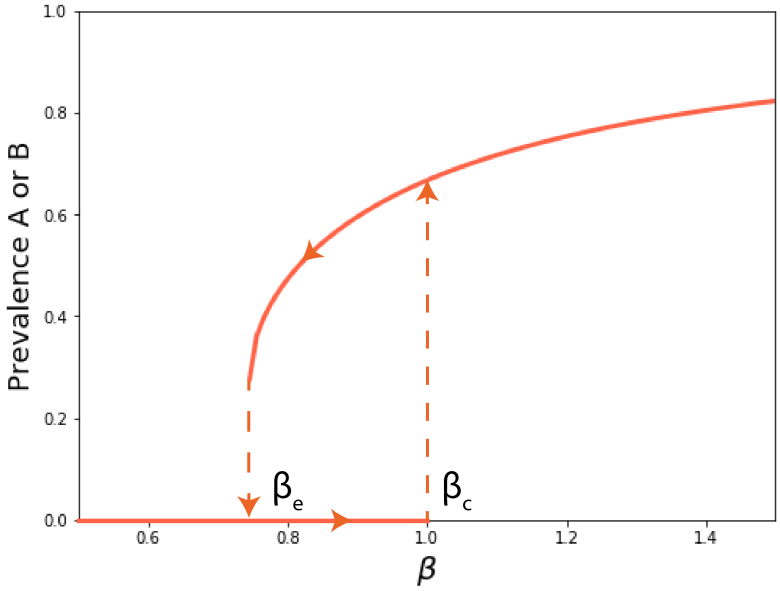

FIGURE 2.6: **Discontinuous transition and hysteresis in cooperative contagion** Solid lines represent stable branches, while dashed lines indicate discontinuous jumps. If the system is prepared in the disease-free state and β is increased past the epidemic threshold β_c, a discontinuous transition to an endemic state is observed. Instead, if the system is prepared in the endemic state (the positive branch) and β is progressively reduced, the disease will be eradicated only below the eradication threshold β_e. Here we set $\mu = 1$ and $C = 6$.

mixing [263]. This result stems from the localized nature of contacts, which enables local strain clusters to occupy different parts of the network. The role of mesoscopic structures, in particular community structure, has been investigated as well [260]. More precisely, it has been found that community structure plays a limited role on the maintenance of diversity, unless inter-community connections are assumed to be extremely sparse.

Other works have focused on the impact of network structure on pathogen phylogeny rather than on macro-ecological patterns [264, 265]. Authors in [265] simulated the spread of a strain population on several contact networks, and measured the resulting phylogenetic tree. Degree heterogeneities were found to alter the shape of phylogenetic trees when contact structure is static in time, in agreement with [264]; however, this effect is eroded when contacts are allowed to vary in time.

Multi-strain models have been used to study the evolution of pathogen traits such as virulence and infectious period. Evolutionary trade-offs between epidemiological traits have been studied in the context of spatially-structured populations [266, 267, 268, 269]. There, it was found that limited parasite dispersal can select for reduced virulence and transmission rate in order to reduce local competition for susceptible hosts [268]. While these results have been obtained for two-dimensional lattices, similar arguments hold also for contact networks [270]. Authors in [269] showed that the impact of spatial structure and dispersal depends also on the actual compartmental structure and additional epidemiological factors, e.g. the magnitude of disease-induced increased mortality. They found for example that spatial structure selects for lower virulence in SIRS dynamics,

making pathogens more “prudent". In SI dynamics with disease-induced mortality, however, virulence may evolve to larger values than those predicted by non-spatial theory.

Chapter 3

Host Contact Dynamics and Diversity in Pathogen Strains

3.1 Introduction

In Chapter 1 we learned that interactions between pathogens can affect their mutual spread. Indeed, competition for hosts due to, e.g., mutual exclusion or cross-immunity, represents an important ecological driver in populations of polymorphic bacteria such as *S. aureus*, *S. pneumoniae* and *N. meningitidis* [79, 27, 75, 76]. Thanks to advances in genomic techniques, our ability to reconstruct bacterial communities has substantially improved during recent years, revealing remarkable ecological diversity in pathogen strain populations.

A central ecological question concerns the processes that give rise to observed macroecological patterns. In the context of multi-strain systems, observed patterns of co-existence and dominance result from the complex interplay of an array of concurrent factors, ranging from heterogeneous strain characteristics to host-related factors [271].

In Chapter 2 we reviewed properties of host-to-host contacts and their impact on epidemic spread. However, despite the large number of works on single- and two-strain models, there has been little effort to investigate the role of contacts on the ecology of large strain assemblies. The latter problem is addressed in my first article, entitled *"Host contact dynamics shapes richness and dominance of pathogen strains"* [1]. In this work we investigated the impact of host contact heterogeneities, community structure and host length of stay on a population of epidemiologically equivalent strains. More in detail, we simulated multi-strain dynamics on synthetic time-varying networks, characterizing simulated ecosystems through ecological indicators. Our results indicate that contact heterogeneities reduce species richness and favor the appearance of dominant strains, while community structure has the opposite effect (although weak). We also show that host length of stay affects strain richness in a non-monotone manner as a consequence of the interplay between host turnover and strain competition. Then we consider *S. aureus* ecology as a case study, leveraging on a combined dataset of *S. aureus* carriage and face-to-face interactions in a French hospital obtained in the context of the I-Bird (individual-based investigation of resistance dissemination) experiment [41]. We show that our parsimonious model, together with contact data, can explain part of variability in *S. aureus*

diversity in a long-term care facility. Our results suggest that host contact structure can affect strain ecology and its accounting into epidemic models may be important for the interpretation of epidemiological and ecological properties of multi-strain systems.

This chapter is structured as follows: in Section 3.2 we introduce tools and concepts from community ecology that we shall use to describe the dynamics of multiple interacting strains. In Section 3.3 give an overview of *S. aureus* ecology, as it represents an important case study in this chapter, and introduce the I-Bird experiment. Section 3.4 contains my first paper associated to this thesis. Additional results complementing the main analysis are reported in Section 3.5. In particular, we further characterize strain ecology through additional ecological measures, namely the domination time and the attack rate. Moreover, we investigate the impact of contact burstiness on strain ecology. First, we extend the family of generative network models considered in Section 3.4 in order to accomodate for generic ICT distributions other than the geometric one. Then we show numerically that bursty activation patterns (induced by a power-law ICT distribution) affect diversity in a way that is similar to contact heterogeneities. In Section 3.6 we relax the assumption of neutrality and consider strains with varying transmissibility. We present a preliminary numerical and theoretical analysis that reveals that mild levels of variation in strains' fitness do not significantly alter the dynamics compared to the neutral case; however, if fitness heterogeneities become larger than a given threshold level, a super-fit strain becomes able to dominate the ecosystem.

3.2 Ecological modeling of multi-strain dynamics

Most multi-strain models in the epidemiological literature consider only two interacting strains. Two-strain models are often amenable to analytical calculations, allowing for an in-depth characterization of co-existence and its conditions. However, it may not be straightforward to apply these insights to larger multi-strain systems.

Several epidemiological works have adopted an ecological perspective, shedding light on ecological consequences of strain interactions. In Section 2.5.5 we reviewed works that explicitly accounted for network structure. Nonetheless, other studies investigated multi-strain dynamics in homogeneous populations. Authors in [272], for example, have studied several communities of *S. aureus*, *S. pneumoniae* and *N. meningitidis*, and found that a minimal transmission model with neutral mutations is able to explain genetic diversity across strains. Authors in [273] found instead that cross-immunity between antigenically similar strains favors the self-organization of a pathogen population into non-overlapping clusters, explaining observed antigenic patterns of *N. meningitidis*.

Tools and concepts from community ecology might shed light on drivers of diversity in multi-strain populations [274, 275]. According to community ecology, the composition of an ecological community is the result of multiple concurrent processes, namely ecological drift, selection, dispersal and speciation [276]. In the context of multi-strain populations, selection is understood as the outcome of strain interactions, fitness differences and ecological niches [275]. In a neutral scenario selection is absent and all strains

share the same reproductive abilities. In this case, community dynamics is driven by ecological drift, i.e. by random processes such as host-to-host transmission, recovery, and strain introductions.

Several ecological models are based on the island-mainland paradigm, where a local community (inhabiting the island) is coupled to a much larger community (occupying the mainland) through migration. The mainland is usually assumed to be unaffected by local island dynamics due to its larger size. In mathematical epidemiology the island might represent an open host population characterized by turnover of individuals. This mechanism provides a continual influx of both new hosts and new strains, replenishing the local strain ecosystem.

3.2.1 Ecological characterization of multi-strain populations

Ecological multi-strain models enable making predictions about the abundance of each strain. The set of abundances N_i is known in community ecology as the species abundance distribution [277, 278, 279]. Within a model with just two strains, one susceptible and one resistant to antibiotics, the frequency of antimicrobial resistance has direct ecological and public health implications. Indeed, works addressing the emergence of antibiotic resistance usually use this quantity as a metric to assess the impact of intervention strategies [26, 73, 25].

For large microbial communities, however, the interpretation of strain abundances is not as straightforward as in the case of just two strains. A possible way to characterize and compare different strain communities consists in using univariate measures that summarize ecological properties of a community [280]. Richness, i.e. the number of co-circulating strains, represents such an example. It must be noted, however, that a single indicator is not sufficient to describe all the facets of ecological diversity. For example, because richness is not sensitive to the magnitude of individual species' abundances, it cannot discriminate between different scenarios that share the same number of strains but with different proportions. In other words, richness cannot quantify evenness. A standard ecological indicator able to quantify evenness is the Shannon Evenness H, which is defined as:

$$H = -\frac{1}{log(N_s)} \sum_i \frac{N_i}{N} log\left(\frac{N_i}{N}\right) , \tag{3.1}$$

where $N = \sum_i N_i$ is the total prevalence and N_s is strain richness. H represents the Shannon entropy of the species abundance distribution, divided by its largest possible value, namely $log(N_s)$. The latter value corresponds to a configuration where all species are equally abundant; thus $H = 1$ in this case. Conversely, H is small when a few species dominate and others are scarcely abundant. Similar insights can be obtained by using the Berger-Parker index, which is defined as the fractional abundance of the most abundant strain, i.e. $BP = \max_i N_i/N$. By definition, the Berger-Parker index lies in the interval $[N_s^{-1}, 1]$. The lower limit is attained in the case of a perfectly even community, whereas the upper limit corresponds to full domination by a single strain.

3.3 Case study: *S. aureus* spread in hospitals

3.3.1 Overview of *S. aureus* ecology

S. aureus is a Gram-positive bacterium that colonizes hosts without necessarily harming them or causing any symptom. Asymptomatic carriage is common, with 30% of the human population actually sharing this condition, and, although apparently harmless, represents a major risk factor for *S. aureus* infection [281]. Spread of *S. aureus* occurs mainly through direct contact, although transmission due to environmental contamination is also possible [282].

S. aureus has raised remarkable concern due to its ability to become resistant to antibiotics. The global burden of antibiotic-resistant *S. aureus* infections has increased since the introduction of penicillin during the early 1940s [3]. As explained in [3], antibiotic resistance in *S. aureus* has emerged through multiple waves, triggered by the introduction of new antibiotics into clinical practice. Methicillin-resistant *S. aureus* (MRSA), which is considered one of the major causes of nosocomial infections [283, 284], has emerged in the 1960s, became endemic in hospitals by the late 1970s and spread to the community by the late 1990s [3].

Several studies probed *S. aureus* strain ecosystem in health-care facilities [285, 286, 41, 287]. The overall picture emerging from these studies is that of a highly diverse ecosystem composed by many rare species and a few dominant strains. The drivers of such diversity are not completely understood. A few studies suggest neutral competition between different *S. aureus* strains [288, 272], whereas others suggest instead different competitive abilities across strains [289, 290, 291] and the existence of multiple host niches [292].

Most models describing the spread of multiple *S. aureus* strains in hospitals consider only two strains. Usually, one of these strains is assumed to be resistant to antibiotic treatment (R), whereas the remaining one is assumed to be susceptible (S). In a few cases, a distinction between hospital- and community-associated resistant strains is also made [293, 294]. R and S strains are often assumed to compete through mutual exclusion, preventing colonized hosts to become either co-infected or super-infected. The protective effect of *S. aureus* carriage is supported by both in vitro and in vivo experiments [295, 296, 77].

A central question to most modeling studies is whether R and S can co-exist at the population level, e.g. in a hospital, and under which conditions. Simple models of competition usually fail at explaining co-existence and rather predict competitive exclusion. The latter outcome arises because a homogeneous population made up by a single host type cannot sustain two strains with different competitive abilities. In other words, simple models assume only one possible ecological niche which can be occupied by a single strain at most. Researchers have thus focused on mechanisms able to boost co-existence between competing bacteria [271]. Antibiotic treatment for example can promote co-existence by limiting the competitive advantage of S over R in treated individuals [297]. In a recent work it has been shown that stratification of the host population in several classes can also promote co-existence, provided that mixing between classes is low and

frequency of treatment varies across classes [23]. Several studies allow new strains to be injected into the host population as a result of, e.g., patients that are already colonized at admission [298, 299], or mutations [272]. In such cases, strain diversity becomes the result of the interplay between extinction and immigration.

The studies mentioned above provide general results regarding the emergence and maintenance of antibiotic resistance; nonetheless, not all of these works are based on mechanistic models specifically designed and calibrated for *S. aureus*. More tailored models should incorporate additional mechanistic ingredients, e.g. selective pressure due to antibiotics [293], compliance to hygiene measures [226] and heterogeneities in carriage types [300].

3.3.2 The I-Bird experiment

The I-Bird experiment was a cohort study that took place in a French long-term healthcare facility in 2009 [301, 41, 209, 210, 42]. The experiment lasted for 6 months, from May to October 2009. Every participant, be it a patient or a staff member, wore a RFID sensor. Signal strength was tuned so that only devices within a small distance (around 1.5 m) and placed directly in front of each other were able to register a contact. Discarding a two months long pilot phase, more than 1 million CPIs were collected, spanning a period of almost 4 months between the 01/07/2009 and the 26/10/2009.

Participants underwent weekly swabs in order to detect carriage of *S. aureus*, *Escherichia coli* and *Klebsiella pneumoniae*. In the case of patients, nasal and rectal swabs as well as swabs from wounds, tracheotomy and other invasive devices were collected. Positive swabs underwent further microbiological examinations. For the case of *S. aureus*, for example, spa-type and antibiotic resistance profile were determined.

Results from microbiological tests provide weekly snapshots of *S. aureus* ecosystem in the hospital. In Fig. 3.1 A we show each strain's abundance weekly time series, as measured from carriage data. We have stacked all time series together, so that the height of the bars indicates the total number of carriers. Each bar also shows how total *S. aureus* carriage decomposes in terms of different strains during a given week. Strain richness and Berger-Parker index are shown as well in Fig. 3.1 B, C respectively.

3.4 First article: Host contact dynamics shapes richness and dominance of pathogen strains

PLOS COMPUTATIONAL BIOLOGY

RESEARCH ARTICLE

Host contact dynamics shapes richness and dominance of pathogen strains

Francesco Pinotti[1], Éric Fleury[2], Didier Guillemot[3], Pierre-Yves Böelle[1], Chiara Poletto[1]*

1 INSERM, Sorbonne Université, Institut Pierre Louis d'Épidémiologie et de Santé Publique (IPLESP), 75012 Paris, France, **2** INRIA, Paris, France, **3** Inserm, UVSQ, Institut Pasteur, Université Paris-Saclay, Biostatistics, Biomathematics, Pharmacoepidemiology and Infectious Diseases (B2PHI), Paris, France

* chiara.poletto@inserm.fr

Citation: Pinotti F, Fleury É, Guillemot D, Böelle P-Y, Poletto C (2019) Host contact dynamics shapes richness and dominance of pathogen strains. PLoS Comput Biol 15(5): e1006530. https://doi.org/10.1371/journal.pcbi.1006530

Editor: James Lloyd-Smith, University of California, Los Angeles, UNITED STATES

Received: September 19, 2018

Accepted: April 29, 2019

Published: May 21, 2019

Data Availability Statement: The contact network and carriage data are available from the http://dx.doi.org/10.6084/m9.figshare.1290932 database.

Funding: FP received funding from "Pierre Louis" School of Public Health of UPMC (www.ed393.upmc.fr). The funders had no role in study design, data collection and analysis, decision to publish, or preparation of the manuscript.

Competing interests: The authors have declared that no competing interests exist.

Abstract

The interaction among multiple microbial strains affects the spread of infectious diseases and the efficacy of interventions. Genomic tools have made it increasingly easy to observe pathogenic strains diversity, but the best interpretation of such diversity has remained difficult because of relationships with host and environmental factors. Here, we focus on host-to-host contact behavior and study how it changes populations of pathogens in a minimal model of multi-strain interaction. We simulated a population of identical strains competing by mutual exclusion and spreading on a dynamical network of hosts according to a stochastic susceptible-infectious-susceptible model. We computed ecological indicators of diversity and dominance in strain populations for a collection of networks illustrating various properties found in real-world examples. Heterogeneities in the number of contacts among hosts were found to reduce diversity and increase dominance by making the repartition of strains among infected hosts more uneven, while strong community structure among hosts increased strain diversity. We found that the introduction of strains associated with hosts entering and leaving the system led to the highest pathogenic richness at intermediate turnover levels. These results were finally illustrated using the spread of *Staphylococcus aureus* in a long-term health-care facility where close proximity interactions and strain carriage were collected simultaneously. We found that network structural and temporal properties could account for a large part of the variability observed in strain diversity. These results show how stochasticity and network structure affect the population ecology of pathogens and warn against interpreting observations as unambiguous evidence of epidemiological differences between strains.

Author summary

Pathogens are structured in multiple strains that interact and co-circulate on the same host population. This ecological diversity affects, in many cases, the spread dynamics and the efficacy of vaccination and antibiotic treatment. Thus understanding its biological and host-behavioral drivers is crucial for outbreak assessment and for explaining trends of

new-strain emergence. We used stochastic modeling and network theory to quantify the role of host contact behavior on strain richness and dominance. We systematically compared multi-strain spread on different network models displaying properties observed in real-world contact patterns. We then analyzed the real-case example of *Staphylococcus aureus* spread in a hospital, leveraging on a combined dataset of carriage and close proximity interactions. We found that contact dynamics has a profound impact on a strain population. Contact heterogeneity, for instance, reduces strain diversity by reducing the number of circulating strains and leading few strains to dominate over the others. These results have important implications in disease ecology and in the epidemiological interpretation of biological data.

Introduction

Interactions between strains of the same pathogen play a central role in how they spread in host populations. [1–7]. In *Streptococcus pneumoniae* and *Staphylococcus aureus*, for instance, several dozen strains can be characterized for which differences in transmissibility, virulence and duration of colonization have been reported in some cases [8, 9]. Strain diversity may also affect the efficacy of prophylactic control measures such as vaccination or treatment. Indeed, strains may be associated with different antibiotic resistance profiles [3, 5, 10, 11], and developed vaccines may only target a subset of strains [2, 3, 12]. With the increasing availability of genotypic information, it has become easy to describe the ecology of population of pathogens and to monitor patterns of extinction and dominance of pathogen variants [13–17]. However, the reasons for multi-strain coexistence patterns (e.g. coexistence between resistant and sensitive strains) or dominance of certain strains (e.g. in response to the selection pressure induced by treatment and preventive measures) remain elusive. One may invoke selection due to different pathogen characteristics, but also environmental and host population characteristics, leading to differences in host behavior, settings and spatial structure may affect the ecology of strains [14–19]. In particular, human-to-human contacts play a central role in infectious disease transmission [20]. This is increasingly well described thanks to extensive high-resolution data—including mobility patterns [21–23], sexual encounters [24], close proximity interactions in schools [25, 26], workplaces [27], hospitals [16, 28–31], etc.—that enable basing epidemiological assessment on contact data with real-life complexity [32, 33]. For instance, the frequency of contacts can be highly heterogeneous leading more active individuals to be at once more vulnerable to infections and acting as super-spreaders after infection [24, 33–35]. Organizational structure of certain settings (school classes, hospital wards, etc.) and other spatial proximity constraints lead to the formation of communities that can delay epidemic spread [36, 37]. Individual turnover in the host population is also described as a key factor in controlling an epidemic [20, 38]. It is likely that, since they impact the spread of single pathogens, the same characteristics could affect the dynamics in multi-strain populations. It was shown, indeed, that network structure impacts transmission with two interacting strains [39–46], the evolution of epidemiological traits [47–49] and the effect of cross-immunity [50, 51]. Yet in these cases, complex biological mechanisms—such as mutation, variations in transmissibility and infectious period, cross immunity—were used to differentiate between pathogens, thereby making the role of network characteristics difficult to assess in its own right.

For this reason, we focused on the dynamical pattern of human contacts and examined whether it contributes to shaping the population ecology of interacting strains under minimal epidemiological assumptions regarding transmission. We described a neutral situation where

all strains have the same epidemiological traits and compete via mutual exclusion (concurrent infection with multiple strains is assumed to be impossible) in a Susceptible-Infected-Susceptible (SIS) framework. We studied the spread of pathogens in a host population during a limited time window, disregarding long-term evolution dynamics of pathogens. More precisely, new strains were introduced through host turnover rather than *de novo* mutation or recombination in pathogens. We quantified the effect of network properties on the ecological diversity in strain populations with richness and dominance indicators. We assessed in turn heterogeneities in contact frequency, community structure and host turnover by comparing simulation results obtained with network models exhibiting a specific feature. We then interpreted *S. aureus* carriage in patients of a long-term care facility in the light of these results.

Results

Multi-strain spread on dynamical networks

We simulated the stochastic spread of multiple strains on a dynamical contact network of individuals (nodes of the network). Individuals can be either susceptible or infected with a single strain at a given time, and, for each strain, β and μ indicate the transmission and the recovery rate respectively. We assumed turnover of individuals, who enter the system with rate λ_{in}, and associated injection of previously unseen strains, carried by incoming individuals with probability p_s. We considered synthetic network models, each displaying a specific structural feature, as well as a real network reconstructed from close-proximity-interaction data collected in a hospital facility. We calibrated all network models to the same average quantities—average population size $\bar{V}$, fraction of active nodes $\bar{a}$, average degree $\bar{k}$ and strength of the community repartition p_{IN}, when applicable—that were chosen to correspond with the hospital network used in the application. Epidemiological parameters were motivated by the duration of *S. aureus* carriage in patients. A larger range of values was explored in some cases to address their impact on the dynamics. We analyze the structure of strain population at the dynamic equilibrium by computing, for each network model, ecological diversity measures, including species richness and evenness/dominance indices [52, 53]. All details about network models, numerical simulations and ecological indicators are described in the Materials and methods section.

Effects of contact heterogeneity

In order to probe the effect of contact heterogeneity on strain ecology we compared a homogeneous model (HOM) in which all nodes have the same activity potential, i.e. they have equal rate of activation to establish contacts, with a heterogeneous model (HET), akin to the activity-driven model described in [34], where the activity potential is different across nodes and is drawn from a power-law distribution.

Fig 1 shows the results of numerical simulations comparing HOM and HET models. Sample epidemic trajectories are reported in Fig 1A. Here every strain is indicated with its own color to display its dynamics resulting from the interaction with the other strains. Fig 1B–1D shows summary statistics in varying strain transmissibility β. The prevalence presents a well-known behavior for both static and dynamic networks (Fig 1B): contact heterogeneities lower the transmissibility threshold above which total prevalence is significantly above zero, thus allowing the spread of pathogens with low transmissibility. At the same time, however, heterogeneities hamper the epidemic spread when β is large, reducing the equilibrium prevalence [35]. Fig 1C shows the average richness, i.e. the number of distinct strains co-circulating. For low values of β HET displays larger richness values compared to HOM. This trend reverses as

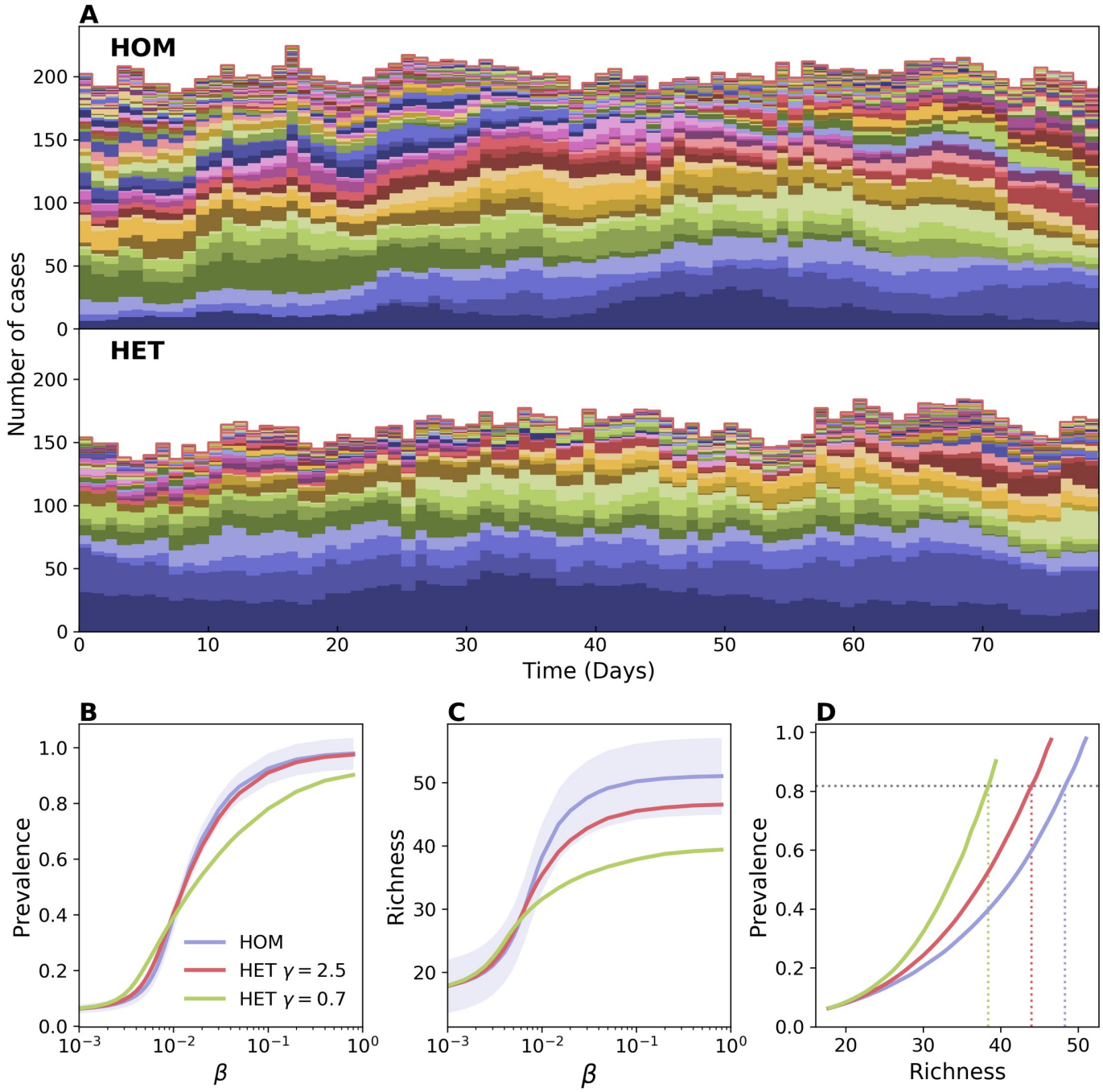

Fig 1. Effect of contact heterogeneity on strain richness. Comparison between a homogeneous (HOM) and a heterogeneous (HET) network. In HOM all nodes have the same activity rate $a_H = 0.285$ and the network average degree is $\bar{k} = 0.89$. In HET the activity rate of each node is drawn randomly from a power-law distribution with support $(\epsilon, 1]$ and the same average value as in HOM. Lower values of the power-law exponent γ correspond to a higher contact heterogeneity. The average degree is the same as in HOM. We chose a population of $\bar{V} = 306$ individuals, average length of stay $\tau = 10$ days, probability of strain injection per incoming individual $p_s = 0.079$, and recovery rate $\mu = 0.00192$ (see Materials and methods). (A) Sample time series of strain abundance for HOM and HET with $\gamma = 0.7$. Each time series is represented with a different color. All abundances are stacked together, so that plot's height represents prevalence. Here $\beta = 0.02$. (B) Average prevalence vs β, and (C) average richness vs β. Two levels of heterogeneity are here considered for HET. For the sake of visualization, the shaded area corresponding to the standard deviation is shown only for HOM. Median and confidence intervals are reported in S1 Fig of the supporting information. (D) Average prevalence vs richness. Dashed lines are shown as a guide to the eye, highlighting variation in richness induced by network topology.

https://doi.org/10.1371/journal.pcbi.1006530.g001

β increases, and the richness is lower in HET consistently with the lower level of prevalence. The relation between richness and prevalence, however, is not straightforward. For instance, the reduction in richness for high β values is important even for the case with limited contact heterogeneity, when prevalence is barely affected. The scaling between prevalence and richness is not linear as β varies (Fig 1D), and the relation between the two quantities varies appreciably among contact networks. In correspondence of a fixed value of prevalence, heterogeneous networks have lower richness—e.g. a prevalence value of ∼0.8 corresponds to ∼20% lower richness in HET with respect to HOM, as highlighted in Fig 1D.

This fact can be explained by the dynamical properties of epidemics on heterogeneous networks. Active nodes, involved in a larger number of contacts, get infected more frequently [35]. Also, a randomly chosen node is likely surrounded by active nodes [33]. As a consequence, injected strains often find their propagation blocked by active infected nodes. In this way, contact heterogeneities enhance the competition induced by mutual exclusion and hamper the wide-spread of emerging strains, similarly to what was found in [46]. This mechanism is further confirmed by looking at the persistence time of strains (S2 Fig in the supporting information). Above the epidemic threshold, it is on average shorter in heterogeneous networks than in homogeneous ones. The distributions are however more skewed in heterogeneous networks, indicating that more strains are going extinct rapidly, while a few others can survive for a long time in the population.

If on the one hand hubs accelerate the extinction of certain strains, on the other they act as super-spreaders, amplifying the propagation of other strains. We find that this impacts profoundly the distribution of strains' abundances, i.e. the strain-specific prevalence. Fig 2A shows that the latter is broader for the HET network, with the most abundant strain reaching a larger proportion of cases. This situation is synthesized by the Berger-Parker index, that quantifies the level of unevenness or dominance of a given ecological system [52, 53]. This is defined as the relative abundance of the most abundant strain (see Materials and methods section). Fig 2B shows that Berger-Parker index increases with β for all networks. This is expected since at low β strains' transmission chains are short and barely interact, while they interfere more at higher values of transmission potential. The Berger-Parker index is always higher in a

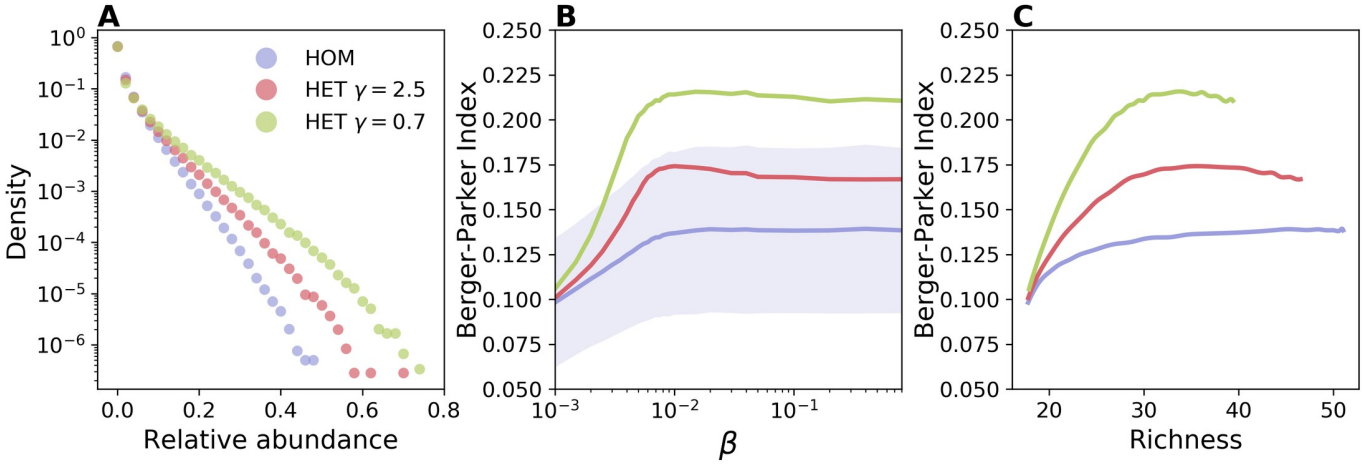

Fig 2. Effect of contact heterogeneity on strain dominance. (A) Distribution of strains' relative abundance, i.e. the frequency of strains infecting a given fraction of the total prevalence, for HOM (blue), HET with $\gamma = 2.5$ (red), and HET with $\gamma = 0.7$ (green). Here $\beta = 0.02$. (B) Berger-Parker index, i.e. the relative abundance of the most abundant strain, as a function of β. For the sake of visualization, the shaded area corresponding to the standard deviation is shown only for HOM. Median and confidence intervals are reported in S1 Fig of the supporting information. (C) Berger-Parker index vs richness. Parameters are the same as in Fig 1.

https://doi.org/10.1371/journal.pcbi.1006530.g002

heterogeneous network, even when the comparison is made at fixed values of richness (Fig 2C). An alternative indicator, the Shannon evenness, shows a similar behavior as displayed in S3 Fig.

The fraction of strains going extinct also depends on stochastic effects in a finite size population. We indeed found that increasing network size, when temporal and topological properties were the same, led to an increase in both persistence time and richness (S4 Fig). This shows that interference among transmission chains is reduced in larger populations. However, the relative abundance distribution remained similar, showing that it is primarily affected by the nodes' activity distribution (S5 Fig).

Eventually, we tested whether additional mechanisms of strain injection were leading to different results. In S6 Fig we assumed new strains to infect susceptible nodes already present in the system with rate q_s, mimicking in this way transmissions originating from an external source, as it can happen in real cases. The plot of S6 Fig shows the same qualitative behavior described here.

Effect of community structure

We considered a community model (COM) with n_C communities in which all nodes are as active as in HOM, but direct a fraction p_{IN} of their links within their community and the rest to nodes in the remaining $n_C - 1$ communities. The closer p_{IN} is to 1, the stronger the repartition in communities is.

Fig 3A and 3B shows that a network with communities displays a higher richness for large β; even when community structure barely affects prevalence (Fig 3B). However, the effect is important only when communities are fairly isolated ($p_{IN} = 0.99$) and the injection from the outside is not so frequent—otherwise the effect is masked by strain injection which occurs uniformly across communities. In particular, for the values of $p_{IN} = 0.78$ and $p_s = 0.079$, chosen to match the hospital application, the difference with the homogeneous case is very small. The limited role of community structure is also confirmed by the fact that once this feature is combined with heterogeneous activation—in a model with the activation scheme of HET and the stub-matching of COM—the latter property has the dominant effect and the richness decreases (S1 Fig).

The relation between richness and prevalence remains the same when adding the injection of new strains due to the transmission from an external source. This mechanism further increases the richness. When β is high and the fraction of infected nodes is close to one, however, such a mechanism is hindered by the fact that susceptible nodes, that can get infected from the external source, are rare (see S6 Fig). This is why richness starts to decrease for high values of β.

We tested the consequences of communities in strain dominance by plotting the Berger-Parker index in Fig 3C. For low β, the behavior of the Berger-Parker index follows the trend in richness. The initial decrease in this indicator is due to the increase in richness, that occurs at constant prevalence and is thus associated to a decrease in the average abundance [54]—green curve corresponding to $p_{IN} = 0.99$ and $p_s = 0.01$. At larger values of β, instead, increased competition levels induced higher dominance levels.

The increase in strain diversity is due to the reduced competition among strains introduced in different communities. When coupling among communities is low, indeed, strains may spend the majority of time within the community they were injected in, thus avoiding strains injected in other communities. Fig 3D confirms this hypothesis by showing the Inverse Participation Ratio (*IPR*) [55] that quantifies uniformity in the repartition of abundance across communities. Values close to zero indicate uniform repartition, while, conversely, values close to 1

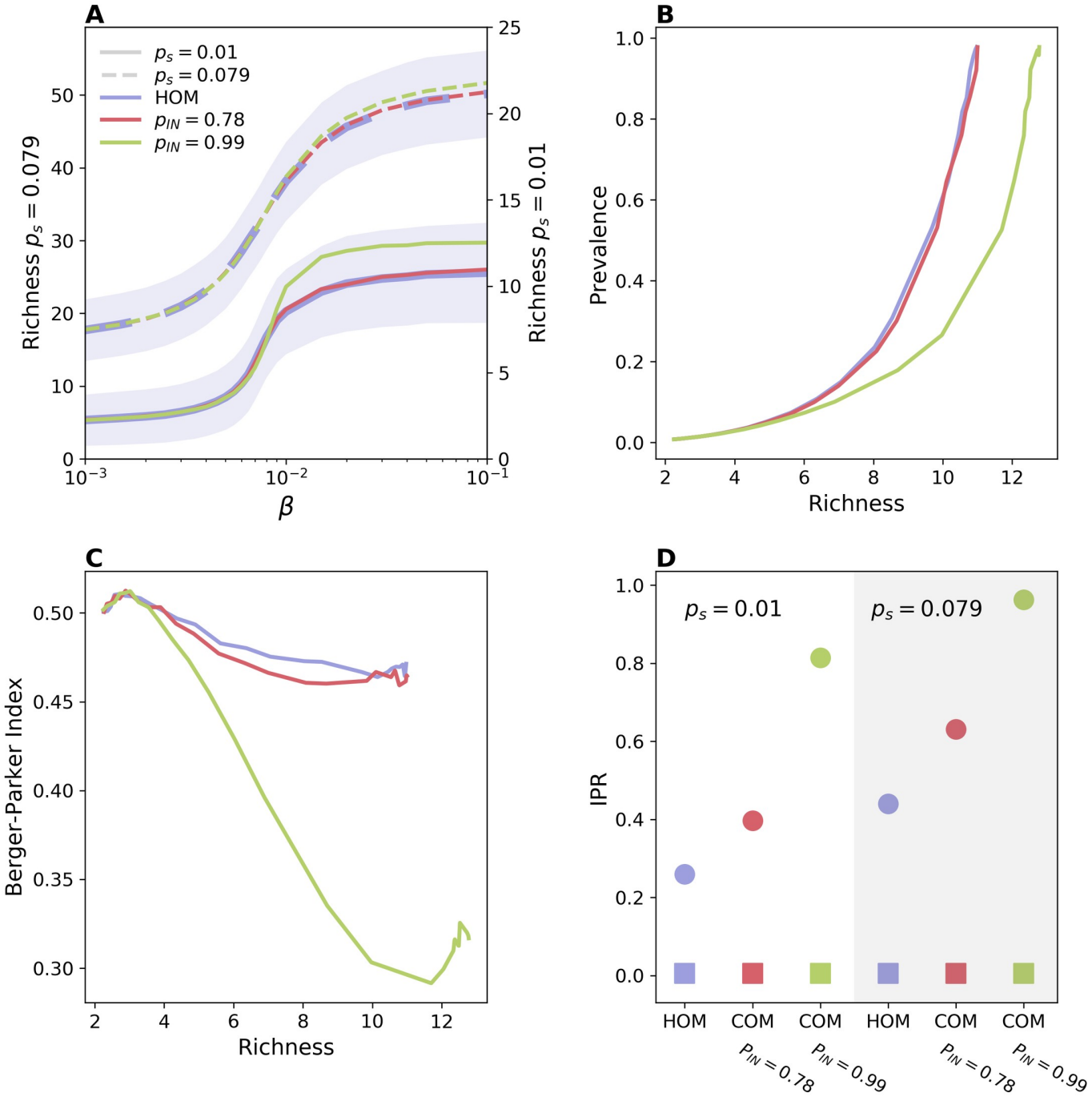

Fig 3. Impact of community structure. (A) Richness vs β for HOM (blue), COM with $p_{IN} = 0.78$ (red), and COM with $p_{IN} = 0.99$ (green). For both COM models we have set $n_C = 6$. Solid lines correspond to $p_s = 0.01$, while dashed lines correspond to $p_s = 0.079$. Solid lines refer to the right y-axis, while dashed ones to the left y-axis. For the sake of visualization, the shaded area corresponding to the standard deviation is shown only for HOM. Median and confidence intervals are reported in S1 Fig of the supporting information. (B) Prevalence vs richness and (C) Berger-Parker index vs richness, for $p_s = 0.01$. (D) Average *IPR* for both $p_s = 0.01$ (white background) and $p_s = 0.079$ (gray background). Here $\beta = 0.02$. Squares correspond to *IPR* obtained from total prevalence while circles correspond to *IPR* obtained from strains' abundances. A value of the *IPR* close to 1 indicates localization over one community. Here no injection due to transmission from an external source is assumed ($q_s = 0$). The effect of this second mechanism is shown in S6 Fig.

https://doi.org/10.1371/journal.pcbi.1006530.g003

indicate that, on average, a strain is confined within a single community for most of the time (more details are reported in the Materials and methods section). The strength of the community structure does not affect the repartition of the total prevalence (squares in the plot), however it alters the average *IPR* value computed from the abundance of single strains, thus strains become more localized as p_{IN} increases. Notice that a certain degree of localization is present also in the homogeneous network, due to those strains causing very few generations before going extinct.

As a sensitivity analysis we tested whether the main results obtained so far are the same in a more realistic situation where additional heterogeneous properties of nodes are accounted for. We consider the case in which infectious duration varies across individuals, as happens for *S. aureus* colonization. S7 Fig shows that the inclusion of three classes differing in recovery rate reduces richness and increases the Berger-Parker index with respect to the homogeneous recovery. However, the effects discussed so far—e.g. reduction and amplification of richness in HET and COM, respectively—are still present.

Effect of turnover of individuals

Node turnover represents another important property of a network that may impact the ecological dynamics of strains for two reasons: incoming individuals contribute to richness by injecting new strains; on the other hand, the removal from the population of infected nodes breaks transmission chains and hampers the persistence of strains. The result of the interplay between these two mechanisms is summarized by the plot of richness as a function of β and node length of stay, τ,—Fig 4A. The figure, obtained with the HOM model, shows two distinct regimes. In the former case, richness decreases as τ increases, because replacement of individuals becomes slower and injections less frequent. In the high β regime, instead, the average richness at fixed β does not depend monotonically on the node turnover but it is instead maximized at intermediate τ. Interestingly, the optimal value of τ decreases as β increases. This

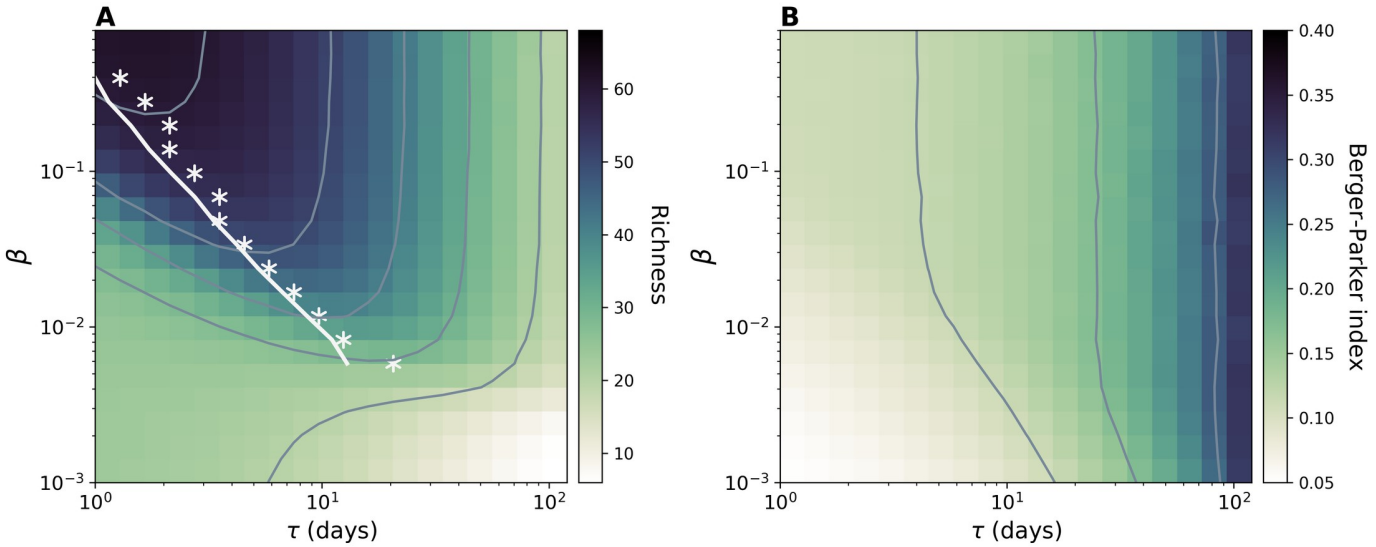

Fig 4. Effects of node length of stay on strain diversity. (A) Average richness and (B) Average Berger-Parker index for simulations on HOM model. Contour plots are shown in both figures. While exploring τ we also set the value of the average network size $\bar{V}$ to 306, thus the injection rate can be computed by the relation $\lambda_{in} = \bar{V}/\tau$. For each value of β we highlight in panel (A) the value of the length of stay corresponding to the maximum richness (white asterisks) together with the analytical prediction (white line) obtained by using Eq (1). Here $\mu = 0.00192$, $\bar{k} = 0.89$, $a_H = 0.28$.

https://doi.org/10.1371/journal.pcbi.1006530.g004

behavior can be explained by looking at the balance between injection and extinction that determines the equilibrium value of richness, $\bar{N}_S$. This reads [56]:

$$\bar{N}_S = \lambda_{in} p_s T_{pers}(\beta, \tau) = \bar{V}\, p_s\, \frac{T_{pers}(\beta, \tau)}{\tau}, \quad (1)$$

where $\lambda_{in} p_s$ is the rate at which new strains are introduced and T_{pers} is the average persistence time of a strain. The trade-off between injection and extinction appears as the ratio between the two time scales, T_{pers} and τ. In the limit $\tau \to 0$ the spread plays no role, even for high β. As τ increases, newly introduced infectious seeds have a higher probability to spread, thus the average extinction time initially increases super-linearly with τ (see S8 Fig in the supporting information) resulting in an increase of richness. However, past a certain value of τ, T_{pers} does not grow super-linearly anymore, thus a further increase in τ is detrimental for pathogen diversity because it is associated to fewer introductions. This general behavior was not altered by the accounting for introductions by transmissions from an external source as shown in S6 Fig.

We derive an approximate formula for T_{pers} considering an emerging strain competing with a single effective strain formed by all other strains grouped together. This formulation, enabled by the neutral hypothesis, makes it possible to write the master equation describing the dynamics and to use the Fokker-Planck approximation to derive persistence times (see Materials and methods section). Analytical results well reproduce the behavior observed in the simulations, and, in particular, the value of the length of stay maximizing richness for different β as shown by the comparison between white stars and continuous line in Fig 4B. The quantitative match for other values of p_s is reported in S9 Fig.

Unlike richness, Berger-Parker index always increases monotonically with the length of stay—Fig 4B. This behavior is due to the correlation of this indicator with average abundance, similarly to what we discussed in the previous section.

Spread of *S. aureus* in a hospital setting

We conclude by analyzing the real-case example of the *S. aureus* spread in a hospital setting [10, 57]. We used close-proximity-interaction (CPI) data recorded in a long-term health-care facility during 4 months by the i-Bird study [16, 28, 31]. These describe a high-resolution dynamical network whose complex structure reflects the hospital organization, the subdivision in wards and the admission and discharge of patients [58]. Together with the measurements of contacts, weekly nasal swabs were routinely performed to monitor the *S. aureus* carriage status of the participants and to identify the spa-type and the antibiotic resistance profile of the colonizing strains.

The modeling framework considered here well applies to this case. The SIS model is widely adopted for modeling the *S. aureus* colonization [59, 60], and the assumption of mutual exclusion is made by the majority of works to model the high level of cross-protection recognized by both epidemiological and microbiological studies [61, 62]. The dynamic CPI network was previously shown to be associated with paths of strain propagation [16]. Consistently, we assumed that transmission is mediated by network links with transmissibility β. In addition, new strains are introduced in the population carried by incoming patients, or through contacts with persons not taking part in the study.

Fig 5A shows weekly carriage and its breakdown in different strains. Prevalence and richness fluctuate around the average values 87,3 ± 6,3 cases and 39,8 ± 2 strains, respectively. Simulation results are reported in Fig 5B, that displays the impact of transmission and introduction rate on richness and prevalence. When q_s is low we find a positive trend between

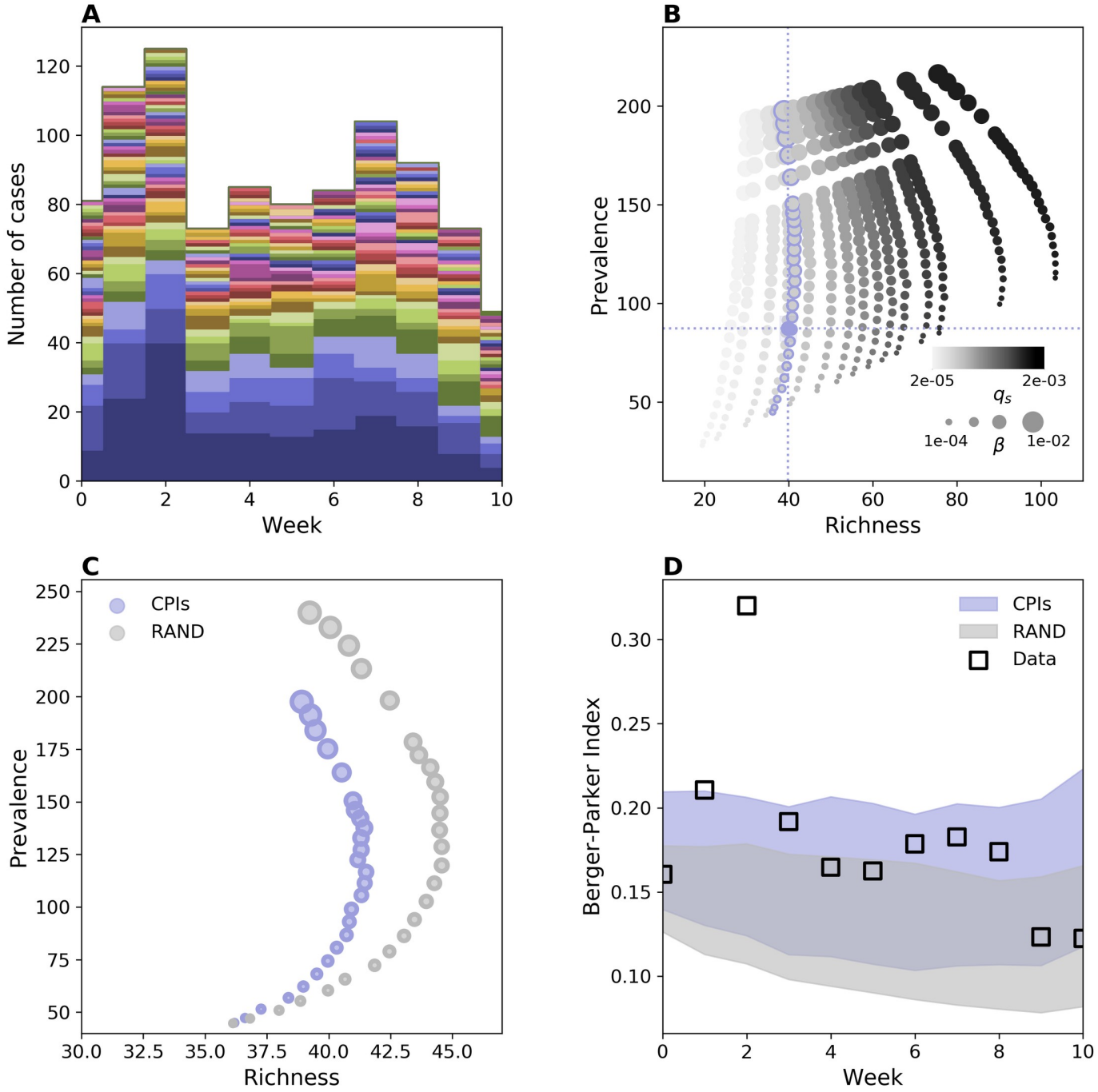

Fig 5. *S. aureus* population structure on hospital network. (A) Weekly carriage data measured during the i-Bird experiment. Each *S. aureus* strain's abundance time series is represented by a different color. All time series have been stacked as in Fig 1A. (B) Prevalence vs. richness from simulations on the hospital network for different β and different rates of introduction, here tuned by the parameter q_s. Blue dashed lines represent the average empirical values. (C) Prevalence vs richness for hospital contact data (blue dots) and RAND null model (grey dots). In RAND contacts are randomized by preserving the first and the last contact of every individual. Markers' size in (B) and (C) is proportional to the value of β. The hospital curve corresponds to the curve in (B) with blue-contour markers. (D) Weekly value of Berger-Parker index in carriage data (squares) along with the same quantity from the simulations. The shaded areas indicate the average plus/minus the standard deviation obtained from 1000 stochastic runs. For each network, parameter values are the ones that reproduce empirical prevalence and richness. Duration of colonization is assumed here to be 35 days [63]. Alternative values of this parameter led to the same qualitative results (S10 Fig).

https://doi.org/10.1371/journal.pcbi.1006530.g005

richness and prevalence, consistently with the synthetic case. For larger values of q_s the trend appears instead different. As transmissibility increases, richness initially grows with prevalence and then decreases after a certain point. This behavior is the same as observed in S6 Fig and stems from the reduction of susceptible nodes, that causes a decline in the expected injection rate—see Materials and methods section.

To quantify the effect of contact patterns on *S. aureus* population ecology we compared simulation results with the ones on a network null model. Specifically, we built the RAND null model that randomizes contacts while preserving just the first and the last contact of every individual. The randomization preserves node turnover, the number of active nodes and links and destroys contact heterogeneities and community structure along with other correlations. Fig 5C shows the comparison for different transmissibility values. The effect of the network is consistent with the theoretical results described for a heterogeneous network, i.e. smaller richness values correspond to the same prevalence in the real network compared to the homogeneous one. We then quantified the level of dominance of the multi-strain distribution by means of the Berger-Parker index. We chose for each network the values of q_s and β that better reproduce empirical richness and prevalence and, interestingly, we found that, for the two cases, same average richness and prevalence correspond to different levels of Berger-Parker index. The Berger-Parker index obtained with the real network is the highest and the one that better matches the empirical values—i.e. the empirical values are within one standard deviation of the mean for almost all weeks. Based on this result we argue that contact heterogeneities, along with the other properties of the contact network, contribute to the increased dominance of certain strains.

Discussion

Multiple biological and environmental factors concur in shaping pathogen diversity. We focused here on the host contact network and we used a minimal transmission model to assess the impact of this ingredient on strain population ecology, quantifying the effects of three main network properties, i.e. heterogeneous activity potential, presence of communities and turnover of individuals. Results show that the structure and dynamics of contacts can alter profoundly strains' co-circulation. Contact heterogeneities were found to shape the distribution of strains' abundances. Highly active nodes are known to play an important role in outbreak dynamics by acting as super-spreaders [33]. At the same time, however, they were found to enhance the interference between the transmission chains of different strains, thus hindering the spread of an emerging variant [46]. Here we showed that the combination of these two dynamical mechanisms reduces the richness and increases the level of heterogeneity in strains' abundances. In particular, hubs could allow strains with no biological advantage to generate a large number of cases and outcompete other equally fit strains. This mechanism may potentially bias the interpretation of biological data. Dynamical models that do not properly account for contact structure could overestimate the difference in strains' epidemiological traits in the attempt to explain observed fluctuations in strain abundance induced in reality by super-spreading events. Moreover, these models could provide biased assessment of transmission vs. introduction rates.

The presence of communities causes the separation of strains and mitigates the effect of competition thus enhancing co-existence. A similar behavior was already pointed out before [46, 51, 59, 64], e.g. for the spread of *S. pneumoniae*, as induced by age assortativity [64], for the case of *S. aureus* where distinct settings were considered [59], and for a population of antigenic distinct strains in presence of cross-immunity [51]. We found that the impact of community structure is not so strong, and it is likely minor when individuals of different

communities have frequent contacts. No appreciable variation was observed, indeed, for p_{IN} = 0.78, chosen to match the inter-ward coupling of the hospital network. Similar results can be expected for school classes or workplace departments presenting a similar level of community mixing. The effect on richness becomes appreciable for low community coupling (e.g. p_{IN} = 0.99 in Fig 3). This is consistent with a certain degree of diversity observed among strains belonging to separated communities, as it is the case of different hospitals [15].

Eventually, the analysis of turnover of individuals revealed major effects on strain diversity, when this mechanism is also the main driver of the introduction of strains in the population. When transmissibility is low richness decreases with host length of stay. When transmissibility is above the epidemic threshold we showed the existence of an optimal value of the length of stay that maximizes strain richness as a result of the interplay between two competing time scales, namely the typical inter-introduction time and the average persistence time of a strain. This provides insights for the spread of bacterial infections in transmission settings, such as hospitals or farms, that are of particular relevance for the spread of antimicrobial resistance and that are characterized by a rapid host turnover [15, 31, 65]. For the case of hospitals, for instance, they suggest that variations in patients' length of stay, as induced by a change of policy, could have appreciable effects on the population structure of nosocomial pathogens.

We adopted a neutral model to better disentangle the relative role of the different network properties. A wide disease-ecology literature addressed the consequences of neutral hypotheses on multi-strain balance in order to provide a benchmark for interpreting the observed co-existence patterns and gauging the effect of selective forces potentially at play [11, 18, 66, 67]. Many of these works addressed, for instance, the co-existence between susceptible and resistant strains of *S. pneumoniae* [11, 66]. However, this assumption was rarely adopted in network models, that consider for the majority strains with different epidemiological traits with the aim of describing pathogen selection and evolution [47–49, 68]. Strains were assumed to have the same infection parameters in [50, 51], where the role of community structure and clustering was analyzed in conjunction with cross-immunity. With respect to these works, the minimal transmission model used here enabled a transparent comprehension of the role of the network. Multiple identical SIS processes can be mapped, in fact, on a single SIS process, in such a way that the wide literature of single SIS processes allows for a better understanding of the behavior recovered in the simulations [32, 33]. Strains can be also grouped in two macro-strains. This strategy allowed us to adopt the viewpoint of an emerging strain and study its competition with the others seen as a unique macro-strain. The associated master equation and Fokker-Planck approximation allowed computing the average extinction time, capturing the key aspects of the dynamics. In a future work this theoretical framework could be extended to consider other network topologies. It could, for instance, be coupled with the activity-block approximation to describe heterogeneous networks. Additional numerical analyses, based on a similar transmission model, could also address other properties known to alter spreading dynamics, such as heterogeneous inter-contact time distribution or topological and temporal correlations.

As a case study, we analyzed the spread of *S. aureus* in a hospital taking advantage of the simultaneous availability of contact and carriage information [16]. The temporal and topological features of the network lead to a lower prevalence and richness with respect to the homogeneous mixing (although the effect was quite small). In addition, similar prevalence and richness values are associated to different dominance levels in different networks—i.e. different values of the Berger-Parker index—with the real network leading to a higher dominance as observed in reality. This behavior can be explained by the theoretical results and can be attributed essentially to the effect of contact heterogeneities, considering that the community structure does not have appreciable effects for this network, as discussed above. The importance of

accounting for host contacts and hospital organization in the assessment of bacterial spread and designing interventions has been recognized by several studies [16, 28–31, 63]. Here we show that this element may be critical also for understanding the population ecology of the bacterium. It is important to note however that, while the realistic network provides results that are closer to the data, this ingredient explains only part of the heterogeneity observed in the abundance. This shows that the contact network is a relevant factor, but other factors should be considered as well. The approach used here is intentionally simplified, as we focused on the main dynamical consequences of the contact network. Clearly, more detailed models can be designed to reproduce more closely the data. A certain degree of variation in the epidemiological traits could be at play, as for example the fitness cost of resistance [8]. Role of hosts in the network (e.g. patients vs. health-care workers), and heterogeneities in health conditions, antibiotic treatment and hygiene practices are also known to affect duration of carriage and chance of transmission [16, 28, 31, 63]. Eventually, we must consider that the comparison of model output with carriage data is also affected by the limitation of the dataset itself, already described in [16]. In particular, the weekly swabs may leave transient colonization undetected. Moreover, while the relevance of CPIs as proxies for epidemiological links has been demonstrated [16], the transmission through the environment (e.g. in the form of fomites) is also possible.

The understanding provided here can be relevant for other population settings, temporal scales and geographical levels. In addition, the modeling framework could be applied to pathogens other than *S. aureus*, such as *human papillomavirus*, *S. pneumoniae* and *Neisseria meningitidis*, for which the strong interest in the study of the strain ecology is justified by the public health need for understanding and anticipating trends in antibiotic resistance, or the long-term effect of vaccination [1, 2, 4, 5]. With this respect, if the simple framework introduced here increases our theoretical comprehension of the multi-strain dynamics, more tailored models may become necessary according to the specific case. In particular, we have considered complete mutual exclusion as the only mechanism for competition. In reality, a secondary inoculation in a host that is already a carrier may give rise to alternative outcomes, such as co-infection or replacement [69]. In addition, infection or carriage may confer a certain level of long-lasting strain-specific protection and/or a short-duration transcendent immunity [11, 50]. Eventually mechanisms of mutation and/or recombination are at play and their inclusion into the model can be important according to the time scale of interest.

Materials and methods

Network models

We provide here details of the generative algorithms used for the contact network models. Network dynamics is implemented in discrete time according to the following rules common to all models:

Turnover dynamics: new nodes arrive according to a Poisson process with rate λ_{in} and leave after a random time drawn from an exponential probability distribution with average τ. After a short initial transient, population size is Poisson distributed with average $\bar{V} = \lambda_{in}\tau$. Upon admission, a node i is assigned with an activity potential a_i, i.e. an activation rate, drawn at random from a given probability distribution $P(a)$. Any node retains this property throughout its whole lifespan.

Activation Pattern: each node i becomes active with rate a_i. It then receives a number of stubs drawn from a zero-truncated Poisson distribution with parameter κ—we require active nodes to engage in at least one contact. The average number of stubs, computed among active

nodes, is thus given by $\kappa/(1 - e^{-\kappa})$, and the average degree can be computed by the latter quantity multiplied by the average activity potential. The active status lasts for a single time step.

Stub-matching: stubs are then matched according to the actual model considered.

We now describe in detail each network model:

HOM: in this model each node has the same probability a_H to be active during each time step; the activity distribution is thus $P(a) = \delta(a - a_H)$, where $\delta(x)$ is the Dirac's delta function. Stubs are matched completely at random in order to form links, according to a configuration model [33]. We discard eventual self-links and multiple links that may occur during the matching procedure.

HET: here each node i has its own activity rate a_i, drawn from a power-law distribution $P(a) \propto a^{-\gamma}$, with $a \in (\epsilon, 1]$. We tune the variance by varying γ—lower γ higher variance. We then set ϵ to have the average activity $\bar{a}$ equal to a_H in HOM. Stub-matching procedure is the same as in HOM. HET model is thus a variant of the activity driven model introduced in [34] with the difference that here contacts are created only among active individuals.

COM: incoming nodes are assigned to one among n_C communities with equal probability—so that communities have the same size on average—and belong to the same community throughout their whole lifespan. Stubs are matched according to the community each node belongs to. Precisely, any stub is matched either with another stub of the same community, with probability p_{IN}, or with a stub of a different community, with complementary probability. Here the stub-matching procedure results in a larger number of lost links—to eliminate multiple links and self-loops—compared to HOM and HET, due to the difficulty in matching stubs within small groups. Thus, the parameter κ has to be adjusted manually to recover the same average degree as in HOM and HET. Each node has the same activity potential a_H as in HOM.

Hospital network and null model

We use a dynamical contact network obtained from CPI data collected during the i-Bird study in a French hospital. Details of the network are already reported in [16]. Briefly, the dataset describes contacts occurring between 592 individuals from July to November 2009. The study involved both patients and health-care workers, distributed in 5 wards, as well as hospital service staff. Every participant wore a wireless device designed to broadcast a signal every 30 s containing information about its ID. Signal strength was tuned so that only devices within a small distance (around 1.5 m) were able to register a contact. CPIs were finally aggregated daily, keeping the information about their cumulative duration within each day.

We discard CPIs relative to the first 2 weeks and the last 4 weeks of dataset, corresponding to a period of adjustments in the measurements and progressive dismissal of the experiment, respectively. Simulations conducted with the CPIs network were compared with results obtained with a null model which we refer to as RAND. According to this randomization scheme the activity of a node is randomized while respecting the constraint that removal and addition of contacts must not alter the time of the first and the last contact of each node (t_S and t_L respectively). Notice that RAND preserves the number of nodes that are present at any time in the network by preserving their first contact t_S and their length of stay $t_L - t_S$. Null models randomizing the latter properties lead to misleading results when node length of stay is heterogeneous and node turnover occurs [70]. RAND also sets all contact weights equal to the average weight value.

Spreading simulations

Spreading dynamics is stochastic and is performed in discrete time. At each time step of duration Δt, we update the state of each node: each infected node transmits the strain it is carrying

to a susceptible neighbor with probability $\beta\Delta t$ and it turns susceptible with probability $\mu\Delta t$. Notice that due to mutual exclusion, an individual can be infected by a single strain at a time [71]. Strain injection is given by the combination of two processes: incoming individuals bring a new strain with probability p_s, and susceptible individuals turn infectious with a new strain with probability $q_s\Delta t$. The two mechanisms mimic respectively incoming infectious individuals (e.g. admission of colonized patients) and transmission from an external source (in the hospital example this corresponds to contacts with individuals that were not participating in the study). The expected injection rate, which accounts for both introduction mechanisms, is thus given by $\iota = \lambda_{\text{in}} p_s + \bar{S} q_s$, where $\bar{S}$ is the average number of susceptible individuals at the equilibrium. In the theoretical analysis in the main paper we assumed $q_s = 0$ for simplicity, thus variations in ι were induced by variations in λ_{in} and p_s. The case $q_s > 0$ was considered in the supporting information.

Simulations on synthetic networks differ from those on the hospital network in the combination of the spreading and network dynamics. In the synthetic network case, at each time step of duration Δt = 1h, both network and spreading dynamics are simulated one after the other. On average, $\lambda_{in}\Delta t$ new nodes enter in the population per time step, while existing nodes can leave with probability $\Delta t/\tau$. Nodes then form contacts according to the specific generative network algorithm. Eventually, transmission and recovery are simulated as explained above. In order to reconstruct the equilibrium dynamics we run simulations for a sufficiently long time span, discarding a transient time of $4 \cdot 10^4$ time steps. We verified that the dynamical properties at the equilibrium are unaffected by initial conditions.

For the hospital example, the network is an external parameter fed into the simulations. Contacts were aggregated daily keeping the information of their total duration. We used this information by considering a weighted network with the link weight, w_{ij}, representing the number of contacts of duration 30 s registered during the day between i and j. We then assumed Δt = 1 day and computed the probability of infection depending on the weight as $1 - (1 - \beta\delta)^{w_{ij}}$, with δ = 30 s. We initialized the system with the same configuration observed in the data, i.e. the initial status for each node is set according to *S. aureus* carriage during the starting week. Simulation length is bound to the hospital contact network duration.

In order to facilitate the comparison between the synthetic and the real scenarios, parameters of the network models were set based on the properties of the hospital network. The average size, the average activity potential and the average degree were set equal to the values estimated from the hospital network, i.e. $\bar{V} = 306$, $\bar{a} = 0.28$, $\bar{k} = 0.89$ respectively. For the COM model the number of communities (n_C = 6) and one of the two explored values of p_{IN} (p_{IN} = 0.78) were also informed by the data. Additional values of $\bar{V}$ and p_{IN} were also tested. Epidemiological parameters were informed by the data in some cases—p_s = 0.079 as computed from carriage data -, or chosen among plausible values for the *S. aureus* colonization—i.e. μ^{-1}, that was set equal to either 21 or 35 days with other values from 14 to 49 days explored in the supporting information. Values of β were explored systematically. For consistency, values of rates throughout the manuscript were always expressed per hour.

Analysis of carriage data

Carriage data was obtained from weekly swabs in multiple body areas, including the nares. Swabs that resulted positive to *S. aureus* were further examined. Spa-type and antibiotic resistance profiles (MSSA or MRSA) were then determined. In this work we regard two strains as different if they differ in spa-type and/or antibiotic resistance profile. We considered carriage data obtained from nasal swabs dismissing other body areas since the anterior nares represent the most important niche for *S. aureus* [72].

Ecological measures and other indicators

We described strain population diversity through standard ecological indicators. The abundance of a strain i, N_i, is the strain-associated prevalence. From this quantity we computed the relative abundance, $f_i = \frac{N_i}{\sum_i N_i}$, and the relative abundance distribution, being the frequency of strains with relative abundance f. The Berger-Parker index is the relative abundance of the dominant strain, i.e. $\max_i f_i$.

To analyze repartition of strains across communities we use the Inverse Participation Ratio (*IPR*) [55]. The general definition of this quantity is the following. Given a vector $\vec{v}$ with l components $\{v_i\}_{i=1,\ldots,l}$, all within the range [0, 1], the *IPR* is given by:

$$IPR = \sum_{i=1}^{l} v_i^4. \tag{2}$$

If all the components are of the order (l^{-1}) then the *IPR* is small. Instead if one component $v_i \sim 1$ then $IPR \sim 1$ too, reflecting localization of $\vec{v}$. The IPR for total prevalence is computed by setting v_i equal to the fraction of infected individuals belonging to community $i = 1, \ldots, l = n_C$, while the *IPR* for a single strain is computed by setting v_i equal to the fraction of individuals infected by that particular strain and belonging to community i. We can extend the *IPR* computation to HOM case by assigning nodes to different groups as in COM but without affecting the stub-matching scheme.

Analytical results for the homogeneous network

In order to estimate the value of the length of stay maximizing the average richness for a given value of β when the contact structure is given by the HOM network we consider a homogeneous mixing version of our system.

Due to Eq (1) the calculation of the average richness reduces to the calculation of the average persistence time. In order to estimate such quantity we focus on a particular strain, labelled as "strain A", which is injected at $t = 0$ and we group all other strains under the label "strain B". We are allowed to do so because all strains have identical parameters. We therefore reduce our initial, multi-strain problem, to a two-strain problem. Since all new strains that will be injected after $t = 0$ will be labeled as strain B, it is clear that A is doomed to extinction since there exists an infinite reservoir of B. The average time to extinction is therefore the average time to extinction of strain A.

Since HOM network realizes quite well homogeneous mixing conditions we regard our system as homogeneously mixed. Within this framework it is sufficient to specify the numbers of hosts infected by strain A (n_A), hosts infected by strain B (n_B) and susceptible hosts (n_s). The master equation for the joint probability distribution $P(n_A, n_B, n_s)$ is given by [73]:

$$\begin{aligned}
\dot{P}(n_A, n_B, n_s) &= \beta' \bar{V}^{-1}(n_A - 1)(n_s + 1)P(n_A - 1, n_B, n_s + 1) \\
&+ \beta' \bar{V}^{-1}(n_B - 1)(n_s + 1)P(n_A, n_B - 1, n_s + 1) \\
&+ \mu(n_A + 1)P(n_A + 1, n_B, n_s - 1) + \mu(n_B + 1)P(n_A, n_B + 1, n_s - 1) \\
&+ \lambda_{out}(n_A + 1)P(n_A + 1, n_B, n_s) \\
&+ \lambda_{out}(n_B + 1)P(n_A, n_B + 1, n_s) + \lambda_{out}(n_s + 1)P(n_A, n_B, n_s + 1) \\
&+ \lambda_{out}\bar{V}p_s P(n_A, n_B - 1, n_s) + \lambda_{out}\bar{V}(1 - p_s)P(n_A, n_B, n_s - 1) \\
&- [(n_A + n_B)(\beta' \bar{V}^{-1} n_s + \mu) + \lambda_{out}(n_A + n_B + n_s) + \lambda_{out}\bar{V}]P(n_A, n_B, n_s),
\end{aligned} \tag{3}$$

Where $\beta' = \beta\bar{k}$. Terms appearing on the right-hand side of the equation represent the

probability flow associated to each transition event. The first four terms describe, in order, the infection due to strain A, the infection due to strain B, the recovery from A and the recovery from B. The remaining terms are then associated to the discharge of either one of the three types of individuals—infected with A, infected with B and susceptibles—and to the admission of infected of type B and susceptibles respectively. In order to obtain some approximate solution to this equation we assume that the average number of individuals $n_A + n_B + n_s$ and the total prevalence $n_A + n_B$ do not fluctuate in time and are therefore equal to $\bar{V}$ and $i(\infty)\bar{V}$ respectively, where $i(\infty)$ is given by:

$$i(\infty) = \frac{\beta' - \mu - \lambda_{out} + \sqrt{(\beta' - \mu - \lambda_{out})^2 + 4\beta'\lambda_{out}p_s}}{2\beta'}. \quad (4)$$

After performing the Van-Kampen size expansion we are left with a Fokker-Planck equation for the density of A $f\left(x = \frac{n_A}{\bar{V}}\right) = P(n_A)$:

$$\partial_t f = -\partial_x(D_1(x)f) + \frac{1}{2\bar{V}}\partial_x^2(D_2(x)f), \quad (5)$$

where $D_1 = \beta'\,(1 - i(\infty))\,x - \mu - \lambda_{out}$ and $D_2 = \beta'\,(1 - i(\infty))\,x + \mu + \lambda_{out}$ are the so-called drift and diffusion coefficients respectively.

According to the theory of stochastic processes [73] the average extinction time $T_{\text{pers}}(x_0)$ (where x_0 represents the initial density of strain A) satisfies:

$$D_1(x_0)\frac{d}{dx_0}\,T_{\text{pers}} + \frac{1}{2\bar{V}}D_2(x_0)\frac{d^2}{dx_0^2}T_{\text{pers}} = -1, \quad (6)$$

with boundary conditions $T_{\text{pers}}(0) = 0$ and $\frac{d}{dx_0}T_{\text{pers}}(i(\infty)) = 0$. The solution is finally given by:

$$T_{\text{pers}}(x_0) = \frac{i(\infty)}{\lambda_{out}p_s}[Ei(-\alpha i(\infty))(e^{\alpha x_0} - 1) - e^{\alpha x_0}Ei(-\alpha x_0) + ln(\alpha x_0) + \gamma_E], \quad (7)$$

where $Ei(x)$ is the exponential integral function and γ_E is Euler-Mascheroni constant. When a new strain is introduced its prevalence is just 1, therefore we estimate the average extinction time using $T_{\text{pers}}(x_0 = \bar{V}^{-1})$.

Supporting information

S1 Text. Multi-strain model with heterogeneous recovery classes. This file contains additional information about simulations with individuals grouped into classes with different recovery rates.
(PDF)

S1 Fig. Richness and Berger-Parker index as a function of transmissibility for HOM, HET, COM and COM+HET models. Each model is displayed on a different column. HET is characterized by activity distribution exponent $\gamma = 0.7$. COM+HET model is simulated using the same activation pattern as in HET with $\gamma = 0.7$ and the same stub-matching procedure as in COM. We consider the case $p_{IN} = 0.99$. The first two rows correspond to $p_s = 0.01$, whereas the last two to $p_s = 0.079$. For each scenario we show the median (solid line), as well as 50% and 95% CI (shaded areas).
(PNG)

S2 Fig. Summary indicators of the persistence time distribution as a function of transmissibility for both HOM and HET models. HOM and HET are displayed in blue and green

respectively. (A), (B) and (C) display distribution's average, coefficient of variation and skewness, respectively. Other parameters are as in Fig 2 in the main text.
(PNG)

S3 Fig. Shannon evenness for HOM model and two instances of HET model. HOM is depicted in blue, whereas instances of HET model with activity distribution exponent $\gamma = 2.5$ and $\gamma = 0.7$ are depicted in orange and green respectively. Shaded blue area represents standard deviation for HOM. We introduce the relative abundance of the i-th strain: $n_i = N_i \Big/ \sum_i N_i$, with N_i the abundance of the strain i (i.e. the number of infected with strain i). Shannon evenness is defined as the normalized Shannon entropy $S(\{n_i\}) = -\mathcal{N}^{-1} \sum_i n_i \ln n_i$, with $\mathcal{N} = \ln N_S$. Parameters are the same as in Fig 1 in the main text.
(PNG)

S4 Fig. Impact of network size. Richness (A,B), average persistence time (C,D), prevalence (E,F) and Berger-Parker index (G,H) as a function of transmissibility for both HOM and HET models (first and second columns respectively). For each value of $\bar{V}$ we compute p_s to have the strain injection rate, $\bar{V} p_s$, the same across the different networks. Other parameters are as in Fig 2 of the main paper. Increasing network size results in a larger number of co-circulating strains, while the re-scaled prevalence and the Berger-Parker index are almost independent of $\bar{V}$. Notice that increasing network size does not lead to any qualitative change in the relation between HOM and HET.
(PNG)

S5 Fig. Relative abundance distribution in varying network size for HOM and HET models. HOM and HET are depicted in blue and green respectively. For each value of $\bar{V}$ we compute p_s to have the strain injection rate, $\bar{V} p_s$, the same across the different networks. Other parameters are as in Fig 2 of the main paper.
(PNG)

S6 Fig. Richness for the different network models with transmission from an external source. The frequency of transmissions from an external source is tuned by q_s, which we set here to 0.0002. (A) Richness for HOM model (blue markers) and HET model with activity distribution exponent $\gamma = 0.7$ (green markers). Here $p_s = 0.079$. (B) Richness index for HOM model (blue markers) and COM model with within-community connection probability $p_{IN} = 0.99$ (green markers). Here $p_s = 0.01$. (C) Richness as a function of β and τ for HOM model. Here $p_s = 0.079$.
(PNG)

S7 Fig. Multi-strain dynamics when recovery rate is heterogeneous across individuals. Here, each node belongs to one out of three classes according to its recovery rate—see description in the dedicated section of this supporting information. We compare HOM (blue), HET (green), COM (red) models with and without heterogeneity in the recovery rate (triangles and circles respectively). Panels show prevalence (A), richness (B) and Berger-Parker index (C). Other parameters are like in Figs 1, 2 and 3 in the main paper ($\gamma = 0.7$ for HET and $p_{IN} = 0.99$ for COM).
(PNG)

S8 Fig. Average persistence time for HOM in varying transmissibility and length of stay. The quantity is computed from the simulations. The dashed gray line represents a linear trend as a guide to the eye. Parameters are the same as in Fig 4 in the main text.
(PNG)

S9 Fig. Comparison between simulations for HOM model and analytical predictions obtained using the Fokker-Planck framework. Solid lines represent average richness obtained by using Eqs (1) and (7) from the main text while dots represent simulations results. Here $\beta = 0.04$ while other parameters are the same as in Fig 4 in the main text.
(PNG)

S10 Fig. Prevalence vs richness for several values of the infectious period and using the CPI network. The value of q_s is the same for the curve highlighted in Fig 5B in the main text, $q_s = 0.00018$. Here dot size is proportional to the magnitude of β.
(PNG)

Acknowledgments

Authors would like to thank Vittoria Colizza, Lulla Opatowski and Laura Temime for useful discussion.

Author Contributions

Conceptualization: Francesco Pinotti, Pierre-Yves Böelle, Chiara Poletto.

Data curation: Francesco Pinotti, Éric Fleury, Didier Guillemot, Pierre-Yves Böelle.

Investigation: Éric Fleury, Didier Guillemot, Pierre-Yves Böelle.

Methodology: Francesco Pinotti, Chiara Poletto.

Supervision: Pierre-Yves Böelle, Chiara Poletto.

Writing – original draft: Francesco Pinotti, Pierre-Yves Böelle, Chiara Poletto.

Writing – review & editing: Francesco Pinotti, Éric Fleury, Didier Guillemot, Pierre-Yves Böelle, Chiara Poletto.

References

1. Schiffman M, Castle PE. Human Papillomavirus: Epidemiology and Public Health. Archives of Pathology & Laboratory Medicine. 2003; 127(8):930–934.
2. Weinberger DM, Malley R, Lipsitch M. Serotype replacement in disease after pneumococcal vaccination. The Lancet. 2011; 378(9807):1962–1973. https://doi.org/10.1016/S0140-6736(10)62225-8
3. Bogaert D, de Groot R, Hermans P. Streptococcus pneumoniae colonisation: the key to pneumococcal disease. The Lancet Infectious Diseases. 2004; 4(3):144–154. https://doi.org/10.1016/S1473-3099(04)00938-7 PMID: 14998500
4. Atkins KE, Lafferty EI, Deeny SR, Davies NG, Robotham JV, Jit M. Use of mathematical modelling to assess the impact of vaccines on antibiotic resistance. The Lancet Infectious Diseases. 2017. https://doi.org/10.1016/S1473-3099(17)30478-4 PMID: 29146178
5. Chambers HF, Deleo FR. Waves of resistance: Staphylococcus aureus in the antibiotic era. Nat Rev Microbiol. 2009; 7(9):629–641. https://doi.org/10.1038/nrmicro2200 PMID: 19680247
6. Reich NG, Shrestha S, King AA, Rohani P, Lessler J, Kalayanarooj S, et al. Interactions between serotypes of dengue highlight epidemiological impact of cross-immunity. J R Soc Interface. 2013; 10(86). https://doi.org/10.1098/rsif.2013.0414 PMID: 23825116
7. Cohen T, Colijn C, Murray M. Modeling the effects of strain diversity and mechanisms of strain competition on the potential performance of new tuberculosis vaccines. Proc Natl Acad Sci U S A. 2008; 105(42):16302–16307. https://doi.org/10.1073/pnas.0808746105 PMID: 18849476
8. Melnyk AH, Wong A, Kassen R. The fitness costs of antibiotic resistance mutations. Evol Appl. 2015; 8(3):273–283. https://doi.org/10.1111/eva.12196 PMID: 25861385
9. Opatowski L, Varon E, Dupont C, Temime L, van der Werf S, Gutmann L, et al. Assessing pneumococcal meningitis association with viral respiratory infections and antibiotics: insights from statistical and

mathematical models. Proceedings Biological Sciences. 2013; 280(1764):20130519. https://doi.org/10.1098/rspb.2013.0519 PMID: 23782877

10. Boucher HW, Corey GR. Epidemiology of Methicillin-Resistant Staphylococcus aureus. Clin Infect Dis. 2008; 46(Supplement_5):S344–S349. https://doi.org/10.1086/533590 PMID: 18462089
11. Cobey S, Lipsitch M. Niche and neutral effects of acquired immunity permit coexistence of pneumococcal serotypes. Science. 2012; 335(6074):1376–1380. https://doi.org/10.1126/science.1215947 PMID: 22383809
12. Murall CL, Bauch CT, Day T. Could the human papillomavirus vaccines drive virulence evolution? Proc R Soc B. 2015; 282(1798):20141069. https://doi.org/10.1098/rspb.2014.1069 PMID: 25429011
13. Aanensen DM, Feil EJ, Holden MTG, Dordel J, Yeats CA, Fedosejev A, et al. Whole-Genome Sequencing for Routine Pathogen Surveillance in Public Health: a Population Snapshot of Invasive Staphylococcus aureus in Europe. mBio. 2016; 7(3):e00444–16. https://doi.org/10.1128/mBio.00444-16 PMID: 27150362
14. Lemey P, Rambaut A, Bedford T, Faria N, Bielejec F, Baele G, et al. Unifying Viral Genetics and Human Transportation Data to Predict the Global Transmission Dynamics of Human Influenza H3N2. PLoS Pathog. 2014; 10(2):e1003932. https://doi.org/10.1371/journal.ppat.1003932 PMID: 24586153
15. Donker T, Reuter S, Scriberras J, Reynolds R, Brown NM, Török ME, et al. Population genetic structuring of methicillin-resistant Staphylococcus aureus clone EMRSA-15 within UK reflects patient referral patterns. Microbial Genomics. 2017; 3(7). https://doi.org/10.1099/mgen.0.000113 PMID: 29026654
16. Obadia T, Silhol R, Opatowski L, Temime L, Legrand J, Thiébaut ACM, et al. Detailed Contact Data and the Dissemination of Staphylococcus aureus in Hospitals. PLOS Computational Biology. 2015; 11(3): e1004170. https://doi.org/10.1371/journal.pcbi.1004170 PMID: 25789632
17. Nekkab N, Astagneau P, Temime L, Crépey P. Spread of hospital-acquired infections: A comparison of healthcare networks. PLOS Computational Biology. 2017; 13(8):e1005666. https://doi.org/10.1371/journal.pcbi.1005666 PMID: 28837555
18. Fraser C, Hanage WP, Spratt BG. Neutral microepidemic evolution of bacterial pathogens. Proceedings of the National Academy of Sciences of the United States of America. 2005; 102(6):1968–1973. https://doi.org/10.1073/pnas.0406993102 PMID: 15684071
19. Robinson K, Fyson N, Cohen T, Fraser C, Colijn C. How the Dynamics and Structure of Sexual Contact Networks Shape Pathogen Phylogenies. PLOS Computational Biology. 2013; 9(6):e1003105. https://doi.org/10.1371/journal.pcbi.1003105 PMID: 23818840
20. Matt J Keeling PR. Modeling Infectious Diseases in Humans and Animals. Princeton University Press; 2008.
21. Wesolowski A, Eagle N, Tatem AJ, Smith DL, Noor AM, Snow RW, et al. Quantifying the impact of human mobility on malaria. Science (New York, NY). 2012; 338(6104):267–270. https://doi.org/10.1126/science.1223467
22. Balcan D, Colizza V, Gonçalves B, Hu H, Ramasco JJ, Vespignani A. Multiscale mobility networks and the spatial spreading of infectious diseases. Proceedings of the National Academy of Sciences of the United States of America. 2009; 106(51):21484–21489. https://doi.org/10.1073/pnas.0906910106 PMID: 20018697
23. Louail T, Lenormand M, Picornell M, Cantú OG, Herranz R, Frias-Martinez E, et al. Uncovering the spatial structure of mobility networks. Nature Communications. 2015; 6:6007. https://doi.org/10.1038/ncomms7007 PMID: 25607690
24. Rocha LEC, Liljeros F, Holme P. Information dynamics shape the sexual networks of Internet-mediated prostitution. Proceedings of the National Academy of Sciences. 2010; 107(13):5706–5711. https://doi.org/10.1073/pnas.0914080107
25. Mastrandrea R, Fournet J, Barrat A. Contact Patterns in a High School: A Comparison between Data Collected Using Wearable Sensors, Contact Diaries and Friendship Surveys. PLOS ONE. 2015; 10(9): e0136497. https://doi.org/10.1371/journal.pone.0136497 PMID: 26325289
26. Salathé M, Kazandjieva M, Lee JW, Levis P, Feldman MW, Jones JH. A high-resolution human contact network for infectious disease transmission. Proceedings of the National Academy of Sciences. 2010; 107(51):22020–22025. https://doi.org/10.1073/pnas.1009094108
27. Génois M, Vestergaard CL, Fournet J, Panisson A, Bonmarin I, Barrat A. Data on face-to-face contacts in an office building suggest a low-cost vaccination strategy based on community linkers. Network Science. 2015; 3(3):326–347. https://doi.org/10.1017/nws.2015.10
28. Duval A, Obadia T, Martinet L, Boëlle PY, Fleury E, Guillemot D, et al. Measuring dynamic social contacts in a rehabilitation hospital: effect of wards, patient and staff characteristics. Scientific Reports. 2018; 8(1):1686. https://doi.org/10.1038/s41598-018-20008-w PMID: 29374222

29. Vanhems P, Barrat A, Cattuto C, Pinton JF, Khanafer N, Régis C, et al. Estimating Potential Infection Transmission Routes in Hospital Wards Using Wearable Proximity Sensors. PLOS ONE. 2013; 8(9): e73970. https://doi.org/10.1371/journal.pone.0073970 PMID: 24040129

30. Voirin N, Payet C, Barrat A, Cattuto C, Khanafer N, Régis C, et al. Combining High-Resolution Contact Data with Virological Data to Investigate Influenza Transmission in a Tertiary Care Hospital. Infection Control & Hospital Epidemiology. 2015; 36(3):254–260. https://doi.org/10.1017/ice.2014.53

31. Assab R, Nekkab N, Crépey P, Astagneau P, Guillemot D, Opatowski L, et al. Mathematical models of infection transmission in healthcare settings: recent advances from the use of network structured data. Current Opinion in Infectious Diseases. 2017; 30(4):410–418. https://doi.org/10.1097/QCO.0000000000000390 PMID: 28570284

32. Holme P, Saramäki J, editors. Temporal Networks. Springer; 2013.

33. Pastor-Satorras R, Castellano C, Van Mieghem P, Vespignani A. Epidemic processes in complex networks. Reviews of Modern Physics. 2015; 87(3):925–979. https://doi.org/10.1103/RevModPhys.87.925

34. Perra N, Gonçalves B, Pastor-Satorras R, Vespignani A. Activity driven modeling of time varying networks. Scientific Reports. 2012; 2:469. https://doi.org/10.1038/srep00469 PMID: 22741058

35. Barthélemy M, Barrat A, Pastor-Satorras R, Vespignani A. Dynamical patterns of epidemic outbreaks in complex heterogeneous networks. Journal of Theoretical Biology. 2005; 235(2):275–288. https://doi.org/10.1016/j.jtbi.2005.01.011 PMID: 15862595

36. Salathé M, Jones JH. Dynamics and Control of Diseases in Networks with Community Structure. PLOS Computational Biology. 2010; 6(4):e1000736. https://doi.org/10.1371/journal.pcbi.1000736 PMID: 20386735

37. Sah P, Leu ST, Cross PC, Hudson PJ, Bansal S. Unraveling the disease consequences and mechanisms of modular structure in animal social networks. Proceedings of the National Academy of Sciences. 2017; 114(16):4165–4170. https://doi.org/10.1073/pnas.1613616114

38. Holme P, Liljeros F. Birth and death of links control disease spreading in empirical contact networks. Scientific Reports. 2014; 4:4999. https://doi.org/10.1038/srep04999 PMID: 24851942

39. Darabi Sahneh F, Scoglio C. Competitive epidemic spreading over arbitrary multilayer networks. Physical Review E. 2014; 89(6):062817. https://doi.org/10.1103/PhysRevE.89.062817

40. Poletto C, Meloni S, Van Metre A, Colizza V, Moreno Y, Vespignani A. Characterising two-pathogen competition in spatially structured environments. Scientific Reports. 2015; 5:7895. https://doi.org/10.1038/srep07895 PMID: 25600088

41. Poletto C, Meloni S, Colizza V, Moreno Y, Vespignani A. Host Mobility Drives Pathogen Competition in Spatially Structured Populations. PLOS Computational Biology. 2013; 9(8):e1003169. https://doi.org/10.1371/journal.pcbi.1003169 PMID: 23966843

42. Sanz J, Xia CY, Meloni S, Moreno Y. Dynamics of Interacting Diseases. Phys Rev X. 2014; 4(4):041005.

43. Karrer B, Newman MEJ. Competing epidemics on complex networks. Phys Rev E. 2011; 84(3):036106. https://doi.org/10.1103/PhysRevE.84.036106

44. Cai W, Chen L, Ghanbarnejad F, Grassberger P. Avalanche outbreaks emerging in cooperative contagions. Nature Physics. 2015; 11(11):936–940. https://doi.org/10.1038/nphys3457

45. Hébert-Dufresne L, Althouse BM. Complex dynamics of synergistic coinfections on realistically clustered networks. Proceedings of the National Academy of Sciences. 2015; 112(33):10551–10556. https://doi.org/10.1073/pnas.1507820112

46. Leventhal GE, Hill AL, Nowak MA, Bonhoeffer S. Evolution and emergence of infectious diseases in theoretical and real-world networks. Nature Communications. 2015; 6:6101. https://doi.org/10.1038/ncomms7101 PMID: 25592476

47. Eames KTD, Keeling MJ. Coexistence and Specialization of Pathogen Strains on Contact Networks. The American Naturalist. 2006; 168(2):230–241. https://doi.org/10.1086/505760 PMID: 16874632

48. Ballegooijen WMv, Boerlijst MC. Emergent trade-offs and selection for outbreak frequency in spatial epidemics. Proceedings of the National Academy of Sciences. 2004; 101(52):18246–18250. https://doi.org/10.1073/pnas.0405682101

49. Lion S, Gandon S. Spatial evolutionary epidemiology of spreading epidemics. Proceedings Biological Sciences. 2016; 283 (1841). https://doi.org/10.1098/rspb.2016.1170 PMID: 27798295

50. Buckee CO, Koelle K, Mustard MJ, Gupta S. The effects of host contact network structure on pathogen diversity and strain structure. PNAS. 2004; 101(29):10839–10844. https://doi.org/10.1073/pnas.0402000101 PMID: 15247422

51. Buckee C, Danon L, Gupta S. Host community structure and the maintenance of pathogen diversity. Proceedings of the Royal Society of London B: Biological Sciences. 2007; 274(1619):1715–1721. https://doi.org/10.1098/rspb.2007.0415

52. Morris EK, Caruso T, Buscot F, Fischer M, Hancock C, Maier TS, et al. Choosing and using diversity indices: insights for ecological applications from the German Biodiversity Exploratories. Ecol Evol. 2014; 4(18):3514–3524. https://doi.org/10.1002/ece3.1155 PMID: 25478144

53. Azaele S, Suweis S, Grilli J, Volkov I, Banavar JR, Maritan A. Statistical mechanics of ecological systems: Neutral theory and beyond. Rev Mod Phys. 2016; 88(3):035003. https://doi.org/10.1103/RevModPhys.88.035003

54. DeBenedictis PA. On the Correlations between Certain Diversity Indices. The American Naturalist. 1973; 107(954):295–302. https://doi.org/10.1086/282831

55. Pastor-Satorras R, Castellano C. Distinct types of eigenvector localization in networks. Scientific Reports. 2016; 6:18847. https://doi.org/10.1038/srep18847 PMID: 26754565

56. Suweis S, Bertuzzo E, Mari L, Rodriguez-Iturbe I, Maritan A, Rinaldo A. On species persistence-time distributions. Journal of Theoretical Biology. 2012; 303:15–24. https://doi.org/10.1016/j.jtbi.2012.02.022 PMID: 22763130

57. van Kleef E, Robotham JV, Jit M, Deeny SR, Edmunds WJ. Modelling the transmission of healthcare associated infections: a systematic review. BMC Infect Dis. 2013; 13:294. https://doi.org/10.1186/1471-2334-13-294 PMID: 23809195

58. Martinet L, Crespelle C, Fleury E, Boëlle PY, Guillemot D. The Link Stream of Contacts in a Whole Hospital. arXiv:180505752 [cs]. 2018;.

59. Kouyos R, Klein E, Grenfell B. Hospital-Community Interactions Foster Coexistence between Methicillin-Resistant Strains of Staphylococcus aureus. PLOS Pathogens. 2013; 9(2):e1003134. https://doi.org/10.1371/journal.ppat.1003134 PMID: 23468619

60. Bonten MJ, Austin DJ, Lipsitch M. Understanding the spread of antibiotic resistant pathogens in hospitals: mathematical models as tools for control. Clinical Infectious Diseases: An Official Publication of the Infectious Diseases Society of America. 2001; 33(10):1739–1746. https://doi.org/10.1086/323761

61. Margolis E, Yates A, Levin BR. The ecology of nasal colonization of Streptococcus pneumoniae, Haemophilus influenzae and Staphylococcus aureus: the role of competition and interactions with host's immune response. BMC Microbiol. 2010; 10:59. https://doi.org/10.1186/1471-2180-10-59 PMID: 20178591

62. Dall'Antonia M, Coen PG, Wilks M, Whiley A, Millar M. Competition between methicillin-sensitive and -resistant Staphylococcus aureus in the anterior nares. J Hosp Infect. 2005; 61(1):62–67. https://doi.org/10.1016/j.jhin.2005.01.008 PMID: 15893854

63. Chang Q, Lipsitch M, Hanage WP. Impact of Host Heterogeneity on the Efficacy of Interventions to Reduce Staphylococcus aureus Carriage. Infect Control Hosp Epidemiol. 2016; 37(2):197–204. https://doi.org/10.1017/ice.2015.269 PMID: 26598029

64. Cobey S, Baskerville EB, Colijn C, Hanage W, Fraser C, Lipsitch M. Host population structure and treatment frequency maintain balancing selection on drug resistance. Journal of The Royal Society Interface. 2017; 14(133):20170295. https://doi.org/10.1098/rsif.2017.0295

65. van Duijkeren E, Ikawaty R, Broekhuizen-Stins MJ, Jansen MD, Spalburg EC, de Neeling AJ, et al. Transmission of methicillin-resistant Staphylococcus aureus strains between different kinds of pig farms. Veterinary Microbiology. 2008; 126(4):383–389. https://doi.org/10.1016/j.vetmic.2007.07.021 PMID: 17765409

66. Gjini E, Valente C, Sá-Leão R, Gomes MGM. How direct competition shapes coexistence and vaccine effects in multi-strain pathogen systems. Journal of Theoretical Biology. 2016; 388:50–60. https://doi.org/10.1016/j.jtbi.2015.09.031 PMID: 26471070

67. Lipsitch M, Colijn C, Cohen T, Hanage WP, Fraser C. No coexistence for free: Neutral null models for multistrain pathogens. Epidemics. 2009; 1(1):2–13. https://doi.org/10.1016/j.epidem.2008.07.001 PMID: 21352747

68. Buendía V, Muñoz MA, Manrubia S. Limited role of spatial self-structuring in emergent trade-offs during pathogen evolution. arXiv:180408463 [q-bio]. 2018;.

69. Sofonea MT, Alizon S, Michalakis Y. Exposing the diversity of multiple infection patterns. Journal of Theoretical Biology. 2017; 419:278–289. https://doi.org/10.1016/j.jtbi.2017.02.011 PMID: 28193485

70. Li M, Rao VD, Gernat T, Dankowicz H. Lifetime-preserving reference models for characterizing spreading dynamics on temporal networks. Scientific Reports. 2018; 8(1):709. https://doi.org/10.1038/s41598-017-18450-3 PMID: 29335422

71. Stanoev A, Trpevski D, Kocarev L. Modeling the Spread of Multiple Concurrent Contagions on Networks. PLOS ONE. 2014; 9(6):e95669. https://doi.org/10.1371/journal.pone.0095669 PMID: 24922541

72. Lauderdale TLY, Wang JT, Lee WS, Huang JH, McDonald LC, Huang IW, et al. Carriage rates of methicillin-resistant *Staphylococcus aureus* (MRSA) depend on anatomic location, the number of sites

cultured, culture methods, and the distribution of clonotypes. Eur J Clin Microbiol Infect Dis. 2010; 29 (12):1553–1559. https://doi.org/10.1007/s10096-010-1042-8 PMID: 20820833

73. Gardiner C. Stochastic Methods: A Handbook for the Natural and Social Sciences. 4th ed. Springer Series in Synergetics. Berlin Heidelberg: Springer-Verlag; 2009.

Supporting Information
Host contact dynamics shapes richness and dominance of pathogen strains

Francesco Pinotti[1], Éric Fleury[2], Didier Guillemot[3], Pierre-Yves Böelle[1], Chiara Poletto[1]

1 Sorbonne Université, INSERM, Institut Pierre Louis d'Épidémiologie et de Santé Publique,Paris,France
2 INRIA, Paris, France
3 Inserm, UVSQ, Institut Pasteur, Université Paris-Saclay, Biostatistics, Biomathematics, Pharmacoepidemiology and Infectious Diseases (B2PHI), Paris, France.

S1 Text: Multi-strain model with heterogeneous recovery classes

In order to test the robustness of our results to the case in which more detailed and realistic ingredients are accounted for, we consider the case in which the recovery rate is heterogeneous across individuals. This mimics a relevant aspect of bacterial colonization, as in e.g. *S. aureus* case. In [1] individuals were subdivided in three main classes with very different carriage duration, i.e. non-carriers, intermittent carriers and persistence carriers. Similarly, we assumed three classes of individuals characterized by different recovery probability per time step, i.e. $\mu^{(1)} = 1$, $\mu^{(2)} = 1.3{\cdot}10^{-3}$ and $\mu^{(3)} = 6.9{\cdot}10^{-4}$. Nodes are distributed in the three classes with probability $p^{(1)} = 0.5$, $p^{(2)} = 0.3$ and $p^{(3)} = 0.2$ [1]. Notice that individuals in the first class recover immediately after a single time step. Recovery rates are chosen so that the average carriage period matches the value used in the main paper.

References

[1] Qiuzhi Chang, Marc Lipsitch, and William P. Hanage. Impact of Host Heterogeneity on the Efficacy of Interventions to Reduce Staphylococcus aureus Carriage. *Infect Control Hosp Epidemiol*, 37(2):197–204, February 2016.

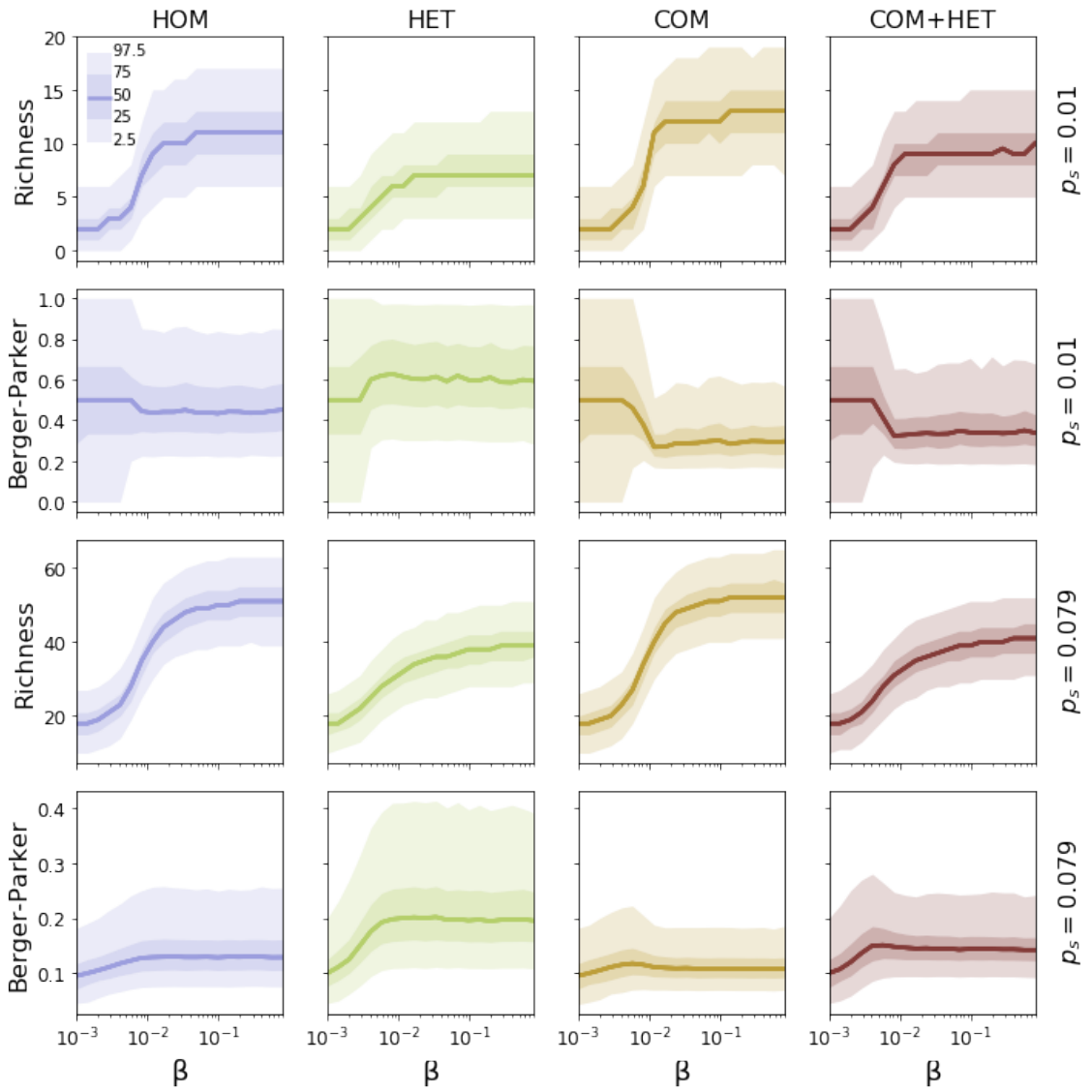

S1 Fig : Richness and Berger-Parker index as a function of transmissibility for HOM, HET, COM and COM+HET models. Each model is displayed on a different column. HET is characterized by activity distribution exponent $\gamma = 0.7$. COM+HET model is simulated using the same activation pattern as in HET with $\gamma = 0.7$ and the same stub-matching procedure as in COM. We consider the case $p_{IN} = 0.99$. The first two rows correspond to $p_s = 0.01$, whereas the last two to $p_s = 0.079$. For each scenario we show the median (solid line), as well as 50% and 95% CI (shaded areas).

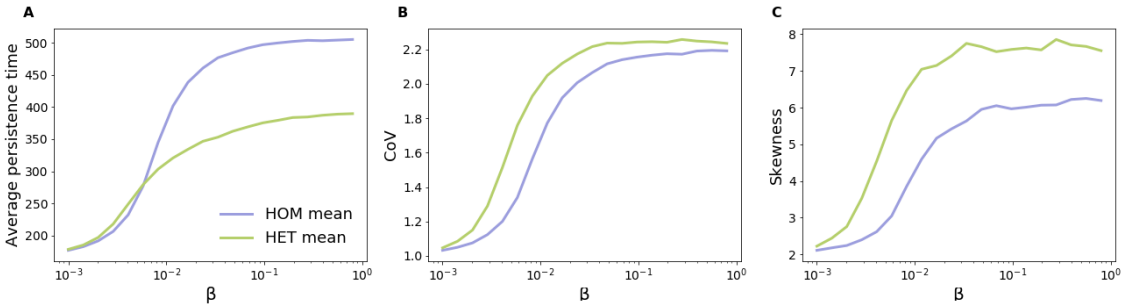

S2 Fig : Summary indicators of the persistence time distribution as a function of transmissibility for both HOM and HET models. HOM and HET are displayed in blue and green respectively. (A), (B) and (C) display distribution's average, coefficient of variation and skewness, respectively. Other parameters are as in Fig 2 in the main text.

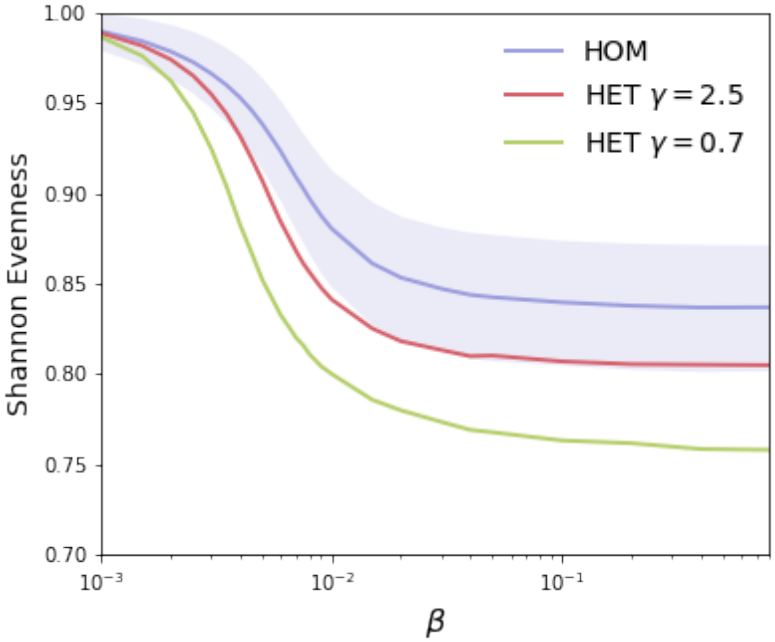

S3 Fig : Shannon Evenness for HOM model and two instances of HET model. HOM is depicted in blue, whereas instances of HET model with activity distribution exponent $\gamma = 2.5$ and $\gamma = 0.7$ are depicted in orange and green respectively. Shaded blue area represents standard deviation for HOM. We introduce the relative abundance of the i-th strain: $n_i = N_i \Big/ \sum_i N_i$, with N_i the abundance of the strain i (i.e. the number of infected with strain i). Shannon evenness is defined as the normalized Shannon entropy $S(\{n_i\}) = -\mathcal{N}^{-1} \sum_i n_i \ln n_i$, with $\mathcal{N} = \ln N_S$. Parameters are the same as in Fig 1 in the main text.

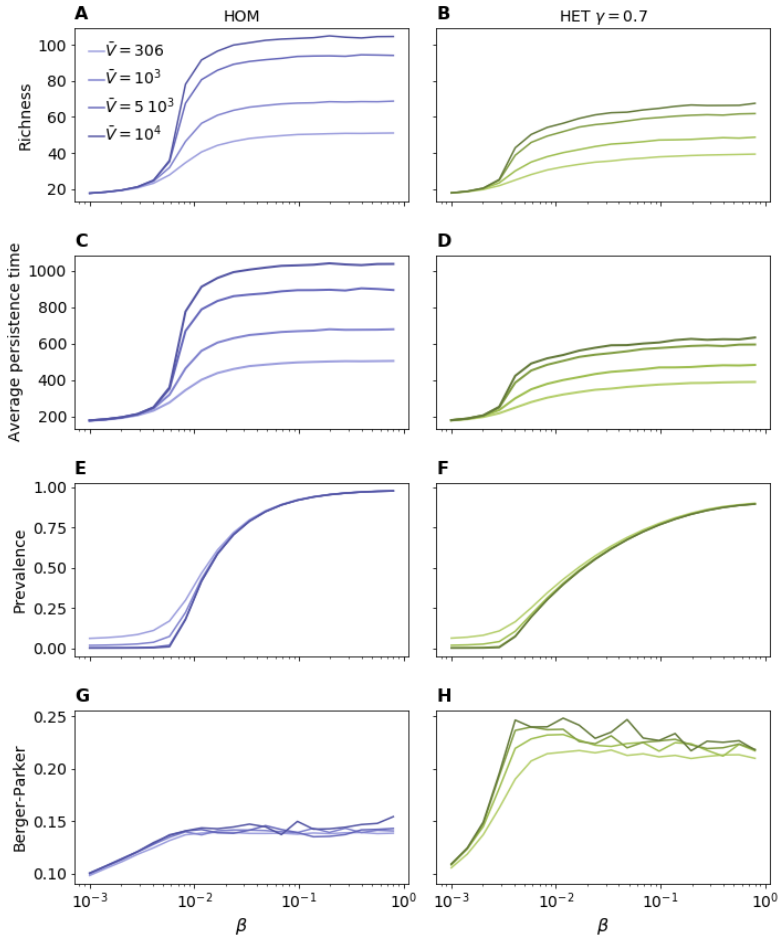

S4 Fig : **Impact of network size.** Richness (A,B), average persistence time (C,D), prevalence (E,F) and Berger-Parker index (G,H) as a function of transmissibility for both HOM and HET models (first and second columns respectively). For each value of $\bar{V}$ we compute p_s to have the strain injection rate, $\bar{V}p_s$, the same across the different networks. Other parameters are as in Fig 2 of the main paper. Increasing network size results in a larger number of co-circulating strains, while the re-scaled prevalence and the Berger-Parker index are almost independent of $\bar{V}$. Notice that increasing network size does not lead to any qualitative change in the relation between HOM and HET.

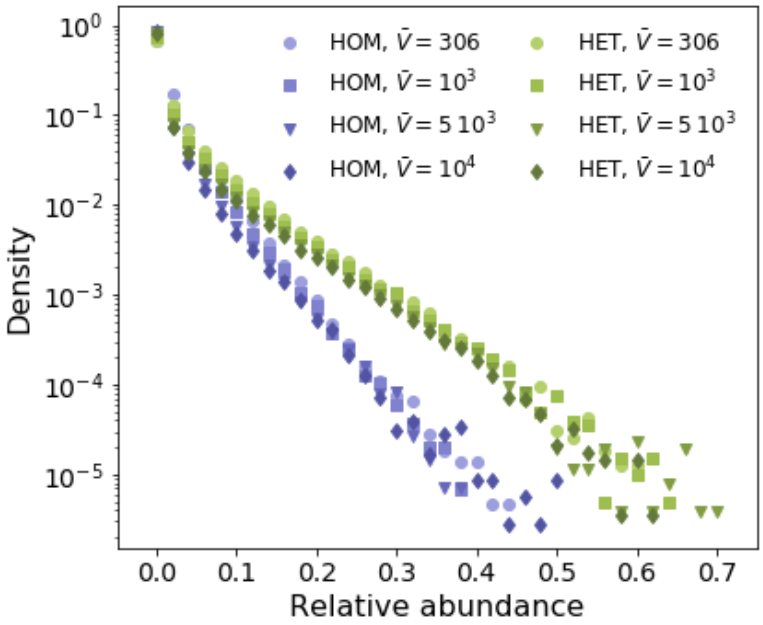

S5 Fig : Relative abundance distribution in varying network size for HOM and HET models. HOM and HET are depicted in blue and green respectively. For each value of $\bar{V}$ we compute p_s to have the strain injection rate, $\bar{V}p_s$, the same across the different networks. Other parameters are as in Fig 2 of the main paper.

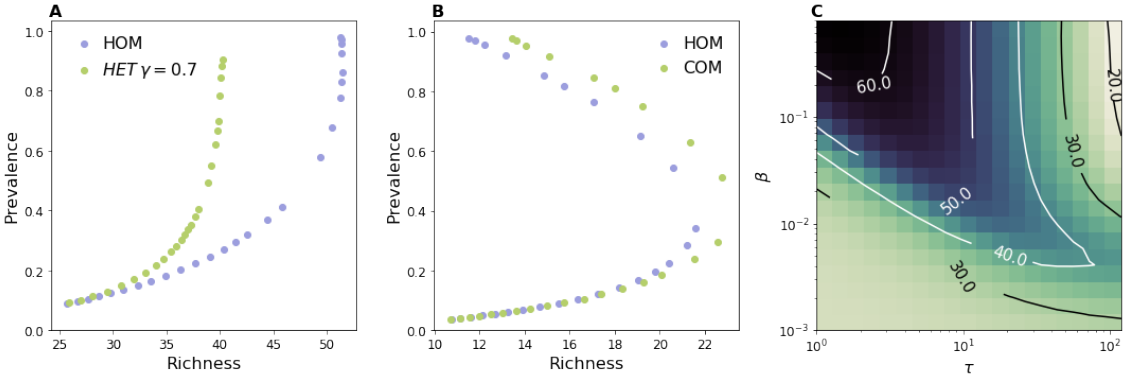

S6 Fig : Richness for the different network models with transmission from an external source. The frequency of transmissions from an external source is tuned by q_s, which we set here to 0.0002. (A) Richness for HOM model (blue markers) and HET model with activity distribution exponent $\gamma = 0.7$ (green markers). Here $p_s = 0.079$. (B) Richness index for HOM model (blue markers) and COM model with within-community connection probability $p_{IN} = 0.99$ (green markers). Here $p_s = 0.01$. (C) Richness as a function of β and τ for HOM model. Here $p_s = 0.079$.

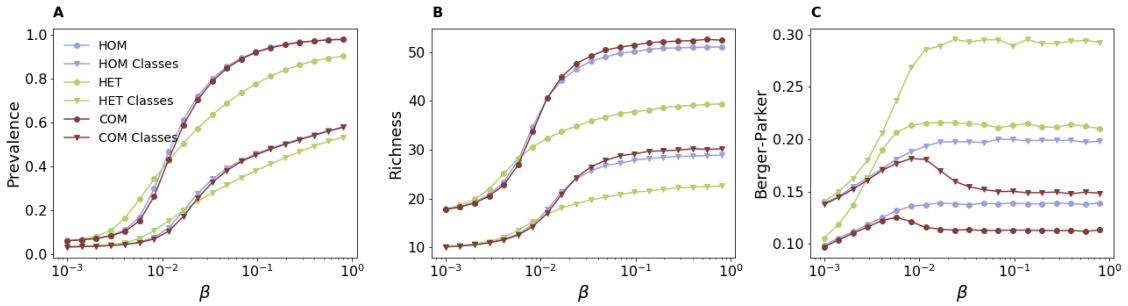

S7 Fig : Multi-strain dynamics when recovery rate is heterogeneous across individuals. Here, each node belongs to one out of three classes according to its recovery rate - see description in the dedicated section of this supporting information. We compare HOM (blue), HET (green), COM (red) models with and without heterogeneity in the recovery rate (triangles and circles respectively). Panels show prevalence (A), richness (B) and Berger-Parker index (C). Other parameters are like in Fig 1, Fig 2 and Fig 3 in the main paper ($\gamma = 0.7$ for HET and $p_{IN} = 0.99$ for COM).

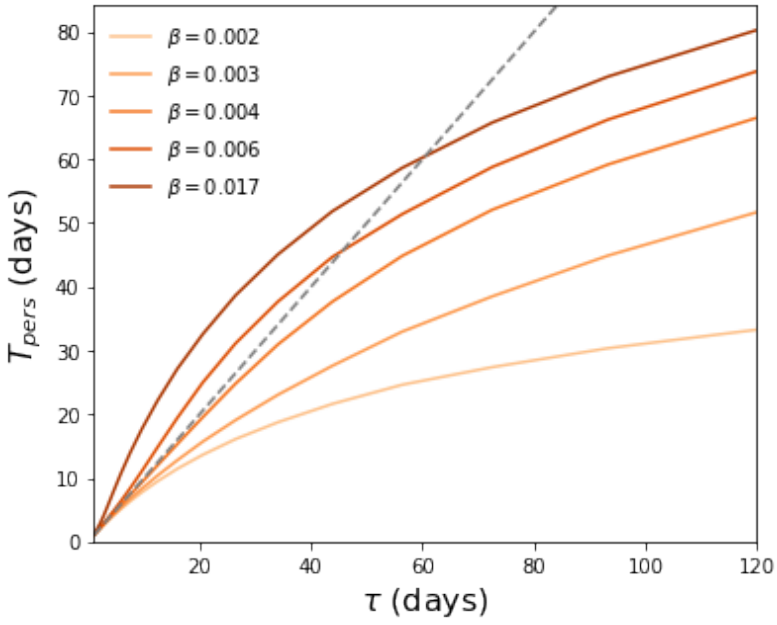

S8 Fig : Average persistence time for HOM in varying transmissibility and length of stay. The quantity is computed from the simulations. The dashed gray line represents a linear trend as a guide to the eye. Parameters are the same as in Fig 4 in the main text.

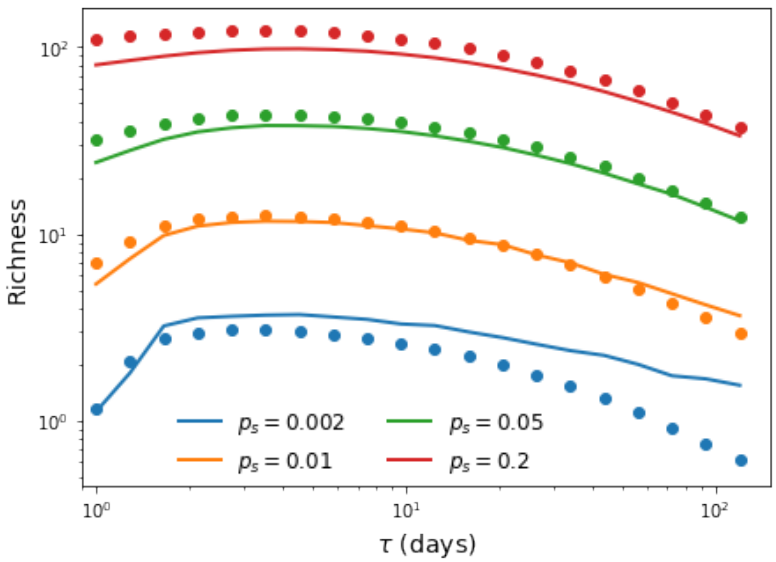

S9 Fig : Comparison between simulations for HOM model and analytical predictions obtained using the Fokker-Planck framework. Solid lines represent average richness obtained by using Eq (1) and Eq (7) from the main text while dots represent simulations results. Here $\beta = 0.04$ while other parameters are the same as in Fig 4 in the main text.

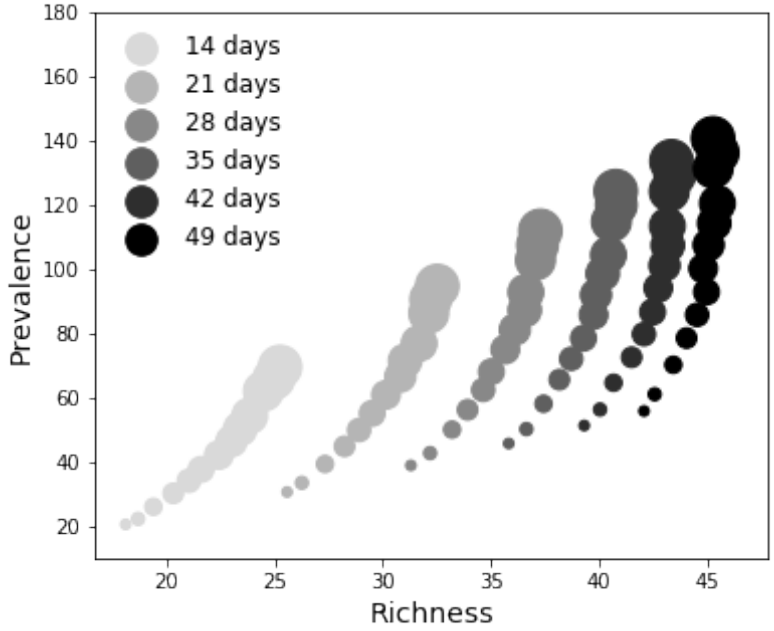

S10 Fig : Prevalence vs richness for several values of the infectious period and using the CPI network. The value of q_s is the same for the curve highlighted in Fig 5B in the main text, $q_s = 0.00018$. Here dot size is proportional to the magnitude of β.

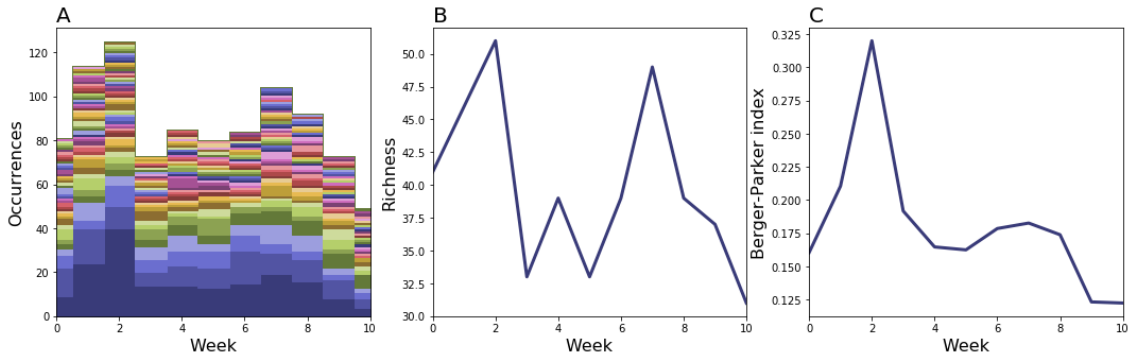

FIGURE 3.1: *S. aureus* **carriage data during the I-Bird study.** (A) Weekly number of carriers associated to each *S. aureus* strain. Each color corresponds to a different strain; all time series have been stacked together. (B) Weekly richness. (C) Weekly Berger-Parker index.

3.5 Additional results: neutral dynamics

3.5.1 Domination time and attack rate

In Section 3.4 we characterized strain ecosystems in terms of diversity measures, including species richness and Berger-Parker index. In this section we investigate the statistics of additional ecological measures in order to better understand the role of contact heterogeneities on diversity in synthetic contact networks.

In particular, we considered the domination time T_{dom}, defined as the time spent by a given strain at the top of the abundance ranking, and the attack rate AR, defined as the number of cases generated by a given strain during its whole lifespan. In other words, AR represents the cumulative incidence of a particular strain. Fig. 3.2 A, B, C show respectively the average value, the standard deviation and the coefficient of variation (CoV) of T_{dom} as a function of transmissibility. Remarkably, the average domination time displays a minimum in correspondence of the epidemic threshold for both HOM and HET, as shown in Fig. 3.2 A. We also notice that T_{dom} is on average larger in HET compared to HOM. At the same time, however, the average attack rate is smaller in HET compared to HOM (Fig. 3.2 D). These two results provide further support to our hypothesis about the twofold role played by hubs. On one hand, hubs act as super-spreaders, boosting the spread of certain strains and favoring dominance. On the other hand, they act as super-blockers towards incoming strains, hence the smaller average attack rate. Our conclusions are further confirmed by the distributions of both T_{dom} and AR which, as evidenced by Fig. 3.2 B,C,E,F, display larger variability in HET compared to HOM. The increased variability in the number of cases in HET reflects observed dominance patterns: a few dominant strains are able to generate many cases while the majority of them hardly generates even a single case. The larger fraction of strains generating none or very few cases explains also the smaller average number of cases observed in HET.

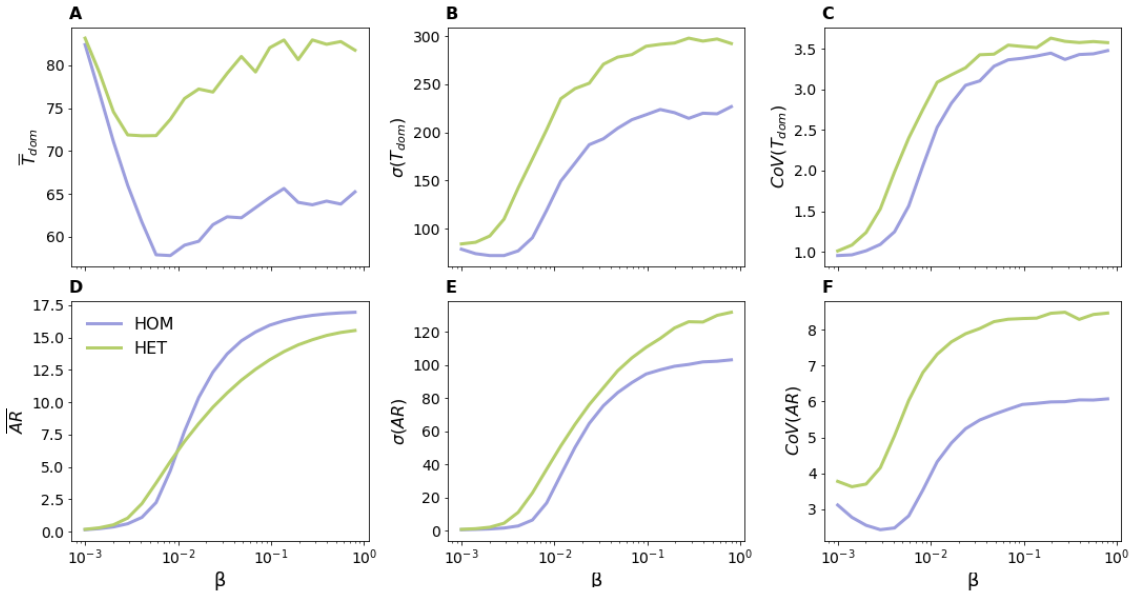

FIGURE 3.2: **Domination time and attack rate statistics.** (A-C) show the average value, standard deviation and coefficient of variation of the domination time T_{dom} for HOM (blue) and HET (green) as a function of transmissibility. (D-F) show the average value, standard deviation and coefficient of variation of the attack rate AR. Parameters are the same as in Fig. 1 of the main paper, reported in Section 3.4.

3.5.2 Impact of bursty contacts on strain diversity

As seen in Chapter 2, individual contact sequences extracted from empirical contact networks usually display bursty behavior. HOM and HET models, which were introduced in Section 3.4, result however in individual ICT sequences that are geometrically distributed.

Here we assess the impact of bursty contact behavior on strain ecology by introducing a general family of generative models which includes HOM and HET as particular cases. The generative algorithm is akin to that introduced in [244] and requires the ICT distribution to be specified a priori. In practice, once a node activates its next ICT is drawn from a distribution $P_{ICT}(t)$. HOM and HET correspond both to a geometric ICT distribution; however, while in HOM all nodes share the same activity potential, in HET the latter is heterogeneous.

We introduce the model BURSTY, which is characterized by a heterogeneous ICT distribution $P_{ICT}(t) = C_0 t^{-\omega}$ with $t \in [1, \dots, t_{max}]$. In order to make a fair comparison with HOM model, we require that BURSTY and HOM share the same average fraction of active nodes or, equivalently, the same average activation probability. We achieve this by first setting the values of C_0, ω and t_{max} such that BURSTY and HOM share the same average ICT (P_{ICT} needs also to be correctly normalized). We thus require that:

$$\bar{t} = \sum_t t P_{ICT}(t) = a_H^{-1} . \tag{3.2}$$

If the population was not affected by turnover, Eq. (3.2) would also guarantee, after an

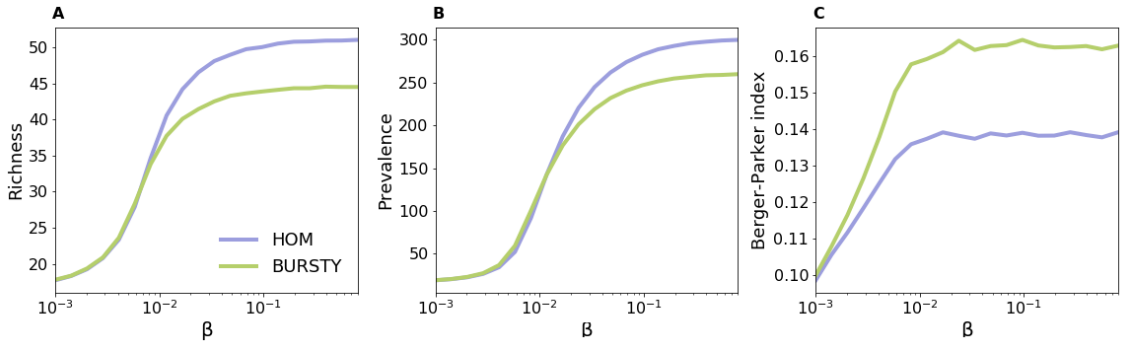

FIGURE 3.3: **Comparison between HOM and BURSTY models.** Here we consider an instance of BURSTY with $t_{max} = 1000$ and $\omega = 2.1$. Here we compare HOM (blue) and BURSTY (green) in terms of (A) richness, (B) prevalence and (C) Berger-Parker index. Other parameters are the same as in Fig. 1 of the main paper, reported in Section 3.4.

initial transient, equality between BURSTY's and HOM's average activation probabilities. Indeed, in BURSTY one needs to wait individual activity sequences to equilibrate in order to identify the average activation probability with $\bar{t}$. In HOM, instead, the activation probability is always identically equal to a_H because of the memoryless property of the geometric distribution. However, equilibration cannot occur in BURSTY as far as node turnover is concerned. Specifically, because each node is removed after τ time steps on average, individual activity sequences do not have "enough time" to equilibrate.

A possible solution is to assume that each individual activity sequence is already at equilibrium when the corresponding node joins the network. We can ensure equilibrium at all times by slightly modifying the generative algorithm: when a new node joins the network, we sample its very first ICT from the (equilibrium) waiting time distribution $P^w_{ICT}(t)$ rather than from P_{ICT} [302]. The waiting time is defined as the time interval between current time and the next activation, and its distribution is given by:

$$P^w_{ICT}(t) = \frac{\sum_{t'=t+1}^{\infty} P_{ICT}(t')}{\bar{t}}\,, \tag{3.3}$$

successive ICTs are instead sampled from P_{ICT} as usual. This recipe guarantees that the fraction of active nodes in the network is equal to $\bar{t}^{-1}$ at all times, irrespective of node turnover. Note that this algorithm is valid for any desired P_{ICT}, not only for the one used in BURSTY. For the case of HOM and HET models, where each node's ICT distribution is geometric (given its activity potential a), we have for example that $P^w_{ICT}(t|a) = P_{ICT}(t|a)$.

In Fig. 3.3 we compare HOM and BURSTY. We find that burstiness has a similar effect to that of activity heterogeneities in that they both lower prevalence and richness while increasing the Berger-Parker index.

3.6 Additional results: non-neutral dynamics

3.6.1 Simulation results

So far we have assumed that the dynamics is neutral, i.e. that all strains share the same epidemiological parameters. In this section we present preliminary results about the case of strains differing in terms of transmissibility. The modeling framework is essentially the same as the one considered so far in this chapter (see Appendix A), except for the number of strains, which is now assumed to be finite. More precisely, we consider a finite pool of S strains whose transmissibilities β_i, $i = 1, \ldots, S$ are identically and independently distributed Gaussian random variables with mean β_0 and variance σ^2 (eventually truncated in the range $[0, 1]$). The neutral case is recovered by setting $\sigma = 0$. Transmissibilities are sampled only once at the beginning of each simulation. Once a new individual is admitted, it has a probability p_s to be already carrying a strain, which is chosen at random from the pool.

We performed extensive numerical simulations on both homogeneous and heterogeneous synthetic contact networks (see Appendix B for a definition of contact networks considered here) and for increasing magnitude of fitness heterogeneities σ. Remarkably, we found that the strain ecosystem displays two different regimes according to σ. Below a critical value σ_c, macro-ecological indicators such as total prevalence, richness and Berger-Parker index are essentially independent from σ. However, as soon as σ crosses a critical value σ_c the ecosystem undergoes a "condensation" phenomenon where a highly transmissible strain becomes dominant by acquiring a finite fraction of total prevalence. This is evidenced by the Berger-Parker index, which sharply increases as σ is increased past σ_c. We denote the critical value σ_c as the condensation threshold.

In Fig. 3.4 we show the average Berger-Parker index for both homogeneous and heterogeneous contact networks as a function of β_0 and σ/β_0 and for several values of the injection probability. The Berger-Parker index is almost constant for σ smaller than σ_c (white dots), while it increases sharply right after such critical value.

We also observe that heterogeneous contact networks provide a lower condensation threshold compared to the homogeneous scenario. Thus, contact heterogeneities not only promote dominance in the neutral scenario but also promote the transition to the condensed regime.

3.6.2 Analytical derivation of the condensation threshold

Here we provide a mathematical derivation of the condensation threshold. For the sake of clarity, we consider here the case of random mixing. The general derivation for a larger class of synthetic contact structures can be found in Appendix B.

We begin by partitioning strains in classes according to their transmissibility. We thus define the density $I(\beta, t)$ of infectious individuals carrying strains with transmissibility in the range $[\beta, \beta + d\beta]$. This quantity evolves in time according to:

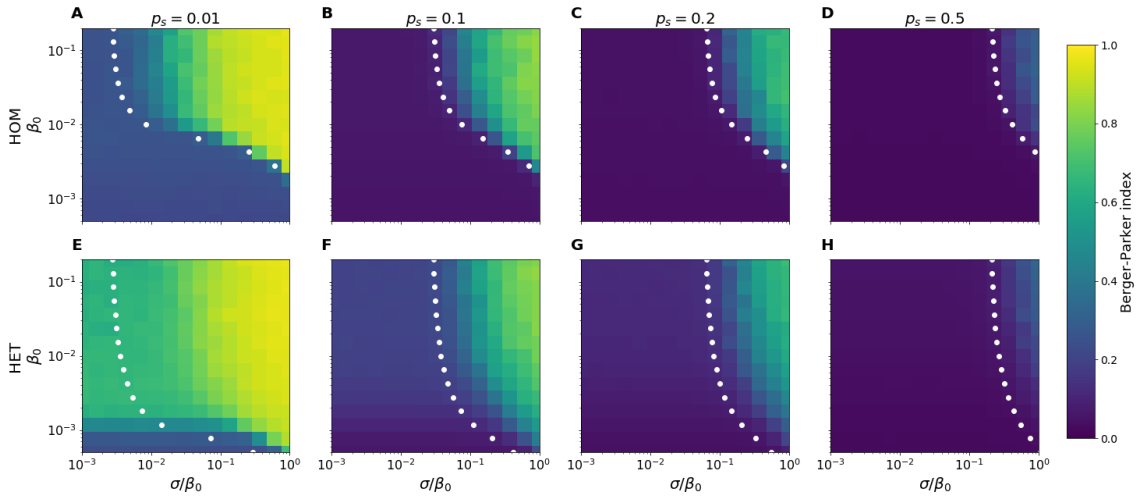

FIGURE 3.4: **Berger-Parker index and the condensation phenomenon.** Berger-Parker index for homogeneous (first row) and heterogeneous (second row) contact networks; details about both networks can be found in Appendix B. Each column corresponds to a different value of p_s. The white dotted line corresponds to the condensation threshold obtained from Eq. (B.12). Parameters: $S = 100$, $\mu^{-1} = 21$ Days, $\tau = 10$ Days. The average activity is $a_H = 0.3$, while the average degree of active nodes is $\tilde{k} = 3$.

$$\frac{d}{dt} I(\beta, t) = \lambda_{in} p_s \rho(\beta) - (\lambda_{out} + \mu) I(\beta, t) + \beta \bar{k} S(t) I(\beta, t) \,, \tag{3.4}$$

where $S(t) = 1 - \int d\beta \, I(\beta, t)$ is the fraction of susceptible individuals. By introducing the dimensionless quantities $\alpha = \lambda_{in} p_s / (\lambda_{out} + \mu)$ and $\omega = \beta \bar{k} / (\lambda_{out} + \mu)$ and by setting the left hand side of Eq. (3.4) to zero, we obtain a set of equations satisfied by the stationary distribution $I(\beta)$:

$$\alpha \rho(\beta) - I(\beta) + \omega S I(\beta) = 0 \,, \tag{3.5}$$

which admits the solution:

$$I(\beta) = \frac{\alpha \rho(\beta)}{1 - \omega(1 - I)} \,. \tag{3.6}$$

By integrating over β we obtain a self-consistence condition that implicitly determines total prevalence:

$$I = \int d\beta I(\beta) = \int d\beta \, \frac{\alpha \rho(\beta)}{1 - \omega(1 - I)} \,. \tag{3.7}$$

The quantity $I(\beta)$ represents the probability that a randomly selected infected individual is carrying a strain with transmissibility β. Therefore $I(\beta)$ can be regarded as the "sampling" distribution. As a consequence of the denominator in Eq. (3.6), $I(\beta)$ is in general different from the input distribution $\rho(\beta)$.

The expression (3.6) for $I(\beta)$ is not new to physicists. In fact, it closely resembles the Bose-Einstein distribution from quantum physics, which describes the statistics of

a gas of bosonic particles. In recent years, the Bose-Einstein distribution has found applications also in theoretical ecology. In particular, it was found to emerge in models of competing species [303], epistasis [304, 305], quasi-species evolution [306, 307, 308, 309] and influenza evolution [309]. The phenomenology presented here is reminiscent of the concept of quasi-species in population genetics. According to this analogy, in the $\sigma < \sigma_c$ regime the pathogen exists as a quasi-species, i.e. as a "cloud" of different strains maintained by the balance between immigration and selection. In this context, the condensation threshold parallels the error threshold concept: as $\sigma > \sigma_c$, immigration cannot balance selection anymore and the quasi-species breaks down in favor of a super-fit strain, eventually accompanied by rarer, less fit immigrant strains.

The main feature of the Bose-Einstein distribution, inherited also by Eq. (3.6), is the existence of a condensed phase. The latter appears for values of σ larger than some crossover value σ_c, i.e. the aforementioned condensation threshold. In order to see this and to determine σ_c, we first notice that the denominator in Eq. (3.6) becomes negative for $\omega > 1/(1-I)$. For $\sigma < \sigma_c$ this is not a problem since the bulk of the input distribution is concentrated far away from such singularity. For $\sigma > \sigma_c$, however, a significant portion of $\rho(\beta)$ lies beyond the singularity and Eq. (3.6) loses its validity because $I(\beta)$ cannot be negative. We may thus estimate σ_c by asking when the tail of the input distribution extends "too much" beyond the singularity in Eq. (3.6). Mathematically, we find σ_c by requiring that the maximum transmissibility over a sample of S strains is on average equal to $(\mu + \lambda_{out})/\bar{k}(1-I)$:

$$\langle \beta_{max} \rangle_S = \frac{\mu + \lambda_{out}}{\bar{k}(1-I)} \,. \tag{3.8}$$

Because transmissibility values are sampled from a Gaussian distribution with average β_0 and variance σ^2, we can write:

$$\langle \beta_{max} \rangle = \beta_0 + \sigma \eta(S) \,, \tag{3.9}$$

where $\eta(S)$ is the average maximum of S independent Gaussian random variables with zero mean and unit variance. Note that, in principle, I depends on σ as well; in practice, however, numerical simulations reveal that I varies slowly with σ within the highly diverse regime. This means that we can obtain a good approximation for σ_c by substituting I with its counterpart I_0 obtained in the purely neutral case (i.e. $\sigma = 0$):

$$I_0 = \frac{\omega_0 - 1 + \sqrt{(\omega_0 - 1)^2 + 4\omega_0}}{2\omega_0} \,, \tag{3.10}$$

where $\omega_0 = \beta_0 \bar{k}/(\mu + \lambda_{out})$. By combining Eqs. (3.8), (3.10) and (3.9), we finally obtain an explicit formula for the condensation threshold:

$$\frac{\sigma_c}{\beta_0} = \frac{1}{\eta(S)} \left(\frac{2}{\omega_0 + 1 - \sqrt{(\omega_0 - 1)^2 + 4\omega_0}} - 1 \right) . \tag{3.11}$$

The dependence on the number of strains S is monotonic decreasing since $\eta(S)$ increases monotonically with S, albeit slowly (asymptotically, $\eta(S) \sim \sqrt{2log(S)}$). This has to be expected since the larger S the larger the chances that a highly transmissible strain appears.

3.6.3 Numerical characterization of the $\sigma < \sigma_c$ regime

The previous analysis reveals that the Berger-Parker index's qualitative behavior differs on the two sides of the condensation threshold. Indeed, for $\sigma < \sigma_c$ the Berger-Parker index is almost constant, whereas as soon as σ crosses σ_c it sharply increases (see Fig. 3.5 A). We interpreted this behavior as the consequence of the "sudden" appearance, for values of σ larger than σ_c, of a dominant strain with high transmissibility.

We found, both numerically and analytically, that the condensation phenomenon arises from the interplay of competition and immigration strength. On one hand, the external strain pool seeks to impose its own distribution for β (i.e. $\rho(\beta)$) on the meta-community. On the other hand, competition for hosts selects those strains with larger fitness. For $\sigma > \sigma_c$ immigration cannot keep up anymore against selection and a dominant strain suddenly appears. It may be, however, that other ecological quantities do not change suddenly at σ_c as the Berger-Parker index does. Perhaps there exist ecological indicators that vary smoothly as σ is increased, bearing signatures of increased selection.

Here, we considered several additional indicators in order to better characterize the strain ecosystem as σ is varied. First, we computed the average excess transmissibility $\bar{\beta}_{exc}$, which is defined as:

$$\bar{\beta}_{exc} = \frac{\bar{\beta} - \beta_0}{\beta_0}, \tag{3.12}$$

where $\bar{\beta} = \int d\beta\, \beta I(\beta)$ is the average sampled transmissibility. We expect $\bar{\beta}_{exc}$ to be small in the $\sigma < \sigma_c$ regime and large in the condensed regime. We see from Fig. 3.5 B that $\bar{\beta}_{exc}$ is indeed small in the highly-diverse phase and its behavior is similar to that of the Berger-Parker index, shown in Fig. 3.5 A.

Next, we computed how much the input distribution $\rho(\beta)$ differs from the sampling distribution $I(\beta)$ in terms of their Kolmogorov-Smirnov distance. The Kolmogorov-Sminov distance behaves smoothly as a function of σ and it is non-null even in the $\sigma < \sigma_c$ regime, as can be seen from Fig. 3.5 C. This means that the sampling distribution $I(\beta)$ carries a significant amount of information about selective forces at play. Nonetheless, using just its average value discounts most of this information, as evidenced by the analysis of $\bar{\beta}_{exc}$.

Finally, we checked whether there is a statistical correlation between the domination time and the transmissibility of the strain at the top of the abundance ranking. Intuitively, we expect a positive correlation between these two quantities since strains with larger transmissibility tend to create more cases. The Spearman rank-order correlation coefficient between domination time and transmissibility indeed indicates a positive correlation, as shown in Fig. 3.5 D. Additionally, the correlation coefficient behaves smoothly

with σ, reaching relatively large values even in the $\sigma < \sigma_c$ regime. Correlation values for larger values of σ are not shown since it is difficult to obtain large samples when the same strain is always dominating.

3.7 Conclusions

In this chapter we investigated the dynamics of multiple strains competing for hosts through mutual exclusion. We adopted an ecological approach, considering an open host population subject to importation of new strains from the community. We explicitly accounted for host-to-host contacts by modeling the host population as a time-varying network. We showed that contact dynamics plays an important role in shaping strain ecology; in particular, we showed that contact heterogeneities, arising from, e.g., activity heterogeneities or from bursty contact behavior, reduce strain diversity, favoring dominance of a few strains even in a neutral scenario. In the case of heterogeneous activity, hubs are responsible for the loss of diversity, boosting the spread of some strains while hampering the spread of newly introduced strains. Community structure had the opposite effect on diversity, although the magnitude of such contribution was found to be marginal. Heterogeneities in strain transmissibility did not alter ecological indicators if sufficiently small in strength. Above a certain threshold, however, we observed a condensation phenomenon where a dominant super-fit strain secures a large finite fraction of infected hosts.

Our results advocate for the importance of host-to-host contacts in shaping strain diversity and warn against interpretations of ecological patterns relying on random-mixing models. Further theoretical research and data analysis are needed in order to better understand the bias introduced by overlooking contact heterogeneities.

Our modeling framework may shed light on ecological questions that, up until now, have been usually addressed in the context of two-strain models. For example, the problem of ecological diversity in large strain communities parallels the problem of co-existence in two-strain systems. On one hand, this link suggests that mechanisms that boost co-existence between two strains might also promote diversity in multi-strain models. On the other hand, however, future research should deal with framing the large body of results arising from two-strain models in the context of strain community dynamics.

A similar ecological perspective might be applied to pathogens other than *S. aureus*, e.g. HPV, *S. pneumoniae*, *N. meningitidis*. In this context, more tailored models are required to describe each specific case. In the case of *S. pneumoniae*, for example, cross-immunity between different strains must be accounted for, whereas in the case of HPV co-infection with multiple types must be allowed, in agreement with empirical observations.

Recruitment of new strains into the population can be driven by mechanisms other than immigration, e.g. mutation and recombination. This is especially true for viral species such as influenza, whose seasonal dynamics is driven by cumulative mutations that enable influenza to continually escape host immunity. When considering longer time horizons, mutation and recombination should be included as well when modeling

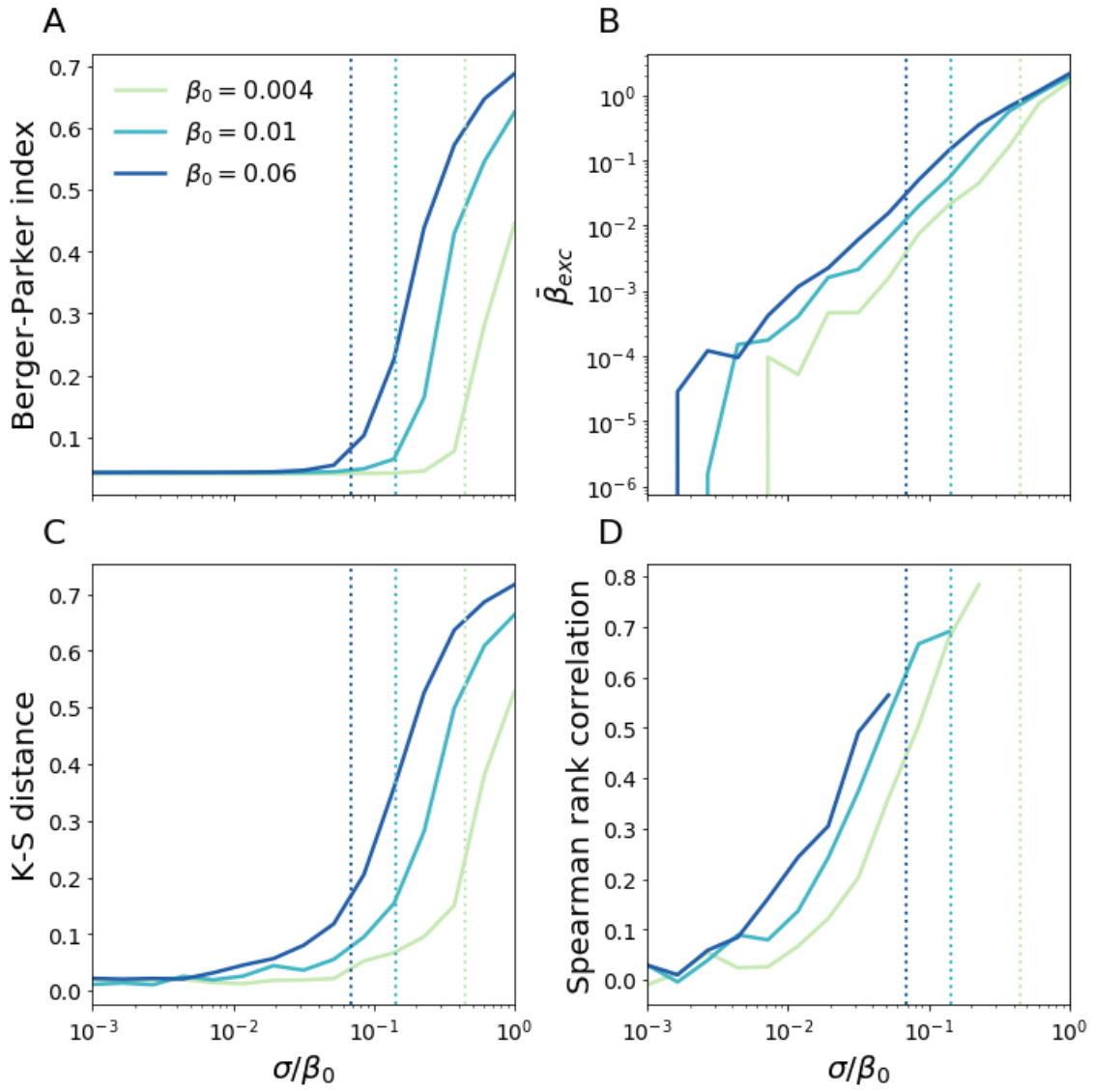

FIGURE 3.5: **Additional ecological indicators.** (A) Berger-Parker index, (B) average excess transmissibility, (C) Kolmogorov-Sminov distance between $\rho(\beta)$ and $I(\beta)$, (D) Spearman rank-order correlation coefficient between domination time and the transmissibility of the dominant strain for three different values of β_0. Simulations are carried using HOM contact network. Dashed lines correspond to the analytical condensation threshold obtained using Eq. (3.11) for each value of β_0. Parameters: $S = 100$, $p_s = 0.2$, $\mu^{-1} = 21$ Days, $\tau = 10$ Days, $a_H = 0.3$, $\tilde{k} = 3$.

the spread of bacteria. These processes can be either neutral from the point of view of the mutant's fitness, or they may confer new traits, e.g. drug resistance.

Chapter 4

The Interplay of Cooperative and Competitive Interactions

4.1 Introduction

In Chapter 3 we focused on the impact of environmental and host-related factors on the dynamics of competing strains. However, co-circulating pathogens might interfere with strain dynamics, altering the outcome of competition. The presence of an additional pathogen may for example cross-regulate the host population through increased mortality or modify the local immunological landscape [28]. Typically, however, interactions between different pathogens or between strains of the same pathogen have been studied separately, making it difficult to draw conclusions about effects of other pathogens on strain diversity. Additionally, non-trivial effects arising from the interplay of diverse interactions might be missed if the latter are treated in isolation.

Synergistic pathogen-pathogen interactions have been observed in several multi-pathogen systems. For example, the current TB-HIV epidemics that is ravaging Sub-Saharan Africa is fueled by the synergy between HIV and Tuberculosis [89]. Immunocompromised individuals carrying HIV are more vulnerable to other pathogens as well, including *P. falciparum* [310] and HPV [311]. Analogously, influenza favors secondary bacterial infections, affecting the spread and burden of *S. pneumoniae* [312, 85].

In this chapter we investigate the interplay between competitive and cooperative interactions in a simple model with two cooperative pathogens, one of which is further structured in two strains that compete through mutual exclusion. Cooperation is mediated by increased susceptibility towards secondary infections. In the second paper associated to this thesis [2] we investigate this model both numerically and analytically, and find that the presence of a cooperative pathogen fundamentally alters competition between strains, leading to a complex phase diagram. In some cases, our model leads to seemingly paradoxical behavior; for example, we find that increasing the cooperative ability of the more transmissible strain can result in its extinction. We find that spatial structure plays an important role. More in detail, we show by means of numerical simulations that spatial separation can support population-level co-existence of both competing strains by creating ecological niches. We show that the latter arise dynamically and select for different trade-offs between transmissibility and cooperative ability.

This chapter is structured as follows: in Section 4.2 we give an overview of multi-pathogen, multi-strain systems where multiple interaction types are simultaneously at play. In Section 4.3 we discuss the role of spatial separation on co-existence of competing strains in spatially structured populations. Section 4.4 contains the second article associated to this thesis.

4.2 Pathogen-pathogen interactions and their impact on multi-strain ecosystems

Several studies highlighted the potential role of pathogen-pathogen interactions in shaping strain diversity. A paradigmatic example is represented by HIV and TB. As seen in Chapter 1, Sub-Saharan Africa has been recently experiencing a joint TB-HIV epidemics [89]. HIV exacerbates almost every aspect of TB infections, increases the risk of TB acquisition and speeds up re-activation of latent TB infections [90]. HIV has been suggested to have played a role in the emergence of Multi-Drug Resistant TB (MDR-TB). Authors in [313] hypothesized that the positive association between HIV and increased risk of mixed infections with multiple TB strains [314] might promote de novo mutations conferring resistance. Antibiotic treatment would then purge non-resistant variants and select for resistant strains.

HIV is known to share a synergy with other pathogens as well. For example, there exists compelling evidence suggesting that HIV interacts with HPV in multiple ways [311]. HIV-positive individuals are at higher risk of acquiring HPV and experience more persistent HPV infections compared to HIV-negative individuals [315, 316]. HPV may in turn increase susceptibility to HIV by weakening the epithelial barrier in the genital tract [317, 318]. HIV is known to co-operate also with vector-borne pathogens such as *Plasmodium falciparum*: HIV increases susceptibility to *P. falciparum* while the latter favors HIV transmission by increasing the viral load of the latter [319, 320, 321, 322, 310]. Such synergy with HIV may affect diversity in *P. falciparum* strains, which are known to compete for the same within-host resources, e.g. red blood cells [323].

As discussed in Chapter 1, the ecology of *S. pneumoniae* is an important factor that must be accounted for in order to design efficient pneumococcal vaccines. At the same time, the reasons behind co-existence patters of multiple *S. pneumoniae* serotypes are not completely understood. Nasopharyngeal colonization with *S. pneumoniae* is known to be affected by other commensal bacteria inhabiting the nasopharynx [324]. While a few bacterial species invariably harm *S. pneumoniae*, e.g. *S. aureus*, other bacteria share a synergy with pneumococcus. *H. influenzae* is known for example to both compete and cooperate with *S. pneumoniae*. Competition has been attributed to *H. influenzae* triggering an innate immune response against *S. pneumoniae* in a serotype-specific manner. The population-level effects of such mechanism on serotype diversity have been investigated in [28]; in particular, serotype-specific interference by *H. influenzae* was suggested to promote co-existence and diversity of *S. pneumoniae* strain populations by favoring clearance of those

serotypes with longer carriage duration, effectively reducing their competitive advantage. Nonetheless, several studies report a positive association between *H. influenzae* and *S. pneumoniae* nasal colonization [325, 326, 327, 328]. *S. pneumoniae* and *H. influenzae* have been found to participate to multi-species biofilm formation, which benefits pneumococcus in that it provides passive protection against antibiotics [329, 330].

Positive interactions between viral pathogens could also affect diversity of bacteria colonizing the nasopharynx [85]. Influenza is known for example to enhance the adhrence of *S. pneumoniae* and *N. meningitidis* to epithelial cells, thus increasing host susceptibility to bacterial colonization. Moreover, influenza infections appear to promote the progression of *S. pneumoniae* carriage to disease [331, 332]. Indeed, several works suggest that influenza-like illnesses are among drivers of seasonal patterns and increased burden of pneumococcal disease [333, 334, 312, 335].

4.3 Factors affecting co-existence between multiple strains

Two strains that compete for the same set of susceptible hosts through complete mutual exclusion cannot coexist in the same host population. More in detail, the strain with the largest fitness value, i.e. with the largest R_0, becomes dominant and drives its competitors to extinction, as discussed in Chapter 1. Co-existence is however possible under certain conditions, e.g. in the case of weak mixing between different host groups [23] and heterogeneous carriage duration [26]. Very few studies addressed the role of additional pathogens on strains' co-existence [28]. Here, we find that co-existence is not possible in a homogeneously-mixed population even in the presence of the cooperative pathogen – under the assumption that the amount of increased susceptiblity between A and each B strain is symmetric –. Instead, competing strains are found to co-exist when host population is structured in different communities. Interestingly, co-existence does not result from spatial structure or cooperation alone, but rather from the interplay of these two ingredients. To better understand this result in the context of the literature we review here previous works on multi-strain competition in a spatially-structured environment.

Spatial separation might be accounted for by subdividing hosts into different communities [260]. Sparse connections between different communities reflect geographical distance between different host groups.

Spatial models are usually classified as either homogeneous or heterogeneous [336]. In the former case, both disease- and host-related parameters are assumed to be uniform in space, whereas in the latter case they may vary from one location to the other. Spatial heterogeneities might reflect for example varying levels of ecological adaptation to different communities. Insights from community ecology reveal that spatially homogeneous models can yield co-existence between multiple species thanks to trade-offs between competitive and dispersal abilities [336]. However, competition for the same resource prevents any of these trade-offs. As a consequence, spatially homogeneous models cannot allow for co-existence of mutually-excluding strains. Authors in [260] showed

that community structure is inefficient at maintaining spatial diversity of cross-reacting strains, suggesting the presence of some degree of local adaptation.

Spatial heterogeneities in epidemiological parameters may guarantee coexistence by allowing for the presence of multiple spatial niches where strains can locally out-compete each other. Authors in [337] have considered for example the case of two competing strains in two patches with hosts diffusing between patches. By engineering the values of epidemiological parameters within each patch, persistence of both strains can be achieved. However, if hosts do not diffuse between patches, co-existence arises only globally, as each patch becomes occupied by only one strain. It can be shown that coexistence at the level of single patches becomes possible if infected individuals are allowed to disperse between patches. A similar result has been obtained by authors in [338], who studied competition between two vector-borne pathogens in a multi-patch environment.

4.4 Second article: Interplay between competitive and cooperative interactions in a three-player pathogen system

Interplay between competitive and cooperative interactions in a three-player pathogen system

Francesco Pinotti[1], Fakhteh Ghanbarnejad[2,3,4], Philipp Hövel[2,5], and Chiara Poletto[1,*]

[1]INSERM, Sorbonne Université, Institut Pierre Louis d'Épidémiologie et de Santé Publique, IPLESP, F75012, Paris, France
[2]Institut für Theoretische Physik, Technische Universität Berlin, Hardenbergstraße 36, 10623 Berlin, Germany
[3]The Abdus Salam International Centre for Theoretical Physics (ICTP), Trieste, Italy
[4]Physics Department, Sharif University of Technology, P.O. Box 11165-9161, Tehran, Iran
[5]School of Mathematical Sciences, University College Cork, Western Road, Cork T12 XF62, Ireland
[*]chiara.poletto@inserm.fr

Abstract

In ecological systems heterogeneous interactions between pathogens take place simultaneously. This occurs, for instance, when two pathogens cooperate, while at the same time multiple strains of these pathogens co-circulate and compete. Notable examples include the cooperation of HIV with antibiotic-resistant and susceptible strains of tuberculosis, or some respiratory infections with *Streptococcus pneumoniae* strains. Models focusing on competition or cooperation separately fail to describe how these concurrent interactions shape the epidemiology of such diseases. We studied this problem considering two cooperating pathogens, where one pathogen is further structured in two strains. The spreading follows a susceptible-infected-susceptible process and the strains differ in transmissibility and extent of cooperation with the other pathogen. We combined a mean-field stability analysis with stochastic simulations on networks considering both well-mixed and structured populations. We observed the emergence of a complex phase diagram, where the conditions for the less transmissible, but more cooperative strain to dominate are non-trivial, e.g. non-monotonic boundaries and bistability. Coupled with community structure, the presence of the cooperative pathogen enables the co-existence between strains by breaking the spatial symmetry

and dynamically creating different ecological niches. These results shed light on ecological mechanisms that may impact the epidemiology of diseases of public health concern.

1 Introduction

Pathogens do not spread independently. Instead, they are embedded in a larger ecosystem that is characterised by a complex web of interactions among constituent elements. Among ecological forces shaping such ecosystems, pathogen-pathogen interactions have drawn increasing attention during recent years due to their population-level impact and public health consequences. Recent advances in serological tests and genotyping techniques have improved our reconstruction of pathogen populations where multiple strains co-circulate, often competing due to cross-protection or mutual exclusion. Examples include tuberculosis [1, 2], *Plasmodium falciparum* [3], *Streptococcus pneumoniae* [4, 5] and *Staphylococcus aureus* [6, 7]. Polymorphic strains can also interact in more complex ways, with both competition and cooperation acting simultaneously, as observed in co-circulating Dengue serotypes [8]. While interfering with each other, strains also interact with other pathogens co-circulating in the same population. Tuberculosis [1], HPV [9] and *P. falciparum* [10], for example, appear to be facilitated by HIV, whereas *S. pneumoniae* benefits from some bacterial infections, e.g. *Moraxella catarrhalis*, and is negatively associated to others such as *S. aureus* [11, 12]. Competition, cooperation and their co-occurrence may fundamentally alter pathogen persistence and diversity, thus calling for a deep understanding of these forces and their quantitative effects on spreading processes.

Mathematical models represent a powerful tool to assess the validity and impact of mechanistic hypotheses about interactions between pathogens or pathogenic strains [13, 14]. The literature on competitive interactions is centered on pathogen dominance and coexistence. Several factors were found to affect the ecological outcome of the competition, including co-infection mechanisms [15, 16, 17, 18], host age structure [19, 20], contact network [21, 22, 23, 24, 25, 26, 27, 28, 29, 30, 31] and spatial organisation [32, 33, 34, 35, 36, 37]. At the same time, models investigating cooperative interactions have driven many research efforts during recent years [38, 39, 40, 41, 42, 43, 44]. Cooperation has been found to trigger abrupt transitions between disease extinction and large scale outbreaks along with hysteresis phenomena where the eradication threshold is lower than the epidemic threshold [38, 42, 39]. These findings were related to the high burden of synergistic infections, e.g. the HIV and tuberculosis co-circulation in many parts of the world. Despite considerable mathematical and computationally-heavy research on interacting pathogens, competition and cooperation have been studied mostly separately. Nevertheless, current understandings about these mechanisms taken in isolation may fail to describe the dynamics arising from their joint interplay, where heterogeneous interactions may shape the phase diagram of co-existence/dominance outcome, along with the epidemic prevalence.

Here we studied the simplest possible epidemic situation where these heterogeneous effects are at play. We introduced a three-player model where two pathogens cooperate, and one of the two is structured in two mutually exclusive strains. This mimics a common situation, where e.g. resistant and susceptible strains of *S. pneumoniae* cooperate with other respiratory infections [11], and allows us to address two important ecological questions:

- How does the interplay between two distinct epidemiological traits, i.e. the transmissibility and the ability to exploit the synergistic pathogen, affect the spreading dynamics?
- How does the presence of a synergistic infection alter the co-existence between competing strains?

We addressed these questions by providing a characterisation of the phase space of dynamical regimes. We tested different modelling frameworks (continuous and deterministic vs. discrete and stochastic), and compared two assumptions regarding population mixing, i.e. homogeneous vs. community structure.

The paper is structured as follows: Section 2 introduces the main aspects of the three-player model. We provide the results of the deterministic dynamical equations in Section 3.1, where we present the stability analysis, together with the numerical integration of the equations, to characterise the phase space of the dynamics. The structuring of the population in two communities is analysed in Section 3.2. In Section 3.3 we describe the results obtained within a network framework comparing stochastic simulations in an Erdős-Rényi and a random modular network. We discuss the implications of our results in Section 4.

2 The model

A scheme of the model is depicted in figure 1a. We considered the case in which two pathogens, A and B, follow susceptible-infected-susceptible dynamics, and we made the simplification that they both have the same recovery rate μ. A and B cooperate in a symmetric way through increased susceptibility, i.e. a primary infection by one of the two increases the susceptibility to a secondary infection by the other pathogen. We assumed that the cooperative interaction does not affect infectivity, thus doubly infected individuals, i.e. infected with both A and B, transmit both diseases at their respective infection rates. B is structured in two strains, B_1 and B_2, that compete through mutual exclusion (co-infection with B_1 and B_2 is impossible) and differ in epidemiological traits. Specifically, we denoted the infection rates for pathogens A and B_i with α and β_i ($i = 1, 2$), respectively. We introduced the parameters $c_i > 1$ to represent the increased susceptibility after a primary infection. In summary, individuals can be in either one of 6 states: susceptible (S), singly infected (A, B_i) and doubly infected with both A and B_i. The latter status is denoted by D_i.

To simplify the analytical expressions we rescaled time by the average infectious period μ^{-1}, which leads to non-dimensional equations. Then, the parameters β_i and α becomes the basic reproductive ratio of each respective palyer.

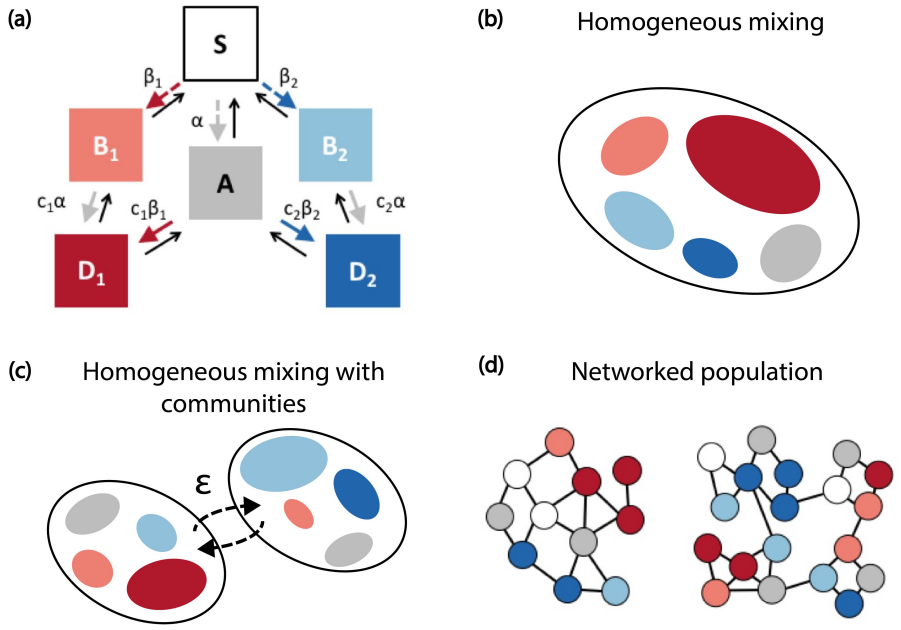

Figure 1: Scheme of the model. (a) Compartmental model. Coloured arrows represent transitions occurring due to infection transmission. Dashed arrows refer to primary infections, while solid arrows refer to secondary ones; transmission parameters are also reported close to each arrow. Black arrows represent recovery transitions. (b-d) Schematic representation of the modelling frameworks and population structures considered. (b) A homogeneously-mixed population (Section 3.1). (c) Two homogeneous populations with across-group mixing ruled by the parameter ϵ (Section 3.2); in (b),(c), colours indicate the infectious density for each compartment. (d) Erdős-Rényi and random modular networks (Section 3.3). Colours indicate the nodes' status.

This implies that the threshold condition $\beta_i, \alpha > 1$ has to be satisfied in order for the respective player to be able to individually reach an endemic state. Assuming a homogeneously mixed population, the mean-field equations describing the spreading dynamics are:

$$\begin{cases} \dot{S} &= A + B_1 + B_2 - \alpha S\, X_A - \beta_1 S\, X_1 - \beta_2 S\, X_2 \\ \dot{B}_1 &= D_1 - B_1 - c_1\alpha B_1\, X_A + \beta_1 S\, X_1 \\ \dot{B}_2 &= D_2 - B_2 - c_2\alpha B_2\, X_A + \beta_2 S\, X_2 \\ \dot{A} &= D_1 + D_2 - A + \alpha S\, X_A - c_1\beta_1 A\, X_1 - c_2\beta_2 A\, X_2 \\ \dot{D}_1 &= -2D_1 + c_1\alpha B_1\, X_A + c_1\beta_1 A\, X_1 \\ \dot{D}_2 &= -2D_2 + c_2\alpha B_2\, X_A + c_2\beta_2 A\, X_2, \end{cases} \tag{1}$$

where the dot indicates a differentiation with respect to time rescaled by μ^{-1},

and quantities S, A, B_i and D_i represent occupation numbers of the compartments divided by the population. The variables X_A, X_i, $i = 1, 2$, indicate the total fractions of individuals carrying A and B_i, respectively, among the singly and doubly infected individuals. They satisfy the equations:

$$\dot{X}_i = X_i\beta_i(S + c_i\, A) - X_i, \tag{2a}$$

$$\dot{X}_A = X_A\alpha(S + c_1 B_1 + c_2 B_2) - X_A. \tag{2b}$$

Without loss of generality, we considered the case in which the strain B_2 is more transmissible than B_1, i.e. $\delta_\beta = \beta_2 - \beta_1 > 0$. Furthermore, we focused on the more interesting case of trade-off between transmissibility and cooperation to limit the parameter exploration: The less transmissible strain, B_1, is more cooperative, $\delta_c = c_1 - c_2 > 0$. If B_2 is more cooperative, we expect it to win the competition. To summarize, our main assumptions are:

- $\delta_\beta = \beta_2 - \beta_1 > 0$,
- $\delta_c = c_1 - c_2 > 0$,
- $c_i > 1 \quad i = 1, 2$.

In the Results section we will first describe the dynamics arising from the deterministic equations (1). We will then consider the case in which the whole population is structured in two groups (see figure 1c). Finally, we will apply the proposed model to contact networks, where nodes represent individuals and transmission occurs through links, and consider transmission and recovery as stochastic processes. Two types of networks will be tested: Erdős-Rényi and random modular networks (see figure 1d).

3 Results

3.1 Continuous well-mixed system

We carried out a stability analysis to classify the outcome of the interaction as a function of the difference in strain epidemiological traits, δ_c and δ_β. Specifically we computed explicit analytical expressions for states' feasibility and stability conditions in several cases. Furthermore, we performed extensive numerical simulations in cases where closed expressions were difficult to obtain. We present the overall behaviour and the main analytical results in this section and we refer to the Supplementary Material for the detailed calculations. In the following, we will use square brackets to indicate final state configurations in terms of persisting strains, thus $[A\&B_1]$ indicates, for instance, the equilibrium configuration where both A and B_1 persist, while B_2 becomes extinct.

Figures 2a,b show the location of stable states with two combinations of α, β_2 and c_1. Results that are obtained for other parameter values are reported in figure S1. No co-existence was found between B_1 and B_2. In principle,

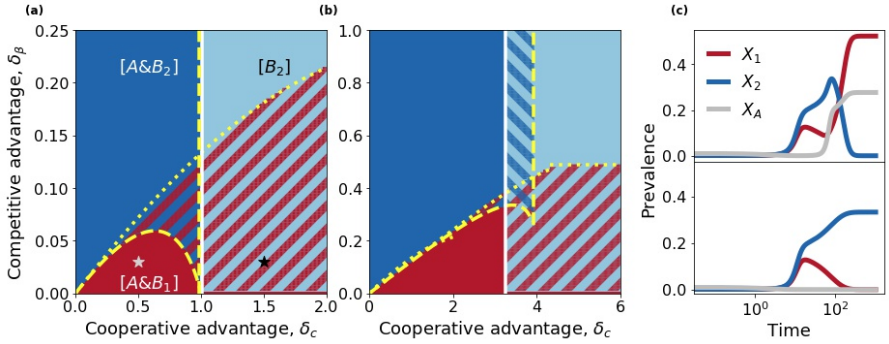

Figure 2: Phase diagram for the well-mixed system. (a),(b) Stable equilibria as a function of δ_β and δ_c for two parameter choices, namely (a) $\alpha = 0.6$, $\beta_2 = 1.5$, $c_1 = 4$, and (b) $\alpha = 0.8$, $\beta_2 = 1.1$, $c_1 = 7$. The three states $[B_2]$, $[A\&B_2]$ and $[A\&B_1]$ are indicated in light blue, dark blue and red, respectively. Hatched regions correspond to bistable and multistable regions. The yellow curves show the analytical boundaries delimiting stability regions for $[A\&B_1]$ and $[A\&B_2]$, while the white one delimits the $[B_2]$'s region. Notice that for $\delta_c > 3$, 6, for panels (a) and (b) respectively, $c_2 < 1$ and the interaction between B_2 and A ceases to be cooperative. This provides naturally a range for x-axis. In panel (b) transmissibility for B_1 is below one for $\delta_\beta > 0.1$. (c) Evolution of total prevalence for A (grey), B_1 (red) and B_2 (blue), considering singly and doubly infected combined. Parameters correspond to the grey and black star markers in panel (a), i.e. $\delta_\beta = 0.03$ and $\delta_c = 0.5$, 1.5 in top and bottom panels, respectively. Dynamical trajectories have been obtained by integrating equations (1) with initial conditions: $B_i(t = 0) = 0.001$, $A(t = 0) = 0.01$.

equations (1) admit a co-existence equilibrium $[A\&B_1\&B_2]$. However, this co-existence was always found to be unstable in the numerical simulations. Persistence of A is only possible together with one of the B strains. The equilibrium solution $[A]$ is unfeasible for $\alpha < 1$ and unstable for $\alpha > 1$, unless both reproductive ratios, β_i, are below the epidemic threshold. Because of the assumption $\delta_\beta > 0$, B_2 outcompetes B_1 in absence of A, in agreement with the principle of competitive exclusion. Therefore the final state $[B_1]$ is always unstable, and persistence of B_1 is possible only in co-circulation with A. On the other hand, B_2 can spread either alone or together with A. Specifically, the $[B_2]$ configuration is feasible for $\beta_2 > 1$. It is stable if and only if $\alpha < \alpha_c$, with

$$\alpha_c = \frac{\beta_2}{c_2(\beta_2 - 1) + 1} \,. \tag{3}$$

This provides a sufficient condition for the persistence of A. Equation (3) can be expressed in terms of δ_c, namely $\delta_c > c_1 - (\beta_2 - \alpha)/[\alpha(\beta_2 - 1)]$, which is visualized as the white boundary in figure 2a,b.

The competition between B_1 and B_2 is governed by the trade-off between

transmission and cooperative advantage. This is described by the boundaries of the $[A\&B_i]$ regions that can be traced by combining the feasibility and stability conditions. These boundaries are plotted in figures 2a,b as dotted and dashed yellow curves for $[A\&B_1]$ and $[A\&B_2]$, respectively. For a solution to be feasible the densities of all states must be non-negative. For absolute parameter values as in figure 2a,b we found that this yields the necessary condition $\alpha\beta_i > 4(c_i-1)/c_i^2$, corresponding to the vertical and horizontal segments. On the other hand, the stability boundary separating $[A\&B_i]$ from any state containing B_j $(j \neq i)$ is given by

$$\beta_j(S^* + c_j A^*) - 1 < 0, \tag{4}$$

where S^* and A^* are the equilibrium densities of S and A, respectively, evaluated in the configuration $[A\&B_i]$. The left-hand side of the equation represents the growth rate of the competitor B_j, appearing in equation (2a), and evaluated in the $[A\&B_i]$ state. Thus, the relation (4) expresses the condition for B_j extinction. Expressed in terms of δ_c and δ_β, the conditions becomes:

$$\begin{aligned}
[A\&B_1] \quad &: \quad \frac{\beta_2(c_1-\delta_c)}{c_1(\beta_2-\delta_\beta)} + \frac{\beta_2\delta_c}{c_1-1}\left(1-\sqrt{1-\frac{4(c_1-1)}{c_1^2(\beta_2-\delta_\beta)\alpha}}\right) = 1 \qquad (5)\\
[A\&B_2] \quad &: \quad \frac{c_1(\beta_2-\delta_\beta)}{\beta_2(c_1-\delta_c)} - \frac{\delta_c(\beta_2-\delta_\beta)}{c_1-\delta_c-1}\left(1-\sqrt{1-\frac{4(c_1-\delta_c-1)}{\beta_2\alpha(c_1-\delta_c)^2}}\right) = 1.
\end{aligned}$$

The intersection among the stability boundaries described above produces a rich state space. For all tested values of α, β_2 and c_1, we found a wide region of the (δ_c, δ_β) space (red-hatched in figures 2a,b) displaying bistability between the $[A\&B_1]$ state and a B_2-dominant state with either $[B_2]$ or $[A\&B_2]$. In certain cases, bistability can also occur between the $[B_2]$ and $[A\&B_2]$ states (blue-hatched region in figure 2b). This has been studied in the past for two cooperating pathogens [42]. We found that the intersection between the latter region and the red-hatched region gives rise to a multistable state.

Interestingly, for all tested parameters we found that the boundary of the $[A\&B_2]$ stability region is not monotonic. As a consequence, for a fixed δ_β a first transition from the $[A\&B_2]$ state to $[A\&B_1]$ is found for small δ_c values. An increase of δ_c leads to a second boundary with a bistable region, where the dominance of B_1 over B_2 depends on initial conditions. The transition for small δ_c is expected: By increasing B_1's advantage in cooperation, a point is reached beyond which B_1's disadvantage in transmissibility is overcome. On the other hand, the second threshold appears to be counter-intuitive. We investigated it more in depth for the case depicted in figure 2a. We plotted the infectious population curves as a function of time for each infectious compartment. We compared $\delta_c = 0.5$, which corresponds to the $[A\&B_1]$ stable state (figure 2c top), and $\delta_c = 1.5$, which leads to a bistable region (figure 2c bottom), where all other parameters are as in figure 2a. Figure 2c shows that B_1 loses the competition at the beginning. However, when B_2 is sufficiently cooperative with A (top), the rise of B_2 leads to a rise in A that ultimately drives B_1 to dominate. For higher

δ_c the strength of cooperation between B_2 and A is not sufficient. The indirect beneficial effect of B_2 over B_1 is not present (bottom), and B_1 can dominate only if initial conditions are favourable.

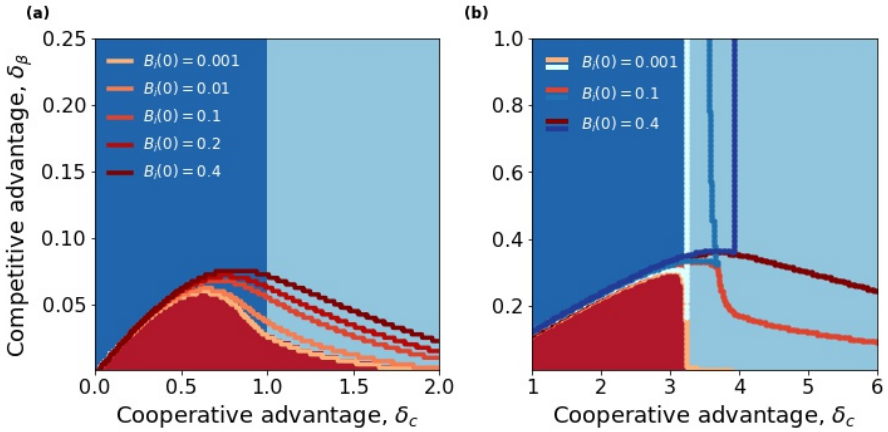

Figure 3: Equilibrium configurations for the well-mixed system. Final outcome obtained by numerically integrating equations (1) for $B_i(t = 0) = 0.001$, $A(t = 0) = 0.01$. (a) $\alpha = 0.6$, $\beta_2 = 1.5$, $c_1 = 4$. Boundaries of the $[A\&B_1]$ state for different initial conditions are indicated by red-scale contours. (b) $\alpha = 0.8$, $\beta_2 = 1.1$, $c_1 = 7$. Here, the boundaries of the $[A\&B_2]$ are shown (in blue shades), together with the ones of $[A\&B_1]$.

In the bistable and multi-stable regions, the outcome of the competition is determined by initial conditions. While a mathematical analysis is complicated due to the multi-dimensionality of the problem, we gained insights into the basins of attraction by numerically integrating equations (1) while exploring different combinations of $B_i(t = 0)$ and $A(t = 0)$. For the bistability between the regions of B_1 and B_2 dominance, we considered the parameter combination of figure 2a and show in figure 3a the states that are reached starting from $B_i(t = 0) = 0.001$ and $A(t = 0) = 0.01$. The bundle of curves with different shades of red (from light to dark) indicates the boundary of the $[A\&B_1]$ equilibrium when $B_1(t = 0)$ and $B_2(t = 0)$ are equally increased. We found that an increase in B_1's initial infected densities favours the $[A\&B_1]$ state, as expected. Interestingly, however, an increase in $B_1(t = 0)$ results in the $[A\&B_1]$ region to expand even when B_2's density increases at the same level. Figure 3b shows that a similar behaviour is found when parameters are as in figure 2b. In this case, the region $[A\&B_2]$ expands together with the $[A\&B_1]$ one. Thus, increased initial frequencies promote co-circulation between B and A. In figure S2 we present a deeper exploration of initial conditions, considering the parameter combination of figure 2a as an example. We found that an increase in the initial level of A also favours B_1. However, the initial advantage (either in $B_1(0)$ or $A(0)$) that is necessary for B_1 to win against B_2 increases as δ_β increases.

The stability diagrams obtained with several parameter sets, explored in a latin-square fashion, is reported in figure S1. This shows that increased transmissibility and cooperativity levels enhance the cooperative interaction of B_i strains with A. This results in an increase in the parameter region for which B_1 together with A dominates over B_2. For instance, the comparison between panels (d) and (f) in the figure shows that, by increasing β_2 from 1.1 to 1.5, the same difference in strain epidemiological traits, δ_c and δ_β, may lead to a switch in dominance from B_2 to B_1.

3.2 Continuous system with communities

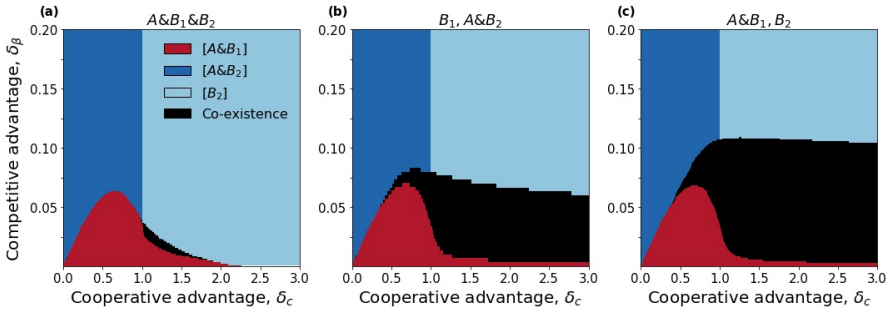

Figure 4: Equilibrium configurations for two interacting communities. Final outcome obtained by numerically integrating the equations when: (a) all strains start in the same community (together with A); (b) B_1 and B_2 start in separate communities, with A starting together with B_2; (c) A starts along with B_1, while B_2 starts separately. Initial density of each pathogen/strain is 0.01. Here $\epsilon = 0.0002$. Other parameters are as in figure 2a.

We now consider a population that is divided into two communities (cf. figure 1c). For simplicity, we assumed that they are of the same size. To differentiate transmission within and across communities, we rescaled the force of infection produced by individuals of a different community by a factor ϵ, and the force of infection of individuals of the same community by $1-\epsilon$. We assumed $0 < \epsilon \leq \frac{1}{2}$ in order to consider the case in which individuals mix more within their community than outside - the limit $\epsilon = \frac{1}{2}$ corresponds to homogeneous mixing.

Given the high number of variables, a stability analysis is difficult in this case. Still, the dynamics can be reconstructed through numerical integration of the equations. Figure 4 shows the final states with fixed ϵ, β_2, C_1 and α. Other parameter values are analysed in figure S3. Figures 4a-c compare different seeding configurations, while keeping the initial density of each pathogen/strain to 0.01: (a) all strains are seeded in community 1 and community 2 is completely susceptible; (b) B_1 is seeded in community 1 while B_2 and A are initially present in community 2 only; (c) B_1 and A are seeded together in community 1, while

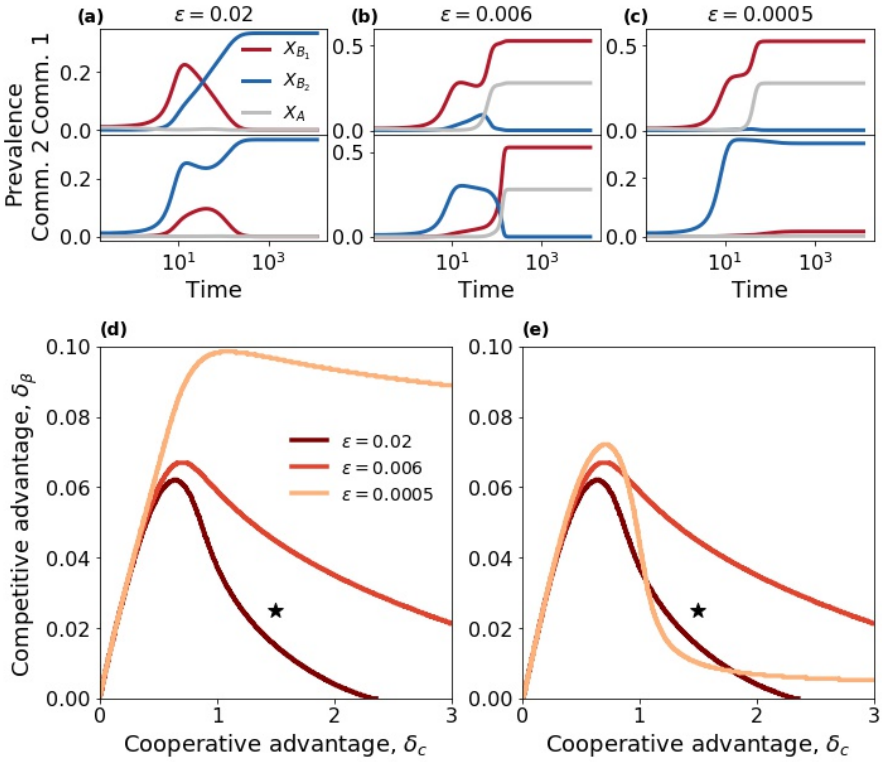

Figure 5: Role of spatial separation for two interacting communities. (a-c) Dynamical trajectories within community 1 and 2 obtained for (a) $\epsilon = 0.02$, (b) $\epsilon = 0.006$, and (c) $\epsilon = 0.0005$. (d,e) Boundaries in the δ_c, δ_β plane delimiting the regions where the dynamics ends up in: (d) B_1 persistence (i.e. $[A\&B_1]$ or full co-existence); (e) $[A\&B_1]$ state. In all panels, A and B_1 are seeded together into one community, while B_2 is seeded into the other community; the initial density of each species is set to 0.01. Trajectories are obtained by setting $\delta_c = 1.5$, $\delta_\beta = 0.025$ (black star in panels (d),(e)). Other parameters are as in figure 2a.

B_2 is seeded in community 2. In all cases we found a diagram with shape similar to figure 3a. However, a new region is now present (indicated in black) where all players co-exist. This occurs when strains are separated since the beginning – see figure S4 for additional seeding configurations. Interestingly, however, this happens also for a tiny region of the parameter space, when all strains are seeded together (panel a), provided that the other community is initially disease-free.

Figure 5 sheds light on the dynamics leading to the outcomes of figure 4. In order to benefit from the cooperative advantage, the B_1 incidence must be above a certain threshold. Figures 5b,c show that incidence of A remains close

to zero, until incidence of B_1 is sufficiently high. With B_2 seeded on a different community (community 2), the direct interaction between the two strains is delayed by the time necessary for B_2 to reach the community of B_1. For high ϵ the delay is short and B_2 reaches community 1 before A incidence starts to raise (figure 5a). On the other hand, for lower ϵ, B_1 has enough time to build up a cooperative protection before the arrival of B_2. This makes it resistant to the invader. At intermediate ϵ, B_1 becomes able to overcome B_2 in community 2. For small ϵ, strains spread in their origin community independently from one another.

In summary, a decrease in ϵ increases the region of B_1 persistence (figure 5d). However, this may be associated to either B_1 dominance or co-existence. Reducing the values of ϵ, the region corresponding to the $[A\&B_1]$ state expands first and shrinks later, leaving the place to the co-existence region. This is shown by the non-monotonous change of the $[A\&B_1]$ region in figure 5e.

When all strains start in the same community, co-existence is enabled by a segregation mechanism similar to the one described above. In this case, separation occurs during the early stage: B_2 rapidly spreads in the other community due to its advantage in transmissibility, and becomes dominant there (cf. figure S5). This enables co-existence in a parameter region where B_1 would otherwise dominate.

Results described so far were obtained with fixed values of β_2, C_1 and α. Additional parameter choices are shown in figure S3. Increasing in α was found to enlarge the B_1 dominance region, as in the well-mixed case. In addition, co-existence becomes possible for $\alpha > 1$ in a very small region of the parameter space.

3.3 Spreading on networks

The continuous deterministic framework analysed so far does not account for stochasticity and for the discrete nature of individuals and their interactions. These aspects may alter the phase diagram and shape the transitions across various regions. We casted our model on a discrete framework in which individuals are represented by nodes in a static network. Possible individual states are still the same as in the mean-field formulation, and infection can spread only between neighbouring nodes. We first considered an Erdős-Rényi graph, where the mixing is homogeneous across nodes. Denoting N the number of nodes and $\bar{k}$ the average degree, the network was built by connecting any two nodes with probability $\bar{k}/(N-1)$. We run stochastic simulations of the dynamics. In order to see the effect of multi-pathogen interactions, we minimised the chance of initial stochastic extinction by infecting a relatively high number of nodes at the beginning: 100 infected for each infectious agent. We then computed the fraction of stochastic simulations ending up in any final state, the average prevalence for each strain (X_1, X_2) in the final state and the average coexistence time. Additional details on the network model and the simulations are reported in the Supplementary Material.

The phase diagram of figure 6a is similar in many aspects to its continuous deterministic version (figure 3a). Three final states are possible, i.e. $[B_2]$, $[A\&B_1]$ and $[A\&B_2]$ (figure 6a). Here, however, the same initial conditions and parameter values can lead to different stochastic trajectories and stationary states. For instance, the red region in the figure corresponds to the case in which the final state $[A\&B_1]$ is reached very frequently; however, the dynamic trajectories can end up also in the $[A\&B_2]$ or in the $[B_2]$ states. The transitions across the different regions of the diagrams can be very different, as demonstrated by figures 6b-g. Panels b,c show the effect of varying δ_c at a fixed δ_β. The transition between $[A\&B_2]$ and $[A\&B_1]$ on the left is sharp. Both the probability of one strain winning over the other and the equilibrium prevalence change abruptly for a critical value of δ_c. Here, the spreading is super-critical for all pathogens: $\beta_1, \beta_2 > 1$ and c_1, c_2 are sufficiently high to sustain the spread of A. The transition is due to the trade-off between B_1 and B_2 growth rates. Conversely, the probability of ending up in the $[B_2]$ state rises slowly, driving the gradual transition from the red to the light blue region on the right. This region appears in correspondence of the bistable region of the continuous/deterministic diagram – figure 2. Here, A undergoes a transition from persistence to extinction, driven by the drop in c_2 (figure S6). This critical regime is characterised by enhanced stochastic fluctuations. When δ_c is fixed and δ_β varies, we found a sharp transition (panels d,e) and a hybrid transition, where the final state probability varies gradually and the equilibrium prevalence (X_1) varies abruptly (panels f,g).

We concluded by analysing the effect of community structure. Each node was assigned to one among n_C communities, which we assumed for simplicity to have equal size N/n_C, and has a number of open connections drawn from a Poisson distribution with average $\bar{k}$. Links were formed by matching these connections according to an extended configuration model, where a fraction ϵ of stubs connects nodes of different communities. In this way the model is the discrete version of the one in Section 3.2.

Mean-field results remain overall valid. The two plots in figure 7 mirror panels a,c of figure 4 and show a similar behaviour. We find evidence of a co-existence region (in black in the figure), where no extinction is observed during the simulation time frame - here set to $2 \cdot 10^6$ time steps, around two orders of magnitude longer than the time needed to observe strain extinction in the Erdős-Rényi case. Such region is larger when the two strains are seeded in separated communities (figure 7b), but it is still visible when strains start altogether (figure 7a). Co-existence occurs less frequently in the latter case, since it requires strains to reach the separation during the spreading dynamics.

Analogously to the continuous deterministic model we found that the separation in communities favours the more cooperative strain. The region where B_1 wins is larger compared to the Erdős-Rényi case (as highlighted by the comparison between the dashed and the continuous curves). In addition, the probability of winning is close to one for a large portion of the $[A\&B_1]$ dominance region.

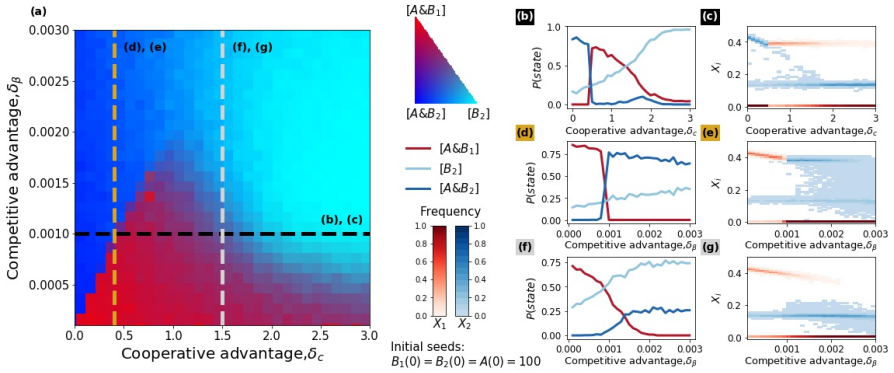

Figure 6: Phase diagram for the Erdős-Rényi network. (a) Frequency of several stationary states, as obtained in numerical simulations. The colour scale in the legend quantifies the proportion of runs ending in the different states among $[B_2]$, $[A\&B_2]$ and $[A\&B_1]$. Here, the extremes of the colour map correspond to the case in which these states are found in 100% of runs. Initial conditions are shown in the figure. (b-g) Equilibrium state probability (left column), and distribution of prevalence in the final state (right column) along the dashed lines in panel (a). Specifically: $\delta_\beta = 0.001$ for (b) and (c); $\delta_c = 0.4$ for (d) and (e); $\delta_c = 1.5$ for (f) and (g). Other parameters are $\mu = 0.05$, $\alpha = 0.009$, $\beta_2 = 0.015$, $c_1 = 4$, $N = 20000$, $\bar{k} = 4$. For convenience, the time step is taken as time unit. It corresponds to 1/20 of the infectious period μ^{-1}.

4 Discussion and conclusion

We presented here a theoretical analysis of a three-player system where both competition and cooperation act simultaneously. We have considered two competing strains co-circulating in the presence of another pathogen cooperating with both of them. Strains differ in epidemiological traits, with one strain being more transmissible but less cooperative than its competitor. Through mathematical analyses and computer simulations we have reconstructed the possible dynamical regimes, quantifying the conditions for dominance of one strain or co-existence. We found that the interplay between competition and cooperation leads to a complex phase diagram whose properties cannot be easily anticipated from previous works that considered competition and cooperation separately.

We showed that it is possible for a more cooperative strain to dominate over a more transmissible one, provided that the difference in transmissibility is not too high. This suggests that the presence of another pathogen (A) might alter the spreading conditions, creating a favourable environment for a strain that would be otherwise less fit. While dominance depends on the difference in epidemiological traits, we found that variations in the absolute cooperation and transmissibility levels may change the hierarchy between strain – analogously to [15] – with a higher spreading potential of either B_i or A favouring the more

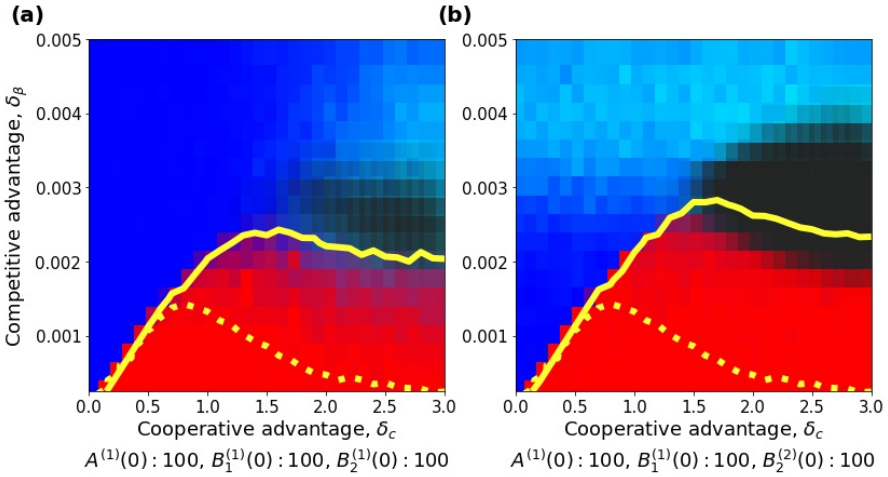

Figure 7: Phase diagram for the random modular network. Frequency of equilibrium configurations, as obtained in the numerical simulations, with (a) A, B_1 and B_2 starting in the same community, and (b) A and B_1 starting from a different community to B_2. Detailed initial conditions are directly shown on each panel. The colour scale is the same as in figure 6. The frequency of runs for which co-existence of all strains was observed after $T_{max} = 2 \cdot 10^6$ time steps is shown with different shades of black. Contour lines representing the 0.5 probability to end up in the $[A\&B_1]$ state are indicated to enable a comparison between the Erdős-Rényi (dashed line) and the random modular network (continuous line). We considered $n_C = 10$ and $\epsilon = 0.003$. Other parameter values are as in figure 6.

cooperative strain.

Interestingly, the cooperative strain can dominate also when A has a sub-critical reproductive ratio ($\alpha < 1$) – when spreading alone – and relies on the synergistic interaction with B strains to persist. The dynamical mechanisms underlying this outcome are complex. We analysed a case with a small difference in cooperativity, and we found that the more transmissible strain, by spreading initially faster, creates the bulk of A infections that in turn favour its competitor. In other words, direct competition for susceptible hosts is not the only force acting between strains: an indirect, beneficial interaction is also at play, mediated by the other pathogen. The dominance outcome is thus the result of the trade-off between these two forces. When the difference in cooperation is higher, two or more stationary configurations are possible. In this scenario, the final outcome is determined also by the initial frequency of each pathogen/strain. We found that, in certain situations, an initial advantage of one strain is able to drive it to dominance. This is in contrast with simpler models of competition, where the final outcome is determined solely by the epidemiological traits. The

outcome, however, is also governed by pathogen A that favours the more cooperative strain. Previous works have analysed multistability in two-pathogen models with cooperation in relation to the hysteresis phenomenon, where the eradication threshold is lower than the epidemic one [42, 38, 41]. A similar mechanism could be at play here. However, the identification of hysteresis loops requires a better reconstruction of the attraction basins. While the numerical work presented here provided some preliminary understanding, a deeper mathematical analysis would be needed in this direction. Multistability is, instead, not present in two-pathogen models with complete mutual exclusion. This dynamical feature emerges, however, in the more general case where strains are allowed to interact upon co-infection [15].

While we did not find stable co-existence among strains in the well-mixed system, co-existence was possible in presence of community structure. In this case, strains can minimise competition for hosts through segregation. Importantly, spatial separation alone is not sufficient to enable co-existence between two strains, when complete mutual exclusion is assumed. This was already known from previous works that showed that community structure must be combined with some level of heterogeneity across communities to enable co-existence, e.g. a strain-specific adaptation to a population or environment to create an ecological niche [36, 34, 45, 46, 47]. Here, communities are homogeneous and co-existence is the result of the interplay between community structure and presence of the cooperative pathogen. When the two strains are seeded in different communities, their interaction occurs after the time lag necessary for one strain to invade the other community. We found that this interval may allow the resident strain to reach the bulk of infections necessary to fend off the invasion. This mechanism is rooted again in the effect of pathogens' frequencies on strain selective advantage. The drivers of strains' co-existence remain an important problem in disease ecology with applications to both vaccination and emergence of anti-microbial resistance. Within-host and population factors have been studied in the past by several modelling investigations. Notably, while co-existence is not possible in models with complete mutual exclusion, this may be enabled in co-infection models [15, 48, 16, 17, 18]. Other models have addressed environmental and host population features, such as age-structure, contacts dynamics and spatial organisation [19, 20, 21, 35]. However, little attention has been dedicated to the effect of an additional co-circulating pathogen. Cobey et al. studied the interaction between *Haemophilus influenzae* and *S. pneumoniae* co-circulating strains [49]. Despite the numerous differences between our model and theirs, their work provides results consistent with ours. Namely, the multi-strain dynamics can be affected by another pathogen.

We simulated the three-player dynamics on networks and we obtained phase diagrams that are similar to the continuous-deterministic counterparts. The discrete/stochastic framework, however, allows for observing the nature of the phase transitions. Several works recently studied the nature of the epidemic transition for two cooperating pathogens, highlighting differences with the single-pathogen case. Cooperation was found to cause discontinuous transitions where the probability of an outbreak and prevalence change abruptly around a crit-

ical value of the transmission rate [39, 42], akin to other complex contagion mechanisms such as the ones found in social contagion [50, 51]. This phenomenon, however, is sensitive to the network topology, with continuous, discontinuous and hybrid, i.e. continuous in the outbreak probability and discontinuous in the prevalence, transitions observed according to the topology of the network [39, 42, 38, 41, 52, 53, 54]. Here we found rich dynamics as the impact of stochastic effects. These effects were less important when the difference between strains' epidemiological traits was small. Conversely, for a higher difference in cooperative factor different outcomes are equally probable. Results presented here are preliminary and limited to two network configurations. Future work should investigate additional network topologies, e.g. a power-law degree distribution, and further values of the network parameters. In addition, more sophisticated numerical analysis (e.g. scaling analysis) would be needed to better classify the nature of the phase transitions.

Concurrence of inter-species cooperation and intra-specie competition is present in many epidemiological situations. Currently, around 90 distinct *S. pneumoniae* serotypes are known to co-circulate worldwide, despite indirect competition mediated by host immune response [4]. The emergence of antibiotic-resistant strains and the development of vaccines able to target only a subset of strains has motivated extensive research on the drivers of *S. pneumoniae* ecology [4, 20, 5]. Strain circulation is facilitated by respiratory infections, e.g. influenza [55, 56] and some bacterial infections [11, 12]. Cooperative behaviour has been observed also between HIV and infections such as HPV, tuberculosis and malaria [9, 10, 57, 1, 58]. This increases the burden of these pathogens and causes public health concern. At the same time, there is evidence that different strains of tuberculosis [2, 59], malaria [3], and HPV [60, 61, 62] may compete. In particular, multidrug-resistant strains of tuberculosis (MDR-TB) are widely spread, although the acquisition of resistance seems to be associated to a fitness cost [58, 63]. The synergistic interaction with HIV could play a role in this emergence and surveillance data suggest a possible convergence between HIV and MDR-TB epidemics in several countries [58]. Our theoretical work highlights ecological mechanisms potentially relevant to these examples. In this regard, an essential aspect of our model is the trade-off between transmissibility and cooperativity in determining strain advantage. Although differences in transmissibility across strains have been documented, e.g. fitness cost of resistance [64], gathering information on strain-specific cooperative advantage remains difficult. The theoretical results illustrated here show the importance of quantifying this component for better describing pathogen ecosystems.

This study also represents the starting point of more complex models where multiple strains are involved and competition and cooperation are acting simultaneously. Patterns of competitive and cooperative interactions could be at play for instance among recently emerged pathogens such as Zika virus [65]. Zika virus has emerged in regions where Dengue and Chikungunya viruses are endemic. Observed patterns of sequential monodominance by one arbovirus at a time at a given location suggest competition between these pathogens [66]. Also, considerable effort is currently devoted to characterising possible positive

interactions between Zika virus and HIV [65]. In some cases, different strains of the same pathogen can interact both competitively and cooperatively, as in the case of Dengue [8, 14]. Primary Dengue infections are characterised by mild symptoms and grant short-term cross-protection against other serotypes. As cross-immunity wanes over time, however, secondary Dengue infections not only become possible but are also associated with severe illness and with increased virulence.

The examples above involve diseases with varying natural history and time scales and should be modelled with different compartmental models – SIR, SI, SIS, SIRS. We decided here to consider two SIS pathogens and the results cannot be readily extended to other models, since the dynamics of disease unfolding alters the outcome of strain interactions. It is important to notice, however, that several dynamical properties of competitive and cooperative interactions, such as dominance vs. co-existence [27] and abrupt transitions [67, 68, 69], hold for both SIS and SIR.

The model studied here is based on certain simplifications. All pathogens are assumed to have the same recovery rate; moreover, cooperation acts in both directions and the same factors c_i quantify the enhancement in susceptibility when A infection occurs before B_i infection and vice versa. These assumptions may not hold for many synergistic pathogens, especially when cooperative benefits are based on different biological mechanisms. For instance, while HIV increases susceptibility against *P. falciparum*, the latter increases HIV's viral load, thus increasing HIV's virulence rather than host susceptibility to HIV [10, 57]. It is likely that, by relaxing these assumptions, our model could exhibit even more complex phase diagrams. Eventually, other aspects of the disease-specific mechanisms and multi-pathogen interactions could affect the results presented here and should be addressed in future works. These include latent infections, which are characteristic, for instance, of tuberculosis [2], partial mutual exclusion among strains [2, 6, 15, 16], or interaction mechanisms other than the ones introduced here (e.g. affecting the infectious period [24]).

In conclusion, we have provided a theoretical study of a dynamical system where both competition and cooperation are at play. We found that a less transmissible and more cooperative strain may dominate; however, the conditions on the parameters for this to happen are non-trivial (non-monotonic) and the outcome critically depends on initial conditions and stochastic effects. When coupled with population structure, the presence of a cooperative pathogen may create the conditions for multi-strain co-existence by dynamically breaking the spatial symmetry and creating ecological niches. These results provide novel ecological insights and suggest mechanisms that may potentially affect the dynamics of interacting epidemics that are of public health concern.

Data availability

The python code used for the mean-field analyses and the C++ code for the stochastic simulations on networks are publicly available at the following link:

https://github.com/francescopinotti92/Competition-Cooperation.

Authors' contributions

FP, FGh, PH, CP conceived and designed the study. FP carried out the analyses. FP, FGh, PH, CP analysed the results. FP, FGh, PH, CP contributed to the writing of the manuscript and approved the final version.

Competing interests

The authors declare no competing interests.

Funding

FP acknowledges support by Pierre Louis Doctoral School of Public Health. FGh and PH acknowledge support by German Academic Exchange Service (DAAD) within the PPP-PROCOPE framework (grand no. 57389088). CP and FP acknowledge support by the Partenariats Hubert Curien within the PPP-PROCOPE (grand no. 35473TK). FGh acknowledges partial support by Deutsche Forschungsgemeinschaft (DFG) under the grant GH 176/1-1 (idonate project: 345463468). PH acknowledges further support by DFG in the framework of Collaborative Research Center 910 (grand no. SFB910). CP acknowledges support from the municipality of Paris through the program Emergence(s).

Research ethics

This section does not apply to this study.

Animal ethics

This section does not apply to this study.

Permission to carry out fieldwork

This section does not apply to this study.

Acknowledgements

We thank Andrew Keane for helpful discussions that made the manuscript more accessible.

References

[1] Jeffrey A. Tornheim and Kelly E. Dooley. Tuberculosis Associated with HIV Infection. *Microbiol. Spectr.*, 5(1):UNSP TNMI7–0028–2016, February 2017. WOS:000397274600026.

[2] Ted Cohen, Caroline Colijn, and Megan Murray. Modeling the effects of strain diversity and mechanisms of strain competition on the potential performance of new tuberculosis vaccines. *Proceedings of the National Academy of Sciences of the United States of America*, 105(42):16302–16307, October 2008.

[3] Kexuan Chen, Ling Sun, Yingxue Lin, Qi Fan, Zhenjun Zhao, Mingming Hao, Guohua Feng, Yanrui Wu, Liwang Cui, and Zhaoqing Yang. Competition between Plasmodium falciparum strains in clinical infections during in vitro culture adaptation. *Infect Genet Evol*, 24:105–110, June 2014.

[4] Sarah Cobey and Marc Lipsitch. Niche and Neutral Effects of Acquired Immunity Permit Coexistence of Pneumococcal Serotypes. *Science*, 335(6074):1376–1380, March 2012.

[5] Lulla Opatowski, Emmanuelle Varon, Claire Dupont, Laura Temime, Sylvie van der Werf, Laurent Gutmann, Pierre-Yves Boëlle, Laurence Watier, and Didier Guillemot. Assessing pneumococcal meningitis association with viral respiratory infections and antibiotics: insights from statistical and mathematical models. *Proceedings. Biological Sciences*, 280(1764):20130519, August 2013.

[6] Thomas Obadia, Romain Silhol, Lulla Opatowski, Laura Temime, Judith Legrand, Anne C. M. Thiébaut, Jean-Louis Herrmann, Éric Fleury, Didier Guillemot, Pierre-Yves Boëlle, and on behalf of the I.-Bird Study Group. Detailed Contact Data and the Dissemination of Staphylococcus aureus in Hospitals. *PLOS Computational Biology*, 11(3):e1004170, March 2015.

[7] Tjibbe Donker, Sandra Reuter, James Scriberras, Rosy Reynolds, Nicholas M. Brown, M. Estée Török, Richard James, East of England Microbiology Research Network, David M. Aanensen, Stephen D. Bentley, Matthew T. G. Holden, Julian Parkhill, Brian G. Spratt, Sharon J. Peacock, Edward J. Feil, and Hajo Grundmann. Population genetic structuring of methicillin-resistant Staphylococcus aureus clone EMRSA-15 within UK reflects patient referral patterns. *Microbial Genomics*, 3(7), 2017.

[8] Nicholas G. Reich, Sourya Shrestha, Aaron A. King, Pejman Rohani, Justin Lessler, Siripen Kalayanarooj, In-Kyu Yoon, Robert V. Gibbons, Donald S. Burke, and Derek A. T. Cummings. Interactions between serotypes of dengue highlight epidemiological impact of cross-immunity. *Journal of The Royal Society Interface*, 10(86):20130414, September 2013.

[9] Katharine J. Looker, Minttu M. Rönn, Patrick M. Brock, Marc Brisson, Melanie Drolet, Philippe Mayaud, and Marie-Claude Boily. Evidence of synergistic relationships between HIV and Human Papillomavirus (HPV): systematic reviews and meta-analyses of longitudinal studies of HPV acquisition and clearance by HIV status, and of HIV acquisition by HPV status. *Journal of the International AIDS Society*, 21(6):e25110, 2018.

[10] Cheryl Cohen, Alan Karstaedt, John Frean, Juno Thomas, Nelesh Govender, Elizabeth Prentice, Leigh Dini, Jacky Galpin, and Heather Crewe-Brown. Increased Prevalence of Severe Malaria in HIV-Infected Adults in South Africa. *Clin Infect Dis*, 41(11):1631–1637, December 2005.

[11] Astrid A. T. M. Bosch, Giske Biesbroek, Krzysztof Trzcinski, Elisabeth A. M. Sanders, and Debby Bogaert. Viral and Bacterial Interactions in the Upper Respiratory Tract. *PLOS Pathogens*, 9(1):e1003057, January 2013.

[12] Eileen M. Dunne, Heidi C. Smith-Vaughan, Roy M. Robins-Browne, E. Kim Mulholland, and Catherine Satzke. Nasopharyngeal microbial interactions in the era of pneumococcal conjugate vaccination. *Vaccine*, 31(19):2333–2342, May 2013.

[13] Pejman Rohani Matt J. Keeling. *Modeling Infectious Diseases in Humans and Animals*. Princeton University Press, 2008.

[14] Sourya Shrestha, Aaron A. King, and Pejman Rohani. Statistical Inference for Multi-Pathogen Systems. *PLOS Computational Biology*, 7(8):e1002135, 2011.

[15] Erida Gjini and Sten Madec. A slow-fast dynamic decomposition links neutral and non-neutral coexistence in interacting multi-strain pathogens. *Theoretical Ecology*, 10(1):129–141, March 2017.

[16] Mircea T. Sofonea, Samuel Alizon, and Yannis Michalakis. From within-host interactions to epidemiological competition: a general model for multiple infections. *Philosophical Transactions of the Royal Society B: Biological Sciences*, 370(1675):20140303, August 2015.

[17] Samuel Alizon. Co-infection and super-infection models in evolutionary epidemiology. *Interface Focus*, 3(6), December 2013.

[18] Samuel Alizon, Jacobus C. de Roode, and Yannis Michalakis. Multiple infections and the evolution of virulence. *Ecology Letters*, 16(4):556–567, April 2013.

[19] Maia Martcheva, Sergei S. Pilyugin, and Robert D. Holt. Subthreshold and superthreshold coexistence of pathogen variants: the impact of host age-structure. *Math Biosci*, 207(1):58–77, May 2007.

[20] Sarah Cobey, Edward B. Baskerville, Caroline Colijn, William Hanage, Christophe Fraser, and Marc Lipsitch. Host population structure and treatment frequency maintain balancing selection on drug resistance. *Journal of The Royal Society Interface*, 14(133):20170295, August 2017.

[21] Ken T. D. Eames and Matt J. Keeling. Coexistence and specialization of pathogen strains on contact networks. *Am. Nat.*, 168(2):230–241, August 2006.

[22] Joel C. Miller. Co-circulation of infectious diseases on networks. *Phys Rev E Stat Nonlin Soft Matter Phys*, 87(6):060801, June 2013.

[23] Faryad Darabi Sahneh and Caterina Scoglio. Competitive epidemic spreading over arbitrary multilayer networks. *Phys. Rev. E*, 89(6):062817, June 2014.

[24] Joaquín Sanz, Cheng-Yi Xia, Sandro Meloni, and Yamir Moreno. Dynamics of Interacting Diseases. *Phys. Rev. X*, 4(4):041005, October 2014.

[25] Jia Li, Zhien Ma, Steve P. Blythe, and Carlos Castillo-Chavez. Coexistence of pathogens in sexually-transmitted disease models. *J. Math. Biol.*, 47(6):547–568, December 2003.

[26] Caichun Chai and Jifa Jiang. Competitive Exclusion and Coexistence of Pathogens in a Homosexually-Transmitted Disease Model. *PLOS ONE*, 6(2):e16467, February 2011.

[27] Brian Karrer and M. E. J. Newman. Competing epidemics on complex networks. *Phys. Rev. E*, 84(3):036106, September 2011.

[28] Naoki Masuda and Norio Konno. Multi-state epidemic processes on complex networks. *Journal of Theoretical Biology*, 243(1):64–75, November 2006.

[29] Gabriel E. Leventhal, Alison L. Hill, Martin A. Nowak, and Sebastian Bonhoeffer. Evolution and emergence of infectious diseases in theoretical and real-world networks. *Nature Communications*, 6:6101, January 2015.

[30] Caroline O'F Buckee, Katia Koelle, Matthew J. Mustard, and Sunetra Gupta. The effects of host contact network structure on pathogen diversity and strain structure. *PNAS*, 101(29):10839–10844, July 2004.

[31] Francesco Pinotti, Éric Fleury, Didier Guillemot, Pierre-Yves Böelle, and Chiara Poletto. Host contact dynamics shapes richness and dominance of pathogen strains. *PLOS Computational Biology*, 15(5):e1006530, May 2019.

[32] Chiara Poletto, Sandro Meloni, Vittoria Colizza, Yamir Moreno, and Alessandro Vespignani. Host Mobility Drives Pathogen Competition in Spatially Structured Populations. *PLOS Computational Biology*, 9(8):e1003169, 2013.

[33] Chiara Poletto, Sandro Meloni, Ashleigh Van Metre, Vittoria Colizza, Yamir Moreno, and Alessandro Vespignani. Characterising two-pathogen competition in spatially structured environments. *Scientific Reports*, 5:7895, January 2015.

[34] Linda J. S. Allen, Nadarajah Kirupaharan, and Sherri M. Wilson. SIS Epidemic Models with Multiple Pathogen Strains. *Journal of Difference Equations and Applications*, 10(1):53–75, January 2004.

[35] Caroline Buckee, Leon Danon, and Sunetra Gupta. Host community structure and the maintenance of pathogen diversity. *Proceedings of the Royal Society of London B: Biological Sciences*, 274(1619):1715–1721, July 2007.

[36] Yixiang Wu, Necibe Tuncer, and Maia Martcheva. Coexistence and competitive exclusion in an SIS model with standard incidence and diffusion, December 2016.

[37] S. Lion and S. Gandon. Spatial evolutionary epidemiology of spreading epidemics. *Proceedings. Biological Sciences*, 283(1841), 2016.

[38] Weiran Cai, Li Chen, Fakhteh Ghanbarnejad, and Peter Grassberger. Avalanche outbreaks emerging in cooperative contagions. *Nature Physics*, 11(11):936–940, November 2015.

[39] Laurent Hébert-Dufresne and Benjamin M. Althouse. Complex dynamics of synergistic coinfections on realistically clustered networks. *PNAS*, 112(33):10551–10556, August 2015.

[40] Deokjae Lee, Wonjun Choi, J. Kertész, and B. Kahng. Universal mechanism for hybrid percolation transitions. *Scientific Reports*, 7(1):5723, July 2017.

[41] Peng-Bi Cui, Francesca Colaiori, and Claudio Castellano. Mutually cooperative epidemics on power-law networks. *Phys. Rev. E*, 96(2):022301, August 2017.

[42] Li Chen, Fakhteh Ghanbarnejad, and Dirk Brockmann. Fundamental properties of cooperative contagion processes. *New J. Phys.*, 19(10):103041, 2017.

[43] Jorge P. Rodríguez, Yu-Hao Liang, Yu-Jhe Huang, and Jonq Juang. Diversity of hysteresis in a fully cooperative coinfection model. *Chaos*, 28(2):023107, February 2018.

[44] Jorge P. Rodríguez, Fakhteh Ghanbarnejad, and Víctor M. Eguíluz. Risk of Coinfection Outbreaks in Temporal Networks: A Case Study of a Hospital Contact Network. *Frontiers in Physics*, 5, 2017.

[45] Zhilan Feng, Ronsong Liu, Zhipeng Qiu, Joaquin Rivera, and Abdul-Aziz Yakubu. Coexistence of competitors in deterministic and stochastic patchy environments. *Journal of Biological Dynamics*, 5(5):454–473, September 2011.

[46] Zhipeng Qiu, Qingkai Kong, Xuezhi Li, and Maia Martcheva. The vector–host epidemic model with multiple strains in a patchy environment. *Journal of Mathematical Analysis and Applications*, 405(1):12–36, September 2013.

[47] Kuang-Hui Lin, Yuan Lou, Chih-Wen Shih, and Tze-Hung Tsai. Global dynamics for two-species competition in patchy environment, March 2014.

[48] Erida Gjini, Carina Valente, Raquel Sá-Leão, and M. Gabriela M. Gomes. How direct competition shapes coexistence and vaccine effects in multi-strain pathogen systems. *Journal of Theoretical Biology*, 388:50–60, January 2016.

[49] Sarah Cobey and Marc Lipsitch. Pathogen diversity and hidden regimes of apparent competition. *Am Nat*, 181(1):12–24, January 2013.

[50] J. Gómez-Gardeñes, L. Lotero, S. N. Taraskin, and F. J. Pérez-Reche. Explosive Contagion in Networks. *Scientific Reports*, 6:19767, January 2016.

[51] Peter Sheridan Dodds and Duncan J. Watts. Universal Behavior in a Generalized Model of Contagion. *Physical Review Letters*, 92(21):218701, May 2004.

[52] Wei Wang, Quan-Hui Liu, Junhao Liang, Yanqing Hu, and Tao Zhou. Coevolution spreading in complex networks. *arXiv:1901.02125 [physics]*, January 2019. arXiv: 1901.02125.

[53] Jorge P. Rodríguez, Fakhteh Ghanbarnejad, and Víctor M. Eguíluz. Particle velocity controls phase transitions in contagion dynamics. *Scientific Reports*, 9(1):1–9, April 2019.

[54] Wonjun Choi, Deokjae Lee, J. Kertész, and B. Kahng. Two golden times in two-step contagion models: A nonlinear map approach. *Phys. Rev. E*, 98(1):012311, July 2018.

[55] Sourya Shrestha, Betsy Foxman, Daniel M. Weinberger, Claudia Steiner, Cécile Viboud, and Pejman Rohani. Identifying the interaction between influenza and pneumococcal pneumonia using incidence data. *Sci Transl Med*, 5(191):191ra84, June 2013.

[56] Lulla Opatowski, Marc Baguelin, and Rosalind M. Eggo. Influenza interaction with cocirculating pathogens and its impact on surveillance, pathogenesis, and epidemic profile: A key role for mathematical modelling. *PLOS Pathogens*, 14(2):e1006770, February 2018.

[57] Laith J. Abu-Raddad, Padmaja Patnaik, and James G. Kublin. Dual infection with HIV and malaria fuels the spread of both diseases in sub-Saharan Africa. *Science*, 314(5805):1603–1606, December 2006.

[58] Charles D. Wells, J. Peter Cegielski, Lisa J. Nelson, Kayla F. Laserson, Timothy H. Holtz, Alyssa Finlay, Kenneth G. Castro, and Karin Weyer. HIV infection and multidrug-resistant tuberculosis: the perfect storm. *The Journal of Infectious Diseases*, 196 Suppl 1:S86–107, August 2007.

[59] D. W. Dowdy, C. Dye, and T. Cohen. Data needs for evidence-based decisions: a tuberculosis modeler's 'wish list'. *Int. J. Tuberc. Lung Dis.*, 17(7):866–877, July 2013.

[60] Margarita Pons-Salort, Véronique Letort, Michel Favre, Isabelle Heard, Benoit Dervaux, Lulla Opatowski, and Didier Guillemot. Exploring individual HPV coinfections is essential to predict HPV-vaccination impact on genotype distribution: a model-based approach. *Vaccine*, 31(8):1238–1245, February 2013.

[61] Penelope Gray, Tapio Luostarinen, Simopekka Vänskä, Tiina Eriksson, Camilla Lagheden, Irene Man, Johanna Palmroth, Ville N. Pimenoff, Anna Söderlund-Strand, Joakim Dillner, and Matti Lehtinen. Occurrence of human papillomavirus (HPV) type replacement by sexual risk-taking behaviour group: Post-hoc analysis of a community randomized clinical trial up to 9 years after vaccination (IV). *International Journal of Cancer*, 145(3):785–796, August 2019.

[62] Carmen Lía Murall, Kevin S. McCann, and Chris T. Bauch. Revising ecological assumptions about Human papillomavirus interactions and type replacement. *Journal of Theoretical Biology*, 350:98–109, June 2014.

[63] S. Gagneux. Fitness cost of drug resistance in Mycobacterium tuberculosis. *Clinical Microbiology and Infection*, 15:66–68, January 2009.

[64] Anita H Melnyk, Alex Wong, and Rees Kassen. The fitness costs of antibiotic resistance mutations. *Evol Appl*, 8(3):273–283, March 2015.

[65] Hussin A. Rothan, Mehdi R. M. Bidokhti, and Siddappa N. Byrareddy. Current concerns and perspectives on Zika virus co-infection with arboviruses and HIV. *Journal of Autoimmunity*, 89:11–20, May 2018.

[66] Tereza Magalhaes, Cynthia Braga, Marli T. Cordeiro, Andre L. S. Oliveira, Priscila M. S. Castanha, Ana Paula R. Maciel, Nathalia M. L. Amancio, Pollyanne N. Gouveia, Valter J. Peixoto-da-Silva Jr, Thaciana F. L. Peixoto, Helena Britto, Priscilla V. Lima, Andreza R. S. Lima, Kerstin D. Rosenberger, Thomas Jaenisch, and Ernesto T. A. Marques. Zika virus displacement by a chikungunya outbreak in Recife, Brazil. *PLOS Neglected Tropical Diseases*, 11(11):e0006055, November 2017.

[67] Peter Grassberger, Li Chen, Fakhteh Ghanbarnejad, and Weiran Cai. Phase transitions in cooperative coinfections: Simulation results for networks and lattices. *Phys. Rev. E*, 93(4):042316, April 2016.

[68] Li Chen, Fakhteh Ghanbarnejad, Weiran Cai, and Peter Grassberger. Outbreaks of coinfections: The critical role of cooperativity. *EPL (Europhysics Letters)*, 104(5):50001, December 2013.

[69] Fatemeh Zarei, Saman Moghimi-Araghi, and Fakhteh Ghanbarnejad. Exact solution of generalized cooperative susceptible-infected-removed (SIR) dynamics. *Physical Review E*, 100(1):012307, July 2019.

Supplementary material for: Interplay between competitive and cooperative interactions in a three-player pathogen system

Francesco Pinotti[1], Fakhteh Ghanbarnejad[2,3,4], Philipp Hövel[2,5], and Chiara Poletto[1,*]

[1]INSERM, Sorbonne Université, Institut Pierre Louis d'Épidémiologie et de Santé Publique, IPLESP, F75012, Paris, France
[2]Institut für Theoretische Physik, Technische Universität Berlin, Hardenbergstraße 36, 10623 Berlin, Germany
[3]The Abdus Salam International Centre for Theoretical Physics (ICTP), Trieste, Italy
[4]Physics Department, Sharif University of Technology, P.O. Box 11165-9161, Tehran, Iran
[5]School of Mathematical Sciences, University College Cork, Western Road, Cork T12 XF62, Ireland
[*]chiara.poletto@inserm.fr

1 Methods

Mean-field dynamics

We studied the mean-field dynamical system described by equations (1) in the main paper by stability analysis and numerical integration. We derived closed-form expressions for all fixed-points and almost all conditions underlying their local stability. We used numerical evaluation of the Jacobian's spectrum to study stability whenever an analytical solution was not possible and to check the accurracy of the analytical results as well. We then numerically integrated the mean-field equations exploring different initial conditions. Numerical integration of the ordinary differential equations was performed in *Python 3.6* using the function *odeint* from the *Scipy* package.

Mean-field dynamics with communities

The epidemic in each population follows the same dynamics as in equations (1) of the main text. The infection terms, however, must be modified in order to account for the different contributions (between and within community) to the force of infection. Specifically, the force of infection due to, e.g. B_1, acting on an individual in community $c = 1, 2$ becomes $\beta_1\left[(1-\epsilon)X_1^{(c)} + \epsilon X_1^{(c')}\right]$, where $c \neq c'$. The two distinct terms appearing in this expression represent the contributions due to infected individuals in the same community (c) and in the other community (c'), respectively. Notice that for 2 interacting populations, as considered in the main paper, we can reduce the number of independent equations from 12 to 10 by exploiting density conservation within each populations, i.e. $\sum_Z Z^{(c)} = 1$, where $Z^{(c)}$ denote the fraction of individuals in state Z and community $c = 1, 2$. Numerical integration of these equations is performed in the same way as in the case of a single population.

Network models

We used the algorithm outlined in [1] to efficiently generate Erdős-Rényi networks. In order to generate modular networks with n_C communities and adjustable community strength, we first group nodes into n_C different communities. Here we chose for simplicity to assign exactly N/n_C nodes to each community. Each node receives a random number of open connections drawn from a Poisson distribution with average $\bar{k}$. We then classify each of these connections as either a within-community or an inter-community stub with probabilities $1-\epsilon$ and ϵ, respectively. Links are finally created by matching stubs. Within-community (between-community) stubs are matched with each other according to a configuration model. We eventually discard self-links, multiple links between any pair of nodes and unmatched stubs. For large networks, the number of discarded stubs is usually negligible compared to the number of links. Notice that this algorithm enables us to independently set both the degree distribution and the strength of the community structure.

Simulating spread of concurrent diseases on networks

Simulations occur in discrete time. During each time step we check first for possible infection events caused by infected nodes and then for recovery events. Every infected node tries to transmit the disease(s) it is carrying to each of its neighbours. Each naive susceptible individual (compartment S) can get infected by pathogen A with probability $1-(1-\alpha)^{n_A}$, where n_A is the number of its susceptible neighbours carrying A. At the same time, a naive susceptible can also be infected by either B_1 or B_2. To avoid co-infections with B_1 and B_2, we loop over the neighbours of the naive node in a random order, checking for each infectious neighbour node if infection occurs or not (according to the corresponding infection probability, i.e. either β_1 or β_2) and stopping iteration at the first successful infection event. Transmission with either B_1 or B_2 can

occur independently from A, thus direct transitions from S to either D_1 or D_2 compartments are allowed. Secondary infections are implemented in a similar way.

For convenience, the simulation time step Δt was taken as the time unit. To avoid possible spurious effects due to time discretisation we set the infectious duration to be longer than the time step, i.e. $\mu^{-1} = 20\Delta t$. During each time step, infected individuals recover from each of the diseases they are carrying with probability μ. As a consequence a doubly infected individual can turn into a fully susceptible individual with probability μ^2. Individuals cannot recover during the same time step they got infected.

For each simulation, we initially choose 100 nodes for each pathogen and set them infected with that pathogen. In the Erdős-Rényi case initially infected nodes are chosen at random, whereas in the case of modular networks the infected seeds are chosen at random within the community where a particular pathogen is seeded. We stop simulations 400 time steps after either B_1 or B_2 becomes extinct, or, alternatively, after reaching the maximum simulation time T_{max}. The former stopping condition is dictated by the need to discern simulations where A is able to persist from those where it becomes extinct right after extinction of either one of the B strains. When any of the stopping conditions is met, we check which pathogens have survived and the corresponding prevalence. To reconstruct the phase diagram of figures 4 and 5 of the main paper we have 500 and 140 simulations for any given point in the parameter space for the Erdős-Rényi and modular networks respectively.

2 Results

2.1 Equilibria and stability analysis for the well-mixed system

Here we enumerate fixed points and study the stability of each equilibrium point by finding the eigenvalues of the corresponding Jacobian matrix $\mathcal{J}$. Because total density is conserved, the effective number of independent equations can be reduced from 6 to 5. Therefore $\mathcal{J}$ is a 5x5 matrix. In the following we eliminate A exploiting total density conservation and consider S, B_1, B_2, D_1, and D_2 as independent variables. A is kept as a placeholder for $1-S-B_1-B_2-D_1-D_2$. The general form of the Jacobian is given by:

$$\begin{pmatrix} \alpha(S^*-X_A^*)-1-\beta_1 X_1^*-\beta_2 X_2^* & S^*(\alpha-\beta_1) & S^*(\alpha-\beta_2) & -1-\beta_1 S^* & -1-\beta_2 S^* \\ c_1\alpha B_1^*+\beta_1 X_1^* & c_1\alpha(B_1^*-X_A^*)+\beta_1 S^*-1 & c_1\alpha B_1^* & 1+\beta_1 S^* & 0 \\ c_2\alpha B_2^*+\beta_2 X_2^* & c_2\alpha B_2^* & c_2\alpha(B_2^*-X_A^*)+\beta_2 S^*-1 & 0 & 1+\beta_2 S^* \\ -c_1(\alpha B_1^*+\beta_1 X_1^*) & c_1\beta_1(A^*-X_1^*)+c_1\alpha(X_A^*-B_1^*) & -c_1(\alpha B_1^*+\beta_1 X_1^*) & c_1\beta_1(A^*-X_1^*)-2 & -c_1\beta_1 X_1^* \\ -c_2(\alpha B_2^*+\beta_2 X_2^*) & -c_2(\alpha B_2^*+\beta_2 X_2^*) & c_2\beta_2(A^*-X_2^*)+c_2\alpha(X_A^*-B_2^*) & -c_2\beta_2 X_2^* & c_2\beta_2(A^*-X_2^*)-2 \end{pmatrix} \tag{1}$$

1. **Disease free state**: $S^* = 1$.

For this equilibrium $\mathcal{J}$ takes the form of an upper triangular matrix. Therefore the eigenvalues can be read off immediately since they coincide with the diagonal elements. In particular: $\lambda \in \{\alpha - 1, \beta_1 - 1, \beta_2 - 1, -2, -2\}$. Stability is therefore ensured if and only if all base transmission rates are smaller than 1.

2. **Pathogen A only ($[A]$)**: $S^* = 1/\alpha, A^* = 1 - 1/\alpha$, which is feasible if and only if $\alpha > 1$.

   In this case one eigenvalue can be found immediately by inspection and it is equal to $1-\alpha$, which is always negative when this equilibrium is feasible (i.e. $\alpha > 1$). The rest of the Jacobian matrix takes a 2x2 block diagonal form with diagonal blocks $J_i^{[A]}$ $(i = 1, 2)$ given by:

$$J_i^{[A]} = \begin{pmatrix} -1 + c_i(1-\alpha)\beta_i/\alpha & 1 + \beta_i/\alpha \\ c_i(\beta_i + \alpha)(1 - \alpha^{-1}) & -2 + c_i\beta_i/\alpha \end{pmatrix}, \tag{2}$$

   whose eigenvalues can be determined by considering the matrix $\Gamma(\lambda) = J_i^{[A]} - \lambda I_2$, where I_n is the nxn identity matrix. We subtract the second column of Γ from the first column obtaining a new matrix Γ'. By construction $\det(\Gamma) = \det(\Gamma')$. Therefore, the characteristic polynomial is the same. Now, however, the latter polynomial already appears in a factorized form, yielding the eigenvalues $\lambda = -2 - c_i(\alpha - 1)$, which is always negative, and $\lambda = -1 + \beta_i c_i(1 - \alpha^{-1}) + \beta/\alpha$, which is negative if and only if $\beta_i < \dfrac{\alpha}{1 + c_i(\alpha - 1)}$. For $\alpha > 1$ (condition for the solution to be feasible, as written above), this is never true if either one of B_i is super-critical.

3. **Strain $\mathbf{B_i}$ only ($[B_i]$)**: $S^* = 1/\beta_i, B_i^* = 1 - 1/\beta_i$, which is feasible if and only if $\beta_i > 1$.

   In the following we will use the index i to refer to strain B_i while the index j will indicate the competitor. Here $\mathcal{J}$ can be broken down into a 2x2 upper triangular matrix and a 3x3 matrix. The former has eigenvalues -2 and $-1 + \dfrac{\beta_j}{\beta_i}$. Therefore, stability requires $\beta_i > \beta_j$. The remaining 3x3 matrix $J_3^{(B_i)}$ takes the form:

$$J_3^{[B_i]} = \begin{pmatrix} \alpha S^* - 1 - \beta_i B_i^* & \alpha S^* - 1 & -2 \\ \alpha c_i B_i^* + \beta_i - 1 & \alpha c_i B_i^* & 2 \\ -c_i(\alpha + \beta_i)B_i^* & -c_i(\alpha + \beta_i)B_i^* & -2 - \beta_i c_i B_i^* \end{pmatrix}, \tag{3}$$

   which can be easily diagonalized by considering the matrix $\Gamma(\lambda) = J_3^{[B_i]} - \lambda I_3$ and performing the following row operations: first add its first row to its second row, then add the second row to its third row; the first row is left unchanged. This procedure enables writing down the characteristic polynomial in an easy-to-factorize form, yielding the eigenvalues $\lambda = 1 - \beta_i$, $\lambda = -2 - c_i(\beta_i - 1)$ and $\lambda = \alpha c_i B_i^* - 1 + \alpha\beta_i^{-1}$. The former two are always

negative when this equilibrium is feasible, while the latter is negative if and only if $\alpha < \dfrac{\beta_i}{1 + c_i(\beta_i - 1)}$, which is never true if the spreading of A is super-critical.

4. A **and** $\mathbf{B_i}$ **syndemic** ($[A\&B_i]$): By using the equilibrium conditions $\dot{X}_i = 0$ and $\dot{X}_A = 0$,

$$\beta_i(S^* + c_i A^*) - 1 = 0, \tag{4}$$

and

$$\alpha(S^* + c_i B_i^*) - 1 = 0, \tag{5}$$

we find that $B_i^* = \dfrac{1 - \alpha S^*}{c_i \alpha}$ and $A^* = \dfrac{1 - \beta_i S^*}{c_i \beta_i}$. By exploiting density conservation, i.e. $D_i^* = 1 - S^* - A^* - B_i^*$, we can express every variable in terms of S^*. The latter is determined by a quadratic polynomial whose roots are given by:

$$S_\pm^* = \frac{1 \pm \sqrt{1 - \dfrac{4}{c_i \beta_i \alpha}\left(1 - \dfrac{1}{c_i}\right)}}{2\left(1 - \dfrac{1}{c_i}\right)}, \tag{6}$$

which exists if $\alpha\beta_i > 4(c_i - 1)/c_i^2$.

Here $\mathcal{J}$ can be broken down into a 2x2 and a 3x3 matrices. The smaller matrix $J_2^{[A\&B_i]}$ is given by:

$$J_2^{[A\&B_i]} = \begin{pmatrix} \beta_j S^* - \alpha c_j X_A^* - 1 & 1 + \beta_j S^* \\ -c_j(\alpha X_A^* + \beta_j A^*) & -2 - \beta_j c_j A^* \end{pmatrix}, \tag{7}$$

which can be easily diagonalised by using row/column operations, yielding the eigenvalues $\lambda = -2 - c_j \alpha X_A^*$ and $\lambda = -1 + \beta_j(S^* + c_j A^*)$. The former is always negative while the latter corresponds to the asymptotic growth rate of X_j. This is the only eigenvalue in which parameters β_j, c_j, which pertain to the competitor strain, appear.

$J_3^{[A\&B_i]}$ instead takes the form:

$$\begin{pmatrix} \alpha(S^* - X_A^*) - \beta_i X_i^* - 1 & S^*(\alpha - \beta_i) & -1 - \beta_i S^* \\ c_i \alpha B_i^* + \beta_i X_i^* & c_i \alpha(B_i^* - X_A^*) - 1 + \beta_i S^* & 1 + \beta_i S^* \\ c_i(\alpha B_i^* + \beta_i X_i^*) & c_i \alpha(X_A^* - B_i^*) + c_i \beta_i (A^* - X_i^*) & -2 + c_i \beta_i (A^* - X_i^*) \end{pmatrix}. \tag{8}$$

Although the spectrum of $J_3^{[A\&B_i]}$ cannot be determined analytically, we can still gain some insight about stability conditions by studying its characteristic polynomial. We do so by first computing $\Gamma(\lambda) = J_3^{[A\&B_i]} - \lambda I_3$. We then consider the matrix Γ' obtained by adding the first row of Γ to the second row and adding the second row to the third row. The characteristic equation takes the form $P(\lambda) = \lambda^3 + a_2\lambda^2 + a_1\lambda + a_0 = 0$. Now, the

Routh-Hurwitz criterion states that in order for all $P(\lambda)$'s roots to have a negative real part, the following conditions must be satisfied: $a_2 > 0$, $a_0 > 0$ and $a_2 a_1 > a_0$. We find that:

$$a_2 = 2 + (c_i + 1)(\alpha X_A^* + \beta_i X_i^*), \tag{9}$$

$$a_1 = \alpha\beta_i c_i^2 X_i^* X_A^* + c_i(2 + \alpha X_A^* + \beta_i X_i^*)(\alpha X_A^* + \beta_i X_i^*) + (1 - c_i)(\alpha^2 X_A^* + \beta_i^2 X_i^*)S^* \tag{10}$$

$$a_0 = \alpha\beta_i c_i^2 X_i^* X_A^* (\alpha + \beta_i)(1 - 2(1 - 1/c_i)S^*), \tag{11}$$

so $a_2 > 0$ always. Substituting $S_\pm^*$ inside the definition of a_0 yields $a_0(S_+^*) < 0$ and $a_0(S_-^*) > 0$. Therefore according to the Routh-Hurwitz criterion the solution S_+^* is never found to be stable. S_-^* is, instead, stable when the condition $a_2 a_1 > a_0$ is satisfied. The feasibility of $[A\&B_i]$ state can be checked numerically as well by requiring that $S^*, A, B_i^*, D_i^* > 0$. In particular, the condition $\alpha\beta_i > 4(c_i - 1)/c_i^2$ ensures that S_-^* is real and positive and explains the vertical boundary delimiting the $[A\&B_2]$ stable region in figure 2b in the main manuscript.

5. **All strains coexist** We first consider the equilibrium conditions $\dot{X}_i = 0$, $i = 1, 2$, given by Eq. (4), which allow us to obtain S^* and A^*:

$$S^* = \frac{c_2\beta_2 - c_1\beta_1}{\beta_1\beta_2(c_2 - c_1)},$$

$$A^* = \frac{\beta_2 - \beta_1}{\beta_1\beta_2(c_1 - c_2)}.$$

Notice that if $\beta_2 > \beta_1$, then we need $c_1 > c_2$ and $c_1\beta_1 > c_2\beta_2$ for this fixed point to be feasible. After some algebra one can obtain a quadratic equation for B_1^*:

$$\begin{aligned}
&\Big(1 + \beta_2 S^*\Big)\Big(1 - S^* - A^*\Big) + c_2^{-1}\Big(S^* - \alpha^{-1}\Big)\Big(1 + \alpha S^* + \alpha c_2(1 - S^*)\Big) + \\
&B_1^*\Bigg\{ - 1 - \beta_2 S^* - \frac{1 + \beta_2 S^*}{1 + \beta_1 S^*}\Big(1 - c_1/c_2 + \alpha c_1 - (\beta_1 + \alpha c_1(1 - c_2^{-1}))S^*\Big) + \\
&\Big(1 - \alpha S^*\Big)\Big(1 - c_1/c_2\Big) + c_1/c_2\Big(1 + \alpha S^* + \alpha c_2(1 - S^*)\Big)\Bigg\} + \\
&B_1^{*2}\alpha c_1\Big(c_1/c_2 - 1\Big)\left(1 - \frac{1 + \beta_2 S^*}{1 + \beta_1 S^*}\right) = 0.
\end{aligned} \tag{12}$$

Once the roots of the latter equations have been found, the remaining fractions can be computed using:

$$B_2^* = c_2^{-1}\Big(\alpha^{-1} - S^* - c_1 B_1^*\Big),$$

$$D_1^* = \frac{1 - \beta_1 S^* + \alpha c_1\Big(1 - S^* - B_1^* - B_2^*\Big)}{1 + \beta_1 S^*} B_1^*,$$

$$D_2^* = 1 - S^* - A^* - B_1^* - B_2^* - D_1^*.$$

By numerically computing these equilibria, we found that they can be feasible under certain conditions on the parameters. The condition for their stability cannot be computed analytically. However, we can still evaluate the Jacobian at the fixed points and then compute its eigenvalues numerically and find that the equilibria are always unstable.

Additional results

References

[1] Vladimir Batagelj and Ulrik Brandes. Efficient generation of large random networks. *Phys. Rev. E*, 71(3):036113, March 2005.

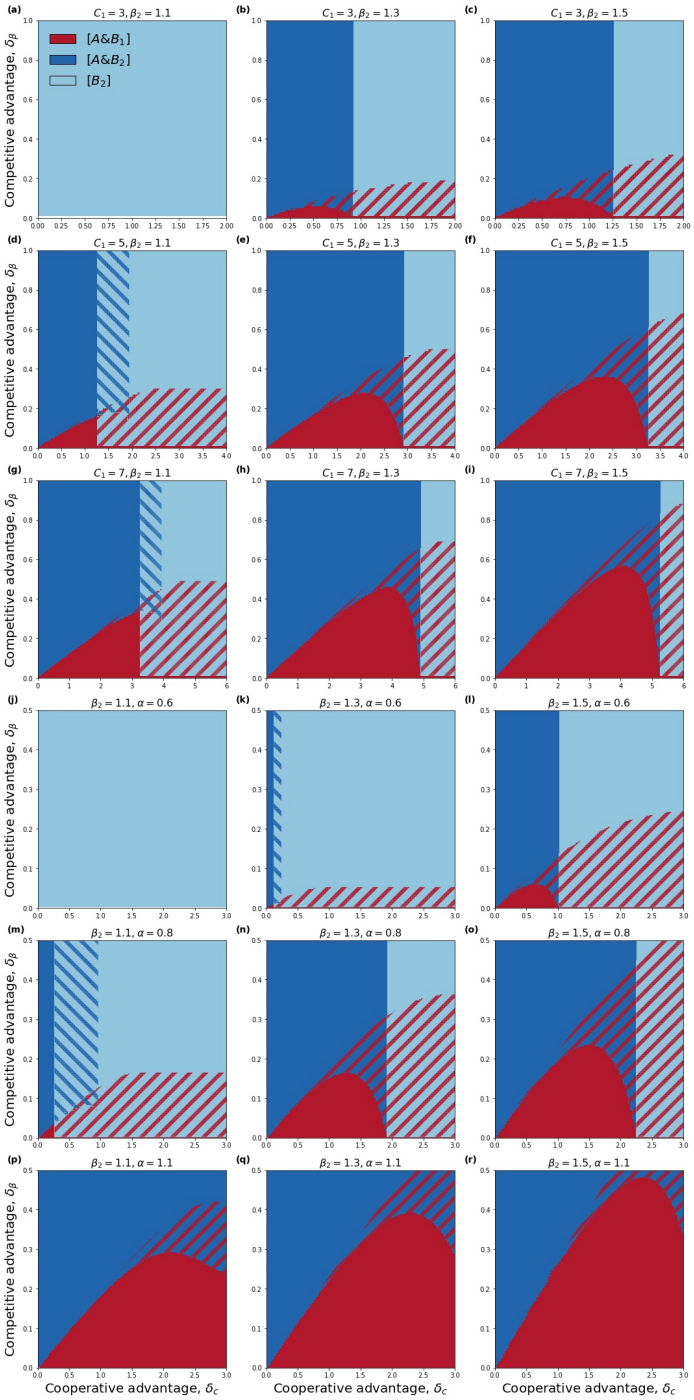

Figure S1: Phase diagram for different values of β_2, α and c_1. (a)-(i) $\alpha = 0.8$. (j)-(r) $c_1 = 4$. The range of β_1 includes values below 1.

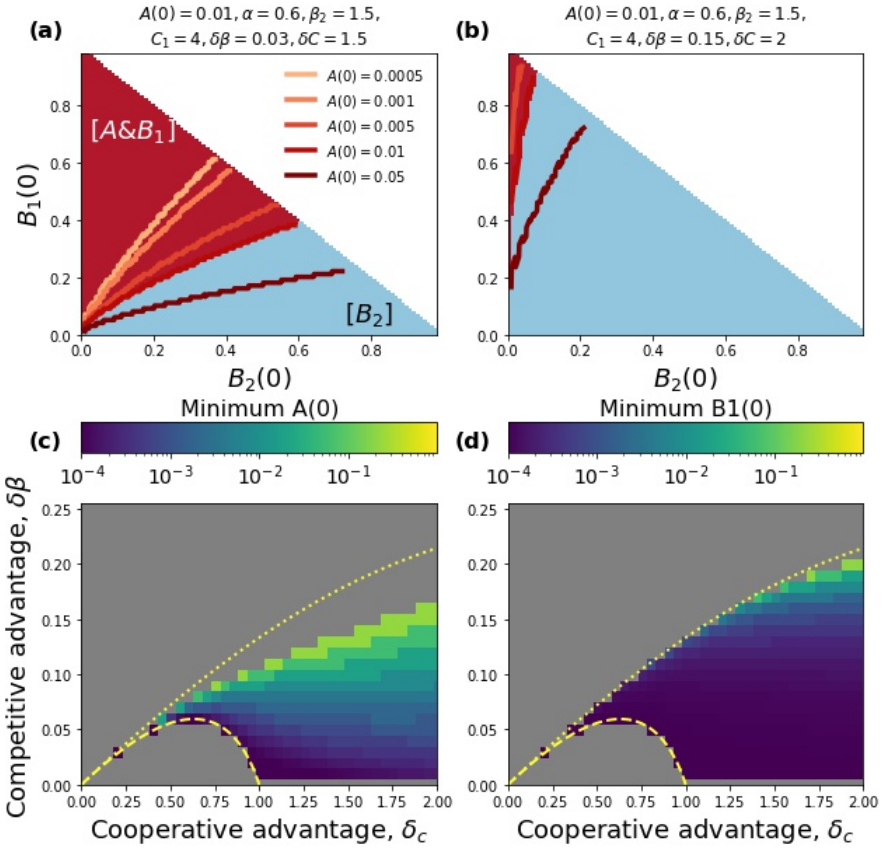

Figure S2: Initial conditions and mean-field dynamics. (a),(b) Final outcome as a function of $B_1(0)$ and $B_2(0)$ with $A(0) = 0.01$. Additional boundaries separating the two dominance regions and corresponding to different values of $A(0)$ are also showed. For each value of $A(0)$ we explore values of $B_1(0)$ and $B_2(0)$ in the simplex $0 \leq B_1(0) + B_2(0) \leq 1 - A(0)$. Prameters were: (a) $\delta_\beta = 0.03$, $\delta_c = 1.5$, (b) $\delta_\beta = 0.15$, $\delta_c = 2$. (c) Minimum amount of $A(0)$ required in order for B_1 to win as a function of δ_β and δ_c, given that $B_1(0) = B_2(0) = 0.001$. (d) Minimum amount of $B_1(0)$ required in order for B_1 to win as a function of δ_β and δ_c, given that $A(0) = 0.01$ and $B_2(0) = 0.001$. Grey regions in (c,d) correspond to either absence of bistability or to parameter choices for which B_1 never wins. This figure shows that a sufficiently large advantage in terms of initial conditions can lead to B_1 winning the competition in the bistable region. Other parameters are the same as in figure 2a of the main manuscript.

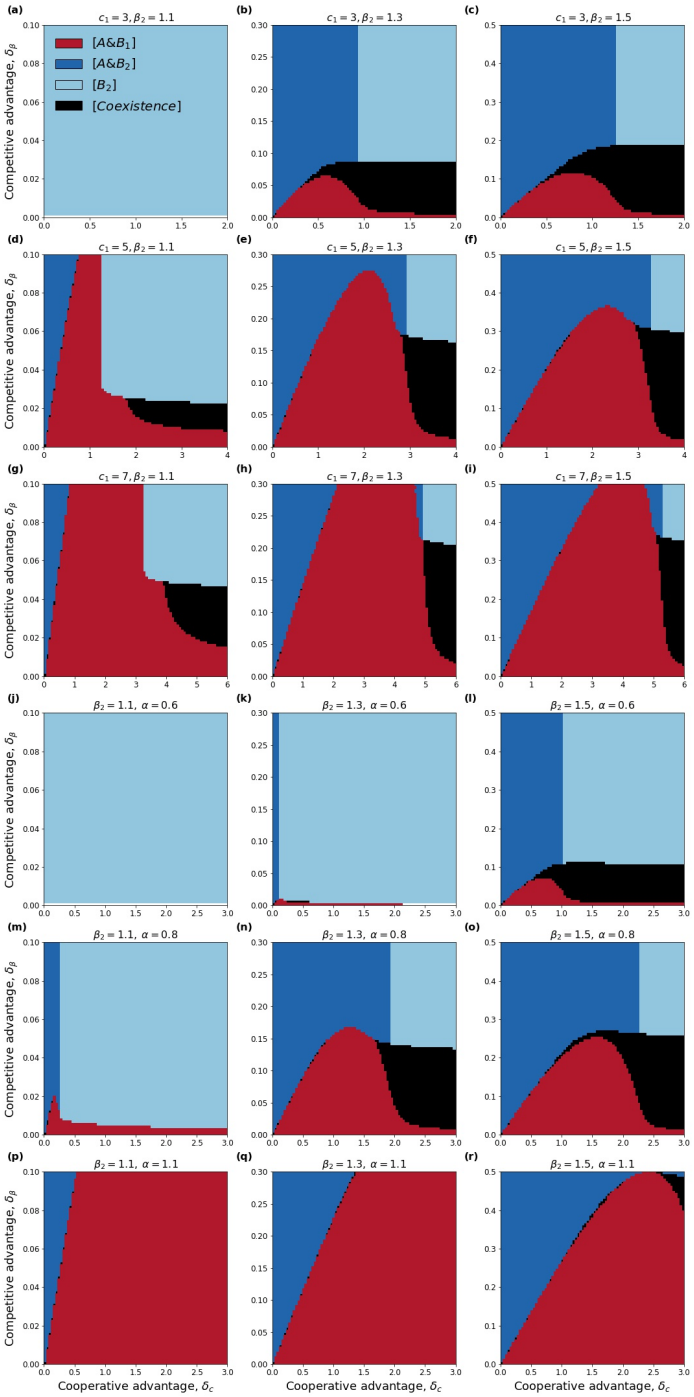

Figure S3: Equilibrium configuration for two interacting communities for different values of β_2, α and c_1. (a)-(i) $\alpha = 0.8$. (j)-(r) $c_1 = 4$. Initial conditions are as in figure 4c of the main paper. Here we have considered values of δ_β and δ_c such that β_1, β_2, c_1 and c_2 are all larger than unity. Increasing values of α have a positive effect on the persistence of B_1.

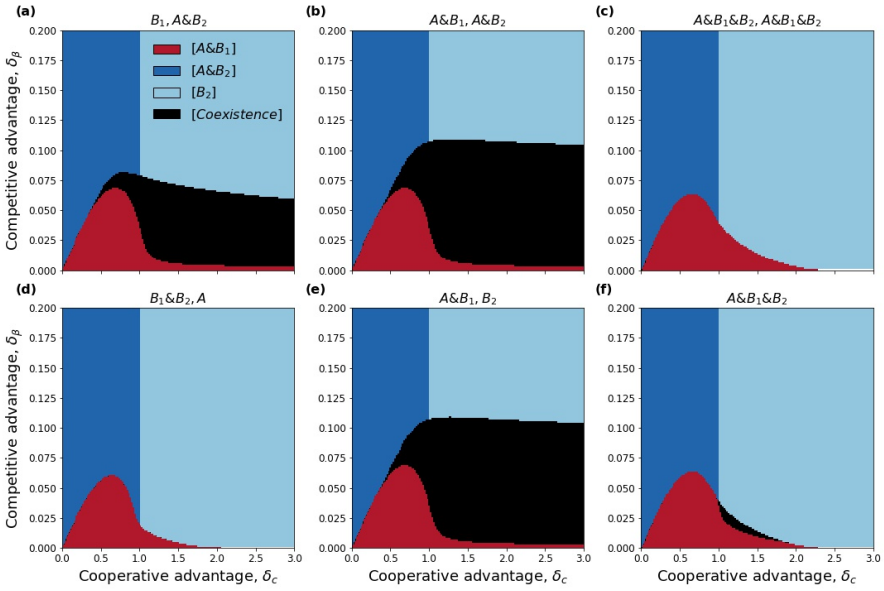

Figure S4: Role of initial conditions in mean-field dynamics with communities. Final outcome as a function of δ_c and δ_β for different initial conditions. The title of each panel indicates in which communities each pathogen is seeded into; the initial density of a pathogen in the community it is seeded into is set to 0.01. Other parameters are as in figure 4 of the main manuscript.

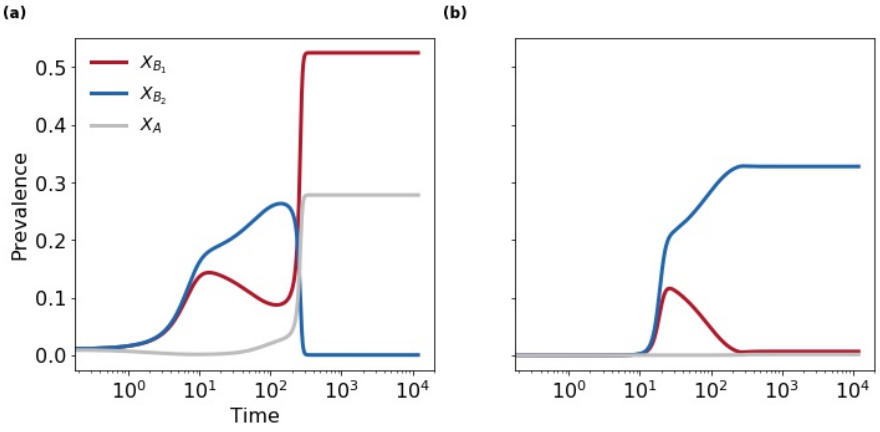

Figure S5: Dynamics with two strains seeded in the same community. Dynamical trajectories of B_1's, B_2's and A's total prevalence (in red, blue and gray respectively) in community 1 (a) and 2 (b). Trajectories were obtained numerically by starting from $B_1^{(1)}(t=0) = B_2^{(1)}(t=0) = A^{(1)}(t=0) = 0.01$. Around $t = 10$, B_2 takes over community 2 as a results of its advantage in transmissibility. At this point B_1's prevalence declines until A gives rise to a new outbreak; the latter ultimately leads to a B_1 dominance in the first community. Here we set $\delta_\beta = 0.025$, $\delta_c = 1.2$ and $\epsilon = 0.0002$. Other parameters are as in figure 2a.

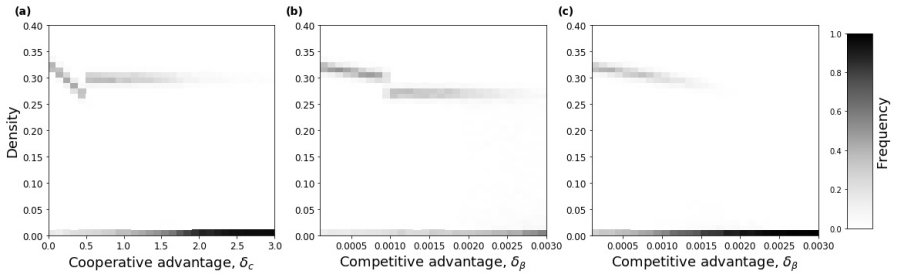

Figure S6: Final-state density of X_A for stochastic simulations on ER networks. (a-c) show the probability of the final state for a given value of X_A. Here we do not differentiate between which final state is attained, i.e. which pathogen persists. (a) has been obtained for $\delta_\beta = 0.001$, while (b) and (c) have been obtained for $\delta_c = 0.4$ and $\delta_\beta = 1.5$, respectively. In (a) we can observe two types of transitions in the behavior of X_A: the sharp transition at $\delta_c = 0.5$ corresponds to a leap from state $[A\&B_2]$ to state $[A\&B_1]$. As δ_c is further increased, extinction of A becomes increasingly probable as the state $[B_2]$ is reached with a higher frequency. This transition is, however, gradual and around $\delta_c = 1.3$ a crossover is reached where states $[A\&B_1]$ and $[B_2]$ are reached with equal probability. Other parameters are as in figure 6.

4.5 Conclusions

In conclusion, strain dynamics is fundamentally altered by interactions with co-circulating pathogens. In particular, we showed that a rich phenomenology emerges in a minimal model accounting for both competitive and cooperative interactions. Importantly, the observed phase diagram is the result of the non-linear interplay between such interactions.

We analytically computed fixed points and the conditions for their stability by means of linear stability analysis. For some parameter choices, stability regions overlap, giving rise to bistable and, eventually, multistable behavior. Within these regions of phase space, epidemiological parameters as well as initial conditions determine the fate of the system. We presented a numerical analysis of initial conditions for a few parameter choices, highlighting the importance of initial conditions. It would be interesting in a future work to study analytically the shape of attraction basins and thus derive necessary and sufficient conditions for each final state to be reached.

Contact structure plays an important role on the dynamics. Community structure, for example, allows population-level co-existence between both strains. In this case, strains are segregated into different communities in order to minimize competition for hosts. Co-existence is ultimately maintained thanks to the cooperative pathogen, whose presence alters the local host environment, dynamically creating multiple ecological niches.

Simulations on Erdős-Rényj and modular networks displayed results analogous to the mean-field case while also shedding light on the nature of various transitions and on the role of initial conditions and stochasticity. Additional network structures, e.g. heterogeneous degrees, clustering and the time evolution of contacts might alter the dynamics as well and thus constitute object of future research.

Our work provides new mechanistic insights on ecological factors driving the dynamics of competing strains. Moreover, it represents a starting point towards more complex models addressing the interplay of multiple biological interactions. With this respect, lifting symmetries in epidemiological parameters within our model is likely to yield more complex dynamical behavior. Asymmetric cooperation between pathogens A and B, for instance, may allow full co-existence by creating inter-dependencies between species involved.

Chapter 5

Conclusions and Perspectives

Diversity in multi-strain assemblies is shaped by many factors, including interference between different strains/pathogens, as well as environmental and host-related factors. In this thesis we explored the effects of host-to-host contacts on strain diversity by means of mathematical modeling.

In Chapter 3 we studied the impact of host contact structure on the dynamics of mutually-excluding strains. More precisely, we investigated the role of relevant contact properties through extensive simulations on synthetic networks of contacts. By considering a neutral epidemiological model, we were able to tease apart the different effects of contact structure, competition for hosts and stochastic effects. Our analysis revealed the importance of contact heterogeneities on strain dynamics: highly active hubs facilitate the spread of some strains while also making it more difficult for new strains to emerge. As a consequence, heterogeneous contacts support less co-circulating strains compared to a homogeneous scenario and at the same time promote dominance of a few strains. The subdivision of hosts into different communities had a positive effect on diversity although its magnitude was small. We also found that strain richness was maximized at intermediate levels of host length of stay. This result, which arises from the balance between strain immigration and extinction, suggests that policies aiming to reduce patients' length of stay could affect the composition of nosocomial pathogens' populations.

Our theoretical results improved our interpretation of *S. aureus* carriage data in a hospital. Indeed, structural and temporal heterogeneities in host-to-host contacts were found to explain part of variability observed in carriage data. Our work may have important implications for the interpretation of strain diversity and for the estimation of strain-specific parameters. For example, because heterogeneous contact patterns appear to contribute to competitive pressure, neglecting the complexity of host behavior may overestimate variation in between-strain transmission potential. This aspect calls for further investigation; indeed, future work could address the bias introduced by the random mixing hypothesis on the estimation of strain-specific parameters.

Our approach was inspired by community ecology. Ecological indicators like, e.g., richness, Berger-Parker index and Shannon Evenness provided quantitative tools to characterize strain ecology and to assess consequences of mechanistic ingredients on ecological diversity. Our epidemiological model was based on parsimonious assumptions. A similar framework could be tailored to specific diseases or outbreaks by accounting for

additional ingredients. Here, for example, we relaxed the hypothesis of strain neutrality and discussed the role of heterogeneous transmissibility. Future work could address additional interaction mechanisms, e.g. super-infection, cross-immunity, and partial exclusion; the inclusion of these additional ingredients would allow us to investigate ecological questions that have been traditionally addressed in the context of two-strain models within our multi-strain framework.

In Chapter 4 we explored the effects of a co-circulating pathogen on the dynamics of two competing strains. We considered a minimal model where different interaction types are simultaneously at play. More in detail, strains were assumed to mutually exclude each other, whereas the interaction with the second pathogen was assumed to be synergistic and mediated by increased susceptibility. The final outcome of competition was dictated not only by the bare transmissibility of each strain but also by their ability to cooperate with the second pathogen. Our analysis revealed a rich phase diagram whose features cannot be fully understood by addressing each interaction alone. In fact, we have shown that certain phenomena arise from the complex interplay of both competitive and cooperative interactions.

Importantly, host spatial separation was found to play an important role, allowing population-level coexistence of all species. Nonetheless, the presence of the cooperative pathogen is key to coexistence since it creates favorable conditions for the less transmissible strain to persist by locally modifying the host environment. Therefore, ecological niches emerge dynamically in our model thanks to trade-offs between competition, cooperation and spatial structure.

Our theoretical analysis represents a first step towards a class of more epidemiologically tailored models. These might include other mechanisms than the ones considered in this work. For example, if long-lasting immunity is conferred upon recovery, one should use a different, SIR-like compartmental structure. Additionally, interactions between unrelated pathogens might not be bi-directional nor be driven by the same biological mechanism. For example, while HIV increases susceptibility against *P. falciparum*, the latter increases the viral load of the former, increasing its transmissibility rather than susceptibility. It is likely that these models will exhibit even more complex behavior than the one reported in this work; for instance, we expect eventual trade-offs between competitive and cooperative abilities to allow for coexistence even in homogeneous populations.

In conclusion, this thesis contributes to the literature of multi-strain interaction on network-structured host populations. We confirm the importance of human contact behavior in shaping strain diversity as well as the importance of simultaneously accounting for both pathogen and host heterogeneities in multi-strain models.

Appendix A

Multi-strain model

A.1 Model description

In this section we provide a detailed explanation of the compartmental model used in Chapter 3. We consider a strain population made up by S strains (S is not necessarily finite). Each strain $l = 1, \dots, S$ is assumed to evolve according to SIS dynamics with transmissibility β_l and recovery rate μ_l. Strains compete for hosts through mutual exclusion, thus an infected individual is completely protected against further infections until it recovers. In a neutral scenario strains are assumed to share the same reproductive abilities. This amounts to the parameter choice: $\beta_l = \beta$ and $\mu_l = \mu \ \forall\, l = 1, \dots, S$. The compartmental model is shown in Fig. A.1.

The host population is assumed to be open: new hosts arrive at rate λ_{in} and are finally discharged at rate λ_{out}. The inverse of λ_{out} represents the average length of stay τ. In this model, the average population size is given by $\bar{N} = \lambda_{in}\tau$. At admission, any individual has a probability p_s to be already carrying a strain. If S is finite, the latter is chosen at random, otherwise it is a completely new, previously unseen strain.

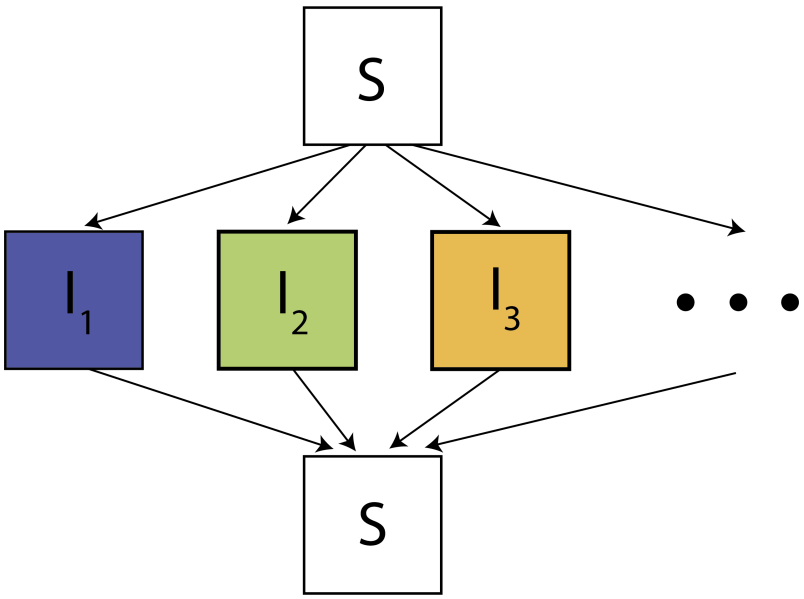

FIGURE A.1: **Compartmental model.** Graphical representation of the compartmental model considered.

In Chapter 3 we considered an additional mechanism through which new strains may be introduced, namely self-infection $S \to I_l$ at rate q_s. This process models the effects of potential contamination sources other than observed contacts, e.g. environmental contamination in the form of fomites or transmission due to unobserved contacts; the latter case might occur when contact structure is actually informed from contact data with missing interactions due to, e.g., imperfect measurements or interactions with individuals that are not included in the study cohort.

A.2 Simulating transmission

Since simulations are carried in discrete time, it is possible for a susceptible individual to engage in concurrent interactions with individuals carrying different strains. How to resolve which strain is transmitted during concurrent interactions?

One possible solution is to proceed as follows: we visit infected neighbors sequentially and in random order. For each of them we check whether transmission occurs or not by taking a draw from a Bernoulli distribution with parameter β_l. The latter represents the probability of transmission given that the currently visited neighbor carries strain l. We keep on iterating over infected neighbors until a successful transmission event occurs. In that case, the strain carried by the "successful" neighbor is transmitted.

We now compute the probability $P_1(n_1, n_2)$ that strain 1 is actually transmitted for the case of two competing strains. Let us assume that a susceptible node is surrounded by n_1 and n_2 neighbors carrying strains 1, 2 respectively. We find that $P_1(n_1, n_2)$ is given by:

$$P_1(n_1, n_2) = \sum_{m_1=1}^{n_1} \sum_{m_2=0}^{n_2} \frac{m_1}{m_1 + m_2} B(m_1|\beta_1, n_1) B(m_2|\beta_2, n_2)\,, \tag{A.1}$$

where $B(x|p, n)$ is the probability that exactly x neighbors out of n are able to transmit the disease successfully and is given by a binomial distribution. The expression (A.1) is obtained by conditioning the probability of strain 1 being transmitted on the numbers of neighbors failing to transmit either strain before a successful transmission event occurs.

$P_1(n_1, n_2)$ can be computed exactly in the neutral case ($\beta_1 = \beta_2 = \beta$). By changing variable from m_2 to $r = m_1 + m_2$ we obtain:

$$\begin{aligned} P_1^{neutral}(n_1, n_2) &= \sum_{m_1=1}^{r} \sum_{r=1}^{n_1+n_2} \frac{m_1}{r} \binom{n_1}{m_1} \binom{n_2}{r - m_1} \beta^r (1-\beta)^{n_1+n_2-r} \\ &= \frac{n_1}{n_1 + n_2} \sum_{r=1}^{n_1+n_2} \binom{n_1 + n_2}{r} \beta^r (1-\beta)^{n_1+n_2-r} \\ &= \frac{n_1}{n_1 + n_2} [1 - (1-\beta)^{n_1+n_2}]\,, \end{aligned} \tag{A.2}$$

the sum over m_1 is performed by multiplying and dividing each term inside the sum by $\binom{n_1+n_2}{r}$ and by recognizing the average value of a hypergeometric random variable. In the case of s concurrent strains we obtain:

$$P_1^{neutral}(\{n_l\}_{l=1,\dots,s}) = \frac{n_1}{\sum n_l}[1-(1-\beta)^{\sum n_l}]\,, \tag{A.3}$$

where $\sum n_l$ is the number of infected neighbors. To derive this result, it is sufficient to use (A.2) and substitute n_2 with the number of infected neighbors that are not carrying strain 1.

If transmission probabilities differ, the sum in Eq. (A.1) cannot be performed analytically. However, we can show that $P_1(n_1, n_2)$ satisfies the following recurrence relation:

$$P_1(n_1,n_2) = \frac{n_1}{n_1+n_2}\beta_1 + \frac{n_1}{n_1+n_2}(1-\beta_1)P_1(n_1-1,n_2) + \frac{n_2}{n_1+n_2}(1-\beta_2)P_1(n_1,n_2-1)\,, \tag{A.4}$$

which follows by conditioning on the outcome of transmission by the first visited neighbor. Specifically, four possible outcomes are possible in our case and correspond to whether the first visited neighbor carries strain 1 or 2 (with probability $n_1/(n_1+n_2)$ and $n_2/(n_1+n_2)$ respectively) and whether transmission occurs or not. If the first strain carries strain 1 but it is not successful at transmission, the probability that some other neighbor transmits strain 1 is given by $P_1(n_1-1,n_2)$ since only n_1-1 "attempts" are left for strain 1. Similarly, if the first neighbor carries strain 2 but does not succeed at transmission, the conditional probability becomes $P_1(n_1,n_2-1)$. If the first neighbor transmits strain 1 or 2, the corresponding conditional probabilities are 1 and 0 respectively. Eq. (A.4) is finally obtained by using the law of conditional probability. This equation, together with the boundary conditions $P_1(n_1,0) = 1-(1-\beta_1)^{n_1}$ and $P_1(0,n_2) = 0$, enables the pre-computation of $P_1(n_1,n_2)$ for any value of n_1 and n_2. In practice, however, we chose to not compute$P_1(n_1,n_2)$ explicitly but to rather simulate transmission as explained at the beginning of this section.

Appendix B

Condensation threshold on networks

B.1 General framework

In this section we detail a general class of generative network models for which we are able to compute the condensation threshold. We consider an activity-driven generative algorithm which yields time-varying networks where each time stamp is created according to the same two-step mechanism outlined in Chapter 3: each node i turns active with probability a_i (drawn at admission from some distribution $P(a)$) and then establishes a random number of contacts with other active individuals. Contacts are obtained by matching stubs according to the configuration model algorithm.

Here we assume that an active node with activity potential a is assigned a random number of stubs $m|a$ given by:

$$m|a = 1 + \chi(a)\,, \tag{B.1}$$

where $\chi(a)$ is a Poisson random variable with average value $\langle\chi(a)\rangle$ that depends, in general, on activity. The average degree of a node with activity a is thus given by:

$$h(a) = a(1 + \langle\chi(a)\rangle)\,, \tag{B.2}$$

where the first factor comes from the probability of being active and the second factor represents the average number of stubs received upon activation.

In order to extend our mathematical framework to this class of contact networks we consider an activity-class approximation where individuals are sorted in different classes according to their activity potential a. We can now write down a set of dynamical equations in the spirit of heterogeneous mean field theory for the density $I(a,\beta)$ of individuals with activity potential a and that simultaneously carry a strain with transmissibility in the range $[\beta, \beta + d\beta]$ [234]. At equilibrium we must have:

$$\alpha P(a)\rho(\beta) - I(a,\beta) + \omega\left[P(a) - \int d\beta I(a,\beta)\right]\sum_{a'}\frac{h(a)h(a')}{\langle h\rangle^2}I(a',\beta) = 0\,, \tag{B.3}$$

where again we have introduced the quantities α and ω, which represent the dimensionless versions of the introduction rate and transmissibility respectively. Notice that the

infection term is given by a sum of contributions from all activity classes, with each term being weighted by the average connectivity between classes a and a', which is proportional to the product of their average degrees $h(a)h(a')$. If all nodes activate with the same probability $\bar{a}$ and $\langle \chi(a) \rangle = \tilde{k} - 1$, independently from a, we recover a homogeneously-mixed population with average degree $\bar{a}\tilde{k}$.

B.2 Analytical results

Once the general mathematical framework B.3 is set, we can derive a general expression for the condensation threshold for the class of network models that we have just introduced.

Our starting point is Eq. (B.3), which we rewrite in matrix form:

$$\sum_{a'} M_{a,a'} I(a', \beta) = \alpha P(a) \rho(\beta) \,, \tag{B.4}$$

where $M_{a,a'} = \delta_{a,a'} - \omega[P(a) - \int d\beta I(a,\beta)]f(a)f(a')$ and $f(a) = h(a)/\langle h \rangle$ is the rescaled degree of individuals with activity a. Eq. (B.4) is a linear system of equations whose solution is given by:

$$I(a,\beta) = \frac{\alpha \rho(\beta)}{1 - \omega \sum_a S(a) f(a)^2} \frac{S(a) f(a)}{\sum_a S(a) f(a)} \,, \tag{B.5}$$

where we introduced the density of susceptible individuals with activity a: $S(a) = P(a) - \int d\beta I(a,\beta)$. The sampling distribution is obtained by summing Eq. (B.5) over all activity classes, yielding:

$$I(\beta) = \frac{\alpha \rho(\beta)}{1 - \omega \sum_a S(a) f(a)^2} \,, \tag{B.6}$$

Eq. (B.6) is akin to the expression for the sampling distribution obtained under the homogeneous mixing assumption. Indeed, by using the same arguments from Chapter 3 we find that condensation occurs when:

$$\langle \beta_{max} \rangle = \frac{\mu + \lambda_{out}}{\langle h \rangle \sum_a S(a) f(a)^2} \,, \tag{B.7}$$

which now depends on network structure as well. The quantity $\sum_a S(a) f(a)^2$, which encodes the dependence on contact structure, can be rewritten as:

$$\sum_a [P(a) - \int d\beta I(a,\beta)] f(a)^2 = \langle f^2 \rangle - \Gamma \,, \tag{B.8}$$

where $\Gamma = \sum_a \int d\beta I(a,\beta) f(a)^2$. Our aim now is to compute Γ. We argue that at stationariety Γ settles around a constant value which varies slowly with σ in the $\sigma < \sigma_c$ regime. Thus, we can estimate the condensation threshold by considering the purely neutral scenario and substitute Γ with its neutral counterpart Γ_0, obtained by assuming that every strain has the same transmissibility β_0. In this case, the equations (B.3) reduce to:

$$-I(a)+\alpha P(a)+\omega_0 f(a)\Big[P(a)-I(a)\Big]\Theta_0=0\,, \tag{B.9}$$

where we introduced $\Theta_0 = \sum_a f(a)I(a)$. Θ_0 represents the average degree of the infected nodes, rescaled by $\langle h\rangle$ and under the assumption of purely neutral dynamics. By multiplying the last equation by $f(a)$ and then summing over a, we find that Γ_0 can be expressed in terms of Θ_0:

$$\Gamma_0=\langle f^2\rangle-\frac{1}{\omega_0}\left(1-\frac{\alpha}{\Theta_0}\right). \tag{B.10}$$

Θ_0 is then found self-consistently by plugging $I(a)$ (obtained from Eq. (B.9)) inside its own definition:

$$\Theta_0=1-(1-\alpha)\sum_a\frac{P(a)f(a)}{1+\omega_0\Theta_0 f(a)}\,. \tag{B.11}$$

Once Θ_0 is found, we can finally estimate σ_c from Eq. (B.7):

$$\frac{\sigma_c}{\beta_0}=\frac{1}{\eta(S)}\left(\frac{\alpha}{\Theta_0-\alpha}\right). \tag{B.12}$$

Although σ_c cannot be expressed explicitly in terms of α and β_0 because of the implicit dependence through Θ_0, we can still obtain additional insight about the condensation threshold by investigating the properties of Θ_0 through Eq. (B.11). We can show for example that $\Theta_0 \geq \alpha$. Also, Θ_0 is found to be an increasing function of β_0, approaching the value 1 as β_0 is increased. This last result stems from the fact that for large β_0 everyone is infected, implying that $\Theta_0 \approx \sum_a f(a) = 1$. Finally, we have the following result:

$$\lim_{\beta_0\longrightarrow 1}\frac{\sigma_c}{\beta_0}=\frac{1}{\eta(S)}\left(\frac{\alpha}{1-\alpha}\right), \tag{B.13}$$

irrespective of the actual choice of $h(a)$ and $P(a)$. Thus, all network models introduced in the previous section share the same limiting value of condensation threshold as the average transmissibility β_0 is increased.

Bibliography

[1] Francesco Pinotti et al. "Host Contact Dynamics Shapes Richness and Dominance of Pathogen Strains". en. In: *PLOS Computational Biology* 15.5 (21-mag-2019), e1006530. ISSN: 1553-7358. DOI: 10.1371/journal.pcbi.1006530.

[2] Francesco Pinotti et al. "Interplay between competitive and cooperative interactions in a three-player pathogen system". In: *Royal Society Open Science* (Under review).

[3] Henry F. Chambers and Frank R. Deleo. "Waves of Resistance: Staphylococcus Aureus in the Antibiotic Era". eng. In: *Nature Reviews. Microbiology* 7.9 (Sept. 2009), pp. 629–641. ISSN: 1740-1534. DOI: 10.1038/nrmicro2200.

[4] Paul M. Sharp and Beatrice H. Hahn. "Origins of HIV and the AIDS Pandemic". In: *Cold Spring Harbor Perspectives in Medicine:* 1.1 (Sept. 2011). ISSN: 2157-1422. DOI: 10.1101/cshperspect.a006841.

[5] J. S. M. Peiris, Y. Guan, and K. Y. Yuen. "Severe Acute Respiratory Syndrome". eng. In: *Nature Medicine* 10.12 Suppl (Dec. 2004), S88–97. ISSN: 1078-8956. DOI: 10.1038/nm1143.

[6] Abdullah Assiri et al. *Hospital Outbreak of Middle East Respiratory Syndrome Coronavirus*. EN. https://www.nejm.org/doi/10.1056/NEJMoa1306742. Research-Article. July 2013. DOI: 10.1056/NEJMoa1306742.

[7] Patrick R. Saunders-Hastings and Daniel Krewski. "Reviewing the History of Pandemic Influenza: Understanding Patterns of Emergence and Transmission". In: *Pathogens* 5.4 (Dec. 2016). ISSN: 2076-0817. DOI: 10.3390/pathogens5040066.

[8] Mark R. Duffy et al. "Zika Virus Outbreak on Yap Island, Federated States of Micronesia". In: *New England Journal of Medicine* 360.24 (June 2009), pp. 2536–2543. ISSN: 0028-4793. DOI: 10.1056/NEJMoa0805715.

[9] Philippe Renault et al. "A Major Epidemic of Chikungunya Virus Infection on Reunion Island, France, 2005-2006". eng. In: *The American Journal of Tropical Medicine and Hygiene* 77.4 (Oct. 2007), pp. 727–731. ISSN: 0002-9637.

[10] D. J Gubler. "The Changing Epidemiology of Yellow Fever and Dengue, 1900 to 2003: Full Circle?" In: *Comparative Immunology, Microbiology and Infectious Diseases*. Advances on Some Vector-Borne Diseases 27.5 (Sept. 2004), pp. 319–330. ISSN: 0147-9571. DOI: 10.1016/j.cimid.2004.03.013.

[11] J. D. Porter and K. P. McAdam. "The Re-Emergence of Tuberculosis". eng. In: *Annual Review of Public Health* 15 (1994), pp. 303–323. ISSN: 0163-7525. DOI: 10.1146/annurev.pu.15.050194.001511.

[12] Katia Koelle et al. "Epochal Evolution Shapes the Phylodynamics of Interpandemic Influenza A (H3N2) in Humans". In: *Science* 314.5807 (2006), pp. 1898–1903. ISSN: 0036-8075.

[13] Caroline Colijn et al. "What Is the Mechanism for Persistent Coexistence of Drug-Susceptible and Drug-Resistant Strains of Streptococcus Pneumoniae?" en. In: *Journal of The Royal Society Interface* 7.47 (June 2010), pp. 905–919. ISSN: 1742-5689, 1742-5662. DOI: 10.1098/rsif.2009.0400.

[14] Sonja Lehtinen et al. "On the Evolutionary Ecology of Multidrug Resistance in Bacteria". en. In: *PLOS Pathogens* 15.5 (13-mag-2019), e1007763. ISSN: 1553-7374. DOI: 10.1371/journal.ppat.1007763.

[15] Stephanie M. Fingerhuth et al. "Antibiotic-Resistant Neisseria Gonorrhoeae Spread Faster with More Treatment, Not More Sexual Partners". en. In: *PLOS Pathogens* 12.5 (19-mag-2016), e1005611. ISSN: 1553-7374. DOI: 10.1371/journal.ppat.1005611.

[16] Magnus Unemo and Christian L. Althaus. "Fitness Cost and Benefit of Antimicrobial Resistance in Neisseria Gonorrhoeae: Multidisciplinary Approaches Are Needed". en. In: *PLOS Medicine* 14.10 (31-ott-2017), e1002423. ISSN: 1549-1676. DOI: 10.1371/journal.pmed.1002423.

[17] M. Lipsitch. "Vaccination against Colonizing Bacteria with Multiple Serotypes". eng. In: *Proceedings of the National Academy of Sciences of the United States of America* 94.12 (June 1997), pp. 6571–6576. ISSN: 0027-8424.

[18] Brian G. Spratt and Brian M. Greenwood. "Prevention of Pneumococcal Disease by Vaccination: Does Serotype Replacement Matter?" English. In: *The Lancet* 356.9237 (Oct. 2000), pp. 1210–1211. ISSN: 0140-6736, 1474-547X. DOI: 10.1016/S0140-6736(00)02779-3.

[19] Margarita Pons-Salort et al. "Exploring Individual HPV Coinfections Is Essential to Predict HPV-Vaccination Impact on Genotype Distribution: A Model-Based Approach". In: *Vaccine* 31.8 (Feb. 2013), pp. 1238–1245. ISSN: 0264-410X. DOI: 10.1016/j.vaccine.2012.11.098.

[20] Keeling, Matt J. and Rohani, Pejman. *Modeling Infectious Diseases in Humans and Animals*. 1st ed. Princeton University Press, 2007. ISBN: 978-0-691-11617-4.

[21] Roy M. Anderson and Robert M. May. *Infectious Diseases of Humans: Dynamics and Control*. Oxford, New York: Oxford University Press, Aug. 1992. ISBN: 978-0-19-854040-3.

[22] Roger Kouyos, Eili Klein, and Bryan Grenfell. "Hospital-Community Interactions Foster Coexistence between Methicillin-Resistant Strains of Staphylococcus Aureus". en. In: *PLOS Pathogens* 9.2 (28-feb-2013), e1003134. ISSN: 1553-7374. DOI: 10.1371/journal.ppat.1003134.

[23] François Blanquart et al. "The Evolution of Antibiotic Resistance in a Structured Host Population". eng. In: *Journal of the Royal Society, Interface* 15.143 (June 2018). ISSN: 1742-5662. DOI: 10.1098/rsif.2018.0040.

[24] Maia Martcheva, Sergei S. Pilyugin, and Robert D. Holt. "Subthreshold and Superthreshold Coexistence of Pathogen Variants: The Impact of Host Age-Structure". eng. In: *Mathematical Biosciences* 207.1 (May 2007), pp. 58–77. ISSN: 0025-5564. DOI: 10.1016/j.mbs.2006.09.010.

[25] Sarah Cobey et al. "Host Population Structure and Treatment Frequency Maintain Balancing Selection on Drug Resistance". en. In: *Journal of The Royal Society Interface* 14.133 (Aug. 2017), p. 20170295. ISSN: 1742-5689, 1742-5662. DOI: 10.1098/rsif.2017.0295.

[26] Sonja Lehtinen et al. "Evolution of Antibiotic Resistance Is Linked to Any Genetic Mechanism Affecting Bacterial Duration of Carriage". en. In: *Proceedings of the National Academy of Sciences* 114.5 (Jan. 2017), pp. 1075–1080. ISSN: 0027-8424, 1091-6490. DOI: 10.1073/pnas.1617849114.

[27] Sarah Cobey and Marc Lipsitch. "Niche and Neutral Effects of Acquired Immunity Permit Coexistence of Pneumococcal Serotypes". In: *Science (New York, N.y.)* 335.6074 (Mar. 2012), pp. 1376–1380. ISSN: 0036-8075. DOI: 10.1126/science.1215947.

[28] Sarah Cobey and Marc Lipsitch. "Pathogen Diversity and Hidden Regimes of Apparent Competition". In: *The American naturalist* 181.1 (Jan. 2013), pp. 12–24. ISSN: 0003-0147. DOI: 10.1086/668598.

[29] Romualdo Pastor-Satorras et al. "Epidemic Processes in Complex Networks". In: *Reviews of Modern Physics* 87.3 (Aug. 2015), pp. 925–979. DOI: 10.1103/RevModPhys.87.925.

[30] Alain Barrat, Marc Barthélemy, and Alessandro Vespignani. *Dynamical Processes on Complex Networks by Alain Barrat*. en. /core/books/dynamical-processes-on-complex-networks/D0173F07E0F05CEE9CF7A6BDAF48E9FC. Oct. 2008. DOI: 10.1017/CBO9780511791383.

[31] Ciro Cattuto et al. "Dynamics of Person-to-Person Interactions from Distributed RFID Sensor Networks". en. In: *PLOS ONE* 5.7 (15-lug-2010), e11596. ISSN: 1932-6203. DOI: 10.1371/journal.pone.0011596.

[32] Marcel Salathé et al. "A High-Resolution Human Contact Network for Infectious Disease Transmission". en. In: *Proceedings of the National Academy of Sciences* 107.51 (Dec. 2010), pp. 22020–22025. ISSN: 0027-8424, 1091-6490. DOI: 10.1073/pnas.1009094108.

[33] Juliette Stehlé et al. “High-Resolution Measurements of Face-to-Face Contact Patterns in a Primary School”. en. In: *PLOS ONE* 6.8 (16-ago-2011), e23176. ISSN: 1932-6203. DOI: 10.1371/journal.pone.0023176.

[34] Juliette Stehlé et al. “Simulation of an SEIR Infectious Disease Model on the Dynamic Contact Network of Conference Attendees”. In: *BMC Medicine* 9 (July 2011), p. 87. ISSN: 1741-7015. DOI: 10.1186/1741-7015-9-87.

[35] Lorenzo Isella et al. “What’s in a Crowd? Analysis of Face-to-Face Behavioral Networks”. In: *Journal of Theoretical Biology* 271.1 (Feb. 2011), pp. 166–180. ISSN: 0022-5193. DOI: 10.1016/j.jtbi.2010.11.033.

[36] Mathieu Génois et al. “Data on Face-to-Face Contacts in an Office Building Suggest a Low-Cost Vaccination Strategy Based on Community Linkers”. en. In: *Network Science* 3.3 (Sept. 2015), pp. 326–347. ISSN: 2050-1242, 2050-1250. DOI: 10.1017/nws.2015.10.

[37] Moses C. Kiti et al. “Quantifying Social Contacts in a Household Setting of Rural Kenya Using Wearable Proximity Sensors”. En. In: *EPJ Data Science* 5.1 (Dec. 2016), p. 21. ISSN: 2193-1127. DOI: 10.1140/epjds/s13688-016-0084-2.

[38] Laura Ozella et al. “Close Encounters between Infants and Household Members Measured through Wearable Proximity Sensors”. en. In: *PLOS ONE* 13.6 (7-giu-2018), e0198733. ISSN: 1932-6203. DOI: 10.1371/journal.pone.0198733.

[39] Lorenzo Isella et al. “Close Encounters in a Pediatric Ward: Measuring Face-to-Face Proximity and Mixing Patterns with Wearable Sensors”. en. In: *PLOS ONE* 6.2 (28-feb-2011), e17144. ISSN: 1932-6203. DOI: 10.1371/journal.pone.0017144.

[40] Philippe Vanhems et al. “Estimating Potential Infection Transmission Routes in Hospital Wards Using Wearable Proximity Sensors”. en. In: *PLOS ONE* 8.9 (Sept. 2013), e73970. ISSN: 1932-6203. DOI: 10.1371/journal.pone.0073970.

[41] Thomas Obadia et al. “Detailed Contact Data and the Dissemination of Staphylococcus Aureus in Hospitals”. en. In: *PLOS Computational Biology* 11.3 (19-mar-2015), e1004170. ISSN: 1553-7358. DOI: 10.1371/journal.pcbi.1004170.

[42] Audrey Duval et al. “Close Proximity Interactions Support Transmission of ESBL-K. Pneumoniae but Not ESBL-E. Coli in Healthcare Settings”. en. In: *PLOS Computational Biology* 15.5 (30-mag-2019), e1006496. ISSN: 1553-7358. DOI: 10.1371/journal.pcbi.1006496.

[43] Ken T. D. Eames and Matt J. Keeling. “Monogamous Networks and the Spread of Sexually Transmitted Diseases”. In: *Mathematical Biosciences* 189.2 (June 2004), pp. 115–130. ISSN: 0025-5564. DOI: 10.1016/j.mbs.2004.02.003.

[44] Peter S. Bearman, James Moody, and Katherine Stovel. “Chains of Affection: The Structure of Adolescent Romantic and Sexual Networks”. en. In: *American Journal of Sociology* 110.1 (July 2004), pp. 44–91. ISSN: 0002-9602, 1537-5390. DOI: 10.1086/386272.

[45] Luis E. C. Rocha, Fredrik Liljeros, and Petter Holme. "Information Dynamics Shape the Sexual Networks of Internet-Mediated Prostitution". en. In: *Proceedings of the National Academy of Sciences* 107.13 (Mar. 2010), pp. 5706–5711. ISSN: 0027-8424, 1091-6490. DOI: 10.1073/pnas.0914080107.

[46] Chaoming Song et al. "Limits of Predictability in Human Mobility". en. In: *Science* 327.5968 (Feb. 2010), pp. 1018–1021. ISSN: 0036-8075, 1095-9203. DOI: 10.1126/science.1177170.

[47] Mikko Kivelä et al. "Multiscale Analysis of Spreading in a Large Communication Network". en. In: *Journal of Statistical Mechanics: Theory and Experiment* 2012.03 (Mar. 2012), P03005. ISSN: 1742-5468. DOI: 10.1088/1742-5468/2012/03/P03005.

[48] Lauri Kovanen et al. "Temporal Motifs Reveal Homophily, Gender-Specific Patterns, and Group Talk in Call Sequences". en. In: *Proceedings of the National Academy of Sciences* 110.45 (Nov. 2013), pp. 18070–18075. ISSN: 0027-8424, 1091-6490. DOI: 10.1073/pnas.1307941110.

[49] Zhi-Qiang Jiang et al. "Calling Patterns in Human Communication Dynamics". en. In: *Proceedings of the National Academy of Sciences* 110.5 (Jan. 2013), pp. 1600–1605. ISSN: 0027-8424, 1091-6490. DOI: 10.1073/pnas.1220433110.

[50] Ming-Xia Li et al. "Statistically Validated Mobile Communication Networks: The Evolution of Motifs in European and Chinese Data". en. In: *New Journal of Physics* 16.8 (Aug. 2014), p. 083038. ISSN: 1367-2630. DOI: 10.1088/1367-2630/16/8/083038.

[51] Lijun Sun et al. "Understanding Metropolitan Patterns of Daily Encounters". en. In: *Proceedings of the National Academy of Sciences* 110.34 (Aug. 2013), pp. 13774–13779. ISSN: 0027-8424, 1091-6490. DOI: 10.1073/pnas.1306440110.

[52] Marta C. González, César A. Hidalgo, and Albert-László Barabási. "Understanding Individual Human Mobility Patterns". eng. In: *Nature* 453.7196 (June 2008), pp. 779–782. ISSN: 1476-4687. DOI: 10.1038/nature06958.

[53] Filippo Simini et al. "A Universal Model for Mobility and Migration Patterns". en. In: *Nature* 484.7392 (Apr. 2012), pp. 96–100. ISSN: 1476-4687. DOI: 10.1038/nature10856.

[54] Cecilia Panigutti et al. "Assessing the Use of Mobile Phone Data to Describe Recurrent Mobility Patterns in Spatial Epidemic Models". en. In: *Royal Society Open Science* 4.5 (May 2017), p. 160950. ISSN: 2054-5703, 2054-5703. DOI: 10.1098/rsos.160950.

[55] Michele Tizzoni et al. "On the Use of Human Mobility Proxies for Modeling Epidemics". en. In: *PLOS Computational Biology* 10.7 (July 2014), e1003716. ISSN: 1553-7358. DOI: 10.1371/journal.pcbi.1003716.

[56] Ken T. D. Eames and Matt J. Keeling. "Coexistence and Specialization of Pathogen Strains on Contact Networks." In: *The American Naturalist* 168.2 (Aug. 2006), pp. 230–241. ISSN: 0003-0147. DOI: 10.1086/505760.

[57] M. E. J. Newman. "Threshold Effects for Two Pathogens Spreading on a Network". In: *Physical Review Letters* 95.10 (Sept. 2005), p. 108701. DOI: 10.1103/PhysRevLett.95.108701.

[58] Brian Karrer and M. E. J. Newman. "Competing Epidemics on Complex Networks". In: *Physical Review E* 84.3 (Sept. 2011), p. 036106. DOI: 10.1103/PhysRevE.84.036106.

[59] Shweta Bansal and Lauren Ancel Meyers. "The Impact of Past Epidemics on Future Disease Dynamics". In: *Journal of Theoretical Biology* 309 (Sept. 2012), pp. 176–184. ISSN: 0022-5193. DOI: 10.1016/j.jtbi.2012.06.012.

[60] Qing-Chu Wu, Xin-Chu Fu, and Meng Yang. "Epidemic Thresholds in a Heterogenous Population with Competing Strains". en. In: *Chinese Physics B* 20.4 (Apr. 2011), p. 046401. ISSN: 1674-1056. DOI: 10.1088/1674-1056/20/4/046401.

[61] Chiara Poletto et al. "Host Mobility Drives Pathogen Competition in Spatially Structured Populations". en. In: *PLOS Computational Biology* 9.8 (15-ago-2013), e1003169. ISSN: 1553-7358. DOI: 10.1371/journal.pcbi.1003169.

[62] Chiara Poletto et al. "Characterising Two-Pathogen Competition in Spatially Structured Environments". en. In: *Scientific Reports* 5 (Jan. 2015), p. 7895. ISSN: 2045-2322. DOI: 10.1038/srep07895.

[63] Gabriel E. Leventhal et al. "Evolution and Emergence of Infectious Diseases in Theoretical and Real-World Networks". en. In: *Nature Communications* 6 (Jan. 2015), p. 6101. ISSN: 2041-1723. DOI: 10.1038/ncomms7101.

[64] Ruud van de Bovenkamp, Fernando Kuipers, and Piet Van Mieghem. "Domination-Time Dynamics in Susceptible-Infected-Susceptible Virus Competition on Networks". In: *Physical Review E* 89.4 (Apr. 2014), p. 042818. DOI: 10.1103/PhysRevE.89.042818.

[65] Laurent Hébert-Dufresne and Benjamin M. Althouse. "Complex Dynamics of Synergistic Coinfections on Realistically Clustered Networks". en. In: *Proceedings of the National Academy of Sciences* 112.33 (Aug. 2015), pp. 10551–10556. ISSN: 0027-8424, 1091-6490. DOI: 10.1073/pnas.1507820112.

[66] Weiran Cai et al. "Avalanche Outbreaks Emerging in Cooperative Contagions". en. In: *Nature Physics* 11.11 (Nov. 2015), pp. 936–940. ISSN: 1745-2481. DOI: 10.1038/nphys3457.

[67] Peter Grassberger et al. "Phase Transitions in Cooperative Coinfections: Simulation Results for Networks and Lattices". In: *Physical Review E* 93.4 (Apr. 2016), p. 042316. DOI: 10.1103/PhysRevE.93.042316.

[68] Li Chen, Fakhteh Ghanbarnejad, and Dirk Brockmann. "Fundamental Properties of Cooperative Contagion Processes". en. In: *New Journal of Physics* 19.10 (2017), p. 103041. ISSN: 1367-2630. DOI: 10.1088/1367-2630/aa8bd2.

[69] Sebastian Funk and Vincent A. A. Jansen. "Interacting Epidemics on Overlay Networks". In: *Physical Review E* 81.3 (Mar. 2010), p. 036118. DOI: 10.1103/PhysRevE.81.036118.

[70] Joaquín Sanz et al. "Dynamics of Interacting Diseases". In: *Physical Review X* 4.4 (Oct. 2014), p. 041005. DOI: 10.1103/PhysRevX.4.041005.

[71] Sanghyuk S. Shin et al. "Mixed Mycobacterium Tuberculosis–Strain Infections Are Associated With Poor Treatment Outcomes Among Patients With Newly Diagnosed Tuberculosis, Independent of Pretreatment Heteroresistance". en. In: *The Journal of Infectious Diseases* (). DOI: 10.1093/infdis/jiy480.

[72] Jeffrey A. Tornheim and Kelly E. Dooley. "Tuberculosis Associated with HIV Infection". English. In: *Microbiology Spectrum* 5.1 (Feb. 2017). WOS:000397274600026, UNSP TNMI7–0028–2016. DOI: 10.1128/microbiolspec.TNMI7-0028-2016.

[73] Caroline Colijn and Ted Cohen. "How Competition Governs Whether Moderate or Aggressive Treatment Minimizes Antibiotic Resistance". eng. In: *eLife* 4 (Sept. 2015). ISSN: 2050-084X. DOI: 10.7554/eLife.10559.

[74] Daniel M Weinberger, Richard Malley, and Marc Lipsitch. "Serotype Replacement in Disease after Pneumococcal Vaccination". In: *The Lancet* 378.9807 (Dec. 2011), pp. 1962–1973. ISSN: 0140-6736. DOI: 10.1016/S0140-6736(10)62225-8.

[75] Nicole Mideo. "Parasite Adaptations to Within-Host Competition". In: *Trends in Parasitology* 25.6 (June 2009), pp. 261–268. ISSN: 1471-4922. DOI: 10.1016/j.pt.2009.03.001.

[76] Farrah Bashey. "Within-Host Competitive Interactions as a Mechanism for the Maintenance of Parasite Diversity". In: *Philosophical Transactions of the Royal Society B: Biological Sciences* 370.1675 (Aug. 2015). ISSN: 0962-8436. DOI: 10.1098/rstb.2014.0301.

[77] Elisa Margolis, Andrew Yates, and Bruce R. Levin. "The Ecology of Nasal Colonization of Streptococcus Pneumoniae, Haemophilus Influenzae and Staphylococcus Aureus: The Role of Competition and Interactions with Host's Immune Response". eng. In: *BMC microbiology* 10 (Feb. 2010), p. 59. ISSN: 1471-2180. DOI: 10.1186/1471-2180-10-59.

[78] O. T. Avery and H. J. Morgan. "THE OCCURRENCE OF PEROXIDE IN CULTURES OF PNEUMOCOCCUS". eng. In: *The Journal of Experimental Medicine* 39.2 (Jan. 1924), pp. 275–287. ISSN: 0022-1007.

[79] Andrew F. Read and Louise H. Taylor. "The Ecology of Genetically Diverse Infections". en. In: *Science* 292.5519 (May 2001), pp. 1099–1102. ISSN: 0036-8075, 1095-9203. DOI: 10.1126/science.1059410.

[80] Daniel M. Weinberger et al. "Epidemiologic Evidence for Serotype-Specific Acquired Immunity to Pneumococcal Carriage". en. In: *The Journal of Infectious Diseases* 197.11 (June 2008), pp. 1511–1518. ISSN: 0022-1899. DOI: 10.1086/587941.

[81] David Goldblatt et al. "Antibody Responses to Nasopharyngeal Carriage of Streptococcus Pneumoniae in Adults: A Longitudinal Household Study". en. In: *The Journal of Infectious Diseases* 192.3 (Aug. 2005), pp. 387–393. ISSN: 0022-1899. DOI: 10.1086/431524.

[82] J. H. C. M. Kreijtz, R. A. M. Fouchier, and G. F. Rimmelzwaan. "Immune Responses to Influenza Virus Infection". In: *Virus Research*. Negative Strand RNA Viruses: To Mark the Retirement of Dr Brian WJ Mahy, Founder and Editor-in-Chief, 1984–2011 162.1 (Dec. 2011), pp. 19–30. ISSN: 0168-1702. DOI: 10.1016/j.virusres.2011.09.022.

[83] Sourya Shrestha et al. "Identifying the Interaction between Influenza and Pneumococcal Pneumonia Using Incidence Data". In: *Science translational medicine* 5.191 (June 2013), 191ra84. ISSN: 1946-6234. DOI: 10.1126/scitranslmed.3005982.

[84] S. Shrestha et al. "Time and Dose-Dependent Risk of Pneumococcal Pneumonia Following Influenza: A Model for within-Host Interaction between Influenza and Streptococcus Pneumoniae". en. In: *Journal of The Royal Society Interface* 10.86 (July 2013), pp. 20130233–20130233. ISSN: 1742-5689, 1742-5662. DOI: 10.1098/rsif.2013.0233.

[85] Lulla Opatowski, Marc Baguelin, and Rosalind M. Eggo. "Influenza Interaction with Cocirculating Pathogens and Its Impact on Surveillance, Pathogenesis, and Epidemic Profile: A Key Role for Mathematical Modelling". en. In: *PLOS Pathogens* 14.2 (15-feb-2018), e1006770. ISSN: 1553-7374. DOI: 10.1371/journal.ppat.1006770.

[86] Michael J. Mina and Keith P. Klugman. "The Role of Influenza in the Severity and Transmission of Respiratory Bacterial Disease". eng. In: *The Lancet. Respiratory Medicine* 2.9 (Sept. 2014), pp. 750–763. ISSN: 2213-2619. DOI: 10.1016/S2213-2600(14)70131-6.

[87] J. S. Abramson et al. "Depression of Monocyte and Polymorphonuclear Leukocyte Oxidative Metabolism and Bactericidal Capacity by Influenza A Virus". eng. In: *Infection and Immunity* 35.1 (Jan. 1982), pp. 350–355. ISSN: 0019-9567.

[88] Agnieszka Rynda-Apple, Keven M. Robinson, and John F. Alcorn. "Influenza and Bacterial Superinfection: Illuminating the Immunologic Mechanisms of Disease". eng. In: *Infection and Immunity* 83.10 (Oct. 2015), pp. 3764–3770. ISSN: 1098-5522. DOI: 10.1128/IAI.00298-15.

[89] Charles D. Wells et al. "HIV Infection and Multidrug-Resistant Tuberculosis: The Perfect Storm". eng. In: *The Journal of Infectious Diseases* 196 Suppl 1 (Aug. 2007), S86–107. ISSN: 0022-1899. DOI: 10.1086/518665.

[90] Haileyesus Getahun et al. "HIV Infection-Associated Tuberculosis: The Epidemiology and the Response". eng. In: *Clinical Infectious Diseases: An Official Publication of the Infectious Diseases Society of America* 50 Suppl 3 (May 2010), S201–207. ISSN: 1537-6591. DOI: 10.1086/651492.

[91] Samuel A. Shelburne et al. "Immune Reconstitution Inflammatory Syndrome: Emergence of a Unique Syndrome during Highly Active Antiretroviral Therapy". eng. In: *Medicine* 81.3 (May 2002), pp. 213–227. ISSN: 0025-7974.

[92] Nicholas G. Reich et al. "Interactions between Serotypes of Dengue Highlight Epidemiological Impact of Cross-Immunity". In: *Journal of the Royal Society Interface* 10.86 (Sept. 2013). ISSN: 1742-5689. DOI: 10.1098/rsif.2013.0414.

[93] Maria G. Guzman, Mayling Alvarez, and Scott B. Halstead. "Secondary Infection as a Risk Factor for Dengue Hemorrhagic Fever/Dengue Shock Syndrome: An Historical Perspective and Role of Antibody-Dependent Enhancement of Infection". en. In: *Archives of Virology* 158.7 (July 2013), pp. 1445–1459. ISSN: 1432-8798. DOI: 10.1007/s00705-013-1645-3.

[94] Benoît Randuineau. "Interactions Entre Pathogènes : Quels Impacts Sur La Santé Publique ?" Thesis. Paris 6, Nov. 2015.

[95] P Rohani et al. "Population Dynamic Interference among Childhood Diseases." In: *Proceedings of the Royal Society B: Biological Sciences* 265.1410 (Nov. 1998), pp. 2033–2041. ISSN: 0962-8452.

[96] P. Rohani et al. "Ecological Interference between Fatal Diseases". eng. In: *Nature* 422.6934 (Apr. 2003), pp. 885–888. ISSN: 0028-0836. DOI: 10.1038/nature01542.

[97] Tereza Magalhaes et al. "Zika Virus Displacement by a Chikungunya Outbreak in Recife, Brazil". en. In: *PLOS Neglected Tropical Diseases* 11.11 (6-nov-2017), e0006055. ISSN: 1935-2735. DOI: 10.1371/journal.pntd.0006055.

[98] Isabel Rodriguez-Barraquer et al. "Impact of Preexisting Dengue Immunity on Zika Virus Emergence in a Dengue Endemic Region". en. In: *Science* 363.6427 (Feb. 2019), pp. 607–610. ISSN: 0036-8075, 1095-9203. DOI: 10.1126/science.aav6618.

[99] Spencer J. Fox, Joel C. Miller, and Lauren Ancel Meyers. "Seasonality in Risk of Pandemic Influenza Emergence". In: *PLoS Computational Biology* 13.10 (Oct. 2017). ISSN: 1553-734X. DOI: 10.1371/journal.pcbi.1005749.

[100] Samit Bhattacharyya et al. "Cross-Immunity between Strains Explains the Dynamical Pattern of Paramyxoviruses". en. In: *Proceedings of the National Academy of Sciences* 112.43 (Oct. 2015), pp. 13396–13400. ISSN: 0027-8424, 1091-6490. DOI: 10.1073/pnas.1516698112.

[101] Jessica A. Kahn et al. "Vaccine-Type Human Papillomavirus and Evidence of Herd Protection After Vaccine Introduction". In: *Pediatrics* 130.2 (Aug. 2012), e249–e256. ISSN: 0031-4005. DOI: 10.1542/peds.2011-3587.

[102] David Mesher et al. "Population-Level Effects of Human Papillomavirus Vaccination Programs on Infections with Nonvaccine Genotypes". In: *Emerging Infectious Diseases* 22.10 (Oct. 2016), pp. 1732–1740. ISSN: 1080-6040. DOI: 10.3201/eid2210.160675.

[103] Penelope Gray et al. "Occurrence of Human Papillomavirus (HPV) Type Replacement by Sexual Risk-Taking Behaviour Group: Post-Hoc Analysis of a Community Randomized Clinical Trial up to 9 Years after Vaccination (IV)". eng. In: *International Journal of Cancer* (Feb. 2019). ISSN: 1097-0215. DOI: 10.1002/ijc.32189.

[104] Andreas Ährlund-Richter et al. "Changes in Cervical Human Papillomavirus (HPV) Prevalence at a Youth Clinic in Stockholm, Sweden, a Decade After the Introduction of the HPV Vaccine". English. In: *Frontiers in Cellular and Infection Microbiology* 9 (2019). ISSN: 2235-2988. DOI: 10.3389/fcimb.2019.00059.

[105] Courtney Covert et al. "Evidence for Cross-Protection but Not Type-Replacement over the 11 Years after Human Papillomavirus Vaccine Introduction". In: *Human Vaccines & Immunotherapeutics* 15.7-8 (Aug. 2019), pp. 1962–1969. ISSN: 2164-5515. DOI: 10.1080/21645515.2018.1564438.

[106] Penelope Gray et al. "Evaluation of HPV Type-Replacement in Unvaccinated and Vaccinated Adolescent Females—Post-Hoc Analysis of a Community-Randomized Clinical Trial (II)". en. In: *International Journal of Cancer* 142.12 (2018), pp. 2491–2500. ISSN: 1097-0215. DOI: 10.1002/ijc.31281.

[107] Lalita Priyamvada et al. "Human Antibody Responses after Dengue Virus Infection Are Highly Cross-Reactive to Zika Virus". eng. In: *Proceedings of the National Academy of Sciences of the United States of America* 113.28 (Dec. 2016), pp. 7852–7857. ISSN: 1091-6490. DOI: 10.1073/pnas.1607931113.

[108] Susana V. Bardina et al. "Enhancement of Zika Virus Pathogenesis by Preexisting Antiflavivirus Immunity". eng. In: *Science (New York, N.Y.)* 356.6334 (Apr. 2017), pp. 175–180. ISSN: 1095-9203. DOI: 10.1126/science.aal4365.

[109] Miguel A. Martín-Acebes, Juan-Carlos Saiz, and Nereida Jiménez de Oya. "Antibody-Dependent Enhancement and Zika: Real Threat or Phantom Menace?" In: *Frontiers in Cellular and Infection Microbiology* 8 (Feb. 2018). ISSN: 2235-2988. DOI: 10.3389/fcimb.2018.00044.

[110] Sally Blower and Daniel Bernoulli. "An Attempt at a New Analysis of the Mortality Caused by Smallpox and of the Advantages of Inoculation to Prevent It. 1766". eng. In: *Reviews in Medical Virology* 14.5 (2004 Sep-Oct), pp. 275–288. ISSN: 1052-9276. DOI: 10.1002/rmv.443.

[111] Ronald Ross. *The Prevention of Malaria*. John Murray; London, 1911.

[112] Michael T. Meehan et al. "Coupled, Multi-Strain Epidemic Models of Mutating Pathogens". In: *Mathematical Biosciences* 296 (Feb. 2018), pp. 82–92. ISSN: 0025-5564. DOI: 10.1016/j.mbs.2017.12.006.

[113] F. Tria et al. "A Minimal Stochastic Model for Influenza Evolution". en. In: *Journal of Statistical Mechanics: Theory and Experiment* 2005.07 (July 2005), P07008–P07008. ISSN: 1742-5468. DOI: 10.1088/1742-5468/2005/07/P07008.

[114] J. R. Gog and J. Swinton. "A Status-Based Approach to Multiple Strain Dynamics". eng. In: *Journal of Mathematical Biology* 44.2 (Feb. 2002), pp. 169–184. ISSN: 0303-6812.

[115] Sébastien Ballesteros, Elisabeta Vergu, and Bernard Cazelles. "Influenza A Gradual and Epochal Evolution: Insights from Simple Models". en. In: *PLOS ONE* 4.10 (20-ott-2009), e7426. ISSN: 1932-6203. DOI: 10.1371/journal.pone.0007426.

[116] Adam J. Kucharski, Viggo Andreasen, and Julia R. Gog. "Capturing the Dynamics of Pathogens with Many Strains". en. In: *Journal of Mathematical Biology* 72.1-2 (Jan. 2016), pp. 1–24. ISSN: 0303-6812, 1432-1416. DOI: 10.1007/s00285-015-0873-4.

[117] Julia R. Gog and Bryan T. Grenfell. "Dynamics and Selection of Many-Strain Pathogens". en. In: *Proceedings of the National Academy of Sciences* 99.26 (Dec. 2002), pp. 17209–17214. ISSN: 0027-8424, 1091-6490. DOI: 10.1073/pnas.252512799.

[118] Marc Lipsitch et al. "No Coexistence for Free: Neutral Null Models for Multistrain Pathogens". In: *Epidemics* 1.1 (Mar. 2009), pp. 2–13. ISSN: 1755-4365. DOI: 10.1016/j.epidem.2008.07.001.

[119] C. G. Whitney et al. "Increasing Prevalence of Multidrug-Resistant Streptococcus Pneumoniae in the United States". eng. In: *The New England Journal of Medicine* 343.26 (Dec. 2000), pp. 1917–1924. ISSN: 0028-4793. DOI: 10.1056/NEJM200012283432603.

[120] Jeff Powis et al. "In Vitro Antimicrobial Susceptibilities of Streptococcus Pneumoniae Clinical Isolates Obtained in Canada in 2002". eng. In: *Antimicrobial Agents and Chemotherapy* 48.9 (Sept. 2004), pp. 3305–3311. ISSN: 0066-4804. DOI: 10.1128/AAC.48.9.3305-3311.2004.

[121] A. Fenoll et al. "Evolution of Streptococcus Pneumoniae Serotypes and Antibiotic Resistance in Spain: Update (1990 to 1996)". eng. In: *Journal of Clinical Microbiology* 36.12 (Dec. 1998), pp. 3447–3454. ISSN: 0095-1137.

[122] A. Fenoll et al. "Antimicrobial Susceptibility and Pneumococcal Serotypes". eng. In: *The Journal of Antimicrobial Chemotherapy* 50 Suppl S2 (Dec. 2002), pp. 13–19. ISSN: 0305-7453. DOI: 10.1093/jac/dkf509.

[123] Keiko Okuma et al. "Dissemination of New Methicillin-Resistant Staphylococcus Aureus Clones in the Community". In: *Journal of Clinical Microbiology* 40.11 (Nov. 2002), pp. 4289–4294. ISSN: 0095-1137. DOI: 10.1128/JCM.40.11.4289-4294.2002.

[124] H. F. Chambers. "The Changing Epidemiology of Staphylococcus Aureus?" eng. In: *Emerging Infectious Diseases* 7.2 (2001 Mar-Apr), pp. 178–182. ISSN: 1080-6040. DOI: 10.3201/eid0702.700178.

[125] Yuki Furuse and Hitoshi Oshitani. "Mechanisms of Replacement of Circulating Viruses by Seasonal and Pandemic Influenza A Viruses". In: *International Journal of Infectious Diseases* 51 (Oct. 2016), pp. 6–14. ISSN: 1201-9712. DOI: 10.1016/j.ijid.2016.08.012.

[126] Xu-Sheng Zhang et al. "Co-Circulation of Influenza A Virus Strains and Emergence of Pandemic via Reassortment: The Role of Cross-Immunity". In: *Epidemics*. Special Issue: Papers from Epidemics3 5.1 (Mar. 2013), pp. 20–33. ISSN: 1755-4365. DOI: 10.1016/j.epidem.2012.10.003.

[127] Irene Man et al. "Capturing Multiple-Type Interactions into Practical Predictors of Type Replacement Following HPV Vaccination". en. In: *bioRxiv* (Jan. 2019), p. 523472. DOI: 10.1101/523472.

[128] Erida Gjini et al. "How Direct Competition Shapes Coexistence and Vaccine Effects in Multi-Strain Pathogen Systems". In: *Journal of Theoretical Biology* 388 (Jan. 2016), pp. 50–60. ISSN: 0022-5193. DOI: 10.1016/j.jtbi.2015.09.031.

[129] Paul S. Wikramaratna et al. "Five Challenges in Modelling Interacting Strain Dynamics". In: *Epidemics*. Challenges in Modelling Infectious DIsease Dynamics 10 (Mar. 2015), pp. 31–34. ISSN: 1755-4365. DOI: 10.1016/j.epidem.2014.07.005.

[130] Mircea T. Sofonea, Samuel Alizon, and Yannis Michalakis. "From Within-Host Interactions to Epidemiological Competition: A General Model for Multiple Infections". en. In: *Philosophical Transactions of the Royal Society B: Biological Sciences* 370.1675 (Aug. 2015), p. 20140303. ISSN: 0962-8436, 1471-2970. DOI: 10.1098/rstb.2014.0303.

[131] Mircea T. Sofonea, Samuel Alizon, and Yannis Michalakis. "Exposing the Diversity of Multiple Infection Patterns". In: *Journal of Theoretical Biology* 419 (Apr. 2017), pp. 278–289. ISSN: 0022-5193. DOI: 10.1016/j.jtbi.2017.02.011.

[132] Joseph Dureau, Konstantinos Kalogeropoulos, and Marc Baguelin. "Capturing the Time-Varying Drivers of an Epidemic Using Stochastic Dynamical Systems". en. In: *Biostatistics* 14.3 (July 2013), pp. 541–555. ISSN: 1465-4644. DOI: 10.1093/biostatistics/kxs052.

[133] Anastasia Chatzilena et al. "Contemporary Statistical Inference for Infectious Disease Models Using Stan". In: *arXiv:1903.00423 [q-bio, stat]* (Mar. 2019). arXiv: 1903.00423 [q-bio, stat].

[134] Clara Champagne et al. "Dengue Modeling in Rural Cambodia: Statistical Performance versus Epidemiological Relevance". In: *Epidemics* 26 (Mar. 2019), pp. 43–57. ISSN: 1755-4365. DOI: 10.1016/j.epidem.2018.08.004.

[135] Ottar N. Bjørnstad, Bärbel F. Finkenstädt, and Bryan T. Grenfell. "Dynamics of Measles Epidemics: Estimating Scaling of Transmission Rates Using a Time Series Sir Model". en. In: *Ecological Monographs* 72.2 (2002), pp. 169–184. ISSN: 1557-7015. DOI: 10.1890/0012-9615(2002)072[0169:DOMEES]2.0.CO;2.

[136] C. L. Althaus et al. "Ebola Virus Disease Outbreak in Nigeria: Transmission Dynamics and Rapid Control". In: *Epidemics* 11 (June 2015), pp. 80–84. ISSN: 1755-4365. DOI: 10.1016/j.epidem.2015.03.001.

[137] Simon Cauchemez et al. "How Modelling Can Enhance the Analysis of Imperfect Epidemic Data". In: *Trends in Parasitology* 35.5 (May 2019), pp. 369–379. ISSN: 1471-4922. DOI: 10.1016/j.pt.2019.01.009.

[138] Julien Riou, Chiara Poletto, and Pierre-Yves Boëlle. "Improving Early Epidemiological Assessment of Emerging Aedes-Transmitted Epidemics Using Historical Data". en. In: *PLOS Neglected Tropical Diseases* 12.6 (4-giu-2018), e0006526. ISSN: 1935-2735. DOI: 10.1371/journal.pntd.0006526.

[139] Patrick Walker et al. "Outbreaks of H5N1 in Poultry in Thailand: The Relative Role of Poultry Production Types in Sustaining Transmission and the Impact of Active Surveillance in Control". In: *Journal of the Royal Society Interface* 9.73 (Aug. 2012), pp. 1836–1845. ISSN: 1742-5689. DOI: 10.1098/rsif.2012.0022.

[140] Thibaut Jombart et al. "OutbreakTools: A New Platform for Disease Outbreak Analysis Using the R Software". In: *Epidemics* 7 (June 2014), pp. 28–34. ISSN: 1755-4365. DOI: 10.1016/j.epidem.2014.04.003.

[141] Kathleen M. O'Reilly et al. "Projecting the End of the Zika Virus Epidemic in Latin America: A Modelling Analysis". In: *BMC Medicine* 16.1 (Oct. 2018), p. 180. ISSN: 1741-7015. DOI: 10.1186/s12916-018-1158-8.

[142] Henrik Salje et al. "Reconstruction of 60 Years of Chikungunya Epidemiology in the Philippines Demonstrates Episodic and Focal Transmission". en. In: *The Journal of Infectious Diseases* 213.4 (Feb. 2016), pp. 604–610. ISSN: 0022-1899. DOI: 10.1093/infdis/jiv470.

[143] Lulla Opatowski et al. "Transmission Characteristics of the 2009 H1N1 Influenza Pandemic: Comparison of 8 Southern Hemisphere Countries". en. In: *PLOS Pathogens* 7.9 (1-set-2011), e1002225. ISSN: 1553-7374. DOI: 10.1371/journal.ppat.1002225.

[144] Steven Riley et al. "Transmission Dynamics of the Etiological Agent of SARS in Hong Kong: Impact of Public Health Interventions". In: *Science* 300.5627 (2003), pp. 1961–1966. ISSN: 0036-8075.

[145] Raymond Gani and Steve Leach. "Transmission Potential of Smallpox in Contemporary Populations". en. In: *Nature* 414.6865 (Dec. 2001), pp. 748–751. ISSN: 1476-4687. DOI: 10.1038/414748a.

[146] Manlio De Domenico et al. "Mathematical Formulation of Multi-Layer Networks". In: *Physical Review X* 3.4 (Dec. 2013), p. 041022. ISSN: 2160-3308. DOI: 10.1103/PhysRevX.3.041022. arXiv: 1307.4977.

[147] Mikko Kivelä et al. "Multilayer Networks". en. In: *Journal of Complex Networks* 2.3 (Sept. 2014), pp. 203–271. ISSN: 2051-1310. DOI: 10.1093/comnet/cnu016.

[148] Ginestra Bianconi. *Multilayer Networks: Structure and Function*. en. Oxford University Press, June 2018. ISBN: 978-0-19-106850-8.

[149] Alberto Aleta and Yamir Moreno. "Multilayer Networks in a Nutshell". In: *Annual Review of Condensed Matter Physics* 10.1 (Mar. 2019), pp. 45–62. ISSN: 1947-5454, 1947-5462. DOI: 10.1146/annurev-conmatphys-031218-013259. arXiv: 1804.03488.

[150] S. Boccaletti et al. "The Structure and Dynamics of Multilayer Networks". In: *Physics Reports*. The Structure and Dynamics of Multilayer Networks 544.1 (Nov. 2014), pp. 1–122. ISSN: 0370-1573. DOI: 10.1016/j.physrep.2014.07.001.

[151] Giulia Menichetti et al. "Weighted Multiplex Networks". en. In: *PLOS ONE* 9.6 (6-giu-2014), e97857. ISSN: 1932-6203. DOI: 10.1371/journal.pone.0097857.

[152] Naoki Masuda and Petter Holme, eds. *Temporal Network Epidemiology*. en. Theoretical Biology. Springer Singapore, 2017. ISBN: 978-981-10-5286-6.

[153] Petter Holme and Jari Saramäki. "Temporal Networks". In: *Physics Reports*. Temporal Networks 519.3 (Oct. 2012), pp. 97–125. ISSN: 0370-1573. DOI: 10.1016/j.physrep.2012.03.001.

[154] Pan Hui et al. "Pocket Switched Networks and Human Mobility in Conference Environments". In: *Proceedings of the 2005 ACM SIGCOMM Workshop on Delay-Tolerant Networking*. WDTN '05. New York, NY, USA: ACM, 2005, pp. 244–251. ISBN: 978-1-59593-026-2. DOI: 10.1145/1080139.1080142.

[155] Vassilis Kostakos, Eamonn O'Neill, and Alan Penn. "Brief Encounter Networks". In: *ACM Transactions on Computer-Human Interaction* 17.1 (Mar. 2010), pp. 1–38. ISSN: 10730516. DOI: 10.1145/1721831.1721833. arXiv: 0709.0223.

[156] A. Scherrer et al. "Description and Simulation of Dynamic Mobility Networks". In: *Computer Networks*. Complex Computer and Communication Networks 52.15 (Oct. 2008), pp. 2842–2858. ISSN: 1389-1286. DOI: 10.1016/j.comnet.2008.06.007.

[157] Nathan Eagle and Alex (Sandy) Pentland. "Reality Mining: Sensing Complex Social Systems". en. In: *Personal and Ubiquitous Computing* 10.4 (May 2006), pp. 255–268. ISSN: 1617-4909, 1617-4917. DOI: 10.1007/s00779-005-0046-3.

[158] Piotr Sapiezynski et al. "Inferring Person-to-Person Proximity Using WiFi Signals". In: *arXiv:1610.04730 [cs]* (Oct. 2016). arXiv: 1610.04730 [cs].

[159] Ken T. D. Eames and Matt J. Keeling. "Modeling Dynamic and Network Heterogeneities in the Spread of Sexually Transmitted Diseases". en. In: *Proceedings of the National Academy of Sciences* 99.20 (Oct. 2002), pp. 13330–13335. ISSN: 0027-8424, 1091-6490. DOI: 10.1073/pnas.202244299.

[160] Romualdo Pastor-Satorras and Alessandro Vespignani. "Epidemic Spreading in Scale-Free Networks". In: *Physical Review Letters* 86.14 (Apr. 2001), pp. 3200–3203. DOI: 10.1103/PhysRevLett.86.3200.

[161] M. E. J. Newman. "Spread of Epidemic Disease on Networks". In: *Physical Review E* 66.1 (July 2002), p. 016128. DOI: 10.1103/PhysRevE.66.016128.

[162] P. Van Mieghem, J. Omic, and R. Kooij. "Virus Spread in Networks". In: *IEEE/ACM Transactions on Networking* 17.1 (Feb. 2009), pp. 1–14. ISSN: 1063-6692. DOI: 10.1109/TNET.2008.925623.

[163] E. Cator, R. van de Bovenkamp, and P. Van Mieghem. "Susceptible-Infected-Susceptible Epidemics on Networks with General Infection and Cure Times". In: *Physical Review E* 87.6 (June 2013), p. 062816. DOI: 10.1103/PhysRevE.87.062816.

[164] James P. Gleeson. "High-Accuracy Approximation of Binary-State Dynamics on Networks". In: *Physical Review Letters* 107.6 (Aug. 2011), p. 068701. DOI: 10.1103/PhysRevLett.107.068701.

[165] Deepayan Chakrabarti et al. "Epidemic Thresholds in Real Networks". In: *ACM Trans. Inf. Syst. Secur.* 10.4 (Jan. 2008), 1:1–1:26. ISSN: 1094-9224. DOI: 10.1145/1284680.1284681.

[166] Claudio Castellano and Romualdo Pastor-Satorras. "Thresholds for Epidemic Spreading in Networks". In: *Physical Review Letters* 105.21 (Nov. 2010), p. 218701. ISSN: 0031-9007, 1079-7114. DOI: 10.1103/PhysRevLett.105.218701. arXiv: 1010.1646.

[167] Eugenio Valdano et al. "Analytical Computation of the Epidemic Threshold on Temporal Networks". In: *Physical Review X* 5.2 (Apr. 2015), p. 021005. DOI: 10.1103/PhysRevX.5.021005.

[168] Y. Moreno, R. Pastor-Satorras, and A. Vespignani. "Epidemic Outbreaks in Complex Heterogeneous Networks". en. In: *The European Physical Journal B - Condensed Matter and Complex Systems* 26.4 (Apr. 2002), pp. 521–529. ISSN: 1434-6036. DOI: 10.1140/epjb/e20020122.

[169] Yamir Moreno, Javier B. Gómez, and Amalio F. Pacheco. "Epidemic Incidence in Correlated Complex Networks". In: *Physical Review E* 68.3 (Sept. 2003), p. 035103. DOI: 10.1103/PhysRevE.68.035103.

[170] Joel C. Miller. "Percolation and Epidemics in Random Clustered Networks". In: *Physical Review E* 80.2 (Aug. 2009), p. 020901. DOI: 10.1103/PhysRevE.80.020901.

[171] Zimo Yang and Tao Zhou. "Epidemic Spreading in Weighted Networks: An Edge-Based Mean-Field Solution". In: *Physical Review E* 85.5 (May 2012), p. 056106. DOI: 10.1103/PhysRevE.85.056106.

[172] Erik Volz. "SIR Dynamics in Random Networks with Heterogeneous Connectivity". en. In: *Journal of Mathematical Biology* 56.3 (Mar. 2008), pp. 293–310. ISSN: 1432-1416. DOI: 10.1007/s00285-007-0116-4.

[173] James P. Gleeson. "Binary-State Dynamics on Complex Networks: Pair Approximation and Beyond". In: *Physical Review X* 3.2 (Apr. 2013), p. 021004. DOI: 10.1103/PhysRevX.3.021004.

[174] Romualdo Pastor-Satorras and Alessandro Vespignani. "Immunization of Complex Networks". In: *Physical Review E* 65.3 (Feb. 2002), p. 036104. DOI: 10.1103/PhysRevE.65.036104.

[175] Petter Holme et al. “Attack Vulnerability of Complex Networks”. In: *Physical Review E* 65.5 (May 2002), p. 056109. DOI: 10.1103/PhysRevE.65.056109.

[176] P. Holme. “Efficient Local Strategies for Vaccination and Network Attack”. en. In: *EPL (Europhysics Letters)* 68.6 (Nov. 2004), p. 908. ISSN: 0295-5075. DOI: 10.1209/epl/i2004-10286-2.

[177] Eben Kenah and Joel C. Miller. *Epidemic Percolation Networks, Epidemic Outcomes, and Interventions*. en. https://www.hindawi.com/journals/ipid/2011/543520/. Research Article. 2011. DOI: 10.1155/2011/543520.

[178] Maria Deijfen. “Epidemics and Vaccination on Weighted Graphs”. In: *Mathematical Biosciences* 232.1 (July 2011), pp. 57–65. ISSN: 0025-5564. DOI: 10.1016/j.mbs.2011.04.003.

[179] Zhen Wang et al. “Statistical Physics of Vaccination”. In: *Physics Reports*. Statistical Physics of Vaccination 664 (Dec. 2016), pp. 1–113. ISSN: 0370-1573. DOI: 10.1016/j.physrep.2016.10.006.

[180] Stanley Wasserman and Katherine Faust. *Social Network Analysis by Stanley Wasserman*. en. /core/books/social-network-analysis/90030086891EB3491D096034684EFFB8. Nov. 1994. DOI: 10.1017/CBO9780511815478.

[181] Fredrik Liljeros et al. “The Web of Human Sexual Contacts”. En. In: *Nature* 411.6840 (June 2001), p. 907. ISSN: 1476-4687. DOI: 10.1038/35082140.

[182] W J Edmunds, C J O’Callaghan, and D J Nokes. “Who Mixes with Whom? A Method to Determine the Contact Patterns of Adults That May Lead to the Spread of Airborne Infections.” In: *Proceedings of the Royal Society B: Biological Sciences* 264.1384 (July 1997), pp. 949–957. ISSN: 0962-8452.

[183] Alex Beutel et al. “Interacting Viruses in Networks: Can Both Survive?” In: *Proceedings of the 18th ACM SIGKDD International Conference on Knowledge Discovery and Data Mining*. KDD ’12. New York, NY, USA: ACM, 2012, pp. 426–434. ISBN: 978-1-4503-1462-6. DOI: 10.1145/2339530.2339601.

[184] Joël Mossong et al. “Social Contacts and Mixing Patterns Relevant to the Spread of Infectious Diseases”. In: *PLoS Med* 5.3 (Mar. 2008), e74. DOI: 10.1371/journal.pmed.0050074.

[185] C. Castillo-Chavez et al. “Epidemiological Models with Age Structure, Proportionate Mixing, and Cross-Immunity”. en. In: *Journal of Mathematical Biology* 27.3 (May 1989), pp. 233–258. ISSN: 1432-1416. DOI: 10.1007/BF00275810.

[186] Jonathan M. Read, Ken T. D. Eames, and W. John Edmunds. “Dynamic Social Networks and the Implications for the Spread of Infectious Disease”. eng. In: *Journal of the Royal Society, Interface* 5.26 (Sept. 2008), pp. 1001–1007. ISSN: 1742-5689. DOI: 10.1098/rsif.2008.0013.

[187] Christophe Fraser et al. "Factors That Make an Infectious Disease Outbreak Controllable". en. In: *Proceedings of the National Academy of Sciences* 101.16 (Apr. 2004), pp. 6146–6151. ISSN: 0027-8424, 1091-6490. DOI: 10.1073/pnas.0307506101.

[188] Ken T. D. Eames and Matt J. Keeling. "Contact Tracing and Disease Control". eng. In: *Proceedings. Biological Sciences* 270.1533 (Dec. 2003), pp. 2565–2571. ISSN: 0962-8452. DOI: 10.1098/rspb.2003.2554.

[189] A. C. Ghani, J. Swinton, and G. P. Garnett. "The Role of Sexual Partnership Networks in the Epidemiology of Gonorrhea". eng. In: *Sexually Transmitted Diseases* 24.1 (Jan. 1997), pp. 45–56. ISSN: 0148-5717.

[190] A. C. Ghani and G. P. Garnett. "Measuring Sexual Partner Networks for Transmission of Sexually Transmitted Diseases". en. In: *Journal of the Royal Statistical Society: Series A (Statistics in Society)* 161.2 (1998), pp. 227–238. ISSN: 1467-985X. DOI: 10.1111/1467-985X.00101.

[191] D. M. Auerbach et al. "Cluster of Cases of the Acquired Immune Deficiency Syndrome. Patients Linked by Sexual Contact". eng. In: *The American Journal of Medicine* 76.3 (Mar. 1984), pp. 487–492. ISSN: 0002-9343. DOI: 10.1016/0002-9343(84)90668-5.

[192] Alden S. Klovdahl. "Social Networks and the Spread of Infectious Diseases: The AIDS Example". In: *Social Science & Medicine* 21.11 (Jan. 1985), pp. 1203–1216. ISSN: 0277-9536. DOI: 10.1016/0277-9536(85)90269-2.

[193] WJ Edmunds et al. "Mixing Patterns and the Spread of Close-Contact Infectious Diseases". In: *Emerging Themes in Epidemiology* 3.1 (Aug. 2006), p. 10. ISSN: 1742-7622. DOI: 10.1186/1742-7622-3-10.

[194] J. L. Wylie and A. Jolly. "Patterns of Chlamydia and Gonorrhea Infection in Sexual Networks in Manitoba, Canada". eng. In: *Sexually Transmitted Diseases* 28.1 (Jan. 2001), pp. 14–24. ISSN: 0148-5717.

[195] J. J. Potterat et al. "Risk Network Structure in the Early Epidemic Phase of HIV Transmission in Colorado Springs". eng. In: *Sexually Transmitted Infections* 78 Suppl 1 (Apr. 2002), pp. i159–163. ISSN: 1368-4973. DOI: 10.1136/sti.78.suppl_1.i159.

[196] R. B. Rothenberg et al. "Social Network Dynamics and HIV Transmission". eng. In: *AIDS (London, England)* 12.12 (Aug. 1998), pp. 1529–1536. ISSN: 0269-9370. DOI: 10.1097/00002030-199812000-00016.

[197] Danon Leon et al. "Social Encounter Networks: Characterizing Great Britain". In: *Proceedings of the Royal Society B: Biological Sciences* 280.1765 (Aug. 2013), p. 20131037. DOI: 10.1098/rspb.2013.1037.

[198] Rania Assab et al. "Mathematical Models of Infection Transmission in Healthcare Settings: Recent Advances from the Use of Network Structured Data". eng. In: *Current Opinion in Infectious Diseases* 30.4 (Aug. 2017), pp. 410–418. ISSN: 1473-6527. DOI: 10.1097/QCO.0000000000000390.

[199] M. M. Triola and R. S. Holzman. "Agent-Based Simulation of Nosocomial Transmission in the Medical Intensive Care Unit". In: *16th IEEE Symposium Computer-Based Medical Systems, 2003. Proceedings.* June 2003, pp. 284–288. DOI: 10.1109/CBMS.2003.1212803.

[200] Janet Raboud et al. "Modeling Transmission of Methicillin-Resistant Staphylococcus Aureus among Patients Admitted to a Hospital". eng. In: *Infection Control and Hospital Epidemiology* 26.7 (July 2005), pp. 607–615. ISSN: 0899-823X. DOI: 10.1086/502589.

[201] Anna Machens et al. "An Infectious Disease Model on Empirical Networks of Human Contact: Bridging the Gap between Dynamic Network Data and Contact Matrices". eng. In: *BMC infectious diseases* 13 (Apr. 2013), p. 185. ISSN: 1471-2334. DOI: 10.1186/1471-2334-13-185.

[202] Xia Wang et al. "A Data-Driven Mathematical Model of Multi-Drug Resistant Acinetobacter Baumannii Transmission in an Intensive Care Unit". In: *Scientific Reports* 5 (Mar. 2015). ISSN: 2045-2322. DOI: 10.1038/srep09478.

[203] E. S. McBryde, A. N. Pettitt, and D. L. S. McElwain. "A Stochastic Mathematical Model of Methicillin Resistant Staphylococcus Aureus Transmission in an Intensive Care Unit: Predicting the Impact of Interventions". eng. In: *Journal of Theoretical Biology* 245.3 (Apr. 2007), pp. 470–481. ISSN: 0022-5193. DOI: 10.1016/j.jtbi.2006.11.008.

[204] Sean L. Barnes et al. "Preventing the Transmission of Multidrug-Resistant Organisms (MDROs): Modeling the Relative Importance of Hand Hygiene and Environmental Cleaning Interventions". In: *Infection control and hospital epidemiology : the official journal of the Society of Hospital Epidemiologists of America* 35.9 (Sept. 2014), pp. 1156–1162. ISSN: 0899-823X. DOI: 10.1086/677632.

[205] Hajo Grundmann et al. "Risk Factors for the Transmission of Methicillin-Resistant Staphylococcus Aureus in an Adult Intensive Care Unit: Fitting a Model to the Data". eng. In: *The Journal of Infectious Diseases* 185.4 (Feb. 2002), pp. 481–488. ISSN: 0022-1899. DOI: 10.1086/338568.

[206] Rania Assab and Laura Temime. "The Role of Hand Hygiene in Controlling Norovirus Spread in Nursing Homes". In: *BMC Infectious Diseases* 16.1 (Aug. 2016), p. 395. ISSN: 1471-2334. DOI: 10.1186/s12879-016-1702-0.

[207] Philip M. Polgreen et al. "Prioritizing Healthcare Worker Vaccinations on the Basis of Social Network Analysis". eng. In: *Infection Control and Hospital Epidemiology* 31.9 (Sept. 2010), pp. 893–900. ISSN: 1559-6834. DOI: 10.1086/655466.

[208] Taro Ueno and Naoki Masuda. "Controlling Nosocomial Infection Based on Structure of Hospital Social Networks". In: *Journal of Theoretical Biology* 254.3 (Oct. 2008), pp. 655–666. ISSN: 0022-5193. DOI: 10.1016/j.jtbi.2008.07.001.

[209] Lucie Martinet et al. "The Link Stream of Contacts in a Whole Hospital". In: *arXiv:1805.05752 [cs]* (May 2018).

[210] Audrey Duval et al. "Measuring Dynamic Social Contacts in a Rehabilitation Hospital: Effect of Wards, Patient and Staff Characteristics". en. In: *Scientific Reports* 8.1 (Jan. 2018), p. 1686. ISSN: 2045-2322. DOI: 10.1038/s41598-018-20008-w.

[211] Tjibbe Donker, Jacco Wallinga, and Hajo Grundmann. "Patient Referral Patterns and the Spread of Hospital-Acquired Infections through National Health Care Networks". en. In: *PLOS Computational Biology* 6.3 (19-mar-2010), e1000715. ISSN: 1553-7358. DOI: 10.1371/journal.pcbi.1000715.

[212] Tjibbe Donker et al. "Hospital Networks and the Dispersal of Hospital-Acquired Pathogens by Patient Transfer". en. In: *PLOS ONE* 7.4 (25-apr-2012), e35002. ISSN: 1932-6203. DOI: 10.1371/journal.pone.0035002.

[213] Jan Ohst et al. "The Network Positions of Methicillin Resistant Staphylococcus Aureus Affected Units in a Regional Healthcare System". en. In: *EPJ Data Science* 3.1 (Dec. 2014), pp. 1–15. ISSN: 2193-1127. DOI: 10.1140/epjds/s13688-014-0029-6.

[214] Juan Fernández-Gracia et al. "Influence of a Patient Transfer Network of US Inpatient Facilities on the Incidence of Nosocomial Infections". en. In: *Scientific Reports* 7.1 (June 2017), pp. 1–9. ISSN: 2045-2322. DOI: 10.1038/s41598-017-02245-7.

[215] Narimane Nekkab et al. "Spread of Hospital-Acquired Infections: A Comparison of Healthcare Networks". en. In: *PLOS Computational Biology* 13.8 (24-ago-2017), e1005666. ISSN: 1553-7358. DOI: 10.1371/journal.pcbi.1005666.

[216] Vittoria Colizza et al. "Modeling the Worldwide Spread of Pandemic Influenza: Baseline Case and Containment Interventions". eng. In: *PLoS medicine* 4.1 (Jan. 2007), e13. ISSN: 1549-1676. DOI: 10.1371/journal.pmed.0040013.

[217] Duygu Balcan et al. "Seasonal Transmission Potential and Activity Peaks of the New Influenza A(H1N1): A Monte Carlo Likelihood Analysis Based on Human Mobility". eng. In: *BMC medicine* 7 (Sept. 2009), p. 45. ISSN: 1741-7015. DOI: 10.1186/1741-7015-7-45.

[218] Segolene Charaudeau, Khashayar Pakdaman, and Pierre-Yves Boëlle. "Commuter Mobility and the Spread of Infectious Diseases: Application to Influenza in France". en. In: *PLOS ONE* 9.1 (9-gen-2014), e83002. ISSN: 1932-6203. DOI: 10.1371/journal.pone.0083002.

[219] Marguta Ramona and Parisi Andrea. "Impact of Human Mobility on the Periodicities and Mechanisms Underlying Measles Dynamics". In: *Journal of The Royal Society Interface* 12.104 (Mar. 2015), p. 20141317. DOI: 10.1098/rsif.2014.1317.

[220] Amy Wesolowski et al. "Quantifying the Impact of Human Mobility on Malaria". eng. In: *Science (New York, N.Y.)* 338.6104 (Oct. 2012), pp. 267–270. ISSN: 1095-9203. DOI: 10.1126/science.1223467.

[221] Caroline O. Buckee et al. "Mobile Phones and Malaria: Modeling Human and Parasite Travel". In: *Travel medicine and infectious disease* 11.1 (2013), pp. 15–22. ISSN: 1477-8939. DOI: 10.1016/j.tmaid.2012.12.003.

[222] Flavio Finger et al. “Mobile Phone Data Highlights the Role of Mass Gatherings in the Spreading of Cholera Outbreaks”. eng. In: *Proceedings of the National Academy of Sciences of the United States of America* 113.23 (June 2016), pp. 6421–6426. ISSN: 1091-6490. DOI: 10.1073/pnas.1522305113.

[223] Linus Bengtsson et al. “Using Mobile Phone Data to Predict the Spatial Spread of Cholera”. en. In: *Scientific Reports* 5 (Mar. 2015), p. 8923. ISSN: 2045-2322. DOI: 10.1038/srep08923.

[224] Sanja Brdar et al. “Unveiling Spatial Epidemiology of HIV with Mobile Phone Data”. In: *Scientific Reports* 6 (Jan. 2016). ISSN: 2045-2322. DOI: 10.1038/srep19342.

[225] Albert-László Barabási. “Scale-Free Networks: A Decade and Beyond”. en. In: *Science* 325.5939 (July 2009), pp. 412–413. ISSN: 0036-8075, 1095-9203. DOI: 10.1126/science.1173299.

[226] Laura Temime et al. “Peripatetic Health-Care Workers as Potential Superspreaders”. eng. In: *Proceedings of the National Academy of Sciences of the United States of America* 106.43 (Oct. 2009), pp. 18420–18425. ISSN: 1091-6490. DOI: 10.1073/pnas.0900974106.

[227] Stefano Bonaccorsi et al. “Epidemic Outbreaks in Two-Scale Community Networks”. In: *Physical Review E* 90.1 (July 2014), p. 012810. DOI: 10.1103/PhysRevE.90.012810.

[228] Wei Huang and Chunguang Li. “Epidemic Spreading in Scale-Free Networks with Community Structure”. en. In: *Journal of Statistical Mechanics: Theory and Experiment* 2007.01 (Jan. 2007), P01014–P01014. ISSN: 1742-5468. DOI: 10.1088/1742-5468/2007/01/P01014.

[229] Xiaoyan Wu and Zonghua Liu. “How Community Structure Influences Epidemic Spread in Social Networks”. In: *Physica A: Statistical Mechanics and its Applications* 387.2 (Jan. 2008), pp. 623–630. ISSN: 0378-4371. DOI: 10.1016/j.physa.2007.09.039.

[230] Marcel Salathé and James H. Jones. “Dynamics and Control of Diseases in Networks with Community Structure”. en. In: *PLOS Computational Biology* 6.4 (8-apr-2010), e1000736. ISSN: 1553-7358. DOI: 10.1371/journal.pcbi.1000736.

[231] Matthieu Latapy, Tiphaine Viard, and Clémence Magnien. “Stream Graphs and Link Streams for the Modeling of Interactions over Time”. en. In: *Social Network Analysis and Mining* 8.1 (Oct. 2018), p. 61. ISSN: 1869-5469. DOI: 10.1007/s13278-018-0537-7.

[232] Naoki Masuda and Renaud Lambiotte. *Guide To Temporal Networks, A*. Anglais. Wspc, July 2016.

[233] Márton Karsai, Hang-Hyun Jo, and Kimmo Kaski. “Bursty Human Dynamics”. In: *arXiv:1803.02580 [physics]* (2018). DOI: 10.1007/978-3-319-68540-3. arXiv: 1803.02580 [physics].

[234] N. Perra et al. "Activity Driven Modeling of Time Varying Networks". en. In: *Scientific Reports* 2 (June 2012), p. 469. ISSN: 2045-2322. DOI: 10.1038/srep00469.

[235] Kao Rowland R et al. "Disease Dynamics over Very Different Time-Scales: Foot-and-Mouth Disease and Scrapie on the Network of Livestock Movements in the UK". In: *Journal of The Royal Society Interface* 4.16 (Oct. 2007), pp. 907–916. DOI: 10.1098/rsif.2007.1129.

[236] Jessica Enright and Rowland Raymond Kao. "Epidemics on Dynamic Networks". In: *Epidemics* 24 (Sept. 2018), pp. 88–97. ISSN: 1755-4365. DOI: 10.1016/j.epidem.2018.04.003.

[237] Eugenio Valdano, Chiara Poletto, and Vittoria Colizza. "Infection Propagator Approach to Compute Epidemic Thresholds on Temporal Networks: Impact of Immunity and of Limited Temporal Resolution". en. In: *The European Physical Journal B* 88.12 (Dec. 2015), p. 341. ISSN: 1434-6028, 1434-6036. DOI: 10.1140/epjb/e2015-60620-5.

[238] Laetitia Gauvin et al. "Randomized Reference Models for Temporal Networks". In: *arXiv:1806.04032 [physics, q-bio]* (June 2018). arXiv: 1806.04032 [physics, q-bio].

[239] Vittoria Colizza et al. "The Role of the Airline Transportation Network in the Prediction and Predictability of Global Epidemics". en. In: *Proceedings of the National Academy of Sciences* 103.7 (Feb. 2006), pp. 2015–2020. ISSN: 0027-8424, 1091-6490. DOI: 10.1073/pnas.0510525103.

[240] Laetitia Gauvin et al. "Activity Clocks: Spreading Dynamics on Temporal Networks of Human Contact". en. In: *Scientific Reports* 3 (Oct. 2013), p. 3099. ISSN: 2045-2322. DOI: 10.1038/srep03099.

[241] Petter Holme and Fredrik Liljeros. "Birth and Death of Links Control Disease Spreading in Empirical Contact Networks". en. In: *Scientific Reports* 4 (May 2014), p. 4999. ISSN: 2045-2322. DOI: 10.1038/srep04999.

[242] Petter Holme. "Temporal Network Structures Controlling Disease Spreading". In: *Physical Review E* 94.2 (Aug. 2016), p. 022305. DOI: 10.1103/PhysRevE.94.022305.

[243] Mingwu Li et al. "Lifetime-Preserving Reference Models for Characterizing Spreading Dynamics on Temporal Networks". en. In: *Scientific Reports* 8.1 (Jan. 2018), p. 709. ISSN: 2045-2322. DOI: 10.1038/s41598-017-18450-3.

[244] Luis E. C. Rocha and Vincent D. Blondel. "Bursts of Vertex Activation and Epidemics in Evolving Networks". en. In: *PLOS Computational Biology* 9.3 (21-mar-2013), e1002974. ISSN: 1553-7358. DOI: 10.1371/journal.pcbi.1002974.

[245] Marc Lipsitch et al. "Transmission Dynamics and Control of Severe Acute Respiratory Syndrome". eng. In: *Science (New York, N.Y.)* 300.5627 (June 2003), pp. 1966–1970. ISSN: 1095-9203. DOI: 10.1126/science.1086616.

[246] Lauren Ancel Meyers et al. "Network Theory and SARS: Predicting Outbreak Diversity". In: *Journal of Theoretical Biology* 232.1 (Jan. 2005), pp. 71–81. ISSN: 0022-5193. DOI: 10.1016/j.jtbi.2004.07.026.

[247] J. O. Lloyd-Smith et al. "Superspreading and the Effect of Individual Variation on Disease Emergence". En. In: *Nature* 438.7066 (Nov. 2005), p. 355. ISSN: 1476-4687. DOI: 10.1038/nature04153.

[248] A J Kucharski and C L Althaus. "The Role of Superspreading in Middle East Respiratory Syndrome Coronavirus (MERS-CoV) Transmission". en. In: *Eurosurveillance* 20.25 (June 2015). ISSN: 1560-7917. DOI: 10.2807/1560-7917.ES2015.20.25.21167.

[249] Naoki Masuda and Norio Konno. "Multi-State Epidemic Processes on Complex Networks". In: *Journal of Theoretical Biology* 243.1 (Nov. 2006), pp. 64–75. ISSN: 0022-5193. DOI: 10.1016/j.jtbi.2006.06.010.

[250] Giovanna Miritello, Esteban Moro, and Rubén Lara. "Dynamical Strength of Social Ties in Information Spreading". In: *Physical Review E* 83.4 (Apr. 2011), p. 045102. DOI: 10.1103/PhysRevE.83.045102.

[251] M. Karsai et al. "Small but Slow World: How Network Topology and Burstiness Slow down Spreading". eng. In: *Physical Review. E, Statistical, Nonlinear, and Soft Matter Physics* 83.2 Pt 2 (Feb. 2011), p. 025102. ISSN: 1550-2376. DOI: 10.1103/PhysRevE.83.025102.

[252] Dávid X. Horváth and János Kertész. "Spreading Dynamics on Networks: The Role of Burstiness, Topology and Non-Stationarity". en. In: *New Journal of Physics* 16.7 (July 2014), p. 073037. ISSN: 1367-2630. DOI: 10.1088/1367-2630/16/7/073037.

[253] B. Aditya Prakash et al. "Winner Takes All: Competing Viruses or Ideas on Fair-Play Networks". In: *Proceedings of the 21st International Conference on World Wide Web*. WWW '12. New York, NY, USA: ACM, 2012, pp. 1037–1046. ISBN: 978-1-4503-1229-5. DOI: 10.1145/2187836.2187975.

[254] Oleg Kogan et al. "Two-Strain Competition in Quasineutral Stochastic Disease Dynamics". In: *Physical Review E* 90.4 (Oct. 2014), p. 042149. DOI: 10.1103/PhysRevE.90.042149.

[255] Jonas I. Liechti, Gabriel E. Leventhal, and Sebastian Bonhoeffer. "Host Population Structure Impedes Reversion to Drug Sensitivity after Discontinuation of Treatment". en. In: *PLOS Computational Biology* 13.8 (21-ago-2017), e1005704. ISSN: 1553-7358. DOI: 10.1371/journal.pcbi.1005704.

[256] Faryad Darabi Sahneh and Caterina Scoglio. "Competitive Epidemic Spreading over Arbitrary Multilayer Networks". In: *Physical Review E* 89.6 (June 2014), p. 062817. DOI: 10.1103/PhysRevE.89.062817.

[257] Jorge P. Rodríguez et al. "Diversity of Hysteresis in a Fully Cooperative Coinfection Model". In: *Chaos: An Interdisciplinary Journal of Nonlinear Science* 28.2 (Feb. 2018), p. 023107. ISSN: 1054-1500. DOI: 10.1063/1.4996807.

[258] Peng-Bi Cui, Francesca Colaiori, and Claudio Castellano. "Mutually Cooperative Epidemics on Power-Law Networks". In: *Physical Review E* 96.2 (Aug. 2017), p. 022301. DOI: 10.1103/PhysRevE.96.022301.

[259] Jorge P. Rodríguez, Fakhteh Ghanbarnejad, and Víctor M. Eguíluz. "Risk of Coinfection Outbreaks in Temporal Networks: A Case Study of a Hospital Contact Network". English. In: *Frontiers in Physics* 5 (2017). ISSN: 2296-424X. DOI: 10.3389/fphy.2017.00046.

[260] Caroline Buckee, Leon Danon, and Sunetra Gupta. "Host Community Structure and the Maintenance of Pathogen Diversity". en. In: *Proceedings of the Royal Society of London B: Biological Sciences* 274.1619 (July 2007), pp. 1715–1721. ISSN: 0962-8452, 1471-2954. DOI: 10.1098/rspb.2007.0415.

[261] Caroline O'F Buckee et al. "The Effects of Host Contact Network Structure on Pathogen Diversity and Strain Structure". en. In: *Proceedings of the National Academy of Sciences* 101.29 (July 2004), pp. 10839–10844. ISSN: 0027-8424, 1091-6490. DOI: 10.1073/pnas.0402000101.

[262] Michelle Girvan et al. "Simple Model of Epidemics with Pathogen Mutation". In: *Physical Review E* 65.3 (Mar. 2002), p. 031915. DOI: 10.1103/PhysRevE.65.031915.

[263] S. Gupta, N. Ferguson, and R. Anderson. "Chaos, Persistence, and Evolution of Strain Structure in Antigenically Diverse Infectious Agents". eng. In: *Science (New York, N.Y.)* 280.5365 (May 1998), pp. 912–915. ISSN: 0036-8075. DOI: 10.1126/science.280.5365.912.

[264] Gabriel E. Leventhal et al. "Inferring Epidemic Contact Structure from Phylogenetic Trees". en. In: *PLOS Computational Biology* 8.3 (8-mar-2012), e1002413. ISSN: 1553-7358. DOI: 10.1371/journal.pcbi.1002413.

[265] Katy Robinson et al. "How the Dynamics and Structure of Sexual Contact Networks Shape Pathogen Phylogenies". en. In: *PLOS Computational Biology* 9.6 (June 2013), e1003105. ISSN: 1553-7358. DOI: 10.1371/journal.pcbi.1003105.

[266] Y. Haraguchi and A. Sasaki. "The Evolution of Parasite Virulence and Transmission Rate in a Spatially Structured Population". eng. In: *Journal of Theoretical Biology* 203.2 (Mar. 2000), pp. 85–96. ISSN: 0022-5193. DOI: 10.1006/jtbi.1999.1065.

[267] W. Marijn van Ballegooijen and Maarten C. Boerlijst. "Emergent Trade-Offs and Selection for Outbreak Frequency in Spatial Epidemics". en. In: *Proceedings of the National Academy of Sciences* 101.52 (Dec. 2004), pp. 18246–18250. ISSN: 0027-8424, 1091-6490. DOI: 10.1073/pnas.0405682101.

[268] Geoff Wild, Andy Gardner, and Stuart A. West. "Adaptation and the Evolution of Parasite Virulence in a Connected World". eng. In: *Nature* 459.7249 (June 2009), pp. 983–986. ISSN: 1476-4687. DOI: 10.1038/nature08071.

[269] Sébastien Lion and Mike Boots. "Are Parasites "prudent" in Space?" eng. In: *Ecology Letters* 13.10 (Oct. 2010), pp. 1245–1255. ISSN: 1461-0248. DOI: 10.1111/j.1461-0248.2010.01516.x.

[270] Minus Van Baalen. *7 Contact Networks and the Evolution of Virulence*.

[271] François Blanquart. "Evolutionary Epidemiology Models to Predict the Dynamics of Antibiotic Resistance". en. In: *Evolutionary Applications* 12.3 (2019), pp. 365–383. ISSN: 1752-4571. DOI: 10.1111/eva.12753.

[272] Christophe Fraser, William P. Hanage, and Brian G. Spratt. "Neutral Microepidemic Evolution of Bacterial Pathogens". In: *Proceedings of the National Academy of Sciences of the United States of America* 102.6 (Feb. 2005), pp. 1968–1973. ISSN: 0027-8424. DOI: 10.1073/pnas.0406993102.

[273] S. Gupta et al. "The Maintenance of Strain Structure in Populations of Recombining Infectious Agents". eng. In: *Nature Medicine* 2.4 (Apr. 1996), pp. 437–442. ISSN: 1078-8956.

[274] Pieter T. J. Johnson, Jacobus C. de Roode, and Andy Fenton. "Why Infectious Disease Research Needs Community Ecology". In: *Science (New York, N.Y.)* 349.6252 (Sept. 2015), p. 1259504. ISSN: 0036-8075. DOI: 10.1126/science.1259504.

[275] Eric W. Seabloom et al. "The Community Ecology of Pathogens: Coinfection, Coexistence and Community Composition". en. In: *Ecology Letters* 18.4 (Apr. 2015), pp. 401–415. ISSN: 1461-0248. DOI: 10.1111/ele.12418.

[276] Mark Vellend. "Conceptual Synthesis in Community Ecology". eng. In: *The Quarterly Review of Biology* 85.2 (June 2010), pp. 183–206. ISSN: 0033-5770.

[277] Thomas J. Matthews and Robert J. Whittaker. "REVIEW: On the Species Abundance Distribution in Applied Ecology and Biodiversity Management". en. In: *Journal of Applied Ecology* 52.2 (2015), pp. 443–454. ISSN: 1365-2664. DOI: 10.1111/1365-2664.12380.

[278] Sandro Azaele et al. "Statistical Mechanics of Ecological Systems: Neutral Theory and Beyond". In: *Reviews of Modern Physics* 88.3 (July 2016), p. 035003. DOI: 10.1103/RevModPhys.88.035003.

[279] Brian J. McGill et al. "Species Abundance Distributions: Moving beyond Single Prediction Theories to Integration within an Ecological Framework". In: *Ecology Letters* 10.10 (Oct. 2007), pp. 995–1015. ISSN: 1461-023X. DOI: 10.1111/j.1461-0248.2007.01094.x.

[280] G. Stirling and B. Wilsey. "Empirical Relationships between Species Richness, Evenness, and Proportional Diversity". eng. In: *The American Naturalist* 158.3 (Sept. 2001), pp. 286–299. ISSN: 1537-5323. DOI: 10.1086/321317.

[281] Heiman FL Wertheim et al. "The Role of Nasal Carriage in Staphylococcus Aureus Infections". en. In: *The Lancet Infectious Diseases* 5.12 (Dec. 2005), pp. 751–762. ISSN: 1473-3099. DOI: 10.1016/S1473-3099(05)70295-4.

[282] Jonathan A. Otter, Saber Yezli, and Gary L. French. "The Role Played by Contaminated Surfaces in the Transmission of Nosocomial Pathogens". eng. In: *Infection Control and Hospital Epidemiology* 32.7 (July 2011), pp. 687–699. ISSN: 1559-6834. DOI: 10.1086/660363.

[283] Eili Klein, David L. Smith, and Ramanan Laxminarayan. "Hospitalizations and Deaths Caused by Methicillin-Resistant Staphylococcus Aureus, United States, 1999–2005". In: *Emerging Infectious Diseases* 13.12 (Dec. 2007), pp. 1840–1846. ISSN: 1080-6040. DOI: 10.3201/eid1312.070629.

[284] Dawn M. Sievert et al. "Antimicrobial-Resistant Pathogens Associated with Healthcare-Associated Infections Summary of Data Reported to the National Healthcare Safety Network at the Centers for Disease Control and Prevention, 2009–2010". en. In: *Infection Control & Hospital Epidemiology* 34.1 (Jan. 2013), pp. 1–14. ISSN: 0899-823X, 1559-6834. DOI: 10.1086/668770.

[285] Olga Sakwinska et al. "Ecological Temporal Stability of Staphylococcus Aureus Nasal Carriage". en. In: *Journal of Clinical Microbiology* 48.8 (Aug. 2010), pp. 2724–2728. ISSN: 0095-1137, 1098-660X. DOI: 10.1128/JCM.02091-09.

[286] Lyndsey O. Hudson et al. "Diversity of Methicillin-Resistant Staphylococcus Aureus (MRSA) Strains Isolated from Inpatients of 30 Hospitals in Orange County, California". en. In: *PLOS ONE* 8.4 (24-apr-2013), e62117. ISSN: 1932-6203. DOI: 10.1371/journal.pone.0062117.

[287] F. Di Ruscio et al. "Epidemiology and Spa-Type Diversity of Meticillin-Resistant Staphylococcus Aureus in Community and Healthcare Settings in Norway". English. In: *Journal of Hospital Infection* 100.3 (Nov. 2018), pp. 316–321. ISSN: 0195-6701, 1532-2939. DOI: 10.1016/j.jhin.2017.12.019.

[288] Olga Sakwinska et al. "Genetic Diversity and Ecological Success of Staphylococcus Aureus Strains Colonizing Humans". In: *Applied and Environmental Microbiology* 75.1 (Jan. 2009), pp. 175–183. ISSN: 0099-2240. DOI: 10.1128/AEM.01860-08.

[289] Ben S. Cooper et al. "Quantifying Type-Specific Reproduction Numbers for Nosocomial Pathogens: Evidence for Heightened Transmission of an Asian Sequence Type 239 MRSA Clone". en. In: *PLOS Computational Biology* 8.4 (12-apr-2012), e1002454. ISSN: 1553-7358. DOI: 10.1371/journal.pcbi.1002454.

[290] Binh An Diep et al. "The Arginine Catabolic Mobile Element and Staphylococcal Chromosomal Cassette Mec Linkage: Convergence of Virulence and Resistance in the USA300 Clone of Methicillin-Resistant Staphylococcus Aureus". en. In: *The Journal of Infectious Diseases* 197.11 (June 2008), pp. 1523–1530. ISSN: 0022-1899. DOI: 10.1086/587907.

[291] Erica M. C. D'Agata et al. "Modeling the Invasion of Community-Acquired Methicillin-Resistant Staphylococcus Aureus into Hospitals". en. In: *Clinical Infectious Diseases* 48.3 (Feb. 2009), pp. 274–284. ISSN: 1058-4838. DOI: 10.1086/595844.

[292] Lyndsey O. Hudson et al. "Differences in Methicillin-Resistant Staphylococcus Aureus Strains Isolated from Pediatric and Adult Patients from Hospitals in a Large County in California". en. In: *Journal of Clinical Microbiology* 50.3 (Mar. 2012), pp. 573–579. ISSN: 0095-1137, 1098-660X. DOI: 10.1128/JCM.05336-11.

[293] Lidia Kardaś-Słoma et al. "Impact of Antibiotic Exposure Patterns on Selection of Community-Associated Methicillin-Resistant Staphylococcus Aureus in Hospital Settings". en. In: *Antimicrobial Agents and Chemotherapy* 55.10 (Oct. 2011), pp. 4888–4895. ISSN: 0066-4804, 1098-6596. DOI: 10.1128/AAC.01626-10.

[294] Lidia Kardas-Sloma et al. "Antibiotic Reduction Campaigns Do Not Necessarily Decrease Bacterial Resistance: The Example of Methicillin-Resistant Staphylococcus Aureus". eng. In: *Antimicrobial Agents and Chemotherapy* 57.9 (Sept. 2013), pp. 4410–4416. ISSN: 1098-6596. DOI: 10.1128/AAC.00711-13.

[295] H. R. Shinefield, J. C. Ribble, and M. Boris. "Bacterial Interference between Strains of Staphylococcus Aureus, 1960 to 1970". eng. In: *American Journal of Diseases of Children (1960)* 121.2 (Feb. 1971), pp. 148–152. ISSN: 0002-922X.

[296] R. Aly et al. "Bacterial Interference among Strains of Staphylococcus Aureus in Man". eng. In: *The Journal of Infectious Diseases* 129.6 (June 1974), pp. 720–724. ISSN: 0022-1899. DOI: 10.1093/infdis/129.6.720.

[297] D J Austin, M Kakehashi, and R M Anderson. "The Transmission Dynamics of Antibiotic-Resistant Bacteria: The Relationship between Resistance in Commensal Organisms and Antibiotic Consumption." In: *Proceedings of the Royal Society B: Biological Sciences* 264.1388 (Nov. 1997), pp. 1629–1638. ISSN: 0962-8452.

[298] Marc Lipsitch, Carl T. Bergstrom, and Bruce R. Levin. "The Epidemiology of Antibiotic Resistance in Hospitals: Paradoxes and Prescriptions". en. In: *Proceedings of the National Academy of Sciences* 97.4 (Feb. 2000), pp. 1938–1943. ISSN: 0027-8424, 1091-6490. DOI: 10.1073/pnas.97.4.1938.

[299] David L. Smith et al. "Persistent Colonization and the Spread of Antibiotic Resistance in Nosocomial Pathogens: Resistance Is a Regional Problem". In: *Proceedings of the National Academy of Sciences of the United States of America* 101.10 (Mar. 2004), pp. 3709–3714. ISSN: 0027-8424. DOI: 10.1073/pnas.0400456101.

[300] Qiuzhi Chang, Marc Lipsitch, and William P. Hanage. "Impact of Host Heterogeneity on the Efficacy of Interventions to Reduce Staphylococcus Aureus Carriage". In: *Infection control and hospital epidemiology* 37.2 (Feb. 2016), pp. 197–204. ISSN: 0899-823X. DOI: 10.1017/ice.2015.269.

[301] Thomas Obadia et al. "Interindividual Contacts and Carriage of Methicillin-Resistant Staphylococcus Aureus: A Nested Case-Control Study". eng. In: *Infection Control and Hospital Epidemiology* 36.8 (Aug. 2015), pp. 922–929. ISSN: 1559-6834. DOI: 10.1017/ice.2015.89.

[302] David R. Cox. *Renewal Theory*. en. Methuen, 1962.

[303] G. Bianconi, L. Ferretti, and S. Franz. "Non-Neutral Theory of Biodiversity". en. In: *EPL (Europhysics Letters)* 87.2 (July 2009), p. 28001. ISSN: 0295-5075. DOI: 10.1209/0295-5075/87/28001.

[304] Richard A. Neher and Boris I. Shraiman. "Competition between Recombination and Epistasis Can Cause a Transition from Allele to Genotype Selection". en. In: *Proceedings of the National Academy of Sciences* 106.16 (Apr. 2009), pp. 6866–6871. ISSN: 0027-8424, 1091-6490. DOI: 10.1073/pnas.0812560106.

[305] Ginestra Bianconi and Olaf Rotzschke. "Bose-Einstein Distribution, Condensation Transition, and Multiple Stationary States in Multiloci Evolution of Diploid Populations". en. In: *Physical Review E* 82.3 (Sept. 2010), p. 036109. ISSN: 1539-3755, 1550-2376. DOI: 10.1103/PhysRevE.82.036109.

[306] J. F. C. Kingman. "A Simple Model for the Balance between Selection and Mutation". In: *Journal of Applied Probability* 15.1 (1978), pp. 1–12. ISSN: 0021-9002. DOI: 10.2307/3213231.

[307] Su-Chan Park and Joachim Krug. "Evolution in Random Fitness Landscapes: The Infinite Sites Model". en. In: *Journal of Statistical Mechanics: Theory and Experiment* 2008.04 (Apr. 2008), P04014. ISSN: 1742-5468. DOI: 10.1088/1742-5468/2008/04/P04014.

[308] Steffen Dereich and Peter Mörters. "Emergence of Condensation in Kingman's Model of Selection and Mutation". en. In: *Acta Applicandae Mathematicae* 127.1 (Oct. 2013), pp. 17–26. ISSN: 1572-9036. DOI: 10.1007/s10440-012-9790-3.

[309] Ginestra Bianconi et al. "Modeling Microevolution in a Changing Environment: The Evolving Quasispecies and the Diluted Champion Process". In: 2011. DOI: 10.1088/1742-5468/2011/08/P08022.

[310] Laith J. Abu-Raddad, Padmaja Patnaik, and James G. Kublin. "Dual Infection with HIV and Malaria Fuels the Spread of Both Diseases in Sub-Saharan Africa". eng. In: *Science (New York, N.Y.)* 314.5805 (Dec. 2006), pp. 1603–1606. ISSN: 1095-9203. DOI: 10.1126/science.1132338.

[311] Katharine J Looker et al. "Evidence of Synergistic Relationships between HIV and Human Papillomavirus (HPV): Systematic Reviews and Meta-Analyses of Longitudinal Studies of HPV Acquisition and Clearance by HIV Status, and of HIV Acquisition by HPV Status". en. In: *Journal of the International AIDS Society* 21.6 (June 2018), e25110. ISSN: 17582652. DOI: 10.1002/jia2.25110.

[312] Matthieu Domenech de Cellès et al. "Characterizing and Comparing the Seasonality of Influenza-Like Illnesses and Invasive Pneumococcal Diseases Using Seasonal Waveforms". en. In: *American Journal of Epidemiology* 187.5 (May 2018), pp. 1029–1039. ISSN: 0002-9262. DOI: 10.1093/aje/kwx336.

[313] Daniela Brites and Sebastien Gagneux. "Old and New Selective Pressures on Mycobacterium Tuberculosis". eng. In: *Infection, Genetics and Evolution: Journal of Molecular Epidemiology and Evolutionary Genetics in Infectious Diseases* 12.4 (June 2012), pp. 678–685. ISSN: 1567-7257. DOI: 10.1016/j.meegid.2011.08.010.

[314] Sanghyuk S. Shin et al. "Advanced Immune Suppression Is Associated With Increased Prevalence of Mixed-Strain Mycobacterium Tuberculosis Infections Among Persons at High Risk for Drug-Resistant Tuberculosis in Botswana". en. In: *The Journal of Infectious Diseases* 211.3 (Feb. 2015), pp. 347–351. ISSN: 0022-1899. DOI: 10.1093/infdis/jiu421.

[315] Gui Liu et al. "HIV-Positive Women Have Higher Risk of Human Papilloma Virus Infection, Precancerous Lesions, and Cervical Cancer". eng. In: *AIDS (London, England)* 32.6 (Mar. 2018), pp. 795–808. ISSN: 1473-5571. DOI: 10.1097/QAD.0000000000001765.

[316] Sheri A. Denslow et al. "Incidence and Progression of Cervical Lesions in Women with HIV: A Systematic Global Review". eng. In: *International journal of STD & AIDS* 25.3 (Mar. 2014), pp. 163–177. ISSN: 1758-1052. DOI: 10.1177/0956462413491735.

[317] Catherine F HOULIHAN et al. "HPV Infection and Increased Risk of HIV Acquisition. A Systematic Review and Meta-Analysis". In: *AIDS (London, England)* 26.17 (Nov. 2012). ISSN: 0269-9370. DOI: 10.1097/QAD.0b013e328358d908.

[318] Pascale Lissouba, Philippe Van de Perre, and Bertran Auvert. "Association of Genital Human Papillomavirus Infection with HIV Acquisition: A Systematic Review and Meta-Analysis". eng. In: *Sexually Transmitted Infections* 89.5 (Aug. 2013), pp. 350–356. ISSN: 1472-3263. DOI: 10.1136/sextrans-2011-050346.

[319] Clara Flateau, Guillaume Le Loup, and Gilles Pialoux. "Consequences of HIV Infection on Malaria and Therapeutic Implications: A Systematic Review". In: *The Lancet Infectious Diseases* 11.7 (July 2011), pp. 541–556. ISSN: 1473-3099. DOI: 10.1016/S1473-3099(11)70031-7.

[320] Christina C. Chang et al. "HIV and Co-Infections". en. In: *Immunological Reviews* 254.1 (July 2013), pp. 114–142. ISSN: 1600-065X. DOI: 10.1111/imr.12063.

[321] James G Kublin et al. "Effect of Plasmodium Falciparum Malaria on Concentration of HIV-1-RNA in the Blood of Adults in Rural Malawi: A Prospective Cohort Study". In: *The Lancet* 365.9455 (Jan. 2005), pp. 233–240. ISSN: 0140-6736. DOI: 10.1016/S0140-6736(05)17743-5.

[322] Cheryl Cohen et al. "Increased Prevalence of Severe Malaria in HIV-Infected Adults in South Africa". en. In: *Clinical Infectious Diseases* 41.11 (Dec. 2005), pp. 1631–1637. ISSN: 1058-4838. DOI: 10.1086/498023.

[323] Kexuan Chen et al. "Competition between Plasmodium Falciparum Strains in Clinical Infections during in Vitro Culture Adaptation". In: *Infection, genetics and evolution : journal of molecular epidemiology and evolutionary genetics in infectious diseases* 24 (June 2014), pp. 105–110. ISSN: 1567-1348. DOI: 10.1016/j.meegid.2014.03.012.

[324] Eileen M. Dunne et al. "Nasopharyngeal Microbial Interactions in the Era of Pneumococcal Conjugate Vaccination". In: *Vaccine* 31.19 (May 2013), pp. 2333–2342. ISSN: 0264-410X. DOI: 10.1016/j.vaccine.2013.03.024.

[325] Peter Jacoby et al. "Modelling the Co-Occurrence of Streptococcus Pneumoniae with Other Bacterial and Viral Pathogens in the Upper Respiratory Tract". eng. In: *Vaccine* 25.13 (Mar. 2007), pp. 2458–2464. ISSN: 0264-410X. DOI: 10.1016/j.vaccine.2006.09.020.

[326] Shabir A. Madhi et al. "Long-Term Effect of Pneumococcal Conjugate Vaccine on Nasopharyngeal Colonization by Streptococcus Pneumoniae–and Associated Interactions with Staphylococcus Aureus and Haemophilus Influenzae Colonization–in HIV-Infected and HIV-Uninfected Children". eng. In: *The Journal of Infectious Diseases* 196.11 (Dec. 2007), pp. 1662–1666. ISSN: 0022-1899. DOI: 10.1086/522164.

[327] Yu-Wen Chien et al. "Density Interactions among Streptococcus Pneumoniae, Haemophilus Influenzae and Staphylococcus Aureus in the Nasopharynx of Young Peruvian Children". eng. In: *The Pediatric Infectious Disease Journal* 32.1 (Jan. 2013), pp. 72–77. ISSN: 1532-0987. DOI: 10.1097/INF.0b013e318270d850.

[328] Osman Abdullahi et al. "The Descriptive Epidemiology of Streptococcus Pneumoniae and Haemophilus Influenzae Nasopharyngeal Carriage in Children and Adults in Kilifi District, Kenya". In: *The Pediatric infectious disease journal* 27.1 (Jan. 2008), pp. 59–64. ISSN: 0891-3668. DOI: 10.1097/INF.0b013e31814da70c.

[329] Kristin E. D. Weimer et al. "Divergent Mechanisms for Passive Pneumococcal Resistance to β-Lactam Antibiotics in the Presence of Haemophilus Influenzae". eng. In: *The Journal of Infectious Diseases* 203.4 (Feb. 2011), pp. 549–555. ISSN: 1537-6613. DOI: 10.1093/infdis/jiq087.

[330] Joshua R. Shak, Jorge E. Vidal, and Keith P. Klugman. "Influence of Bacterial Interactions on Pneumococcal Colonization of the Nasopharynx". In: *Trends in microbiology* 21.3 (Mar. 2013), pp. 129–135. ISSN: 0966-842X. DOI: 10.1016/j.tim.2012.11.005.

[331] Jonathan A. McCullers. "Insights into the Interaction between Influenza Virus and Pneumococcus". In: *Clinical Microbiology Reviews* 19.3 (July 2006), pp. 571–582. ISSN: 0893-8512. DOI: 10.1128/CMR.00058-05.

[332] Kirsty R. Short et al. "Interactions between Streptococcus Pneumoniae and Influenza Virus: A Mutually Beneficial Relationship?" eng. In: *Future Microbiology* 7.5 (May 2012), pp. 609–624. ISSN: 1746-0921. DOI: 10.2217/fmb.12.29.

[333] Daniel M. Weinberger et al. "Seasonal Drivers of Pneumococcal Disease Incidence: Impact of Bacterial Carriage and Viral Activity". eng. In: *Clinical Infectious Diseases: An Official Publication of the Infectious Diseases Society of America* 58.2 (Jan. 2014), pp. 188–194. ISSN: 1537-6591. DOI: 10.1093/cid/cit721.

[334] Daniel M. Weinberger et al. “Pneumococcal Disease Seasonality: Incidence, Severity and the Role of Influenza Activity”. eng. In: *The European Respiratory Journal* 43.3 (Mar. 2014), pp. 833–841. ISSN: 1399-3003. DOI: 10.1183/09031936.00056813.

[335] Matthieu Domenech de Cellès et al. “Unraveling the Seasonal Epidemiology of Pneumococcus”. eng. In: *Proceedings of the National Academy of Sciences of the United States of America* 116.5 (Jan. 2019), pp. 1802–1807. ISSN: 1091-6490. DOI: 10.1073/pnas.1812388116.

[336] Priyanga Amarasekare. “Competitive Coexistence in Spatially Structured Environments: A Synthesis”. en. In: *Ecology Letters* 6.12 (Dec. 2003), pp. 1109–1122. ISSN: 1461-0248. DOI: 10.1046/j.1461-0248.2003.00530.x.

[337] Linda J. S. Allen, Nadarajah Kirupaharan, and Sherri M. Wilson. “SIS Epidemic Models with Multiple Pathogen Strains”. In: *Journal of Difference Equations and Applications* 10.1 (Jan. 2004), pp. 53–75. ISSN: 1023-6198. DOI: 10.1080/10236190310001603680.

[338] Zhipeng Qiu et al. “The Vector–Host Epidemic Model with Multiple Strains in a Patchy Environment”. In: *Journal of Mathematical Analysis and Applications* 405.1 (Sept. 2013), pp. 12–36. ISSN: 0022-247X. DOI: 10.1016/j.jmaa.2013.03.042.